Vilnius University

CENTER FOR PHYSICAL SCIENCE AND TECHNOLOGY

Ieva

KRANAUSKAITĖ

Size and synergy effects on electrical properties of composites with nanocarbon inclusions

DOCTORAL DISSERTATION

Physical Sciences

Physics (02P)

VILNIUS 2018

This dissertation was prepared in Vilnius university in 2014 – 2018.

Scientific supervisor:

dr. Jan Macutkevič (Vilnius university, Physical sciences, Physics 02P)

The dissertation will be defended at joint scientific council:

Chairman – **prof. dr. Vytautas Balevičius** (Vilnius university, physical sciences, physics 02P)

Members:

Prof dr. Kęstutis Arlauskas (Vilnius university, physical sciences, physics 02P)

Doc. dr. Renata Butkutė (Vilnius university, physical sciences, physics 02P)

Prof. dr. Ričardas Makuška (Vilnius university, physical sciences, chemistry 03P)

Doc. dr. Tomas Šalkus (Vilnius university, physical sciences, physics 02P)

The dissertation will be defended at public meeting of scientific council on 25 th September, 2018, 15:00 at National centrer for physical sciences and technology, B336 room. Address: Sauletekio av. 3, Vilnius, Lithuania.

The dissertation is available at the libraries of Vilnius university, Center for physical sciences and technology and at website of Vilnius university: https://www.vu.lt/lt/naujienos/ivykiu-kalendorius

NACIONALINIS FIZINIŲ IR TECHNOLOGIJŲ MOKSLO CENTRAS

Ieva

KRANAUSKAITĖ

Dalelių dydžio ir sinergijos įtaka elektrinėms kompozitų su anglies nanodalelėmis savybėms

DAKTARO DISERTACIJA

Fiziniai mokslai

Fizika (02P)

VILNIUS 2018

Disertacija rengta 2014 – 2018 metais Vilniaus universitete

Mokslinis vadovas:

Dr. Jan Macutkevič (Vilniaus universitetas, fiziniai mokslai, fizika 02P)

Disertacija ginama viešame Gynimo tarybos posėdyje:

Pirmininkas – **prof. dr. Vytautas Balevičius** (Vilniaus universitetas, fiziniai mokslai, fizika 02P)

Nariai:

Prof dr. Kęstutis Arlauskas (Vilniaus universitetas, fiziniai mokslai, fizika 02P)

Doc. dr. Renata Butkutė (Vilniaus universitetas, fiziniai mokslai, fizika 02P)

Prof. dr. Ričardas Makuška (Vilniaus universitetas, fiziniai mokslai, chemija 03P)

Doc. dr. Tomas Šalkus (Vilniaus universitetas, fiziniai mokslai, fizika 02P)

Disertacija ginama viešajame Gynimo tarybos posėdyje 2018 m. rugsėjo mėn. 25 d. 15 val. Nacionalinio fizinių ir technologijų mokslų centro B336 auditorijoje. Adresas: Saulėtelio al. 3,Vilnius, Lietuva.

Disertaciją galima peržiūrėti Vilniaus universiteto ir Fizinių ir technologijos mokslų centro bibliotekose, ir Vilniaus universiteto svetainėje adresu: https://www.vu.lt/lt/naujienos/ivykiu-kalendorius

Aknowledgments

I would like to thank all the people who have helped and supported me for the past four years during my doctoral studies.

First of all, I am grateful to my scientific supervisor dr. Jan Macutkevič for supervision, help in achieving goals and preparing the thesis.

Sincere gratitude to the prof. Jūras Banys for the advice and guidance throughout the years in the laboratory.

Also I would like to thank all the colleagues and students in laboratory for help with experiments, collaboration in projects, discussions and friendly atmosphere.

Abbrevations

AC – alternating current

CB – carbon black

CG – coarse graphite

CNT – carbon nanotubes

CVD – chemical vapor deposition

DND – detonation nanodiamonds

DC – direct current

EMI – electromagnetic interference

EMT – effective medium theory

EG – exfoliated graphite

FG – fine graphite

FIT – fluctuation induced tunneling

GNP – graphene nanoplatelets

IPA - isopropanol

MG – medium graphite

MWCNT – multiwalled carbon nanotubes

NG – natural graphite

PDMS – polydimethylsiloxane

PMMA – poly(methyl methacrylate)

PA – polyamide

PC – polycarbonate

PE – polyethylene

PP – polypropylene

PS – polystyrene

PTFE – polytetrafluoroethylene

PVC – poly(vinyl chloride)

PVDF – polyvinylidene fluoride

PT – percolation threshold

PU – polyurethane

ROM – rule of mixure

SEM – scanning electron microscopy

TEM – transmission electron microscopy

Vol. % - volume percent

VRH – variable range hopping

Wt. % - weight percent

Contents

1 Introduction

In the large field of nanotechnology, polymer nanocomposites became a prominent area of current research and development. The electrical properties of these composites increase interest of scientific community due to potential applications and the accumulation of knowledge regarding their structure and properties relationship. The most attractive option in this field is the possibility to control macroscopic properties of nanocomposites at the nanoscale.

The combination of the insulating polymer as a host matrix and conducting carbon materials as filler gives as result a material with whole new set of properties that are not found in the individual components giving a rise to a novel class of electrical engineering materials [1, 2]. The electromagnetic response of polymer composites filled with low concentration of various conductive fillers, in particular nano- and micro-sized carbon allotropes, is important with respect to a variety of phenomena and related applications, including antistatic, radar wave absorbing materials and electromagnetic coatings [3-5]. In electronics, conductive polymer composites find applications as adhesives and circuit elements [6]. Technological advances in nanocomposites – the fusion of traditional polymers and the developing field of nanotechnology – have demonstrated that polymers filled with nanocarbons (carbon nanotubes, carbon blacks, carbon onions, etc.) possess unique properties including improved strength and durability, electrical conductivity, flame resistance, UV absorption, and reduced permeability [3].

At the same time, using nano-sized carbon materials raise a lot of challenges. The nanoparticles tend to increase viscosity and form agglomerates due to van der Waals forces, which lead to insufficient conductive network and higher percolation threshold. It is an important task to reach as low as possible percolation threshold in order to maintain the mechanical properties of polymers and to save the cost of generally expensive fillers. Very low percolation threshold could be observed in composites filled with long chain-like carbon black aggregates [7], but the lowest values were generally observed

in composites based on carbon nanotubes [8]. Nevertheless, the percolation threshold of composites based on the same polymer matrix and the same carbon nanotubes could be very different [9]. That means it is influenced by the distribution of the filler in a polymer matrix, which is governed by composite preparation technique. The good dispersion in polymer matrix often requires carbon's chemical modification, doping, functionalization, oxidation, etc., which in turn can have negative influence on physical and electromagnetic composite properties [10]. Another promising solution is an attempt combining two carbon fillers into a hybrid structure, which could lead to synergy effect of both fillers, improving mechanical, thermal and electrical characteristics. In addition, the use of different shape of nanoparticles enables to increase the efficiency at smaller filler contents. Therefore, it is hard to predict theoretically the final hybrid filler composite properties.

Broadband dielectric measurements can provide valuable information for inherent physical effects as well as describing overall electrical response.

1.1 Aim of the work

The aim of the dissertation is to systematically investigate size and synergy effects of composites filled with nanocarbon inclusions on broadband dielectric and electrical properties.

The main tasks of the work:

- To investigate dielectric and electrical properties of composites filled with different size of onion-like carbon aggregates in wide frequency (20 Hz – 1 THz) and temperature (30 K – 500 K) ranges.
- To investigate dielectric and electrical properties of composites filled with different length of carbon nanotubes, which were prepared by the same conditions, in wide frequency (20 Hz – 1 THz) and temperature (30 K – 500 K) ranges.
- To investigate dielectric properties of composites filled with different size graphite particles in wide frequency (20 Hz – 1 THz) and temperature (30 K – 500 K) ranges.
- To investigate synergy effects in electrical properties of hybrid filler OLC/MWCNT and GNP/MWCNT composites in wide frequency (20 Hz – 1 THz) and temperature ranges.

1.2 Scientific novelty

The dielectric and electrical properties of carbon based polymer composites containing onion-like carbon (OLC), carbon nanotubes (CNT), graphite and graphene nanoplatelets (GNP) for the first time were investigated in very wide frequency range from 20 Hz to 1 THz and temperature range from 30 K to 500 K.

For the first time the electrical properties of OLC composites with different aggregate size were investigated in such wide frequency and temperature ranges, and that was established that the electrical percolation threshold and the transition to the insulating state are dependent from aggregate size. The synergy effects were discovered in hybrid filler OLC/MWCNT composites.

For the first time composites filled with different length, but same diameter of MWCNTs were investigated in wide frequency and temperature range. That was established that electrical properties are rather independent from CNT aspect ratio, but are dependent from CNT distribution in polymer matrix.

For the first time composites with different size of graphite particles were investigated below percolation threshold and the size effect in these composites was revealed.

1.3 Statements presented for defence

1. In OLC composites the electrical percolation threshold is lower for composites with smaller size of OLC aggregates.
2. Electrical conductivity and percolation threshold values are dependent to the CNTs distribution in composite polymer matrix.
3. In composites with graphite inclusions the dielectric permittivity value increases with graphite particle size and could be modified by small amount of carbon particles even below the percolation threshold.
4. Composites filled with hybrid OLC/MWCNT and GNP/MWCNT fillers exhibit an increase in electrical conductivity because of synergy effect between different types of carbon particles.

1.4 Author's contribution

The author of this dissertation carried out dielectric spectroscopy experiments independently, analyzed the results, prepared articles and presentations.

1.5 List of publications included into the thesis

1. J. Macutkevic, **I. Kranauskaite**, J. Banys, S. Moseenkov, V. Kuznetsov, O. Shenderova, Metal-insulator transition and size dependent electrical percolation in onion-like carbon/polydimethylsiloxane composites, *Journal of Applied Physics* **115**, 213702 (2014).

2. **I. Kranauskaite**, J. Macutkevic, P. Kuzhir, N. Volynets, A. Paddubskaya, D. Bychanok, S. Maksimenko, J. Banys, R. Juskenas, S. Bistarelli, A. Cataldo, F. Micciulla, S. Bellucci, V. Fierro, A. Celzard, Dielectric properties of graphite-based epoxy composites, *Physica status solidi A*, **211** (7), 1623 – 1633 (2014).

3. **I. Kranauskaite**, J. Macutkevic, J. Banys, E. Talik, V. Kuznetsov, N. Nunn, O. Shenderova, Synergy effects in the electrical conductivity behavior of onion-like carbon and multiwalled carbon nanotubes composites, *Physica status solidi B* **252** (8), 1799 – 1803 (2015).

4. **I. Kranauskaite**, J. Banys, E. Talik, V. Kuznetsov, N. Nunn, O. Shenderova, Electric/dielectric properties of composites filled with onion-like carbon and multiwalled carbon nanotubes, *Lithuanian Journal of Physics* **55** (2), 126 – 131 (2015).

5. **I. Kranauskaite**, J. Macutkevic, J. Banys, V. Kuznetsov, S. Moseenkov, N. Rudyna, D. Krasnikov, Length-dependent broadband electricproperties of PMMA composites filledwith carbon nanotubes, *Physica Status Solidi A* **213** (4), 1025 – 1033 (2016).

6. **I. Kranauskaitė**, J. Macutkevic, A. Borisova, A. Martone, M. Zarrelli, A. Selskis, A. Aniskevich, J. Banys, Enhancing electrical conductivity of MWCNT/epoxy composites by GNP particles, *Lithuanian Journal of Physics*, **57** (4), 195–203 (2017).

7. **I. Kranauskaite**, J. Macutkevic, J. Banys, V. Kuznetsov, M. Letellier, V. Fierro, A. Celzard, O. Shenderova, Size-dependent electrical and thermal properties of onion-like carbons/polyurethane composites, *Polymer composites*, DOI 10.1002/pc.24816 (2018).

Other publications:

1. P. Kuzhir, A. Paddubskaya, A. Plyushch, N. Volynets, S. Maksimenko, J. Macutkevic, **I. Kranauskaite**, J. Banys, E. Ivanov, R. Kotsilkova, A. Celzard, V. Fierro, J. Zicans, T. Ivanova, R. Merijs Meri, I. Bochkov, A. Cataldo, F. Micciulla, S. Bellucci, Ph. Lambin, Epoxy composites filled

with high surface area-carbon fillers: Optimization of electromagnetic shielding, electrical, mechanical, and thermal properties, *Journal of Applied Physics* **114**, 164304 (2013).

2. S. Bellucci, S. Bistarelli, A. Cataldo, F. Micciulla, **I. Kranauskaite**, J. Macutkevic, J. Banys, N. Volynets, A. Paddubskaya, D. Bychanok, P. Kuzhir, S. Maksimenko, V. Fierro, A. Celzard, Broadband Dielectric Spectroscopy of Composites Filled With Various Carbon Materials, *IEEE Transactions on Microwave Theory and Techniques* **63** (6), 2024 – 2031 (2015).

3. Š. Bagdzevičius, **I. Kranauskaitė**, R. Grigalaitis, K. Bormanis, A. Sternberg, J. Banys, Chemical strain effects and changed lattice dynamic in (Sr1-1.5xBix)TiO3 ceramics (x ≤ 0.15), *Ferroelectrics* **497** (1), (2016).

4. **I. Kranauskaite**, J. Macutkevic, D. Bychanok, D. Meisak J. Banys, Broadband electrical properties of carbon nanotubes epoxy composites, Nanomeeting 2017 proceedings "Physics, chemistry and applications of nanostructures, World Scientific Publishing Co. Pte. Ltd (2017).

1.6 List of presentations

Oral presentations:

1. **I. Kranauskaite**, J. Macutkevic, J. Banys, V. Kuznetsov, S. Moseenkov, "Dielectric properties of multiwalled carbon nanotubes composites", "EMRS fall meeting 2015", Warsaw, Poland, (2015).

2. **I. Kranauskaite**, J. Macutkevic, A. Borisova, A. Martone, M. Zarrelli, A. Selskis, A. Aniskevich, J. Banys, Dielectric/electrical properties of polymer composites filled with carbon nanotubes, "Modern Multifunctional Materials and Ceramics", Vilnius, Lithuania (2017).

3. **I. Kranauskaite**, J. Macutkevic, J. Banys, V. Kuznetsov, M. Letellier, V. Fierro, A. Celzard, O. Shenderova, Electrical properties of onion-like

carbon composites, "Modern Multifunctional Materials and Ceramics", Vilnius, Lithuania (2018).

Poster presentations:

1. **I. Kranauskaite**, J. Macutkevic, J. Banys, D. Krasnikov, S. Moseenkov, V. Kuznetsov, „Influence of carbon nanotube length on composite dielectric properties", European Conference on Application of Polar Dielectrics (ECAPD 2014), Vilnius, Lithuania (2014).

2. **I. Kranauskaite**, J. Macutkevic, J. Banys, D. Krasnikov, S. Moseenkov, V. Kuznetsov, "Dielectric Properties of Composites with Carbon Nanotubes in PMMA Matrix", "Functional materials and nanotechnologies 2014" (FMNT 2014), Riga, Latvia (2014).

3. **I. Kranauskaite**, J. Macutkevic, J. Banys, V. Kuznetsov, S. Moseenkov, "Electric and dielectric properties of composites filled with multiwalled carbon nanotubes", 41-oji Lietuvos nacionalinė fizikos konferencija (LNFK 41), Vilnius, Lithuania (2015).

4. **I. Kranauskaite**, J. Macutkevic, J. Banys, V. Kuznetsov, S. Moseenkov, "Dielectric properties of polymer composites filled with multiwalled carbon nanotubes", "European meeting on ferroelectricity" (EMF 2015), Porto, Portugal (2015).

5. **I. Kranauskaite**, J. Macutkevic, J. Banys (presenter), V. Kuznetsov, S. Moseenkov, „Dielectric/electric properties of composites filled with multiwalled carbon nanotubes", „Pacifichem 2015", Honolulu, USA (2015).

6. **I. Kranauskaite**, J. Macutkevic, A. Borisova, A. Martone, M. Zarrelli, A. Aniskevich, J. Banys, M. Giordano, Electrical properties of MWCNT, GNP and hybrid MWCNT/GNP composites, "ISAF/ECAPD/PFM", Darmstadt, Germany (2016).

7. **I. Kranauskaite**, J. Macutkevic, A. Borisova, A. Martone, M. Zarrelli, A. Aniskevich, J. Banys, M. Giordano, „Electrical properties of

MWCNT, GNP and hybrid MWCNT/GNP composites", "LUP-2016", Palanga, Lithuania (2016).

8. **I. Kranauskaite**, J. Macutkevic, D. Bychanok, D. Meisak, J. Banys, Broadband electrical properties of carbon nanotubes epoxy composites, konferencija Nanomeeting-2017, Minsk, Belarus (2017).

9. **I. Kranauskaite**, J. Macutkevic, A. Borisova, A. Martone, M. Zarrelli, A. Selskis, A. Aniskevich, J. Banys, Elektrinės kompozitų su anglies nanovamzdeliais ir grafenu savybės, Lietuvos nacionalinė fizikos konferencija LNFK 42, Vilnius, Lithuania (2017).

10. **I. Kranauskaite**, J. Macutkevic, D. Bychanok, D. Meisak, J. Banys, Kompozitų su anglies nanovamzdeliais elektrinių savybių tyrimas, Lietuvos nacionalinė fizikos konferencija LNFK 42, Vilnius, Lithuania, (2017).

11. **I. Kranauskaite**, J. Macutkevic, A. Borisova, A. Martone, M. Zarrelli, A. Selskis, A. Aniskevich, J. Banys (presenter), Improving electrical properties of multiwall carbon nanotubes/polymer composites by graphene nanoplatelets, "Functional materials and nanotechnologies 2017" (FMNT 2017), Tartu, Estonia (2017).

12. **I. Kranauskaite**, J. Macutkevic, A. Borisova, A. Martone, M. Zarrelli, A. Aniskevich, V. L. Kuznetsov, S. I. Moseenkov, V. Fierro, A. Celzard, J. Banys, Dielectric/electrical properties of graphite, MWCNT and hybrid MWCNT/GNP composites, Workshop on nanocomposite polymers for 3D-printing of high-tech structures, Namur, Belgium (2018).

13. **I. Kranauskaite**, J. Macutkevic, A. Borisova, A. Martone, M. Zarrelli, A. Selskis, A. Aniskevich, J. Banys, Electrical properties of composites filled with carbon nanotubes and graphene nanoplatelets, Fundamental and Applied NanoElectroMagnetic, THz circuits, materials, devices (FANEM), Minsk, Belarus (2018).

14. **I. Kranauskaite**, J. Macutkevic, A. Borisova, A. Martone, M. Zarrelli, A. Selskis, A. Aniskevich, J. Banys, Enhancing electrical conductivity

8

of MWCNT/epoxy composites with graphene nanoplatelets, EMRS spring meeting 2018, Strasbourg, France (2018).

15. **I. Kranauskaite**, J. Macutkevic, A. Borisova, A. Martone, M. Zarrelli, A. Selskis, A. Aniskevich, V. L. Kuznetsov, S. I. Moseenkov, V. Fierro, A. Celzard, J. Banys (presenter), Dielectric/electrical properties of graphite, MWCNT and hybrid MWCNT/GNP composites, European Conference on Applications of Polar Dielectrics (ECAPD-2018), Moscow, Russia (2018).

2 Overview

A composite is a multi-phase system combined from two or more materials, or phases, with significantly different physical and chemical properties. Composites consist of a matrix material and a filler. In the case of carbon based polymer composites, polymer is a matrix and carbon particles are the filler. By choosing an appropriate combination of the matrix and the filler, a new material could be produced that meets requirements of particular applications. Composites also provide design flexibility and they are light as well as strong and resistant to environmental impacts.

In this chapter separate composite components – polymers and carbon materials, and composite as a whole system will be described giving information about known physical properties and theoretical models.

2.1 Types of polymer

A polymer long-chain molecule is composed of many repeated units, monomers. These large polymer molecules have complex shapes and form solids that could be either amorphous or crystalline. Most of the polymers applied in industrial field are organic synthetic polymers, which contain mainly carbon atoms, sometimes in combination with hydrogen, oxygen and nitrogen. The nature of the chemical bonding directly influences the electrical properties of the polymer material [11].

All polymers could be divided into two major groups based on their thermal processing behavior. Both types of polymers behave in a similar fashion, except at the high temperatures. Polymers that can be heat-softened in order to process into desired form are called thermoplastics. Thermoplastic materials generally fall within two classes of molecular arrangement, amorphous and semi-crystalline. In comparison, thermosets are polymers whose individual chains have been chemically linked by covalent bonds during polymerization or by subsequent chemical or thermal treatment during

fabrication [12]. Thermosets are typically hard and brittle at the room temperature, and it is unable to flow at high temperatures.

Both thermoplastics and thermosets have their advantages and disadvantages. Thermosets are highly resistant to temperature and chemical effects, are cost-effective, meanwhile cannot be remolded and reshaped and cannot be recycled. Thermoplastics have high strength, are chemical resistant, recyclable, eco-friendly manufactured, but are relatively expensive in comparison with thermosets and can melt if heated.

2.2 Transitions in polymer

The bulk polymeric system can behave as a solid or as a rubbery (viscoelastic material, which is highly deformable or as a melt in dependence on temperature). This is demonstrated in Fig. 2.1 where temperature dependence of modulus is presented. At low temperatures the polymer system behaves like a glassy solid with modulus in order of 10^9 Pa s. At certain temperature shear modulus decrease by several orders of magnitude and the system has viscoelastic properties. From this step-like change the glass transition temperature T_g can be estimated.
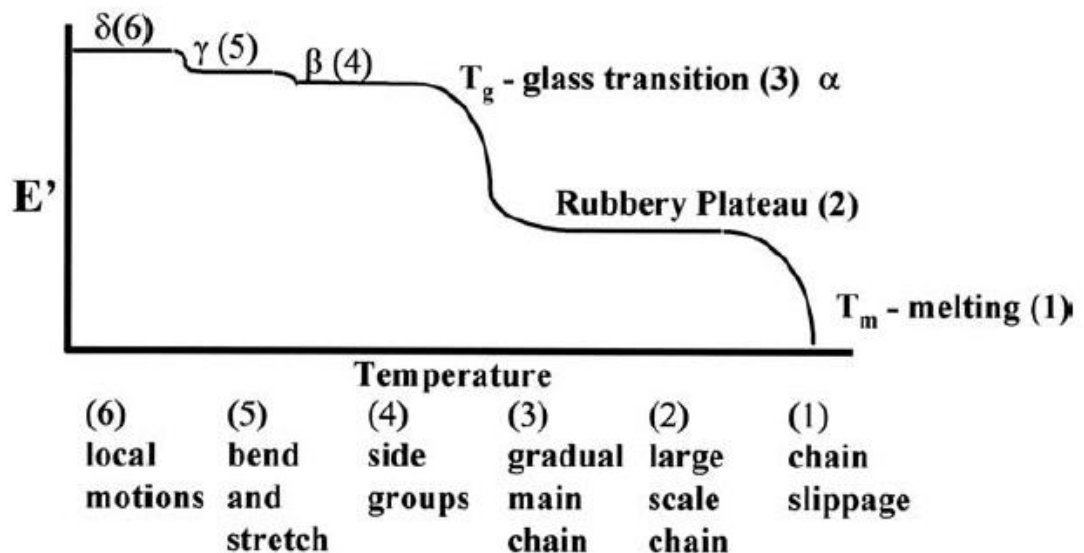

Fig. 2.1. Effect of temperature on the macroscopic stiffness of polymers [13]

The thermal transitions in polymers could be described in terms of either free volume changes [13] or relaxation times [14]. According to a simplistic approach, the polymer molecule could be treated as a crankshaft mechanism with a collection of mobile segments that have some degree of free movement (Fig. 2.2) [13]. From this model various temperature dependent transitions seen in polymer could be simply described. The effect of temperature on the macroscopic stiffness of both thermoplastic and thermoset polymers are shown schematically in Fig. 2.1.
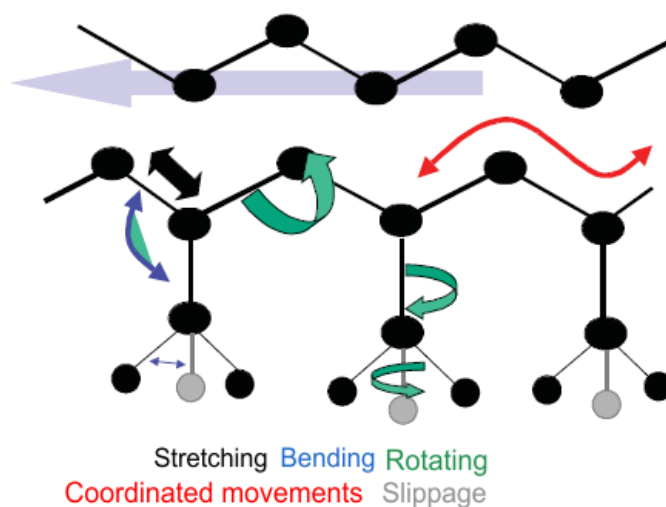

Stretching Bending Rotating
Coordinated movements Slippage

Fig. 2.2. The crankshaft model. Arrows shows various motions of polymer chain [13]

At low temperature molecules are tightly compressed and polymer pass through the solid state transitions associated with local polymer chain motions (Fig. 2.2). As the temperature increases, free volume of the chain segment increases, that means its ability to move in various directions also increases. The localized bond and side chain movements are called gamma transition, T_γ. At higher temperatures T_β transition occurs, that could be associated with rotation of chain segment around covalent bond. As the heating continues, polymers exhibit a decrease in stiffness near a characteristic temperature called the glass transition temperature (T_g or T_α) at which polymer undergo from glassy to rubbery state (Table 2.1). This transition is due to an increase in mobility of large segments of the main polymeric chain.

Table 2.1. Glass transition temperatures for some common polymers [15-17]

Polymer	Glass transition temperature T_g (°C)
Poly(carbonate) (PC)	145
Polytetrafluoroethylene (PTFE)	115
Poly(methylmethacrylate) (PMMA)	105
Polystyrene (PS)	95
Poly(vinyl chloride) (PVC)	80
Polyethylene terephthalate (PET)	70
Polyamide (PA)	47–60
Polypropylene (PP isotactic)	0
Polyvinyl fluoride (PVF)	−20
Polyvinylidene fluoride (PVDF)	−35

Finally, at higher temperatures than T_g large-scale chain slippage occurs, except for thermosets (epoxies), where cross-links prevent the chains from slipping past each other [18]. Semi-crystalline materials do not exhibit a clear T_g, although for these polymers the main transition occurs at T_m when crystalline regions break down.

2.3 Polarization in polymer

Polymers are electrical insulators and the electrical properties of polymer matrix composites refer to dielectric relaxation. When an electric field is applied to dielectric material, the atomic and molecular charges are in separation of positive and negative charges, and material is polarized. There are four types of polarization mechanisms, which occur in dielectric materials [11]:

1) Electronic polarization – also known as atomic polarization; the shift of the electrons with respect to the nucleus;

2) Orientational polarization – also known as dipolar polarization; molecules with permanent dipole moment orient according to the direction of applied electric field;

3) Ionic polarization – the cations and anion of an ionic material get displaced in opposite directions;

4) Charge polarization.

There are two main polarization mechanisms in polymeric materials – polarization due to charge migration, which gives rise to conductivity [19] and polarization due to orientation of permanent dipoles. The orientation of permanent dipoles involves cooperative motions of molecular segments in a viscous medium with time scales measurable by dielectric spectroscopy. The time dependent loss of orientation of dipoles upon removal of the electric field is called dipole relaxation. Some polymeric structures and elements display the high polarisibility such as aromatic rings, sulphur, iodine and bromine. In opposite, fluorine has a low polarisibility due to small atomic radius and concentrated negative charge.

Polymers could be polar and nonpolar depending on chain geometry. Polar polymers include PMMA, PVDF, PVC, PA, PC, while nonpolar – PTFE, PE, PP, PS. Polymers, which contain multiple carbon-carbon bonds have higher relative dielectric permittivity since the bond polarisability of multiple bonds are higher than of single carbon-carbon bond. For nonpolar polymers the dielectric permittivity is independent of the alternating current frequency and is equal to 3 or less. Polar polymers at low frequency (100 Hz) generally have dielectric permittivity between 3 and 5.

The orientation of dipoles in an electric field is relatively slow process in frequencies below 10^{12} Hz. The arrangement of all molecules consist of their average orientations to the direction of electric field. When dielectric material is applied to alternating electrical field and dipoles are unable to follow the rate of change of the oscillating applied electric field, the relative dielectric permittivity is expressed by complex form:

$$\varepsilon^* = \varepsilon' - i\varepsilon'', \tag{2.1}$$

where ε' is a real part of complex dielectric permittivity, ε'' is an imaginary part of complex dielectric permittivity, $\tan\delta = \dfrac{\varepsilon''}{\varepsilon'}$ is called dielectric loss factor. ε' and ε'' are experimentally observed to characterize the dielectric dispersion over the range of frequencies.

In terms of a single relaxation time Debye model the dielectric relaxation behaviour relating dielectric permittivity and relaxation time is determined by the following equation [20]:

$$\varepsilon^* = \varepsilon_\infty + \frac{\Delta\varepsilon}{1+i\omega\tau},$$ (2.2)

where ε_∞ is contribution of high frequency processes to dielectric permittivity, $\Delta\varepsilon$ is relaxation strength, τ is dielectric relaxation time that is needed for dipoles to return to their equilibrium position.

Polymer materials are rather complex systems characterized by broader and usually assymmetric relaxation peak and distribution of relaxation times. Therefore, the frequency dependencies of dielectric permittivity could be analysed by Cole-Cole or Havriliak-Negami equations depending on the motional processes of polymeric systems. The major dielectric relaxations in polymers are due to localized fluctuations within a backbone segment associated with „dielectric glass transition" (α-relaxation) or local rotational fluctuations of a short side chain in the glassy state (β-relaxation). The α-relaxation is located at lower frequencies or higher temperatures than the β- or secondary relaxation. The β-relaxation spectra are generally broad, mostly symmetric and could be described by Cole-Cole equation [21]:

$$\varepsilon^* = \varepsilon_\infty + \frac{\Delta\varepsilon}{1+(i\omega\tau_{CC})^\alpha},$$ (2.3)

where τ_{CC} is the Cole-Cole relaxation time, which is equal to mean relaxation time ($\tau_{cc} = \langle\tau\rangle$) and is most probable relaxation time, α is the width of the distribution of relaxation times ($0 < \alpha \leq 1$). With increasing temperature the width of the β-relaxation peak decreases and the shape of the relaxation function is due to distribution of both the activation energy and the preexponental factor, related to a distribution of molecular environments of the relaxing dipole. The temperature dependence of the relaxation rate or relaxation time of β-relaxation can be described in general by Arrhenius law:

$$\tau = \tau_0 \exp\left[-\frac{E_A}{k_B T}\right],$$ (2.4)

where τ_0 is the preexoponential factor, k_B is the Boltzmann constant, E_A is the activation energy, which depends on both the internal rotational barriers and

the environment of fluctuating unit. Typical values for E_A are from 20 to 50 kJ mol^{-1}.

In general, the α-relaxation shows in the frequency domain a broad and assymmetric peak. This functional shape could be described by Havriliak-Negami function [22]:

$$\varepsilon^* = \varepsilon_\infty + \frac{\Delta\varepsilon}{(1+(i\omega\tau_{HN})^\alpha)^\gamma}, \tag{2.5}$$

where γ is parameter, which describes assymetry of corresponding spectrum, τ_{HN} is the Havriliak-Negami relaxation time. It is important to note, that $\tau_{HN} \neq \langle\tau\rangle$ and the mean relaxation time could be calculated [23]:

$$\langle\tau\rangle = \ln\tau_{HN} + \frac{\Psi(\gamma)+Eu}{1-\alpha}, \tag{2.6}$$

where $\Psi(\gamma)$ is a digamma function, Eu is Euler constant (Eu $\approx$ 0.5772).

The width of α-relaxation peak for polymers depends on various factors such as temperature, structure of the chain or crosslinking density. It becomes narrower with increasing temperature and broadens dramatically with crosslinking. In contrast to the β-relaxation process the shape of relaxation function of the dynamic glass transition is not related to a distribution of relaxation times due to spacial heterogeneities.

The temperature dependence of relaxation time of the α-relaxation ussually cannot be parameterized by Arrhenius law. Close to the glass transition temperature it can be described by Vogel-Fulcher equation:

$$\tau = \tau_0\exp\left[-\frac{E_A}{k_B(T-T_0)}\right], \tag{2.7}$$

where τ_0 is preexoponential factor, k_B is the Botzman constant, E_A is activation energy, T_0 or T_{VF} is glass transition temperature of a process as cooling rate becomes infinitely slow.

2.4 Carbon inclusions for composites

Carbon is remarkable element for an ability of its atoms to bond together in different allotropic forms. The various forms of carbon, having their unique properties, are used in composite preparation include carbon black, graphite, graphene, carbon nanotubes and fullerenes (Fig. 2.3).
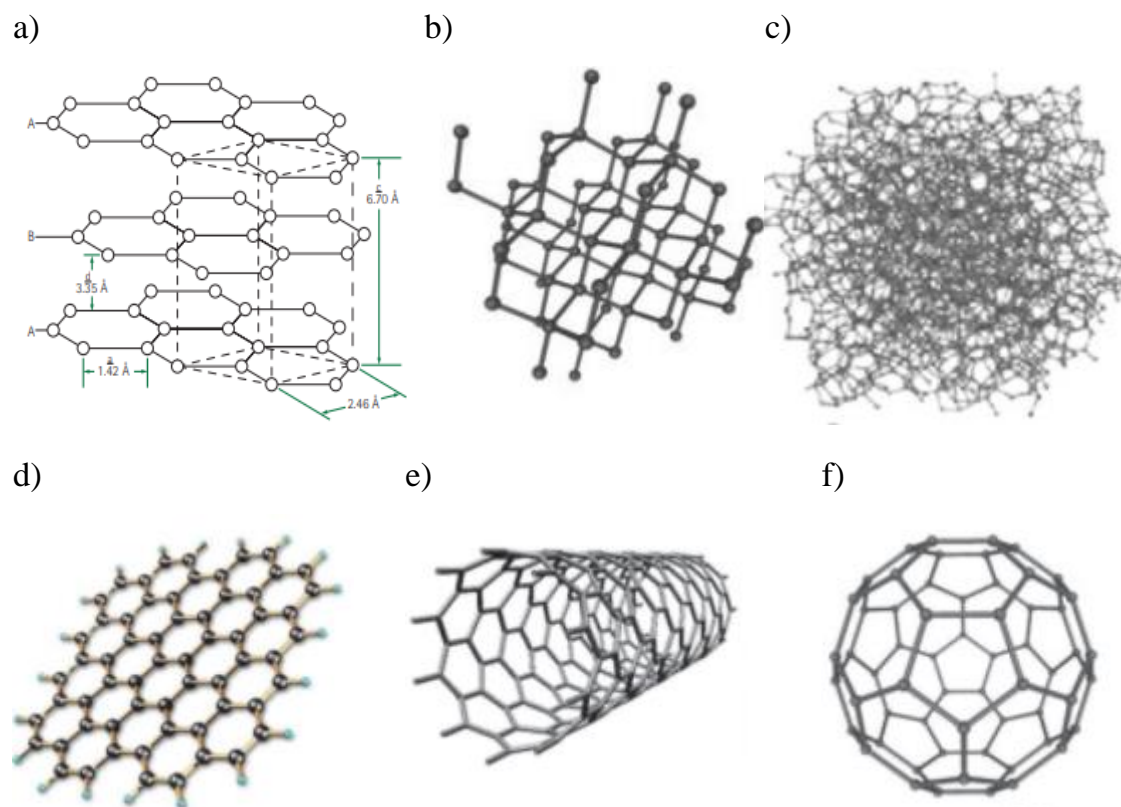
Fig. 2.3. Some stuctures of carbon allotropes: a) graphite, b) diamond, c) amorphous carbon, d) graphene, e) carbon nanotube, f) fullerene [24-26]

Amorphous carbon, graphite and diamond are three naturally occurring allotropes of carbon. Carbon black (CB) is a form of amorphous carbon having high surface area to a volume, which has good adhesive properties with polymer matrix and was the most commonly used carbon filler for years. Amorphous carbon could be carbonized and oxidized in order to form highly porous carbon. Highly porous activated carbons can be used together with other forms of carbon like carbon nanotubes or graphene in composites for electrodes production.

Graphite is composed of series stacked parallel layer planes of hexagonally linked carbon atoms. The atoms within the hexagonal rings are bonded covalently. The spacing between the layer planes is relatively large (0.335 nm), these adjacent planes are connected by van der Waals bonds [24]. The density of graphite is 2.26 g/cm^3. Electrically, graphite is a conductor in the basal plane and insulator normal to basal plane. In a bulk state, graphite is anisotropic and

layered material, which can be separated to form graphite flakes and graphene nanoplatelets (GNP) by intercalation and exfoliation.
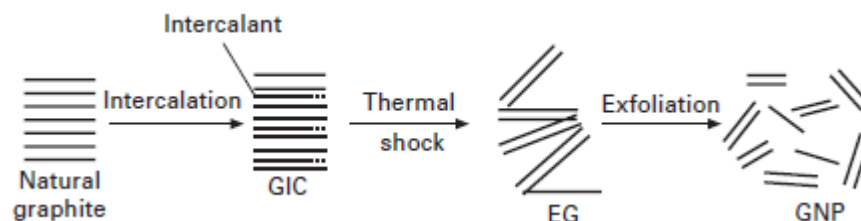

Fig. 2.4. Schematic illustration of GNP production

Intercalating natural graphite flakes the exfoliated graphite (EG) is produced. Exfoliated graphite has porous, accordion-like elongated structure, which consist of deformed graphene sheets. This type of the graphite could be used as more effective filler replacing CB and natural graphite at electrically conductive composite preparation.

Graphene nanoplatelets (GNPs) are two-dimensional disc-like particles with the thickness of several to several tens of graphene sheets produced by exfoliating EG via ultrasonication.

Various other forms of graphite are available: graphite oxide, chemically reduced graphene (CRG), thermally reduced graphite oxide (TRG).

Since the discovery of carbon nanotubes (CNTs) [25], they attract scientist's attention due to their unique mechanical, electrical, optical and thermal properties. CNTs have high aspect ratio with varying diameter from 1 to 100 nm and length up to millimeters [26]. There are two types of of CNTs – single walled (SWCNT) and multiwalled carbon nanotubes (MWCNT). MWCNTs consist of two or more concentric graphene sheets coaxially arranged around central hollow core with interlayered separation.

Fullerene molecules are composed of carbon atoms in the form of hollow sphere, ellipsoid or tube. Spherical fullerenes are also referred to as buckyballs, which could be enclosed in concentric layers forming onion-like structure. They are predicted to have properties different from other carbon nanostructures as nanotubes or nanodiamonds due to their highly symmetrical

structure and may find applications as components of magnetic recording systems [27] or electromagnetic shielding (EMI) materials [28].

2.5 Conductivity

Electrical conductivity in solids sums all energy dissipative effects including charge carriers migration and frequency dielectric dispersion [29]. The complex electrical conductivity and complex dielectric permittivity are related to each other by:

$$\sigma^* = \sigma'(\omega) + i\sigma''(\omega) = i\omega\varepsilon_0\varepsilon^*(\omega). \tag{2.8}$$

The real and imaginary part of complex electrical conductivity:

$$\sigma'(\omega) = \varepsilon_0\varepsilon''\omega, \tag{2.9}$$

$$\sigma''(\omega) = \varepsilon_0\varepsilon'\omega, \tag{2.10}$$

where $\varepsilon_0 = 8.85 \cdot 10^{-12}$ F m^{-1} is the vacuum permittivity. Very often, at the constant temperature, frequency dependence of the real part of complex electrical conductivity could be expressed by Jonscher's equation [30]:

$$\sigma' = \sigma_{DC} + A\omega^s, \tag{2.11}$$

where σ_{DC} is DC (direct current) conductivity, which is a measure of long range movements of charge carries, $A\omega^s$ represents AC (alternating current) conductivity. *A* and *s* are parameters depending on temperature and the concentration of the composite filler [31]. At low frequencies the conductivity aquire constant frequency independent values and above critical frequency (f_{cr}) conductivity increases as a power law. The critical frequency is defined as crossover frequency at which AC conductivity differs from the DC plateau. DC conductivity and the static effective permittivity ε_s are connected with the critical frequency f_{cr} according to the relations [32–34]:

$$\sigma_{DC} = \varepsilon_s\varepsilon_0 f_{cr}, \tag{2.12}$$

$$f_{cr} = \frac{\sigma_{DC}}{\varepsilon_0\varepsilon_s}, \tag{2.13}$$

$$\sigma_{DC} \sim f_{cr}^z, \tag{2.14}$$

where z is an exponent, which characterizes the relation between the capacitive and conductive networks in the composite.

For dielectric-conductor composites electrical conductivity increases with increasing conductive particles content while for pure dielectric and for low filler content DC conductivity is negligible (Fig. 2.5). This clearly indicates the critical concentration for the transition from insulating to conductive behaviour.
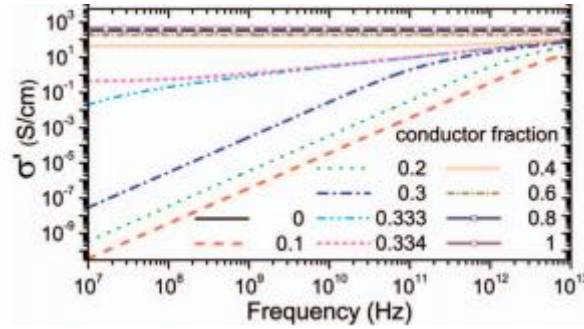

Fig. 2.5. Electrical conductivity spectra of conductor-dielectric composites at different fractions of conductive particles [35]

The transition from insulating to conductive behaviour could be described in terms of percolation theory.

2.6 Percolation theory

The percolation theory is a model in probability theory, which displaying a phase transition of the system. This means that there is a parameter in the model at which the behavior of the system drastically changes [36]. The percolation is a standard model for structurally disordered systems, with widespread applications in nature, which could be applied for insulator-conductor composites.

In the view of electrical conduction in polymer composites, usually, polymer is an insulating material and electrons are free to flow through conductive filler particles. If filler particles contact with each other, the continuous path is formed for electrons to travel through. For illustration, lets consider a square lattice, where each site is randomly occupied with probability p or is empty with probability $1 - p$ (Fig. 2.6 a) [37].

20

At low concentration φ the system is insulating, the conductive particles are either isolated or form small clusters and no conducting path exists. The electrical conductivity values of the composite are close to the polymer matrix. At some certain critical concentration (φ_c), called percolation threshold, the conductive network through the composite is formed. Above φ_c composite is a conductor and below is an insulator. At the percolation threshold region, conductivity increases significantly with very small increase in filler amount until conductive network is completed (Fig. 2.6 b).
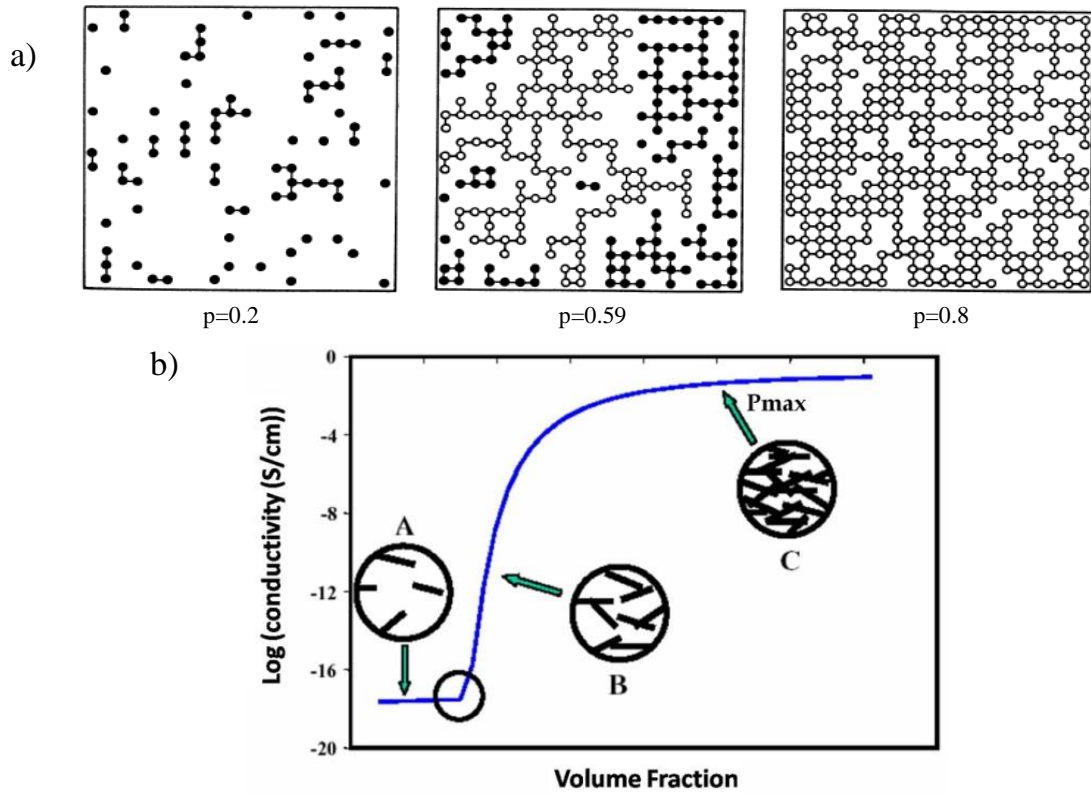

Fig. 2.6. a) Square lattice. Circles represent the occupied sites for different concentrations. Filled circles – finite clusters, open circles – infinite cluster [37]; b) Percolation curve [38]

The percolation theory predicts the relationship between conductivity and the concentration of the filler by following power law [39]:

$$\sigma(\varphi) \propto \sigma_0(\varphi - \varphi_c)^t, \qquad (2.15)$$

above percolation threshold and

$$\sigma(\varphi) \propto \sigma_m(\varphi_c - \varphi)^{-s}, \qquad (2.16)$$

below percolation threshold. Here φ_c is the percolation threshold, φ is the conductive filller concentration, σ_0 and σ_m are the conductivy of the filler and the matrix respectively, t and s are the critical exponent, which depends on the dimension of the lattice and vary in range $1.6 - 2$ [40, 41]. The dielectric permittivity follows the same power law, but with different exponent.

The theoretical percolation threshold value could be estimated according to excluded volume theory, which includes the geometry of particle. The geometry of filler particles is defined by their aspect ratio A (A is >1). In the case of ellipsoids, $A = D/t$, where D is diameter (lateral size or mean width) and t is thickness. For cylindrical particles $A = l/d$, where l is length and d is diameter. That was established that percolation threshold is linearly proportional to the 1/A [42].

The excluded volume considered to be two-dimensional area that surrounds same shaped object. In composite materials, when particles are not densely packed, the percolation threshold is not linked to the volume of the additive (V), but to its excluded volume V_e [43]. Considering that the critical number density of inclusions in polymer is N_c, the total excluded volume $\langle V_{ex} \rangle$ could be defined as $\langle V_{ex} \rangle = N_c \langle V_e \rangle \approx const.$, where $\langle V_e \rangle$ is the excluded volume of an inclusion averaged over orientation distribution. The lower and upper limits of $\langle V_{ex} \rangle$ correspond to a random orientation and stictly parallel cases [43]. The critical volume fraction Φ_c in three dimensions is linked to an excluded volume as follows:

$$\Phi_c = 1 - exp\left(-\frac{\langle V_{ex} \rangle V}{\langle V_e \rangle}\right) = 1 - ex\,p(-N_c V). \qquad (2.17)$$

Assuming that filler particles are randomly dispersed flakes or flattened ellipsoids of aspect ratio A, then $\langle V_{ex} \rangle$ is equal to 1.8 and 2.8 in extreme cases of infinitely thin disks and spheres, respectively. Critical volume fraction gets values in range:

$$1 - exp\left(-\frac{2 \times 1.8}{\pi A}\right) \le \Phi_c \le 1 - exp\left(-\frac{2 \times 2.8}{\pi A}\right). \qquad (2.18)$$

Critical volume and weight concentrations are related to each other through the following relationship:

$$\varphi_c = \frac{1}{1+\left(\frac{\rho_m}{\rho_f}\right)\left(\frac{1-\Phi_c}{\Phi_c}\right)}, \tag{2.19}$$

where ρ_m and ρ_f are the densities of matrix and filler, respectively.

For elongated, rod-like particles critical volume fraction could be estimated [44]:

$$1 - exp\left(-\frac{1.4\times\left[\frac{A\pi}{4}+\frac{\pi}{6}\right]}{\frac{A^2}{2}+2A\pi+\frac{4\pi}{3}}\right) \leq \Phi_c \leq 1 - exp\left(-\frac{2.8\times\left[\frac{A\pi}{4}+\frac{\pi}{6}\right]}{\frac{A^2}{2}+2A\pi+\frac{4\pi}{3}}\right), \tag{2.20}$$

where A is the aspect ratio, in this case the ratio of the length and diameter.

Applying excluded volumes to disk-like and rod-like particles the following relation is achieved:

$$\Phi_c \propto \frac{1}{A}, \tag{2.21}$$

where A is the aspect ratio of disk-like or rod-like particle.

Simplistically, the theoretical percolation threshold could be calculated by following equations:

$$\Phi_c = \frac{1}{2A} \tag{2.22}$$

for rod-like particles. And

$$\Phi_c = \frac{21.2}{A} \tag{2.23}$$

for disc-like particles.

Percolation theory describes the transition from insulating to conductive behaviour of composites and determines critical concentration, which is needed for conductive path to form. But on the other hand, the mechanism of the conductivity cannot be described by the percolation theory. The classical percolation theory follows the properties assuming that charge transport of the conductive composites could be attributed to the formation of the conductive path where conductive inclusions are in geometrical contact. However, in such systems there is no such obvious nearest neighbour bonding, but the percolation theory is still applicable.

2.7 Conductivity mechanism in composites

In composites, when conductive particles are incorporated into polymer matrix, they become a part of the composite structure rather than separate component. Above percolation threshold, when percolative network is formed and the minimal distance between conductive particles is reached the electrical conductivity in composite occurs. The electrical transport in composites with geometrically disconnected conductive particles, placed in insulating polymer matrix, refers to both jump over a potential barrier and tunneling of charges and could be explained by the combination of fluctuation induced tunneling (FIT) model and variable range hopping model (VRH).

The variable range hopping model, or Mott law, describes the electrical properties of disordered materials and could be expressed by following formulas [45]:

$$\sigma_{DC}(T) = \sigma_0 exp\left[-\left(\frac{T_M}{T}\right)^\gamma\right] \tag{2.24}$$

for the DC conductivity and

$$f_{cr} = f_\infty \exp\left[-\left(\frac{T_m}{T}\right)^\gamma\right] \tag{2.25}$$

for the critical frequency. Where γ is related to dimension d of the transport process $\gamma = 1/(1 + d)$, where d=1, 2, 3 for one-dimensional (1D), two-dimensional (2D) and three-dimensional (3D) hopping respectively; σ_0 and f_∞ are the pre-exponenetial factor meaning the conductivity and the frequency at very high temperature, T_M is the Mott's characteristic temperature, which determines the thermally activated hopping among localized states at different temperatures:

$$T_M = \frac{24}{\pi k_B L_c^3 N(E_F)}, \tag{2.26}$$

where k_B is the Boltzmann constant, L_c is the localization length, $N(E_F)$ is the density state of Fermi level. Electrons can hop from one localized state to another with probability $P \propto exp\left(-\frac{2R}{L_c} - \frac{\Delta E}{k_B T}\right)$, where R – distance between two localized states, ΔE – energy difference of two states [45]. The hopping probability is determined by the distance and the energy difference.

For one-dimensional hopping conductivity, the DC hopping length reads:

$$R_{dc} = \sqrt{\frac{\Delta r}{2\,\alpha\,T}},$$ (2.27)

while the AC hopping length is:

$$R_{ac} = \frac{1}{2}\alpha \ln \frac{f_{fon}}{f_{cr}},$$ (2.28)

where Δ determines uniform distribution of carriers energies, r is distance between two nearest conductive particles, α-1 is the localization length, and f_{fon} is attempt frequency. As the VRH model is widely used to describe electrical conductivity of disordered materials, but the experimental results of carbon nanotubes electrical investigations show similar behaviour, which indicates that electrical conductivity of CNTs is a result of two-dimensional variable range hopping mechanism [46]. The electrical properties of carbon nanotubes are determined by the diameter and the helicity, and due to that carbon nanotubes could be semiconducting or metallic [47] and the individual multiwalled carbon nanotubes should show metallic behaviour [48]. However, the studies of an individual multiwalled carbon nanotubes show structural defects and disordered structure, and the electrical conductivity increases with increasing temperature [49, 50].

When conductive particles are dispersed in a polymer matrix charge transport between adjacent particles, separated by insulating polymer, is governed by the electron tunneling. The potential barrier for electrons to tunnel is determined mainly by the distance between conductive particles. If the concentration of conductive particles is too low, there are large distances between particles and potential barrier is high. The conductivity could be increased by larger conductive particles content.

The electrical conductivity above percolation threshold is temperature dependant and could be described by fluctuation induced tunneling model [51]:

$$\sigma_{DC} = \sigma_0 exp\left[-\frac{T_1}{(T+T_0)}\right],$$ (2.29)

25

where σ_0 is a pre-exponenetial factor, T_1 can be regarded as a measure of the energy for an electron to cross the insulator gap between the conductive particles, T_0 is the temperature above which thermally activated conductivity over barrier occurs. If the temperature T<T_0, then the conductivity becomes the normal tunneling and is temperature independent. The tunneling model parameters T_1 and T_0 are related with microscopic parameters by following equations:

$$T_1 = wA\beta_0/8\pi k \qquad (2.30)$$

and

$$T_0 = 2T_1/\pi\chi w, \qquad (2.31)$$

where χ=$(2mV_0)^{0.5}$/h and β_0=$4V_0$/e w, m and e are the electron mass and charge respectively, V_0 is the potential barrier amplitude, w is the interparticle distance (gap width), and A is the area of capacitance formed by the junction. From equations (2.30) and (2.31) it follows that T_1/T_0 is proportional to the gap width w and potential barrier V_0 amplitude.

The DC conductivity is thermally activated while AC conductivity is less temperature dependent.

2.8 Factors that affect conductivity and percolation

From the percolation theory it is observed that the critical concentration or percolation threshold depends on particle shape and particle size, and is inversely propotional to the aspect ratio. However, experimental results reveal discrepancy with theoretical predictions – the percolation threshold is substantially higher or sometimes even lower than the reciprocal aspect ratio (Fig. 2.7) [52]. Such large variations of percolation threshold values show that despite filler particles shape and size, the composite processing conditions, type of the polymer and geometrical arrangement and distribution of the filler particles are important [53,54]. Even low concentration of conductive particles could lead to higher electrical conductivity and lower percolation threshold than high loadings due to formation of very effective conductive network. In contrary, high concentration of conductive particles, especially CNTs, could

cause large agglomeration. The agglomeration of the filler causes a loss of the interfacial volume and creates microscale/nanoscale defects affecting electrical conductivity and percolation threshold value [55].
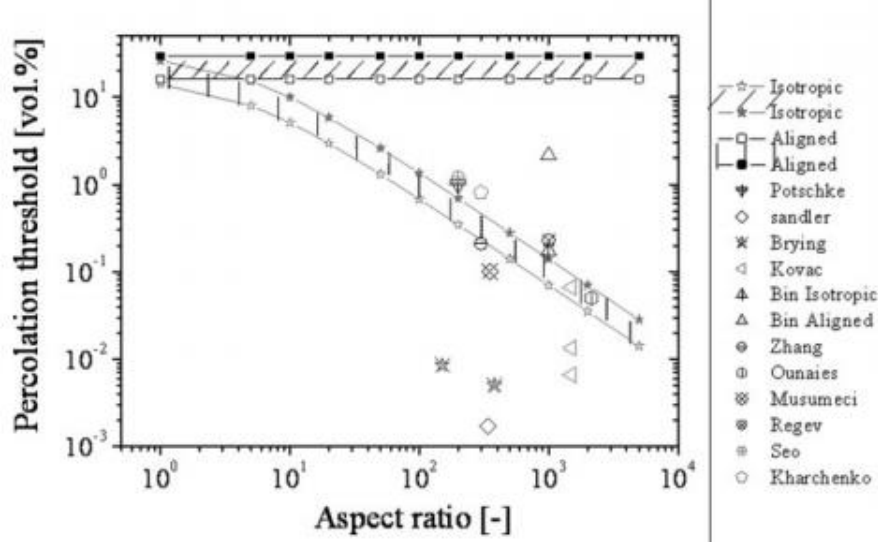

Fig. 2.7. The theoretical percolation threshold for aligned and isotropic composite systems and reported experimental results in the literature [52]

The theoretical percolation threshold calculated by excluded volume theory describes rigid and straight fibers, which homogeneously distributed within a polymer matrix. CNTs have a relatively large aspect ratio, are flexible and forming entangled complicated structure. According to improved interparticle distance approach [56], the composite could be divided into cubic elements containing particle in the center (Fig. 2.8). Depending on dispersion state the conductive particles could be single or a bundle, two extreme cases could be considered: all CNTs are perfectly dispersed in the matrix (Fig. 2.8 a) and all the CNTs are agglomerated (Fig. 2.8 b). In practical composites both individual, perfectly dispersed CNTs and agglomerates of CNTs exist (Fig. 2.8 c). The percolation threshold of these composites could be expressed by following equation [57]:

$$P_c = \frac{\xi \varepsilon \pi}{6} + \frac{(1-\xi) 27 \pi d^2}{4 l^2}, \qquad (2.32)$$

where ξ is the volume fraction of agglomerated CNTs, ε is the localized volume content of CNTs in an agglomerate, l and d are length and diameter of

individual CNT respectively. This model shows that the dispersion has great effect to the percolation threshold, but it cannot be simply estimated how the value of percolation threshold would change when dispersion of the particles is improved.
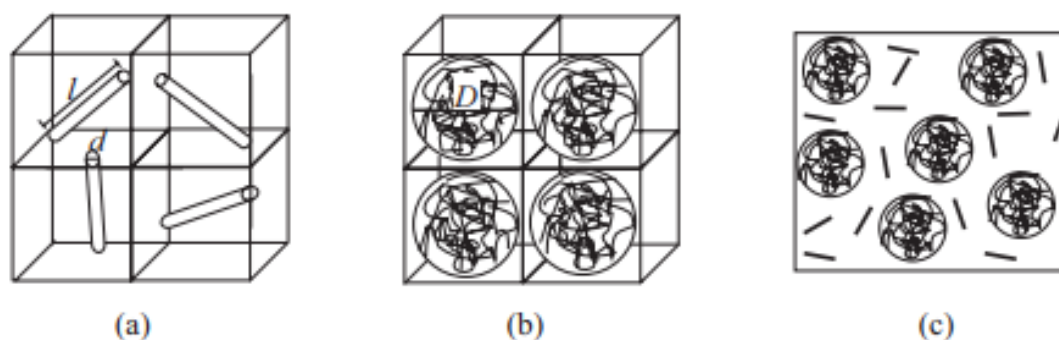

Fig. 2.8. CNT reinforced polymer nanocomposites containing a) perfectly disperced cylindrical CNTs, b) CNTs all in the form of agglomerates, c) a mixture of individual CNTs and agglomerates [57]

The electrical conductivity of composite could be increased by improving the dispersion, reducing agglomeration of conductive inclusions in polymer matrix. The dispersion of filler could be possibly improved by certain composite preparation methods, modification of carbon particles or polymer matrix and introducing additional filler of another type.

There are different composite preparation techniques such as shear mixing, direct mixing, melt blending and ect. Carbon particles could be additionally ultrasonicated in order to reduce agglomeration. *J. Li et al.* [56] have investigated the dependence of composites processing method to percolation threshold value (Fig. 2.9). The lowest percolation threshold value was observed for the conditions „B", where CNTs were dispersed by ultrasonication breaking the CNT agglomerates and decreasing particle size. The highest percolation threshold was for composites produced by shear mixing method (conditions „A"). The large and tightly entangled CNT agglomerates were formed. No percolation threshold was observed for the condition „D", where several treatment steps were combined – ball-milling, ultrasonication and silanizing. That suggests that CNTs were damaged and

broken into very short pieces resulting the reduction of the CNT aspect ratio. In some case the direct mixing of CNTs appears to be promising and the easiest method to achieve effective conductive network formation and the lower percolation threshold value, although it brings inhomogeneity of the polymer [58].
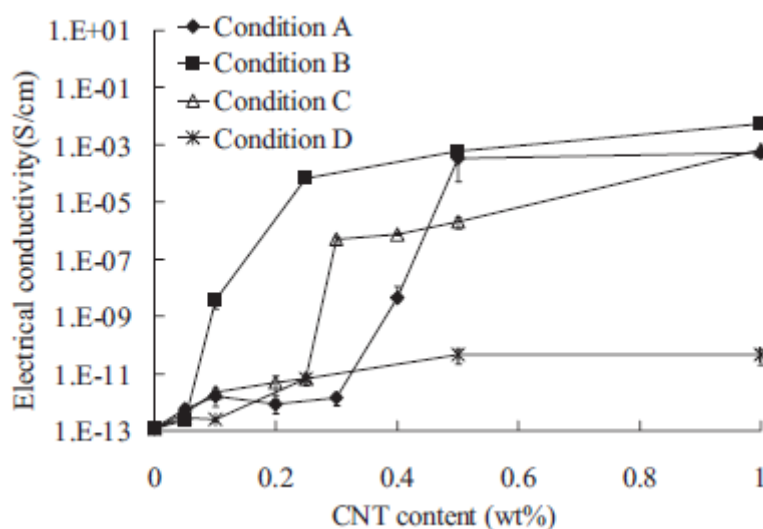

Fig. 2.9. Electrical conductivity of nanocomposite as a function of CNT content for different composite preparation conditions [56]

The studies showed that incorporating hybrid filler, which means that two or more filling materials are incorporated into a single matrix, such as MWCNT together with carbon black and TiO_3 particles [59, 60] or MWCNT with non-conductive nanodiamonds led to more even dispersion in polymer phase and lower percolation threshold. The properties of such hybrid materials could be explained by synergy effect. Synergy refers to interaction of the elements whose combination gives a greater effect than the sum of effects of the individual elements. In the case of composites, synergy is an improvement of the properties. That means that in conductive composite preparation, using different types of the filler, the total filler content could be reduced due to formation of extra effective co-supporting network of the fillers. The increase in conductivity of hybrid filler composites could result in the reduction of tunneling distances that occur, when CNTs are mixed together with other type

of the particles, for example CB [60]. Certain amount of CNTs could be replaced by alternative conductive particles if dispersion is sufficient and these particles possess re-agglomeration tendencies. Herewith, the reduction of the filler content leads to the better electrical and thermal conductivity either possible improvement of mechanical properties. The synergistic effect in ternary composites could be explained by two theoretical situations. The MWCNT form fractal-like structure with the branches in the network, which do not contribute to the effective conductive pathway. An incorporation of CB filler changes MWCNT network structure and leads to formation of new condutive pathways between MWCNT branches. Since the tunneling distance between carbon nanotubes determines the overall conductivity in CNT/polymer composites [61], the increase in conductivity of hybrid filler composites may result directly from the reduction of tunneling distances that occur when CB particles are placed among MWCNTs [60]. And the second case, when CB is added to the existing MWCNT conductive pathway, it is expected that the conductivity should be increased.

According to the excluded volume theory, the hybrid filler composites should obey the following relation [62]:

$$\frac{m_1}{p_{c,1}} + \frac{m_2}{p_{c,2}} = 1, \qquad (2.33)$$

where m_1 and m_2 are the mass fraction of the first and second filler respectively, and $p_{c,1}$ and $p_{c,2}$ are the mass percolation threshold in composites filled with a single filler of first and second filler, respectively. When the sum of the equation is lower than predicted (<1), it could be considered that the synergy effect is achieved.

To summarize, it is important to choose suitable percentage of conductive filler particles and the appropriate preparation method to achieve desired physical properties while taking into account time consumption and the cost.

3 Experimental

In this chapter the composite preparation technique and experimental methods, which were applied to collect data, are presented and discussed.

3.1 Composite preparation

In this section the preparation techniques, which were used to produce composites will be presented in details. The following groups of composites were prepared, which contain different types of polymer and carbon particles:

- Polydimethylsiloxane (PDMS) and polyurethane (PU) filled with different sizes of onion-like carbon (OLC);
- PU filled with hybrid OLC/MWCNT filler;
- Poly(methyl methacrylate) filled with different length of MWCNT;
- Bisphenol A epoxy resin filled with graphite particles;
- RTM6 epoxy resin filled with hybrid GNP/MWCNT filler.

All composites were prepared in collaboration with scientific groups from other institutions: Frascati National Laboratory, National Institute of Nuclear Physics (Frascati, Italy); IJL – UMR Université de Lorraine, ENSTIB (Épinal, France); Boreskov Institute of Catalysis SB RAS (Novosibirsk, Russia); Research Institute of Nuclear Problems of Belarus State University (Minsk, Belarus); International Technology Center (Raleigh USA).

3.1.1 Onion-like carbon composites preparation

The OLC/PDMS and OLC/PU composites were fabricated using OLC particles with different average aggregate size and concentration.

The OLC were prepared in following procedure. Detonation nanodiamonds (DND) were obtained by detonation of a mixture of trinitrotoluene (TNT) and $1,3,5$ – trinitroperhydro – $1,3,5$ – triazine (RDX) in CO_2 atmosphere, followed by oxidation of sp2 carbon in the mixture of concentrated sulfuric acid and chromic anhydride at $110°C$, washed with water, and dried. It is known that

DND exists in the form of strong aggregates (up to few hundred nanometers in size) with coherent and incoherent interfaces between primary ND particles of 4-7 nm in size [63]. Polydispersed DND material was fractionated by centrifugation into fractions with average aggregate size of 40 nm, 100 nm and 250 nm, correspondingly. Volumetric aggregate sizes were measured by a dynamic light scattering technique in water suspensions of DNDs. Fractions of the DNDs were heated in vacuum (10−4 Torr) at 1650°C for 3 h providing fractions of the OLC with aggregate sizes corresponding to the sizes of the starting DND fractions (approximately 250 nm, 100 nm and 40 nm, correspondingly).

Two different polymers were used as a polymer matrix and composites were prepared:

1) The polydimethylsiloxane (PDMS), *Sylgard*, was purchased from *Dow-Corning* as a two part material. When forming OLC/PDMS composites, an intermediate solvent (isopropanol (IPA)) was employed that served as a dispersion medium for the nanoparticles prior to mixing with the polymer matrix. The nanoparticles were dispersed in the solvent and sonicated to break up large agglomerates, then the suspension was combined with uncured PDMS and the IPA solvent subsequently removed by vacuum. Curing of the PDMS-nanoparticle mixture at 60°C for 2 hours and 40°C overnight resulted in films with good nanoparticle dispersion.

2) Preparing OLC/PU composites, OLC were subsequently mixed at different mass ratios with a Clear Gloss MINWAX® Fast-Drying Polyurethane (PU) containing 60 % of volatile compounds. After mixing with the OLC powder, the polymer suspension was stirred at 400 rpm overnight at 313 K. Then, the suspension was casted on a polytetrafluoroethylene (PTFE) substrate and dried overnight at 318 K and room pressure. The samples were thus recovered in the form of films whose typical thicknesses ranged from 0.1 to 0.8 mm, depending

on the OLC concentration that modified the viscosity of the corresponding suspensions.

3.1.2 Hybrid OLC/MWCNT/PU composites preparation

The composites containing up to 2 wt. % inclusions of MWCNTs, up to 7 wt. % of OLC, and hybrid filler MWCNT/OLC containing up to 7 wt.% of OLC and constant concentration of MWCNT – 0.5 wt.% were produced by following procedure.

Polyurethane films with nano-additives were prepared using Clear Gloss MINWAX® Fast-Drying Polyurethane. Nano-additives include MWCNT (20 nm diameter, 5 – 10 micrometer length) purchased from *Amorphous Carbon Materials, Inc*. and OLC derived by vacuum annealing of detonation nanodiamonds (DND). Aggregates of DND consisting of 5 nm primary particles were heated in vacuum ($10-4$ Torr) at 1650 ^{o}C for 3 hours, providing aggregates of OLC with aggregate sizes corresponding to the sizes of the starting DND fractions (approximately 100 nm). Stock suspensions of nano additives (~0.5 - 1.0 % w/v) were prepared in an alcohol solvent and sonicated with a horn-based sonicator for 30 minutes. 7 g of polyurethane (PU) was heated at a hot-plate at 60°C under magnetic stirring. The alcohol based suspension containing the desired amount and type of the nano-additives was added dropwise to the polyurethane while maintaining stirring. After the alcohol suspension was combined with the PU, the alcohol was evaporated from the PU-nanoadditive mixture. The samples were then cast on a PTFE substrate and cured at 40°C for 24 hours. After curing, the samples were annealed at 180°C for 0.5 h in order to homogenize nanofiller distribution.

3.1.3 MWCNT/PMMA composites preparation

All of nanotubes used were synthesized by CVD technique (670 ^{o}C, Ar/C_2H_4 1:1, 400 sccm) with Fe-Co/Al_2O_3 catalyst [64]. This catalyst possesses the high activity (>120 g_{MWCNT}/g_{cat}·h) and provides MWCNT of a high purity (no amorphous carbon) and a narrow diameter distribution (d_{mean}=9 nm).

Traces of the catalyst were removed by refluxing with HCl (1:1) for 6 h with subsequent rinsing with distilled water and drying at 60°C. Oxidized MWCNTs were produced by refluxing with nitric acid (conc.) for 2h with subsequent rinsing with distilled water and drying at 60°C. This procedure provides formation of 1.5-2 oxygen-containing groups on the MWCNT surface [65]. To obtain MWCNT of a small length, carbon nanotubes were subjected to mechanical activation in a high-power planetary ball mill (the acceleration of the balls was 200 m/s^2, the ball/powder weight ratio was 900:10 and 900:20, the ball diameter – 5 mm, the milling time was of 2 min; mill was designed by ISSC SB RAS (Russia)). Thereby, there were four forms of MWCNTs:

1) MWCNT which were only refluxed with HCl (the mean length ~ 50 μm) – "long" MWCNT. These nanotubes in majority consist of tangle agglomerate (the nanotubes length 20-50 μm).

2) MWCNT which were refluxed with HCl and then grinded in mill with the ball/powder weight ratio of 900:10 (the mean length 328±20 nm) – "short" MWCNT.

3) MWCNT which were refluxed with HCl and then grinded in mill with the ball/powder weight ratio of 900:20 (the mean length 438±20 nm) – "medium" MWCNT.

4) MWCNT which were refluxed with HCl, oxidized with HNO_3 and then grinded in mill with the ball/powder ratio of 900:20 (the mean length 335±20 nm) – "OX-short" MWCNT.

PMMA/MWCNT composites were produced via the coagulation precipitation technique [64]. PMMA (MW=120000, *Sigma Aldrich*) solution in N-methylpyrrolidone (NMP) was ultrasonicated with the MWCNT hinge and then introduced to an excessive amount of water (1.5 l, 318 K). Due to the immediate dissolution of NMP in water, the precipitation of the MWCNT/ PMMA composites results in spongy species with gray/black color (depending on the MWCNT loading). Composites then were filtered, washed from NMP residuals and dried in air at 333 K. The composite powder was hot pressed at

453 K with subsequent cooling into the press for 30 min (T~313-323 K). The films with the thickness of 0.4-0.5 mm and different MWNCT content (0.25, 0.5, 1.0, 2.0, 4.0 % wt.) were obtained.

3.1.4 Graphite/epoxy composites preparation

EPIKOTE™ 828 resin was used as composite matrix. It is a medium viscosity liquid epoxy resin produced from bisphenol A resin and epichlorhydrin. It contains no diluent. EPIKOTE 828 provides good pigment wetting, good resistance to filler settling, high level of mechanical and chemical resistance properties in cured state. Several series of composite samples, using Epikote 828, curing agent called A1 (i.e., a modified TEPA) and 0.25, 0.5, 1, 1.5 and 2 wt. % of various graphite fillers were fabricated.

The following graphite particles were used as filler in epoxy resin:

- Exfoliated graphite (EG) was purchased from Mersen (France), and was obtained by intercalation of natural graphite flakes with sulphuric acid followed by a very fast heating. Accordion-like particles were thus produced, leading to a material of low packing density, around 0.003 g cm^{-3} [66]. Typically, the diameter of the EG particles is in the range 0.3 - 0.5 mm.

- Three types of artificial graphite flakes, supplied by *Timcal G+T* (Switzerland) under the name TIMREX® KS, were used: coarse graphite (CG), medium graphite (MG), and fine graphite (FG), having mean flake diameters between 100 and 200 μm, between 44 and 75 μm, and between 15 and 44 μm, respectively. TIMREX® KS grades are synthetic graphite commercialized for being used as conductive additives up to 10 % in the positive electrode of secondary lithium batteries [67]. They have relatively small single crystal domains in the particle, resulting in a relatively high isotropic electrical conductivity. Their particles are flattened spheroids giving excellent processability and rheological behaviour in liquid dispersions.

35

- Natural graphite (NG) is obtained from Madagascar as filler. The latter is composed of shiny, rather large flakes having typical diameters within the range 500 - 750 µm.

The resin was degassed under vacuum (1–3 mbar) for 12-14 hours, and then was put into an oven at 65°C. In the meantime, the graphite particles were dispersed in propanol, and the suspension was submitted to an ultrasonic bath for 1.5 h. Afterwards the alcoholic suspension of graphite was mixed with the resin. The obtained mixture was placed inside an oven at 130–150 °C for evaporating the alcohol. The curing agent A1 was added to the mixture of resin and filler through slow manual mixing for about 7 min. The blend was then poured into moulds of dimensions 1 cm × 1 cm × 7 cm, and left as such for 20 hours for the curing process at room temperature, and finally 4 hours in an oven at 80°C. When the process was completed, the samples were removed from the moulds.

3.1.5 GNP/MWCNT/epoxy composites preparation

Composites were prepared with multiwalled carbon nanotubes (MWCNT) and graphene nanoplatelets in an epoxy resin matrix. The epoxy resin is a mono-component thermosetting resin RTM6 (HexFlow®), which is already degassed. It is the premixed epoxy-amine system for service temperatures from -60 °C up to 180 °C, specifically developed to fulfill the requirements of the aerospace industries in advanced resin transfer moulding process. This resin is characterized by a high ultimate glass transition temperature (200°C) and the low viscosity (50 MPa) within the range 100-120 ^{o}C.

MWCNTs N7000 were purchased from Nanocyl (Belgium) and they were produced via the catalytic carbon vapor deposition process. The mean length of MWCNT is 0.1 – 10 µm, the diameter 10 nm. The MWCNT filler content is 0.015 – 0.30 wt. %. Graphene nanoplatelets (GNPs) were purchased from PuntoQuantico (Italy). The average particle (lateral) size is 20 – 50 µm, the specific surface area 60-80 m^2/g, and the average density 2.43 g/cm^3. Filler contents were chosen 0.015 – 3.0 wt.%. Using both carbon nanofillers hybrid

nanocomposites with total filler content 0.3 wt.%. The ratio of MWCNT and GNP was selected as 1:1, 1:2, 1:5, 2:1, 5:1 were produced.

The epoxy resin/carbon nanofiller nanocomposites were prepared using 150 g of resin mixed with carbon particles in different contents for a constant time (70 min) at temperature 85 °C with a nominal speed 6000 rpm. The mixer used in this work was a T25 digital ULTRA -TURRAX high-performance disperser by *IKA* with an output power 500 W and the frequency 50 Hz. A disperser horn was directly put into the warmed up to 60 °C resin and MWCNTs mixture. The disperser used produce extremely strong shear and thrust forces due to high accelerations acting on the material, and additionally high turbulence occurs in the shear gap between rotor and stator, which provides optimum mixing of the components.

3.2 Experimental methods

The dielectric spectroscopy is a useful tool to study molecular dynamics of polymers and herewith of polymer composites. With this method broad dynamic range could be covered up to terahertz region. Polymer motional processes which take place for polymeric systems on different time scales can be investigated in broad frequency and temperature range. Moreover, information on structural state of the material can be indirectly extracted by taking the molecular mobility as a probe for the structure. The complex dielectric permittivity $\varepsilon^* = \varepsilon' - i\varepsilon''$ of composites was investigated in wide temperature (30 K – 300 K) and frequency range (20 Hz – 1 THz).

In frequency range from 20 Hz to 1 MHz measurements were carried out with LCR meter (HP4284 A) measuring capacitance and the loss tangent. According to planar capacitor formula, the real and imaginary parts of complex dielectric permittivity could be calculated as follows:

$$C_S - C_0 = \frac{\varepsilon_0 S}{d}(\varepsilon - 1), \tag{3.1}$$

$$\varepsilon' = \frac{(C_S - C_0)d}{\varepsilon_0 S} + 1, \tag{3.2}$$

$$\varepsilon'' = \frac{C_S \cdot tg\delta_S - C_0 tg\delta_0}{C_S - C_0}, \tag{3.3}$$

where C_S and $tg\delta_S$ are capacitance and loss tangent of system with the sample, C_0 and $tg\delta_0$ are capacitance and loss tangent of the system without the sample, d and S are the thickness and area of the sample respectively, ε_0 is the vacuum permittivity.

The samples were cylindical shape with parallel surfaces. The diameter and the thickness were 9 mm and 1-3 mm respectively. Silver paste was used for the contacts.

In the frequency range from 1 MHz to 3 GHz measurements were performed by coaxial dielectric spectrometer with vector network analyzer (Agilent 8714ET) by measuring complex reflection coefficient R[*] and phase. Complex reflection coefficient is related with sample and system impedance:

$$R^* = \frac{Z_S^* - Z_0}{Z_S^* + Z_0}, \tag{3.4}$$

Where Z_S^* and Z_0 is an impedance of the sample and the system (50 Ω) respectively.

Since $R^* = R(\cos\varphi - i \cdot \sin\varphi)$, the impedance of the sample:

$$Z_S^* = \frac{Z_0(1 + 2R\cos\varphi + r^2)}{1 - R^2 - 2iR\sin\varphi}. \tag{3.5}$$

Capacitance could be calculated through to the following relation:

$$Z_S^* = \frac{1}{\omega(C_S' + iC_S'')}. \tag{3.6}$$

According to planar capacitor formula, real and imaginary parts of complex dielectric permittivity could be calculated as follows:

$$\varepsilon' = \frac{d}{\varepsilon_0 S}\left(\frac{-2R\sin\varphi}{\omega Z_0(1 + 2R\cos\varphi + R^2)} - C_0\right) + 1, \tag{3.7}$$

$$\varepsilon'' = \frac{d}{\varepsilon_0 S}\left(\frac{1 - R^2}{\omega Z_0(1 + 2R\cos\varphi + R^2)}\right), \tag{3.8}$$

where d and S is the thickness and area of the sample respectively, ε_0 is the vacuum permittivity.

The samples were cylindrical shape with diameter 1 mm and les than 1 mm thickness. Silver paste was used for the contacts.

Microwave measurements (27 GHz – 40 GHz) were carried out using rectangular waveguide method and measuring the releflection and transmission

coefficients with scalar network analyzer (R2-408R, ELMIKA, Vilnius, Lithuania). The shape of the sample is cylindrical rod placed in the middle and perpendicular to the longer wall of the waveguide, parallel to the electric field of main TE_{10} modes.
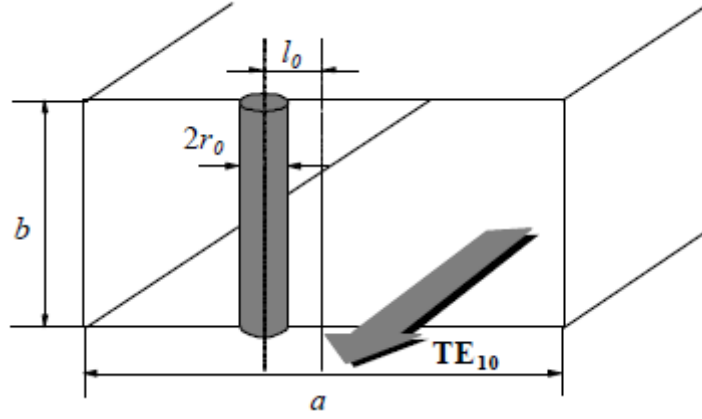

Fig 3.1. The cylindrical sample placed in the waveguide

Complex dielectric permittivity could be found from nonlinear equations $\varepsilon^* = f(R^*)$ or $\varepsilon^* = f(R, T)$. For calculating the complex dielectric permittivity the optimization problem could be solved:

$$R = f_1(\varepsilon', \varepsilon'') \text{ and } T = f_2(\varepsilon', \varepsilon'').$$ (3.9)

The optimization procedure is stopped and the values of dielectric permittivity are obtained, when inequalities are satisfied:

$$|R - f_1(\varepsilon', \varepsilon'') < \delta| \text{ and } |T - f_2(\varepsilon', \varepsilon'') < \delta|,$$ (3.10)

where δ is the accuracy of calculations.

In frequency range from 100 GHz to 1 THz measurement were performed by time domain terahertz spectrometer (EKSPLA, Vilnius, Lithuania). The ultrashort optical pulses are generated by Ti:Saphir laser with 76 MHz repetition rate and 150 fs pulse duration. The emitter and detector are low temperature grown GaBiAs photoconductive antenna. The subpicosecond pulses of THz radiation are detected after propagation through a sample $(S_s(\omega))$and identical lengh of a free space $(S_0(\omega))$.
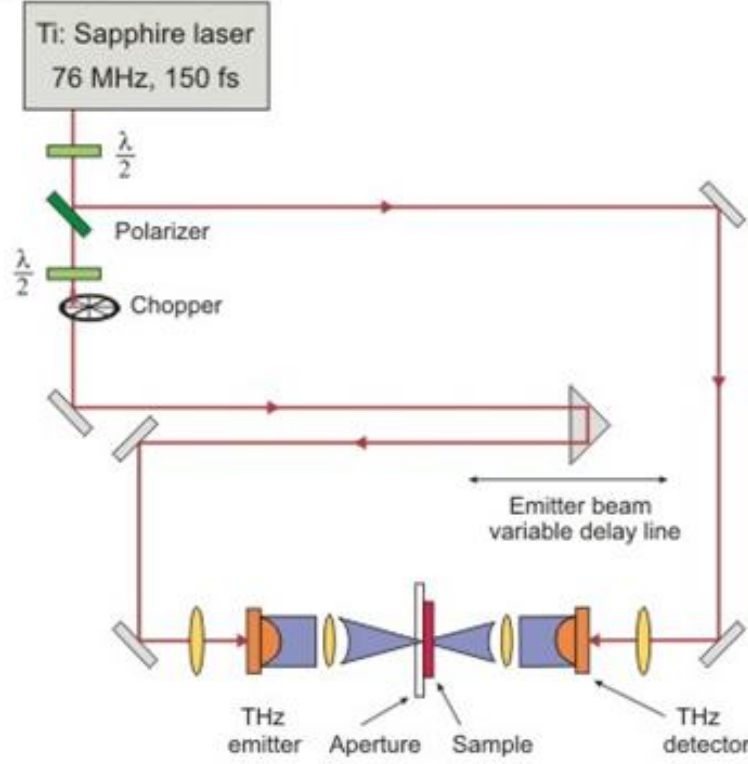
Fig.3.2. Time domain terahertz spectrometer scheme

The ratio of these signals:

$$\frac{S_s(\omega)}{S_0(\omega)} = \rho(\omega) \cdot e^{-i\varphi(\omega)}, \quad (3.11)$$

where $\rho(\omega)$ is the phase and $\varphi(\omega)$ is the amplitude.

Complex refractive index is expressed by $\tilde{n}(\omega) = n_s(\omega) - ik_s(\omega)$. The real and imaginary part of complex refractive index of the sample is:

$$n_s(\omega) = \varphi(\omega) \cdot \frac{c_0}{\omega d} + 1, \quad (3.12)$$

$$k_s(\omega) = \ln\left(\frac{4n_s(\omega)}{\rho(\omega) \cdot (n_s(\omega)+1)^2}\right) \cdot \frac{c_0}{\omega d}, \quad (3.13)$$

where c_0 is the speed of light in vacuum, d – the thickness of the sample. The imaginary part of the refractive index is related to the power absorption coefficient as follows:

$$k_s = c_0 \alpha_s(\omega)/2\omega, \quad (3.14)$$

where

$$\alpha_s(\omega) = \frac{2}{d} \cdot \ln\left(\frac{4n_s(\omega)}{\rho(\omega) \cdot (n_s(\omega)+1)^2}\right) \quad (3.15)$$

40

The real and imaginary part of complex dielectric permittivity, $\varepsilon^* = \varepsilon' - i\varepsilon''$, $\varepsilon^* = (\tilde{n}(\omega))^2$ could be calculated:

$$\varepsilon'_s = (n_s(\omega))^2 - [c_0\alpha_s(\omega)/2\omega]^2, \qquad (3.16)$$

$$\varepsilon''_s = 2n_s(\omega)k_s(\omega) = c_0 n_s(\omega)\alpha_s(\omega)/\omega. \qquad (3.17)$$

4 Results and discussion

This chapter is devoted for the results, analysis and discussion of dielectric and electrical properties of investigated composites. They will be discussed separately by the type of carbon filler – onion-like carbon, carbon nanotubes, graphite and hybrid filler composites. The dielectric measurements are supplemented by the pictures of scanning electron microscopy (SEM) and transmission electron microscopy (TEM) which determine microscopic structure of the investigated composites. The detailed list of the samples is presented in Table 4.1.

Table 4.1. Detailed list of the samples

Sample	Matrix	Filler	Filler concentrations
FG	Epoxy resin EPIKOTE™ 828	Fine graphite	0 – 2 wt. %
NG		Natural graphite	
MG		Medium graphite	
CG		Coarsed graphite	
EG		Exfoliated graphite	
PMMA/MWCNT	PMMA	Multiwalled carbon nanotubes	0 – 4 wt. %
OLC/PDMS	PDMS	Onion-like carbon	0 – 10 vol. %
OLC/PU	PU	Onion-like carbon	0 – 14 vol. %
OLC/MWCNT/PU		Onion-like carbon / Multiwalled carbon nanotubes	OLC/MWCNT ratios 7 wt. %/0.5 wt.% 5 wt. %/0.5 wt.%
MWCNT	Epoxy resin RTM6	Multiwalled carbon nanotubes	0 – 0.3 wt. %
GNP		Graphene nanoplatelets	0 – 3 wt. %
`GNP/MWCNT		Graphene nanoplatelets / Multiwalled carbon nanotubes	GNP/MWCNT ratios 1:5, 1:2, 1:1, 2:1, 5:1, total content 0.3 wt. %

4.1 Onion-like carbon (OLC) composites

In this section composites filled with onion-like carbons (OLCs) are presented, which might be used for applications requesting high electrical conductivity, for example as an antistatic materials, for electrostatic discharge, dissipation, electromagnetic interference shielding, temperature, pressure and gas sensors. OLCs are indeed stable, multi-shelled imperfect fullerenes, exhibiting electrical conductivity as high as about several hundred S/m at room temperature [63]. Many dielectric investigations of OLC composites were performed below percolation threshold, where the complex dielectric permittivity of composites increases slowly with OLC concentration according to the Maxwell-Garnett theory [68, 69]. Also the percolative behaviour and critical exponents of OLC based composite above percolation threshold were revealed [70]. OLC composites, similarly to CB composites, may have complex aggregate structure, which could have strong impact on the electrical percolation threshold [71]. Therefore, the OLC aggregate size effect on composite's dielectric and electrical properties needs to be investigated.

The dielectric and electrical properties of OLC based composites with two different polymer matrixes of polyurethane (PU) and polydimethylsiloxane (PDMS) were investigated in wide frequency (20 Hz – 1 THz) and temperature (30 – 500 K) ranges. OLC particles, which were used, are 40 nm, 100 nm and 250 nm average aggregate sizes. The concentration of the filler particles is up to 14 vol. %. PU is thermosetting polymer while PDMS is a semi-crystalline thermoplastic with very low glass transition temperature (150 K). In addition, hybrid filler OLC/MWCNT/PU composites were investigated in order to reveal possible synergy effect due to combination of different sizes and types of the particles.

Low magnification and high resolution TEM images of OLC particles are presented in Fig. 4.1.
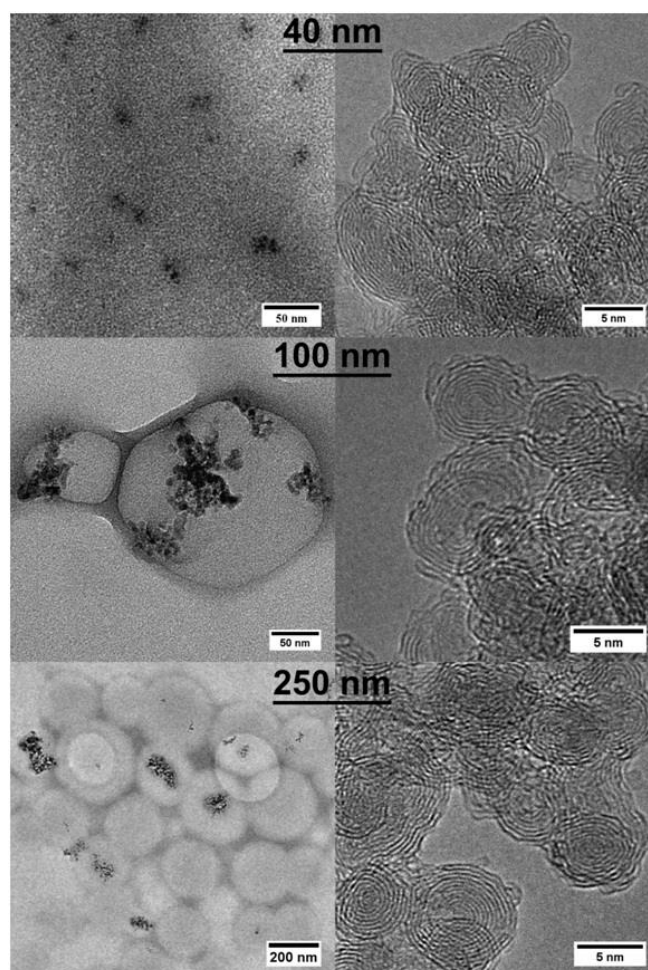
Fig. 4.1. TEM images of OLC with 40 nm, 100 nm and 250 nm average aggregate size. Left part – low magnification images of aggregates deposited on the amorphous carbon layer of TEM grid. Right part presents of high resolution TEM images of OLC aggregates [72]

It can be seen that the primary OLC particles consist of enclosed defective fullerene-like shells, which in turn are combined into tight aggregates with joint graphene layers similar to what is known for some carbon blacks. Therefore, it is likely that OLC form chainlike clusters. Whereas the latter don't have any particular shape, they can probably deform easily when submitted to shear stress during the preparation of the composite: chains of carbon onions arranged in a pearl necklace structure are thus expected to be produced in the polymer matrix [72].

4.1.1 OLC/PDMS composites

SEM images of OLC/PDSM composites with up to 10 vol. % OLC are presented in Fig. 4.2. Composites with small content of OLC are very soft and

flexible while increasing OLC loading (more than 5 vol. %) results in formation of brittle films.
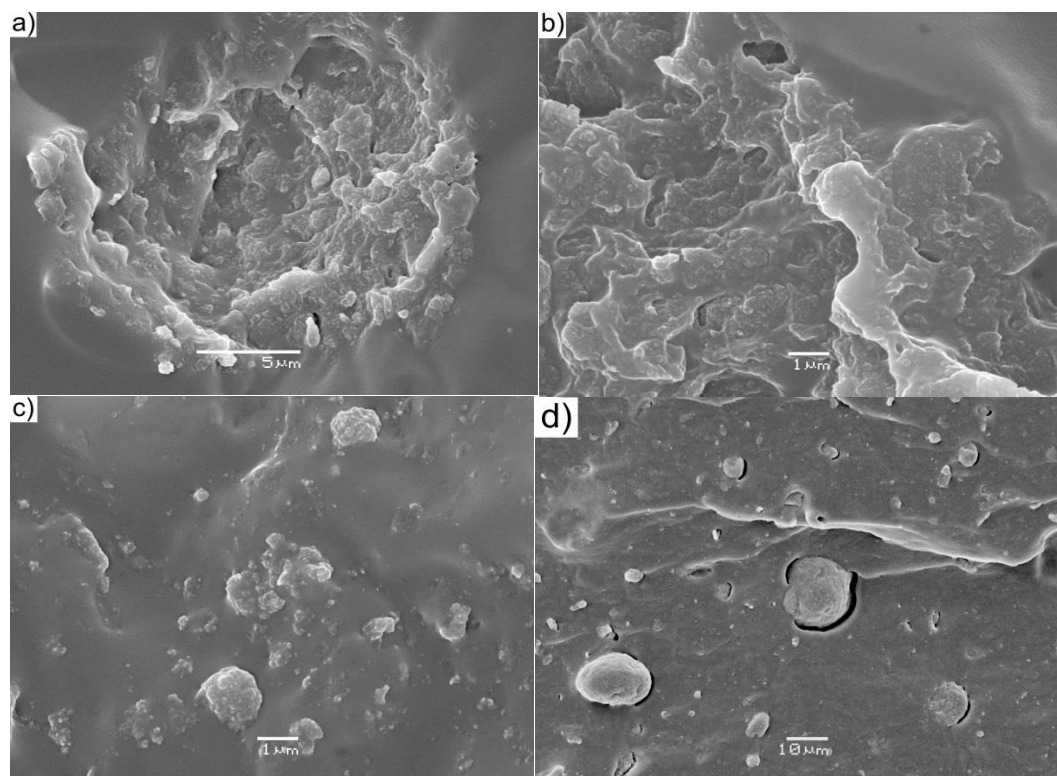
Fig. 4.2. SEM images of OLC/PDSM composites: a) 1 vol.%, b) 5 vol.%, c) 10 vol.%, OLC aggregates 250 nm; d) 6.8 vol.% OLC, aggregates 40 nm [72]

It can be assumed that the broken surfaces are spread along the direction with diminished strength and with the highest concentration of OLC agglomerates, revealing the distribution of the aggregates in these regions. In samples with the lowest OLC content secondary agglomerates (of micron size) can be observed as well as individual primary aggregates of OLC (Fig. 4.2 d) [72]. Increase in OLC content, up to 5 vol. % and more, results in increased sizes of clustered aggregates, however small aggregates also can be observed. Thus, OLC/PDSM composites exhibit a fractal structure of the aggregates similar to carbon black composites [73].

The frequency dependencies of real parts of complex dielectric permittivity (ε') and electrical conductivity (σ') of PDSM composites with different loadings of 250 nm OLC at room temperature are shown in Fig. 4.3.
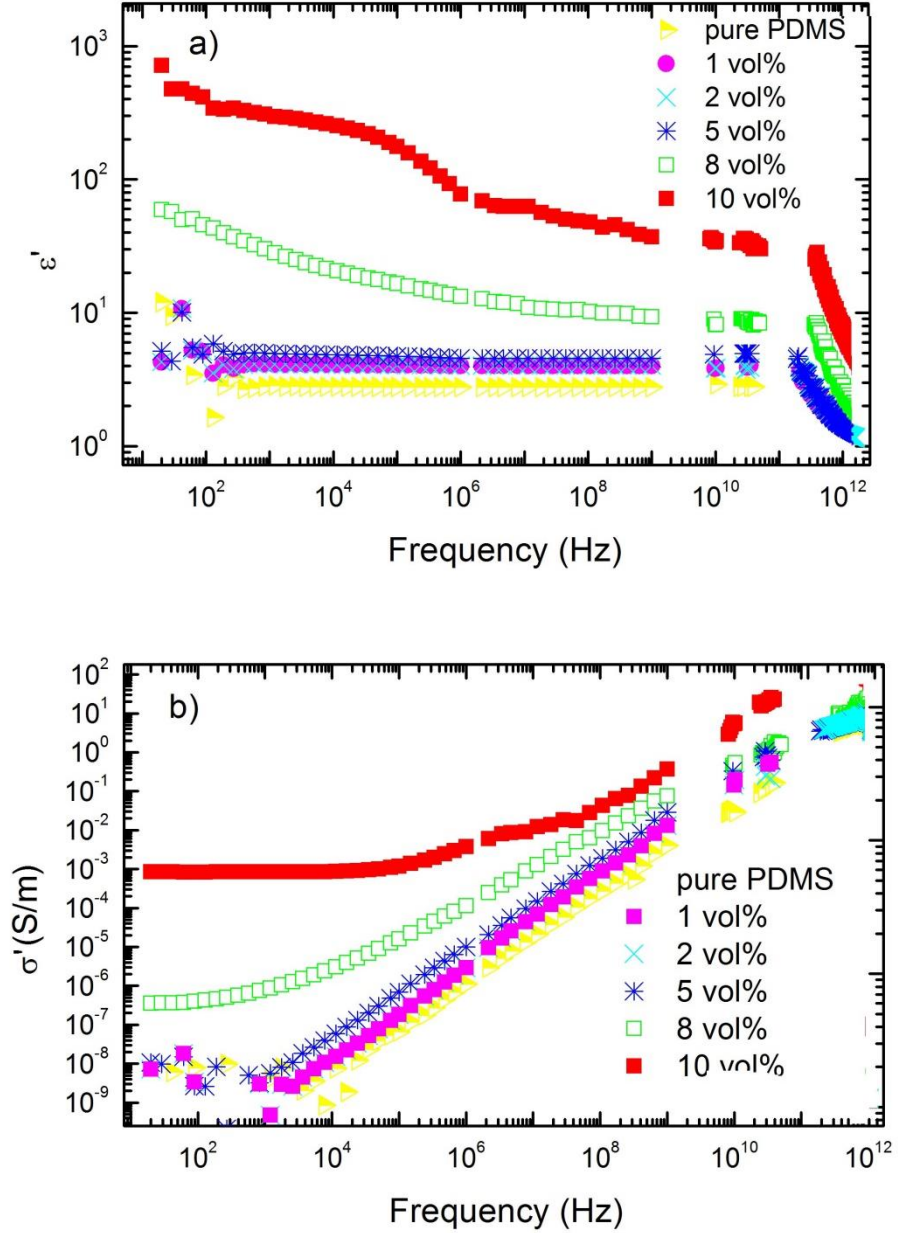
Fig. 4.3.Frequency dependencies of dielectric permittivity and electrical conductivity for OLC/PDSM (250 nm OLC inclusions) composites at room temperature

The values of the dielectric permittivity and electrical conductivity for composites with lower than 5 vol. % OLC fraction are very low and similar to PDMS without inclusions. However, the dielectric permitivity starts to increase for composites with 8 vol. % inclusions. The electrical percolation threshold could be indicated by sharp increase of dielectric permittivity and electrical conductivity values by several orders of magnitude. At low frequencies (below 1 kHz) DC electrical conductivity plateau is clearly expressed in conductivity

spectra of composites with 8 vol.% inclusions, indicating that the percolation threshold in OLC/PDMS composites with 250 nm OLC inclusions is in a range from 5 vol. % to 8 vol. %.

The dielectric permittivity is in the order of 10^3 and the electrical conductivity is about 0.001 S/m at low frequencies for the composites with 10 vol. %. These values are very high and similar to the values of functionalized carbon nanotubes composites near the percolation threshold [74]. In the microwave frequency range the value of complex dielectric permittivity for the presented composites is higher in comparison with the carbon black composites [75]. The different trends are observed in the frequency spectra of the dielectric permittivity, which are related with the Maxwell – Wagner contribution to the dielectric permittivity [76]. The high values of loss tangent at low frequencies indicate a high absorption ability of electromagnetic waves by composite with 10 vol. % of OLC. A flat frequency dependence of the real part of dielectric permittivity in the frequency range 8 - 53 GHz is also observed is in carbon black and carbon nanotubes composites [77, 78]. A rapid decrease with frequency of the real part of the dielectric permittivity above 100 GHz is typical for phonon related dielectric dispersion and this part of the spectra above 100 GHz obtained for PDSM without inclusions is in good agreement with results presented in [79].

In order to reveal the influence of the OLC concentration and aggregate size to the electrical properties and percolation threshold, the dielectric permittivity and the electrical conductivity at the frequency 129 Hz and room temperature for all investigated composites are plotted as a function of the concentration (Fig. 4.4).
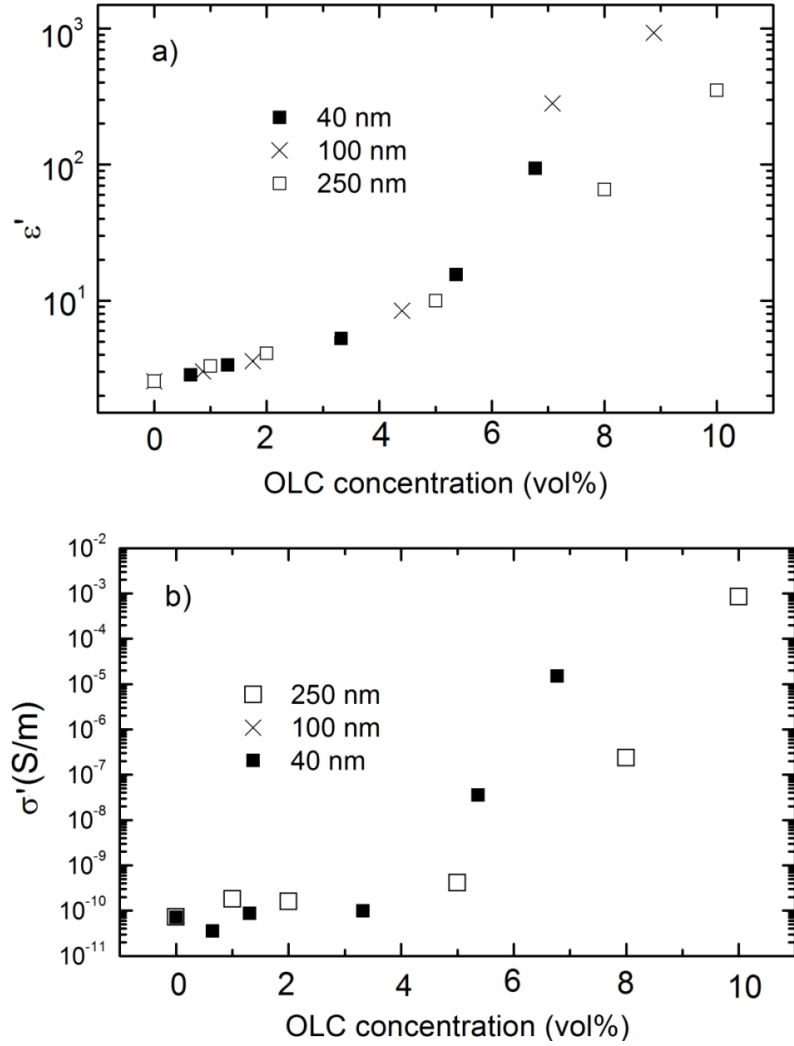
Fig. 4.4. Concentration dependencies of the real parts of complex a) dielectric permittivity, b) electrical conductivity of OLC/PDSM composites for 40 nm, 100 nm, 250 nm aggregate size at room temperature

The frequency spectra of composites with 250 nm at concentrations 10 vol. % and 8 vol. % (Fig. 4.3), 100 nm at concentrations 8.9 vol. % and 7.1 vol. % and 40 nm aggregate size at concentration 6.8 vol. % (not shown) a frequency independent DC plateau can be observed at low frequencies, so that the conductivity at 129 Hz for these composites coincide with the DC conductivity. Therefore, the percolation threshold is close to ~ 10 vol. % for composites with 250 nm, ~ 7.1 vol. % - with 100 nm and ~ 6.8 vol. % - with 40 nm OLC aggregates, correspondingly. Thus, the lowest percolation threshold is observed in the composites with 40 nm OLC aggregate size. Below the percolation threshold the effective permittivity ε' at 129 Hz was fitted

according to the power law (Eq. 2.16) [80]. The obtained parameters are ε_m=2.55 for all types of OLC, while p_c=8 vol. % and s=1.35 were obtained for 250 nm OLC, p_c=7.1 vol. % and s=1.25 for 100 nm OLC, s=6.7 vol. % and q=1.04 for 40 nm OLC aggregates, correspondingly. At concentrations close to the percolation threshold, the percolation theory predicts the value of the exponent close to 2 in any three-dimensional medium [81]. So, obtained values of the critical index are in agreement with the percolation theory. In order to increase the determination accuracy of p_c and s, many more samples with different OLC concentrations should be investigated at concentrations close to the critical value. According to the percolation theory for the two phase randomly distributed composite whose fillers are spherical the percolation threshold should be about 0.16 volume fraction [81]. Nevertheless, the critical volume fraction is lower than it is expected from theory.

Temperature dependence of the effective permittivity and the electrical conductivity of OLC/PDSM composites with 250 nm OLC inclusions at 10 vol.% is presented in Fig. 4.5 at different frequencies from room temperature up to 500 K.
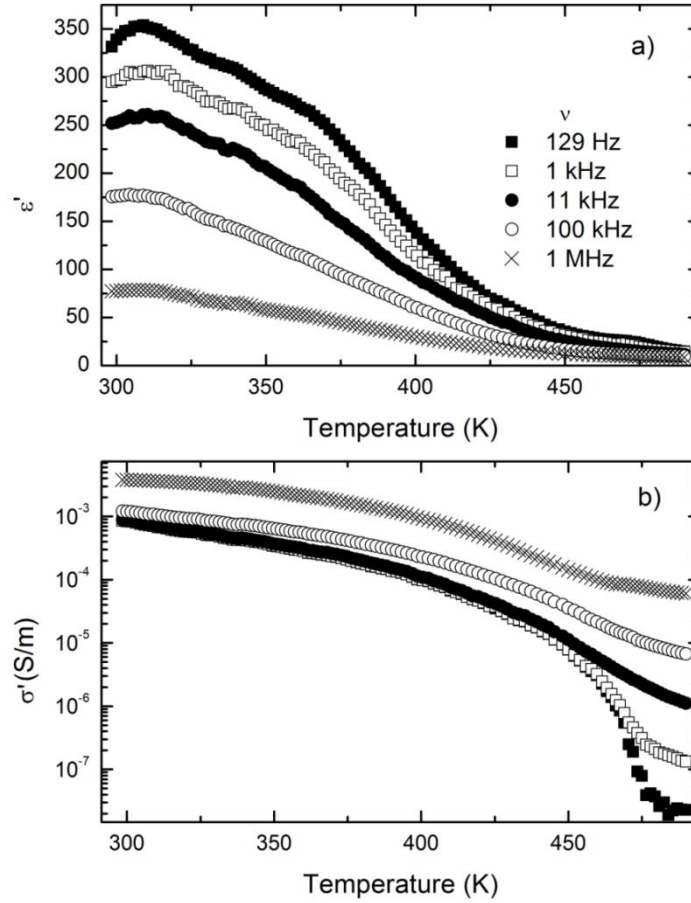
Fig. 4.5. Temperature dependencies of real parts of complex a) dielectric permittivity, b) electrical conductivity of OLC/PDSM composites (with 250 nm OLC 10 wt.% inclusions) at different frequencies (high temperature region)

Both the dielectric permittivity and the electrical conductivity decrease during heating, however the most pronounced decrease occurs at temperatures above 450 K and at lower frequencies (below 11 kHz). In order to understand the phenomena the electrical conductivity was plotted as a function of the frequency at various representative temperatures in Fig. 4.6.
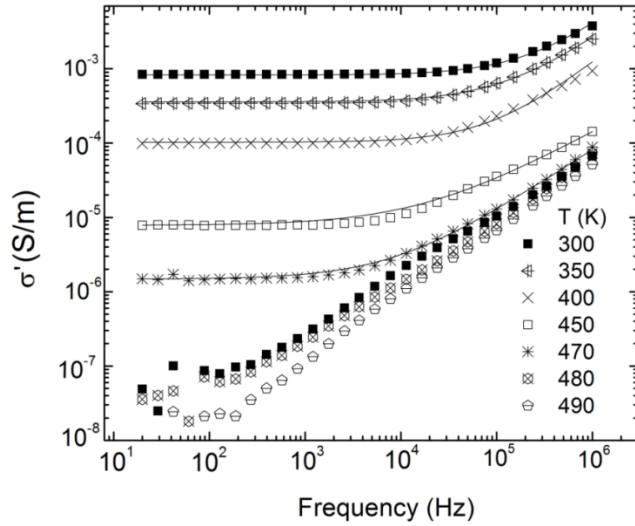
Fig. 4.6. Frequency dependence of real part of electrical conductivity of OLC/PDSM composites (with 250 nm OLC 10 wt. % inclusions) at different temperatures (high temperature region). Solid lines are fits of Jonscher's equation

During heating not only was the electrical conductivity decreased, but also substantially changes in the shape of the conductivity spectrum took place. A frequency independent conductivity (DC conductivity) is observed at lower frequencies and at lower temperatures. Above 470 K no DC conductivity is observed in the conductivity spectra of the investigated composites. The frequency spectra of the conductivity was fitted with the empirical Jonscher's equation. DC conductivity values for all composites above the percolation threshold are presented in Fig. 4.7 a. From this fit, it is possible to calculate the critical frequency f_{cr}, at which the value of the conductivity $\sigma'(f)$ deviates from the DC plateau. The experimental value for f_{cr} has been defined as the frequency at which the value of the conductivity is 10 % higher than the DC conductivity value. The results are plotted in Fig. 4.7 b.
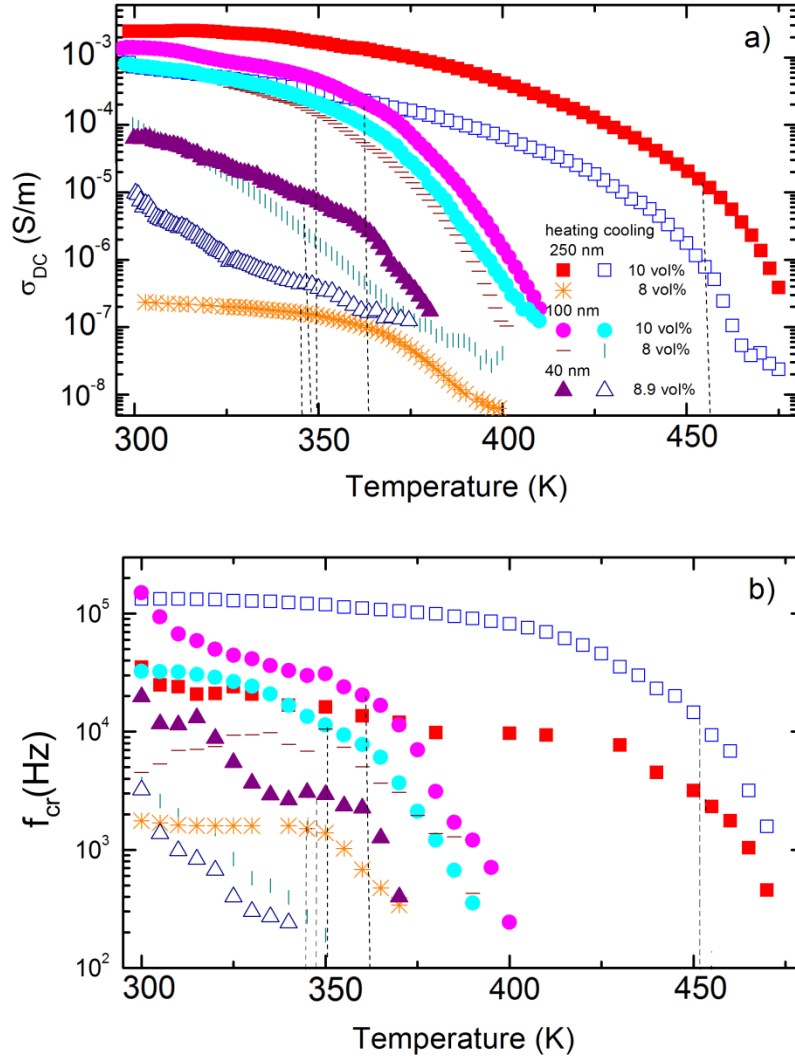
Fig. 4.7. Temperature dependencies of OLC/PDSM composites: a) DC conductivity, b) critical frequency (high temperature region). The dotted lines indicate a limit between a „slow" decreasing of DC conductivity and critical frequency with temperature and a „rapid" decreasing" of these parameters

It can be clearly seen that both the DC conductivity and the critical frequency f_{cr} are almost temperature independent at lower temperatures and rapidly decrease close to the specific temperature, which depends on the OLC aggregate size and concentration. Above this temperature no DC conductivity occurs in the composites, therefore a conductor-insulator phase transition is observed. The complex dielectric permittivity of a PDSM polymer matrix without inclusions only very slowly increases with temperature, no anomaly is revealed and its value remains quite low ($\varepsilon' < 5$ and $\varepsilon'' < 1.5$) in the temperature region 300 – 500 K. The transition temperature was obtained as a temperature,

at which DC conductivity disappears and the results are presented in Table 4.1. The transition temperature increases with OLC concentration and OLC aggregate size.

Table 4.1 The metal-insulator transition temperatures for OLC/PDSM composites

OLC type	Concentration (vol.%)	Transition temperature (K)
250 nm	10	476
	8	382
100 nm	8.9	413
	7.1	401
40 nm	6.8	398

The DC conductivity (σ_{DC}) and critical frequency (f_{cr}) are almost temperature independent at temperatures far from the conductor-insulator transition temperature, and according to the relation $\sigma_{DC} \sim f_{cr}^z$, in this temperature region critical exponent z is almost zero. Close to the conductor-insulator transition temperature both DC conductivity and critical frequency rapidly decreases and the critical exponent is ~1.5 in this temperature region for all composites. This indicates a strong dependence on the distances between OLC clusters of both effective permittivity and electrical conductivity close to the metal- insulator transition temperature [82]. Upon heating both the electrical conductivity and the dielectric permittivity decrease due to very different thermal expansion properties of the PDSM polymer matrix and OLC. The volume of OLC clusters remains almost the same, while the polymer matrix volume increases rapidly with heating.

At low frequencies the electrical conductivity in the investigated composites can occur via several mechanisms: 1) electron hopping in the infinite OLC clusters, 2) serial transport by hopping in finite clusters and a tunneling between these finite clusters, 3) tunneling between finite and infinite clusters. Due to the rapid polymer matrix expansion only tunneling

53

conductivity decreases because the distance for electron tunneling is increased. At higher temperatures (above the conductor-insulator transition temperature) the DC electrical conductivity disappears, when the mean distance between the OLC clusters exceeds a critical value at which no more tunneling is possible. Thus, electrical transport in the OLC/PDSM composites is governed by hopping in finite clusters and tunneling between these finite clusters.

With increasing OLC concentration or aggregate size the mean distance between the OLC clusters decreases and therefore the electrical conductivity is increased. The volume concentration of OLC clusters φ_i can be calculated as $\varphi_i = \frac{V_{OLC}}{(V_{OLC}+V_{PDMS})}$, where V_{OLC} is the volume of OLC in the composite and V_{PDSM} is the volume of matrix in the composite. Assuming that V_{OLC} is almost temperature independent, φ_i could be proportional to $1/V_{PDMS}$. Thus, the volume concentration decreases upon heating and when it reaches a critical value, a transition into the insulator state occurs, which is followed by vanishing of both DC conductivity and critical frequency. This is clearly seen in Fig. 4.7 where a slow decrease of both conductivity and critical frequency is observed on heating, as well as a rapid decrease close to the conductor-insulator temperature. The transition into an insulator state can be explained by the decrease of OLC volume concentration below some critical concentration.

For the lower OLC concentrations (8 vol. % of 250 nm OLC aggregates) the conductor-insulator transition is irreversible, i.e. after annealing above the transition temperature the value of composite dielectric permittivity remains low upon cooling (Fig. 4.7). In this case the destroyed OLC network does not recover with polymer matrix shrinkage upon cooling and the composite is an insulator at room temperature after annealing. At higher OLC concentrations the behavior of the DC conductivity and the critical frequency is reversible (Fig. 4.7), i.e. upon cooling the values of DC conductivity and critical frequency are partially recovered.

A decrease in conductivity of percolative composites during heating was observed in other composites [82], however in these composites no conductor-

insulator transition occured due to finite matrix conductivity at higher temperature. In contrast, no DC conductivity and any electrical or dielectric anomaly was observed in the PDMS polymer up to 500 K. Above room temperature the conductor-insulator transition usually occurs in vanadium oxide related compounds [83], however in this case the phase transition temperature can be easily changed by changing the OLC filler concentration and type. Moreover, in vanadium oxide related materials the high temperature phase is conductive and low temperature is non-conductive [83], while in OLC/PDMS composites the high temperature phase is not conductive. This is due to the fact that in OLC/PDMS composites at higher temperatures the distances between the OLC clusters is too big and tunneling electrical conductivity does not occur in the composite. Thus, the OLC/PDMS composites can be useful in various applications, where a temperature dependent behavior is required.

At low temperatures dielectric permittivity and electrical conductivity increase during cooling and reach a maximum close to the glass transition temperature (150 K) of pure PDMS matrix (Fig. 4.8).
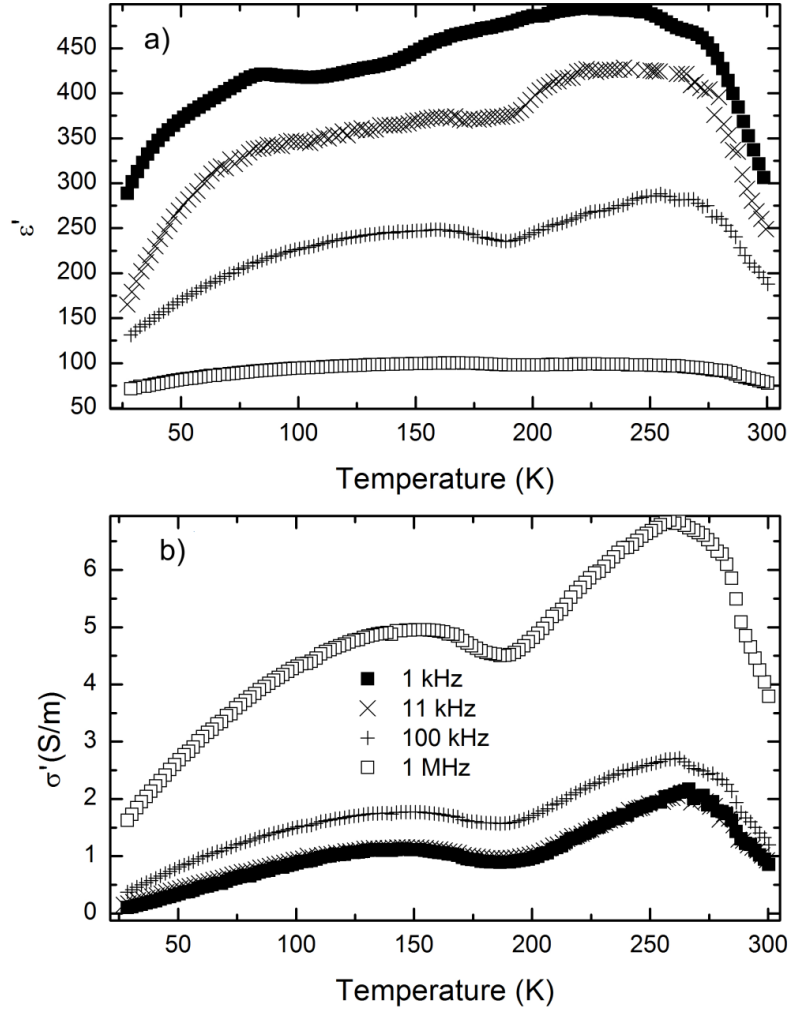
Fig. 4.8. Temperature dependencies of real parts of complex a) dielectric permittivity, b) electrical conductivity of OLC/PDSM composites (with 250 nm OLC 10 vol.% inclusions) at different frequencies (low temperature region)

The behavior can be explained by a rapid shrinkage of the PDMS matrix upon cooling down to the glass transition temperature. A similar behavior was observed also in other polymer composites [78]. At low temperatures (below 170 K) both the effective permittivity and the electrical conductivity decrease upon cooling. Conductivity spectra $\sigma'(f)$ were fitted with Jonscher's equation (Fig. 4.9).
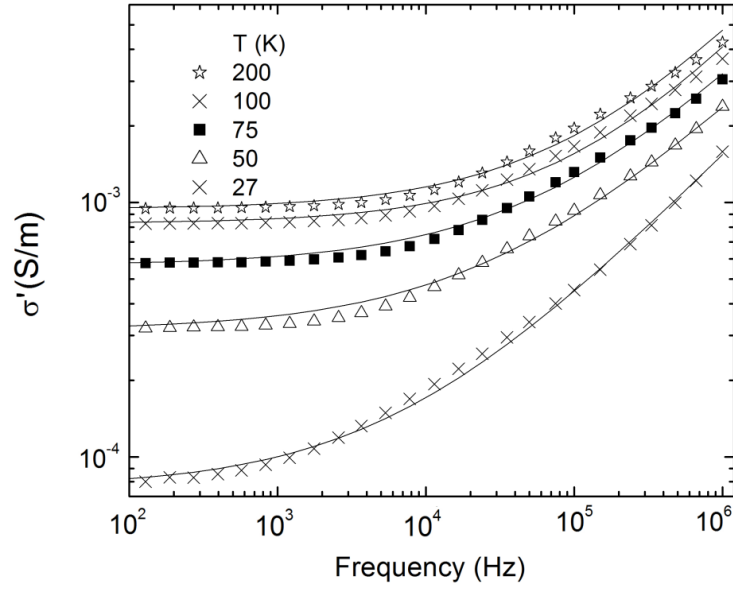
Fig. 4.9. Frequency dependence of the real part of complex electrical conductivity of OLC/PDSM (with 250 nm OLC inclusions 10 vol.% inclusions) at different temperatures (low temperature region). Solid lines are the fits of Jonscher's equation

For temperatures below 170 K, the DC conductivity data fit well to the fluctuation induced tunneling model (Fig. 4.10). Obtained parameters are listed in Table 4.2. Thus, the ratio T_1/T_0 should decrease with the OLC concentration, as it was observed in the composites with 100 nm OLC aggregates.
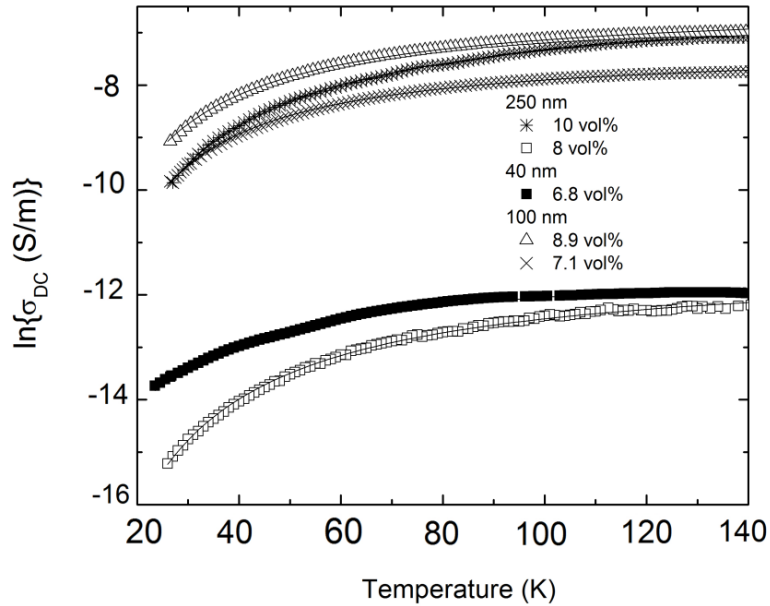

Fig. 4.10. Temperature dependence of DC conductivity of OLC/PDSM composites. Solid lines are fits of tunneling model (low temperature region)

Table 4.2. Tunneling model fit parameters for DC conductivity at low temperatures

OLC size	Concentration (vol. %)	T_1 (K)	T_0 (K)
250 nm	10	110	4.2
	8	38	8.3
100 nm	8.9	75	2
	7.1	83	5
40 nm	6.8	70	5.2

However, below 100 K not only the DC conductivity but also the shape of the conductivity spectra is temperature dependent (Fig. 4.9). This means that the critical frequency is also temperature dependent. It could be assumed that the temperature dependence of the DC conductivity at lower temperatures (below 100 K) can be fitted by the general Mott expression for variable range hopping (Fig. 4.11). A similar behavior is also valid for the critical frequency f_{cr}.
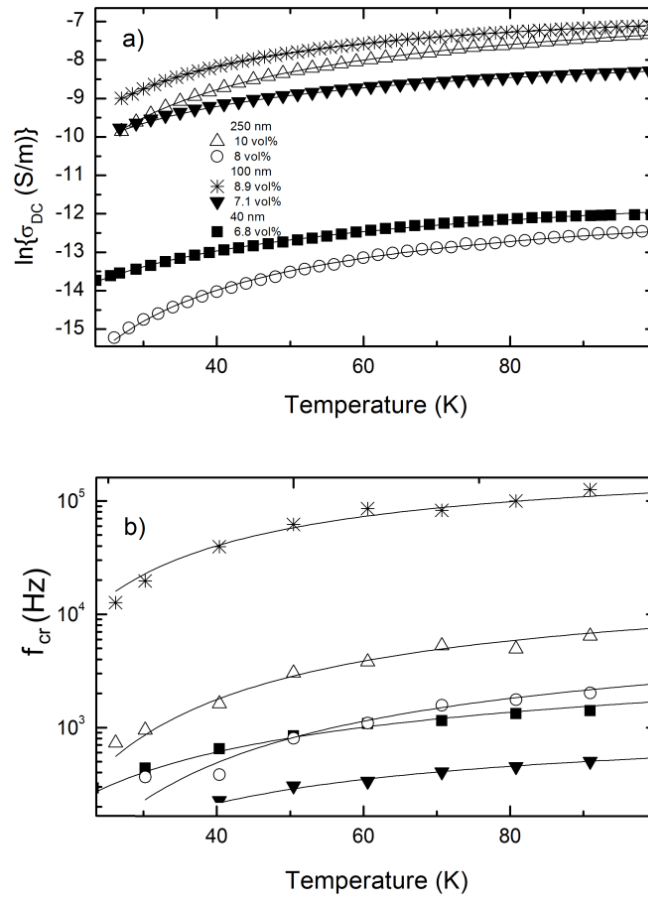

Fig. 4.11.Temperature dependencies of OLC/PDSM composites: a) DC conductivity b) critical frequency. Solid lines are the fits of Mott's law (low temperature region)

Table 4.3. Mott law fit parameters for DC conductivity at low temperatures

OLC size	Concentration (vol.%)	σ_{dc0} (mS/m)	T_M (K)	n	f_∞ (kHz)
250 nm	10	2.13	122	1.15	25
	8	0.01	117	1.09	0.89
100 nm	8.9	1.45	61	0.9	224
	7.1	0.43	57	1.02	67
40 nm	6.8	0.012	69	1.16	3.1

The value of n is close to 1 for all investigated composites, and this is typical for pure OLC powder [63]. Thus, electrical transport in OLC/PDMS composites occurs via electron tunneling between OLC aggregates and a quasi-one-dimensional hopping inside the OLC clusters.

4.1.2 OLC/PU composites

SEM images of OLC/PU composites with different aggregate sizes are presented in Fig. 4.12. It can be concluded that OLC particles are well dispersed in all cases, since all areas strictly look equal, without obvious aggregation or depletion at any place.
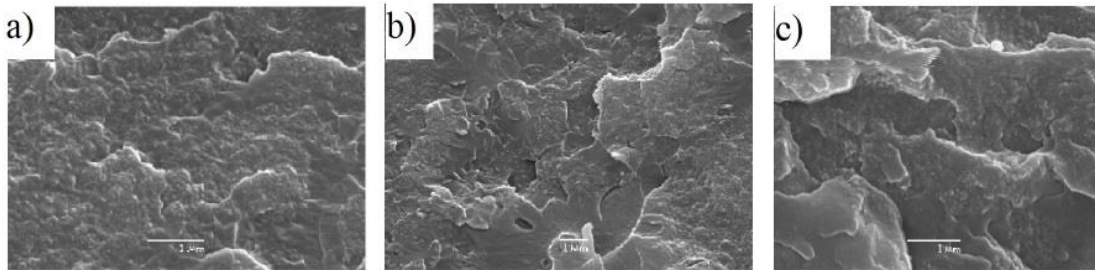

Fig. 4.12. SEM images of composite films based on polyurethane matrix filled with: a) 14 vol. % of OLC of aggregate size 100 nm, b) 11 vol. % of OLC of aggregate size 40 nm; c) 3.5 vol. % of OLC of aggregate size 100 nm [84]

The frequency dependence of dielectric permittivity and electrical conductivity for 100 nm aggregate size OLC/PU composites are presented in Fig. 4.13.
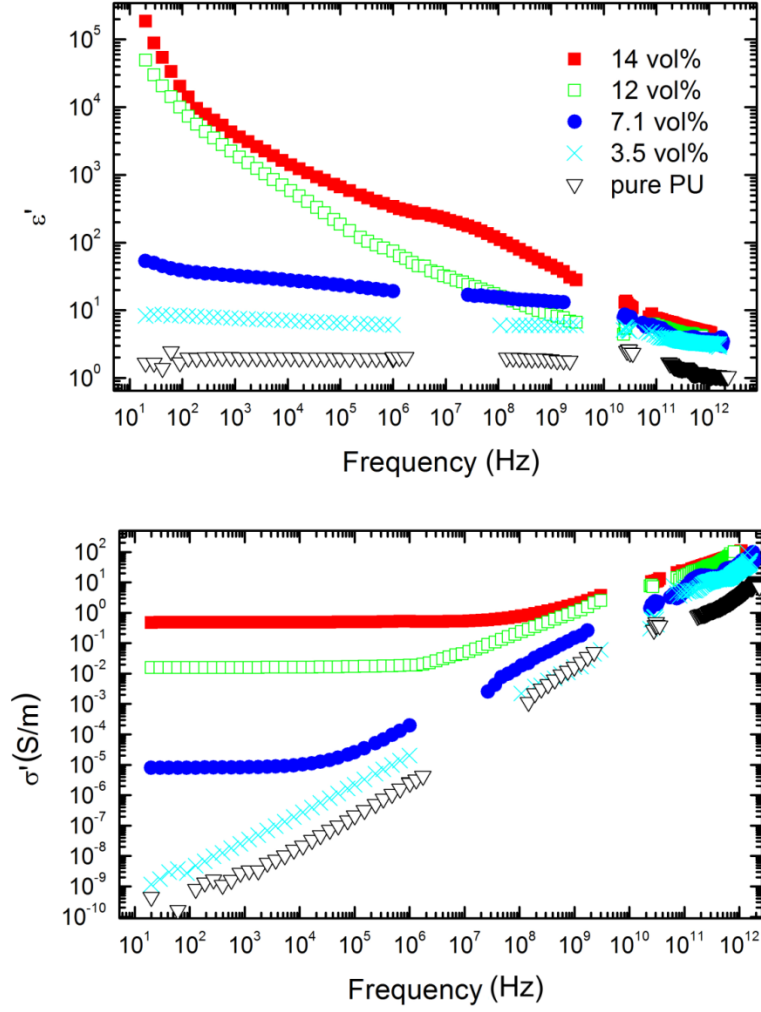
Fig. 4.13. Frequency dependencies of real parts of complex dielectric permittivity and electrical conductivity of OLC/PU composites with 100 nm OLC inclusions at room temperature

The dielectric permittivity of composites with 3.5 vol. % of OLC inclusions and PU without inclusions is very low (less than 10) and almost constant in a wide frequency range, while the electrical conductivity of these materials strongly increases with frequency and no DC conductivity can be observed. Dielectric losses (which are strongly related with electrical conductivity) of these materials are also very low and caused by PU molecules dynamics [71]. Above an OLC concentration of 7 vol. %, the dielectric permittivity starts decreasing with frequency, where a constant conductivity can be observed at low frequency (DC conductivity), as well as two different dielectric dispersions obviously related to Maxwell-Wagner relaxation [85].

The concentration dependence of both dielectric permittivity and electrical conductivity for different OLC aggregate sizes is presented in Fig. 4.14. The electrical conductivity values were selected at 129 Hz frequency, since above the percolation threshold those values correspond to the DC conductivity. The percolation threshold in composites with large (100 nm) OLC aggregates is close to 7.1 vol. % concentration, while similar considerations of composites with small (40 nm) OLC aggregates allowed determining the percolation threshold value close to 5.4 vol. %. Assuming that chains of carbon onions arranged in a pearl necklace structure are formed in the composite it is expected that aggregates based on small-sized OLC are more easily deformable, leading to more elongated aggregates in the polymer and hence to a lower percolation threshold. The percolation threshold value close to 5.4 vol. % for 40 nm OLC is slightly lower than the percolation threshold observed in OLC/PDMS composites for the same aggregate size. The huge values of dielectric permittivity and electrical conductivity in the microwave range (for example at 30 GHz) of composites above the percolation threshold indicate that those composites are suitable for electromagnetic shielding.
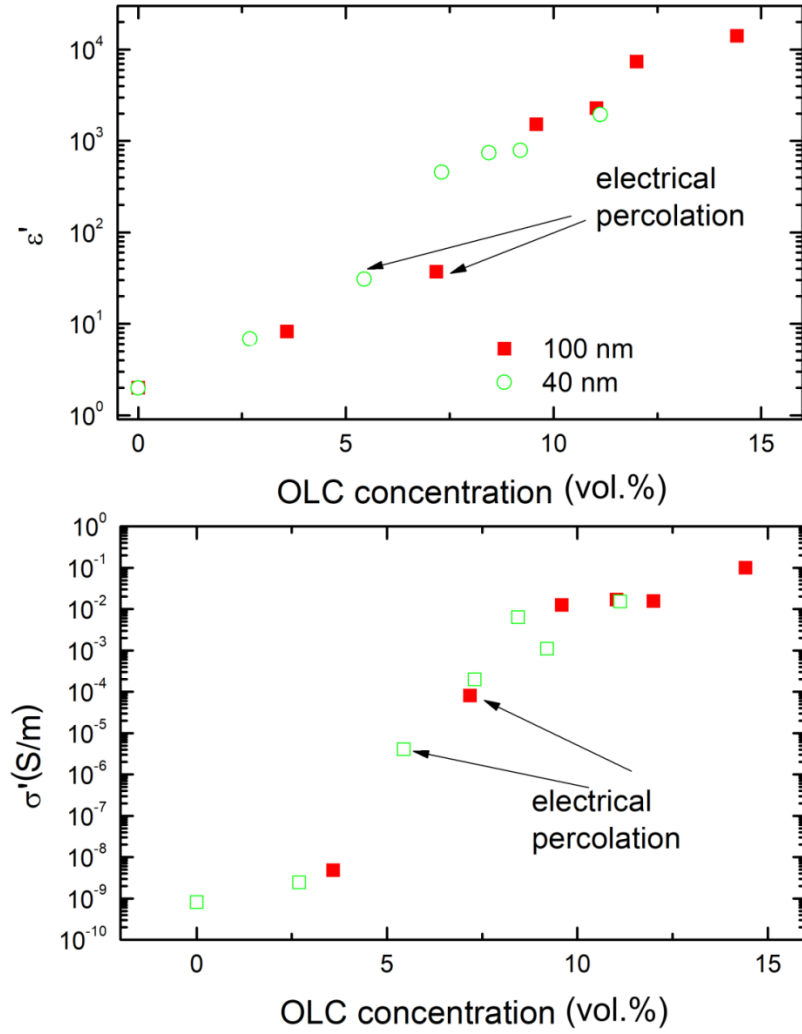
Fig. 4.14. Concentration dependencies of real parts of complex dielectric permittivity and electrical conductivity of OLC/PU composites for different aggregate size at frequency at room temperature

Frequency dependencies of the electrical conductivity of composites with 7.1 vol. % of OLC at different temperatures are presented in Fig. 4.15. At low frequency, and as expected just above the percolation threshold, a frequency-independent plateau (DC conductivity) is observed but at higher frequency the conductivity increases as a power law of frequency. On cooling, the DC conductivity decreases and the changes of conductivity behaviour can be fitted by Jonscher's equation.
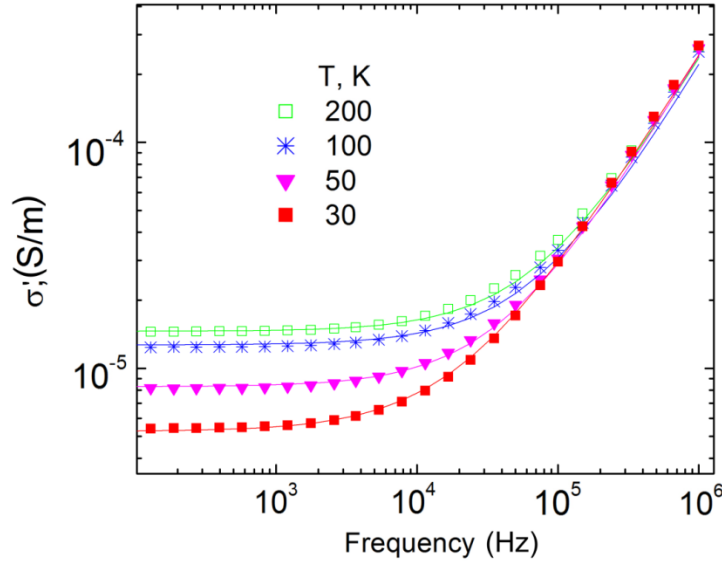
Fig. 4.15. Frequency dependence of real part of complex electrical conductivity of OLC/PU (with 100 nm OLC inclusions at 7.5 vol. %) at different temperatures (low-temperature region

Below room temperature, the DC conductivity can be described by fluctuation-induced tunneling model (Fig. 4.16).
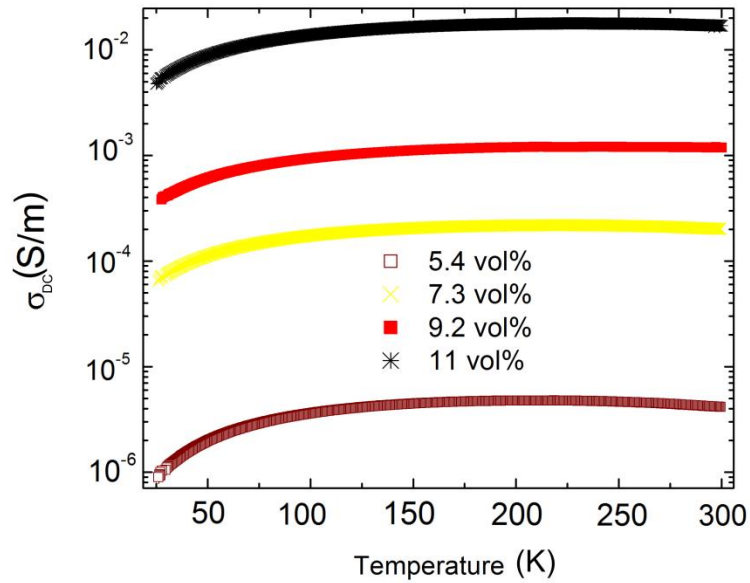

Fig. 4.16. Temperature dependence of DC conductivity for OLC/PU composites below room temperature

However, at even lower temperatures, typically below 100 K, Mott's law describes also quite well the temperature dependence of the electrical conductivity.
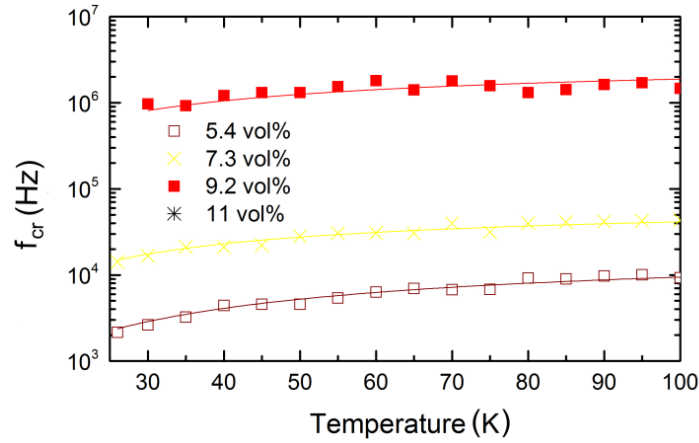
Fig. 4.17. Temperature dependence of critical frequency of OLC/PU composites in the low-temperature region. Solid ines are the fits of Mott's law

The corresponding parameters of tunneling model and Mott's law fits are gathered in Table 4.4. It can be seen that the values of σ_0 derived from both fits to the experimental data are quite consistent with each other.

Table 4.4. Tunneling fit and Mott's law fit parameters for DC conductivity at low temperatures.

OLC size (nm)	Concentration (vol. %)	Tunneling fit parameters			Mott's law parameters			
		σ_{DC0}, (mS/m)	T_1 (K)	T_0 (K)	σ_0 (mS/m)	T_m (K)	n	ω_0 (kHz)
100	7.2	0.93	53	11	1.12	55	1.51	14
	9.5	16.9	36	7	17	31	1.24	268
	11	27	39	8	35.7	45	1.73	2213
	12	10.5	31	7	99	29	1.41	481
	14	250	36	8	254	29	1.09	-
40	5.4	0.006	63	3	25.73	78	1.35	21
	7.3	0.285	54	9	0.33	56	1.46	81
	8.4	8.18	58	6	9.28	54	1.12	830
	9.2	1.6	62	15	2	64	1.62	402
	11	22.7	53	7	25.73	54	1.37	-

The dimensionality for all composites is close to 0.5, which is typical for OLC particles obtained by annealing nano-diamonds at 1600 K [63]. Below 100 K, the critical frequency decreases on cooling according to the Mott's law (Eq. 2.25). According to Eq. 2.27 and Eq. 2.28 and assuming that both localisation length and attempt frequency don't depend on temperature and concentration, it can be concluded that the increase of critical frequency f_{cr} with OLC concentration seen in Fig. 4.17 is related to the decrease of AC hopping length, while the increase of critical frequency with temperature is related to the decrease of AC hopping length. Thus, the electrical transport in PU matrices filled with OLC of different aggregate sizes proceeds by electron hopping inside OLC clusters and by tunneling between clusters.

4.1.3 OLC/MWCNT/PU

Scanning electron microscopy (SEM) images of composites filled with onion-like carbon, carbon nanotubes and hybrid OLC/MWCNT filler are presented in Fig. 4.18.
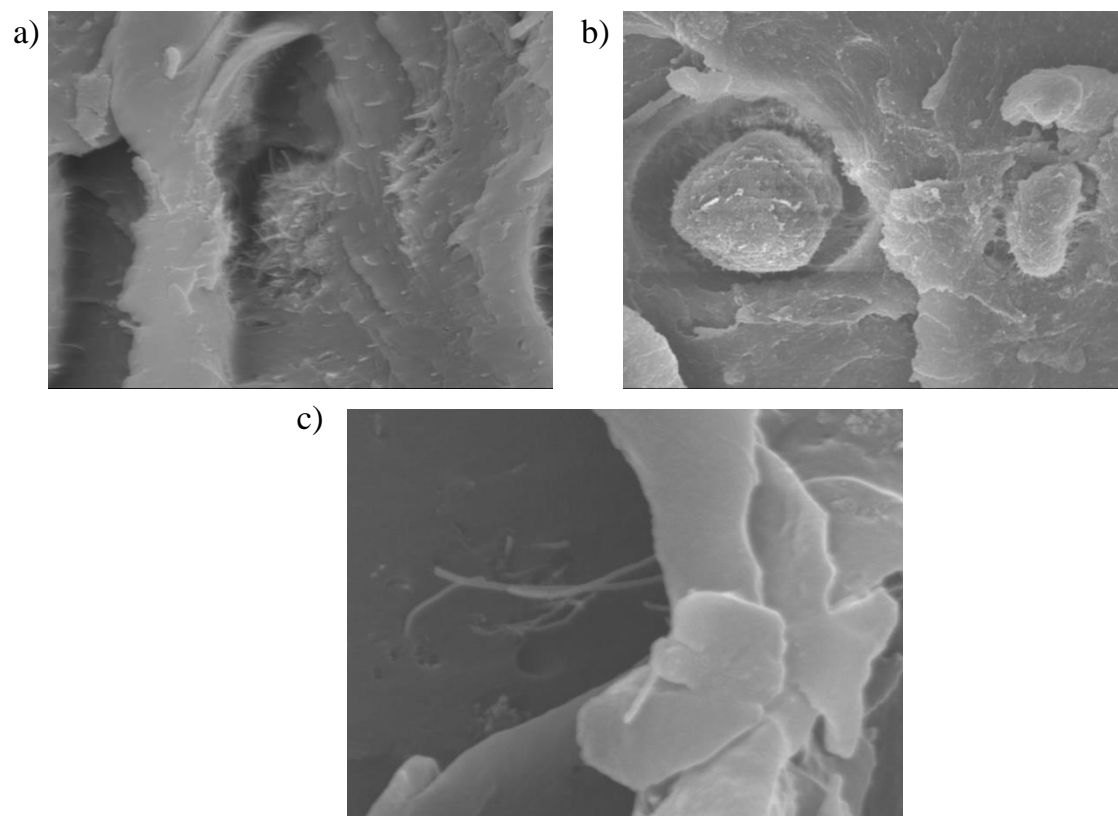

Fig. 4.18. SEM images of composites filled with: a) 2 wt.% of MWCNT, b) 2 wt.% of OLC and c) hybrid 2 wt.% of OLC and 0.5 wt.% of CNT [80]

All composites demonstrate good quality, with carbon inclusions being reasonably well dispersed. However, the best dispersion of particles is observed in hybrid filler MWCNT/OLC composites.

Frequency dependencies of the dielectric permittivity and electrical conductivity of hybrid filler composites with 0.5 wt.% of CNT and different concentrations of OLC and polyurethane are presented in Fig. 4.19.
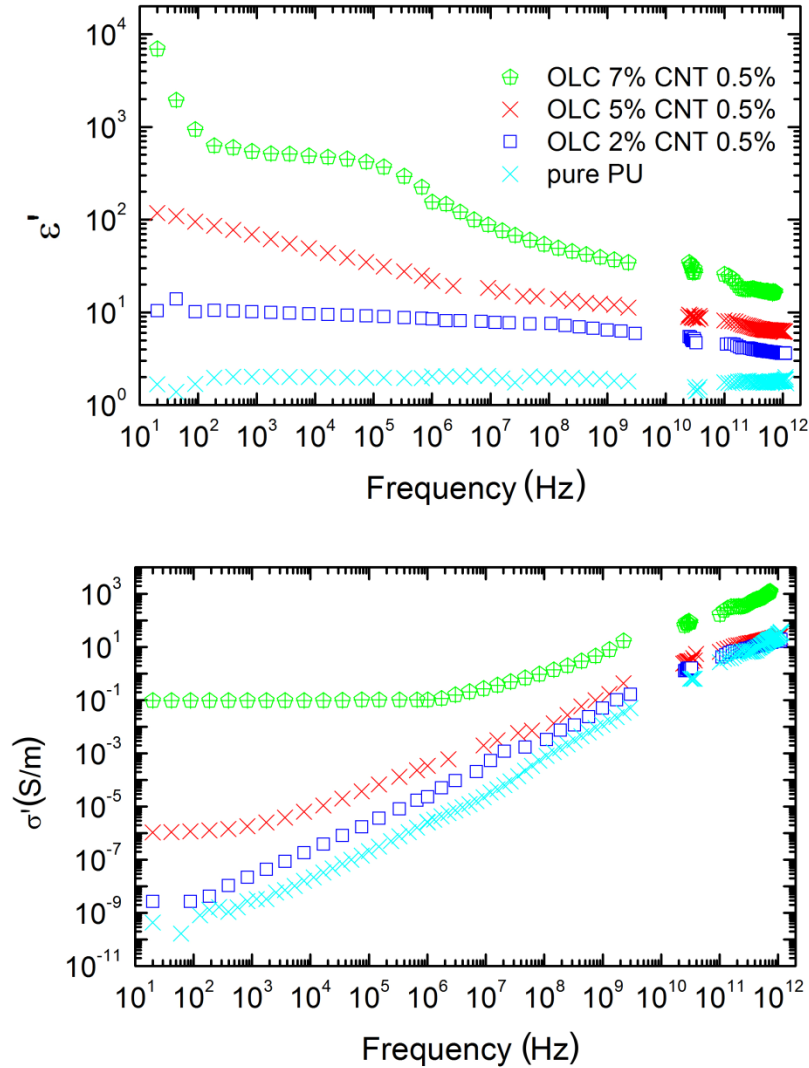

Fig. 4.19. Frequency dependencies of real parts of complex dielectric permittivity and electrical conductivity for composites with hybrid filler CNT/OLC inclusions at room temperature

The dielectric/electrical properties of composites filled with 2 wt.% of OLC and 0.5 wt.% CNT inclusions are similar to pure PU polymer properties. However, the values of dielectric permittivity and electrical conductivity for

composites filled with 5 wt. % of OLC and 0.5 wt. % of CNT are considerably higher (at low frequencies the value of dielectric permittivity is 100x higher, and the value of electrical conductivity is as high as 1 µS/m) and a frequency independent DC conductivity plateau is observed in the conductivity spectra. Thus, the percolation threshold in hybrid OLC/MWCNT composites is close to 5 wt. % OLC and 0.5 wt. % of MWCNT. In contrast, the values of dielectric permittivity and electrical conductivity for the composites with only 5 wt. % of OLCs are $\varepsilon'=16$, $\sigma=6.5 \cdot 10^{-9}$ S/m and for the composites with only 0.5 wt.% CNTs are $\varepsilon'=4.5$, $\sigma=2.5 \cdot 10^{-9}$ S/m at room temperature and frequency 129 Hz. Therefore, the synergy effect is clearly observed in the composite containing a mixture of 5 wt. % of OLCs and 0.5 wt. % of MWCNTs. The value of the percolation threshold in PU filled with OLC inclusions was substantially higher – 7 wt. %.

According to the excluded volume theory, the hybrid filler composites should obey the Eq. 2.33 [62]. For the investigated composites with 5 wt. % of OLC and 0.5 wt. % inclusions, the equation transforms into the inequality $\frac{5}{7} + \frac{0.5}{x} < 1$, where x is greater than 2. Thus, the percolation threshold in hybrid filler OLC/MWCNT composites is lower than the value predicted by equation, and the synergy effect is evident.
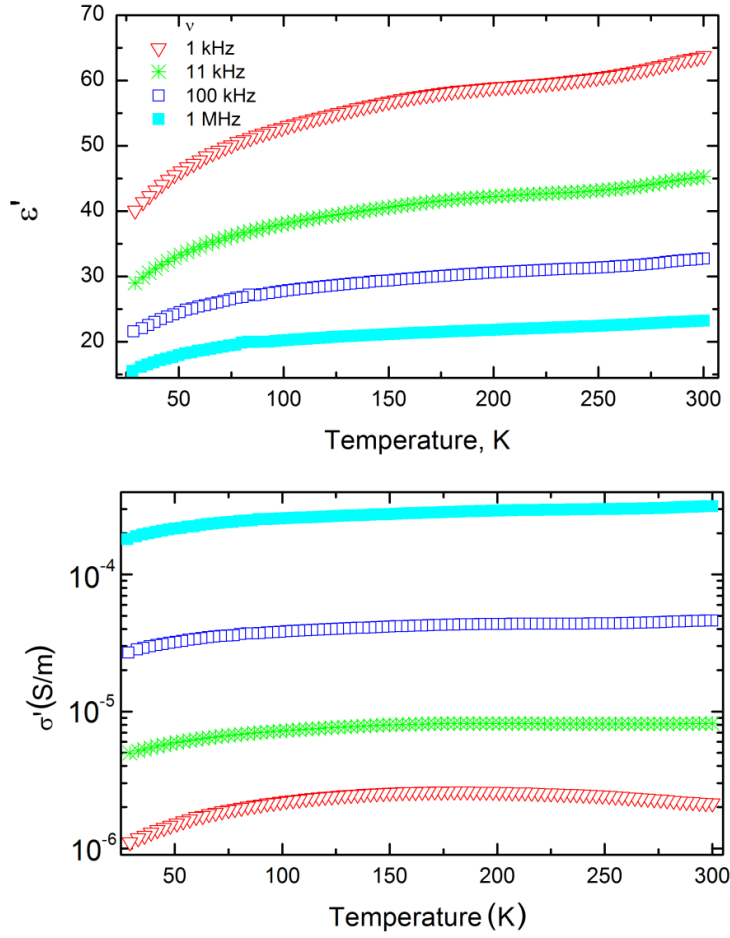
Fig. 4.20. Temperature dependencies of real parts of complex dielectric permittivity and electrical conductivity for composites with 5 wt. % of OLC and 0.5 wt. % of MWCNT inclusions.

At low temperatures, both the dielectric permittivity and the electrical conductivity decrease in OLC/MWCNT/PU composites (Fig. 4.20). However, the most pronounced reduction occurs at temperatures below 100 K. A similar behaviour was observed in other OLC/MWCNT/PU and OLC/PU composites and is in a good agreement with the data presented in the literature for composites with nanocarbon inclusions [87]. Electrical conductivity spectra follows Jonscher's equation and the DC conductivity data fit well to the fluctuation induced tunneling model (Fig. 4.21). All tunneling model fitting parameters are presented in Table 4.5.
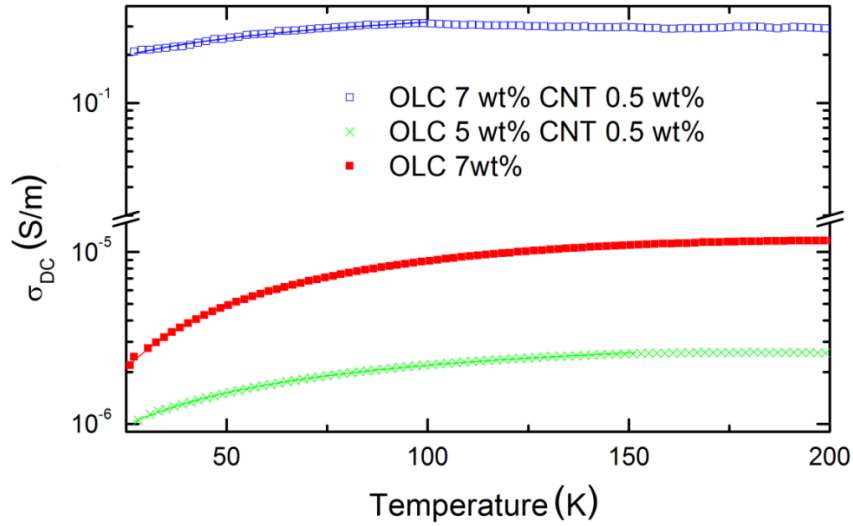
Fig. 4.21. Temperature dependence of DC conductivity of composites with various nanocarbon inclusions. Solid lines are the fits of tunneling model

Table 4.5. Tunneling model fit parameters

Inclusions	$T_1(K)$	$T_0 (K)$	$\sigma_0 (S/m)$
7 wt.% of OLC	88.4	15.2	$1.9 \cdot 10^{-5}$
5 wt.% of OLC and 0.5 wt.% of CNT	76.7	29.9	$3.99 \cdot 10^{-6}$
7 wt.% of OLC and 0.5 wt.% of CNT	63.5	44.7	0.49

The T_1/T_0 values are lower for the hybrid filler composites in comparison to single filler OLC composites. That could be explained by the better distribution of carbon inclusions in hybrid OLC/MWCNT filler composites and the lower interparticle distance these composites.

Summary

The lowest percolation thresholds were observed for composites with the smallest size of the OLC aggregates (~40 nm) for both PDMS and PU composites, 6.8 vol. % and 5.4 vol. % respectively. The 40 nm size OLC particles are more likely to be deformed, leading to more elongated aggregates in the polymer and hence to a lower percolation threshold. The electrical percolation occurs mainly due to electron tunneling between OLC clusters. The electrical properties of the composites above the percolation are mainly governed by electron tunneling between OLC clusters and electron hopping in quasi-one-dimesnional chains inside clusters.

High values of the dielectric permittivity and the electrical conductivity of the composites above the percolation are similar to the values for carbon nanotubes and that indicate OLC based composites suitability for electromagnetic shielding applications. In addition, PDMS composites can be useful in various electronic applications as a soft flexible material with high dielectric permittivity and electrical conductivity values in a wide frequency range. At higher temperatures the transition into the insulator state occurs, due to the very different thermal properties of the PDMS polymer matrix and OLC particles. The transition temperature increases with the OLC aggregate size and concentration.

Since the dielectric properties of composites with OLC inclusions are very attractive, they can be improved by addition of small amounts of MWCNTs due to the strong synergy effect. In composites with hybrid OLC/MWCNT inclusions, the dielectric permittivity and the electrical conductivity increase due to the reduction of the average distance between nanocarbon clusters.

4.2 MWCNT/PMMA composites

Depending on the CNT concentration and the type the values of the dielectric permittivity, the electrical conductivity and the loss tangent of composites filled with the CNT can be very different, and that is very important for composite applications, for example, as electromagnetic shielding or dissipation coatings [87]. Nevertheless, the most investigations of composites filled with the CNTs are performed only at room temperature and in narrow frequency range [74]. Although, the concentration dependence of dielectric permittivity and electrical conductivity of MWCNT composites were investigated in broad frequency range [88, 89], but the impact of the MWCNT's aspect ratio on composite broadband dielectric properties is still unclear.

It is very important to study the composites produced under the same preparation conditions with the difference only in the nanotubes length. In this section the investigations of the influence of the carbon nanotubes length and surface compound on composite broadband (20 Hz – 1 THz) dielectric and electrical properties in a wide temperature range will be presented and discussed.

Composites contain PMMA matrix, which is thermoplastic polymer with a glass transition temperature around 380 K and different length of MWCNT:

1. The nanotubes length 20-50 μm MWCNT – "long" MWCNT,
2. The mean length 328±20 nm – "short" MWCNT,
3. The mean length 438±20 nm – "medium" MWCNT,
4. The mean length 335±20 nm – "OX-medium" MWCNT (MWCNTs were additionally oxidized),

while diameter for all nanotubes were d=9 nm and the concentration of MWCNT were 0.25 – 4 wt. %.

For SEM analysis composite films were broken at 77 K in order to decrease the PMMA elasticity. In order to avoid charging effects, composites were gold coated with the layer thickness of 6–8 nm [90].
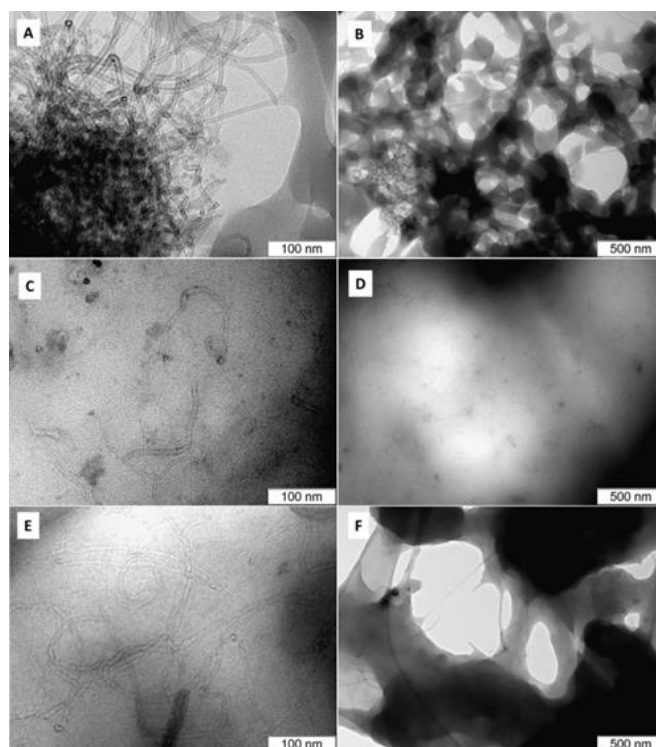
Fig. 4.22. TEM images of composite powders: A,B – "long" MWCNT /PMMA 1.0 %; C, D – "short" MWCNT/PMMA 1.0 %; E,F – "OX-medium" MWCNT/PMMA 1.0 % [90]

TEM study of the composite powders produced with "long" MWCNT before hot pressing demonstrates non-uniform distribution of nanotubes on PMMA surface. Polymer nanotubes are not fully covered with polymer. Both covered and "naked" nanotube surface areas are observed. The diffusion of polymer species inside the nanotube tangle is also limited. MWCNT agglomerates of several microns in size, which were not disintegrated by ultra-sonication, and areas of the nanotube surface without any polymer species were observed (Fig. 4.22 a, b). Melting of the PMMA/MWCNT powder allows the polymer molecules penetrate inside the MWCNT aggregates. Nevertheless, a non-uniform distribution of MWCNT was obtained. Thus, SEM study of composite breaks demonstrates areas of high and almost negligible concentration of the nanotubes (Fig. 4.23, marked with dotted lines).
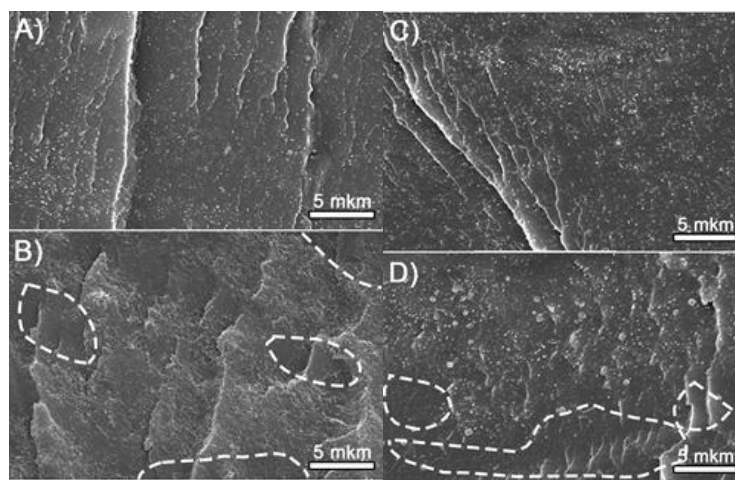
Fig. 4.23. SEM images of the composite film breaks obtaned after cracking at liqiud nitrogen temperature. Brigth fragments (dots or villus are attributed to nanotubes): a) – "short" MWCNT/PMMA 2.0 wt.%, b) "long" MWCNT/PMMA 2.0 wt.%, c) "OX-medium" MWCNT/PMMA 2.0%, d) "medium" MWCNT/PMMA 2 wt.%. Dotted lines demonstrate the regions with the negligible concentration of the nanotubes [90]

Composites with "medium" MWCNT inclusions demonstrate the intermediate distribution of carbon nanotubes in polymer. Although, no big agglomerate structures were observed, but areas with the almost negligible concentration of nanotubes were observed in the composite breaks (Fig. 4.23 d, marked with dotted lines).

The frequency dependence of the real parts of the complex dielectric permittivity and the complex electrical conductivity with different concentrations of „short" MWCNT at room temperature is presented in Fig. 4.24. The values of the dielectric permittivity and the electrical conductivity of composites with 0.25 wt. % inclusions are quite low and are similar to the PMMA polymer matrix properties. In contrast, at higher MWCNT concentrations the value of the dielectric permittivity is high enough (higher as 10^3 for composite with 4 wt. % inclusions) and the frequency independent conductivity plateau is observed in the frequency dependence of the electrical conductivity.
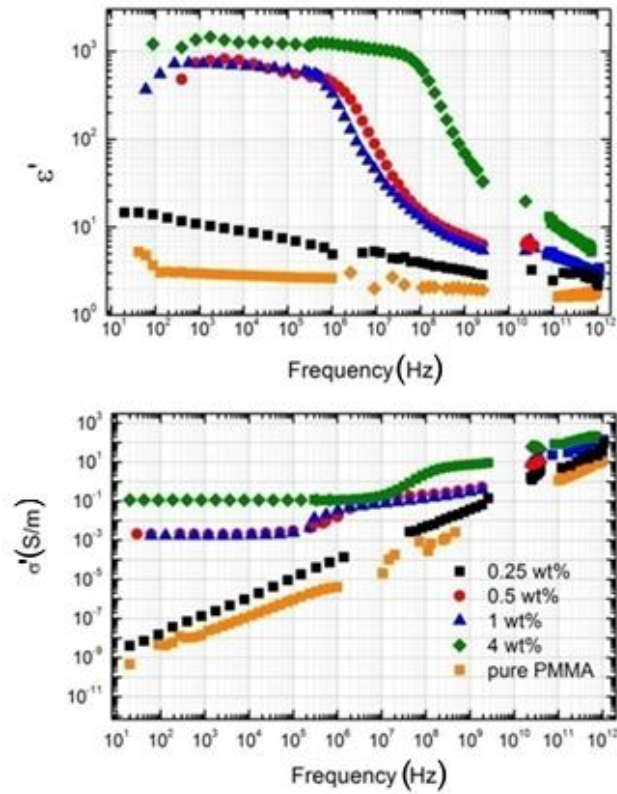
Fig. 4.24. Frequency dependencies of real parts of complex dielectric permittivity and electrical conductivity for composites with different concentrations of "short" MWCNT inclusions at room temperature

The percolation threshold of composites with „short" MWCNT is close to 0.5 wt.%. In all other studied composites at different MWCNT concentrations the electrical percolation also occurs. The percolation threshold can be easily established from the concentration dependence of the dielectric permittivity and the electrical conductivity, indeed close to the percolation threshold the values of both parameters increase rapidly (Fig. 4.25) and a typical DC conductivity plateau is observed in the frequency dependence of the conductivity (not shown). By this way it was established that the percolation threshold in composites with "ox-medium" and "long" MWCNT is a range from 1 wt. % to 2 wt. %, in composites with "medium" MWCNT is in a range from 0.5 wt. % to 1 wt. %. The small decrease in the DC conductivity and the dielectric permittivity when the concentration of the "shortest" MWCNT increases from 0.5 wt. % to 1 wt. % is related to the local fluctuation of the

74

CNT distributions [91]. Thus, the percolation threshold decreases with the mean MWCNT length.
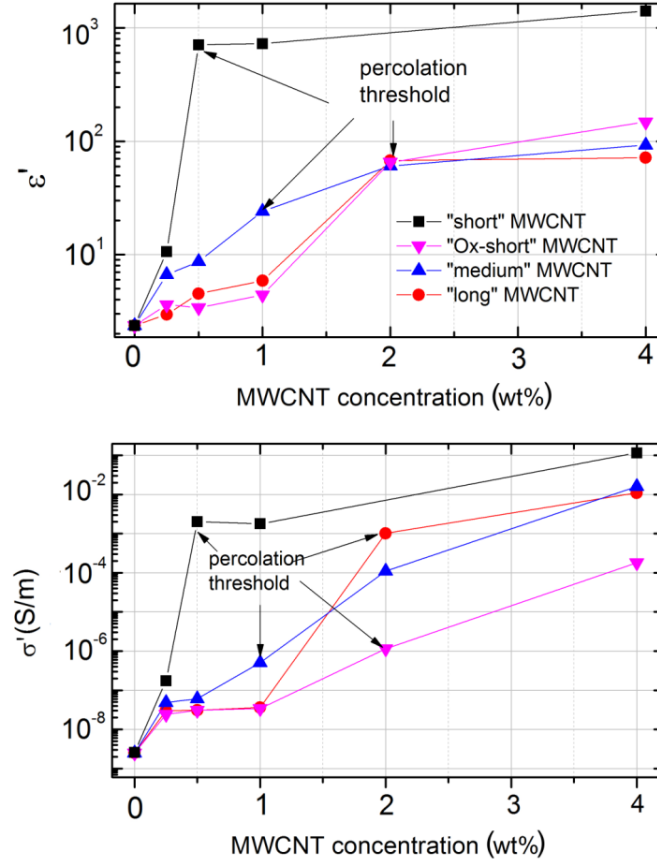

Fig. 4.25. Concentration dependencies of real parts of the complex dielectric permittivity and the electrical conductivity for all composites at room temperature

Firstly, it should be admitted that the percolation threshold values for composites with the threaded MWCNT are close to the values predicted by the excluded volume theory. Secondly, for the „short" MWCNT it was proposed another model for the percolation threshold [92, 93]:

$$\varphi_c = \frac{9H(1-H)}{-9H^2 + 15H + 2}$$

where H is related with the aspect ratio in the following way:

$$H(p) = \frac{1}{A^2 - 1} \left[\frac{p}{\sqrt{A^2 - 1}} \ln(A + \sqrt{(A^2 - 1)} - 1 \right]$$

According to these equations the percolation threshold is almost independent of the aspect ratio when the aspect ratio is in the range from 20 to 100, so it should be for composites with not threaded MWCNT. However, usually composites comprise individual, perfectly dispersed carbon nanotubes and the agglomerates of carbon nanotubes. Therefore, if the volume fraction of agglomerated MWCNT is different in composites with different aspect ratio MWCNT, the percolation threshold can be lower in composites with „short" MWCNT. This assumption is also supported by SEM investigations. Moreover, below the percolation threshold the values of the dielectric permittivity and the electrical conductivity are also the highest for composites with the „short" nanotubes and decrease with the mean MWCNT length. The effect is related with the fact that the dielectric permittivity and the electrical conductivity close to the percolation threshold increase according to the power law [94]. Thus, in all composites below the percolation threshold, the lower percolation threshold value is accompanied by the higher value of the dielectric permittivity and the electrical conductivity. In contrast above the percolation threshold the dielectric permittivity value of all composites is very similar, except composites with the „short" MWCNT where the dielectric permittivity and the electrical conductivity values are the highest.

The frequency dependencies of the complex dielectric permittivity for the composite with the „short" MWCNT inclusions at different temperatures and temperature dependence of relaxation time below percolation threshold are presented in Fig. 4.26. The position of the maximum of imaginary part of dielectric permittivity is temperature dependent and shifts to higher frequencies. A broad dielectric dispersion is observed in temperature range from 360 K to 380 K and could be related with the β relaxation processes in the PMMA matrix [95]. At higher temperatures (above 370 K) an increase in the complex dielectric permittivity is related with the electrical conductivity effects. For all other investigated composites below the percolation threshold the values of the complex dielectric permittivity are similar to PMMA matrix properties.
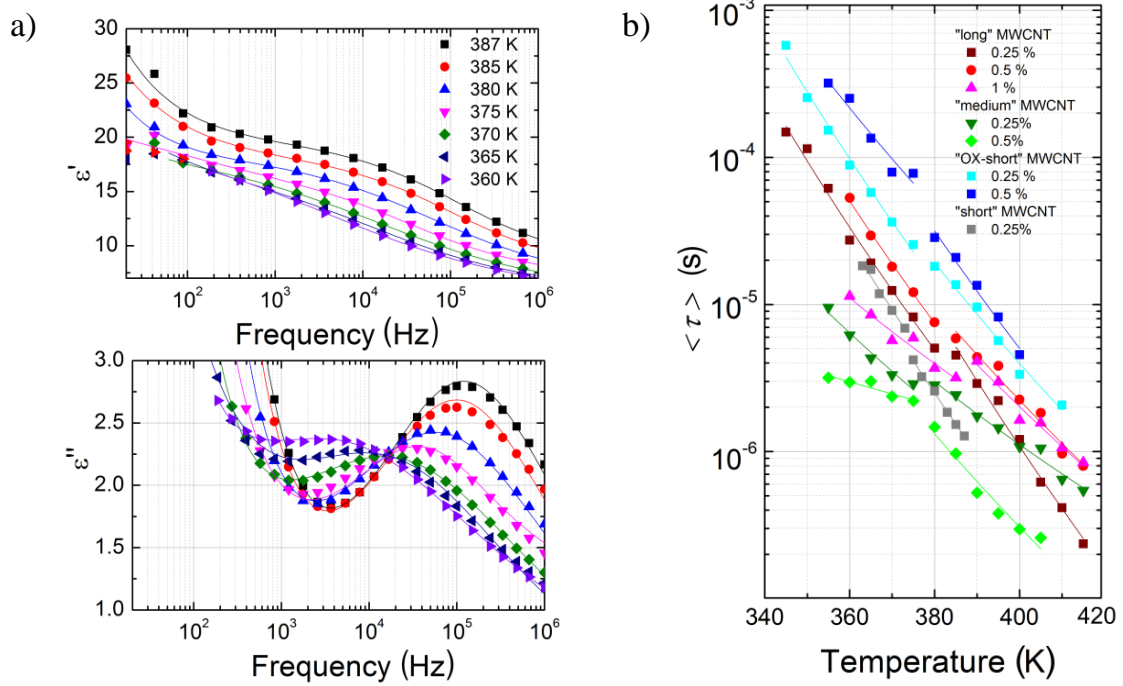
Fig. 4.26. a) Frequency dependence of the complex dielectric permittivity for the composites with the „short" MWCNT inclusions. The MWCNT concentration is 0.25 wt. % (below the percolation threshold). Solid lines are fits of the Havriliak-Negami equation; b) Temperature dependence of the mean relaxation time for all investigated composites below the percolation threshold. Solid lines are the fits of the Arrhenius law

Frequency dependencies were analysed by using Havriliak-Negami equation. The value of mean relaxation time is the lowest in composites with the shortest nanotubes and for the composites with higher MWCNT concentration (Fig. 4.26 b). The temperature dependence of the mean relaxation time fits Arrhenius law. The mean relaxation time has a change in the slope close to the glass transition temperature (~380 K) [96]. Therefore, the mean relaxation time fits Arrhenius law separately below and above the glass transition temperature. The obtained parameters are presented in Table 4.6. Obtained values of parameters for PMMA without inclusions are in good agreement with the data presented in [96, 97]. In composites with non treated MWCNT the activation energy strongly decreases with decreasing MWCNT concentration.

Table 4.6. Arrhenius fit parameters for temperature dependence of mean relaxation time

MWCNT mean length	MWCNT concentration (wt.%)	Temperature region	τ_0 (s)	U (eV)
pure PMMA		$T<T_g$	$8.5 \cdot 10^{-17}$	0.95
		$T>T_g$	$2.86 \cdot 10^{-20}$	1.2
50 μm	0.25	$T<T_g$	$4.9 \cdot 10^{-21}$	1.1
		$T>T_g$	$4.9 \cdot 10^{-24}$	1.3
	0.5	$T<T_g$	$8.2 \cdot 10^{-21}$	1.1
		$T>T_g$	$1.9 \cdot 10^{-18}$	0.9
	1	$T<T_g$	$3.8 \cdot 10^{-14}$	0.6
		$T>T_g$	$1.4 \cdot 10^{-17}$	0.9
438 nm	0.25	$T<T_g$	$1.3 \cdot 10^{-15}$	0.7
		$T>T_g$	$8.1 \cdot 10^{-15}$	0.6
	0.5	$T<T_g$	$2.7 \cdot 10^{-9}$	0.6
		$T>T_g$	$2.8 \cdot 10^{-19}$	0.9
335 nm	0.25	$T<T_g$	$1.3 \cdot 10^{-20}$	1.1
		$T>T_g$	$3.7 \cdot 10^{-19}$	1
	0.5	$T<T_g$	$3.4 \cdot 10^{-17}$	0.9
		$T>T_g$	$3.5 \cdot 10^{-21}$	1.2
328 nm	0.25	$T<T_g$	$3.4 \cdot 10^{-22}$	1.2
		$T>T_g$	$1.4 \cdot 10^{-22}$	1.2

Above the percolation threshold all composites exhibit non-zero DC conductivity in the whole temperature range. The frequency dependence of electrical conductivity for composites with the „short" MWCNTs and concentration 0.5 wt. % at different temperatures is presented in Fig. 4.27.
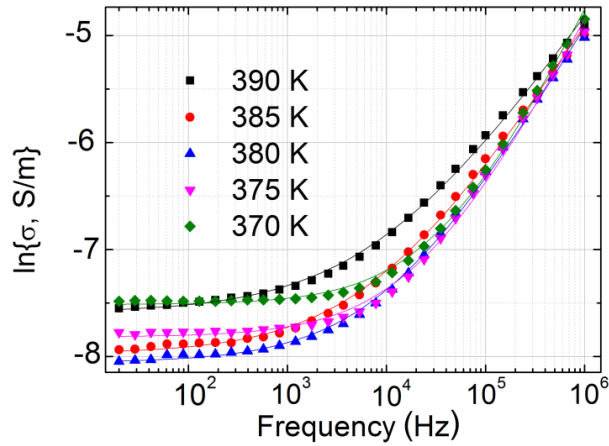
Fig. 4.27. Frequency dependence of real part of complex electrical conductivity of composites with „short" MWCNT inclusions at different temperatures (high temperature region), filler concentration is 0.5 wt.% (above percolation threshold). Solid lines are fits of Jonscher's equation

At low frequencies the conductivity is frequency independent (the DC conductivity) and at the higher frequencies the conductivity increases according to the power law (AC conductivity). The frequency dependence of the electrical conductivity was fitted with the Jonscher's equation [30]. The DC conductivity exhibit a different behaviour at low temperatures (below the room temperature) and at high temperatures (above the room temperature).
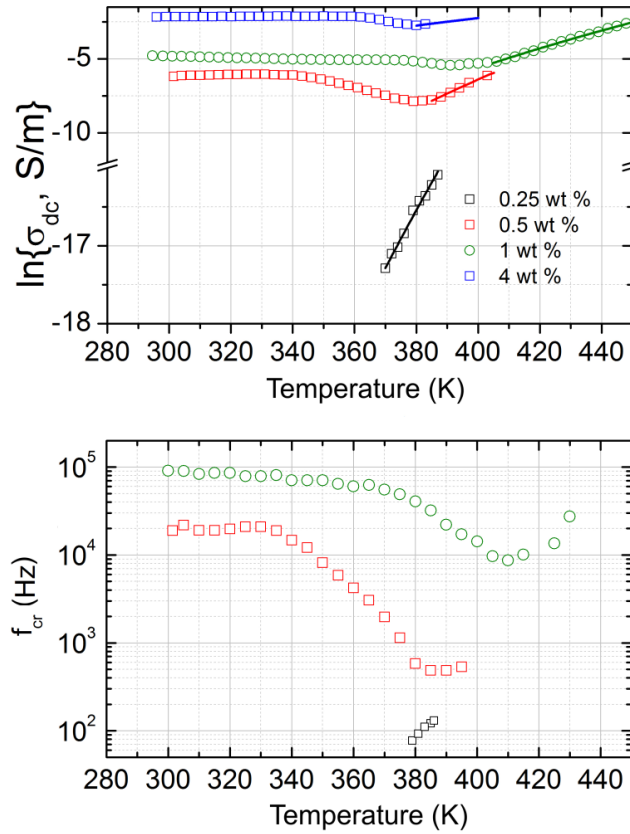
Fig. 4.28. Temperature dependencies of DC conductivity and critical frequency of composites with the „short" MWCNT inclusions (high temperature region)

Above room temperature the temperature dependence of the DC conductivity and the critical frequency have three different areas: 1) DC conductivity and the critical frequency are almost temperature independent at low temperatures, 2) the DC conductivity and critical frequency decreases with the temperature in intermediate temperature range, 3) the DC conductivity and the critical frequency increases with the temperature at higher temperatures. The decrease of the conductivity and the critical frequency is related with very different thermal properties of the PMMA matrix and the MWCNT. On heating the PMMA matrix suddenly expands, while the volume of MWCNT remains the same. In this way the average distance for charge carriers increase and the electrical conductivity decrease. At higher temperatures the electrical conductivity effects were observed even in the composites below the percolation threshold and also in PMMA. At these higher temperatures the conductivity of the composites above the percolation threshold increases due to

80

the finite polymer matrix conductivity. However, the DC conductivity for PMMA can not be determined, because it occurs below low frequency limit (20 Hz). The DC conductivity at these higher temperatures follows the Arrhenius law. Obtained activation energy values are summarized in Table 4.7. One can be concluded that the activation energy decreases with the MWCNT concentration above the percolation threshold. At the higher temperatures the electrical transport occurs due to the finite PMMA matrix conductivity and due to the tunneling between MWCNT clusters.

Table 4.7. Concentration dependence of DC conductivity activation energy

MWCNT mean lenght	MWCNT concentration (wt. %)	E_a (eV)
50 µm	2	0.92
	4	0.2
438 nm	1	1
	2	0.66
	4	0.21
335 nm	2	0.1
	4	0.33
328 nm	0.25	0.9
	0.5	1.3
	1	0.95
	4	0.33

The conductivity related with the electrical transport in the MWCNT network is weakly temperature dependent, at the same time the electrical conductivity of the PMMA matrix follows the Arrhenius law, similarly as in other polymers [98]. With the increasing MWCNT concentration the contribution of matrix conductivity to the total conductivity decreases and together temperature dependence of total electric conductivity becomes more flat. At low temperatures (below 200 K) the DC conductivity decreases according to the electrical tunneling model. Obtained parameters are listed in Table 4.8

Table.4.8 Concentration dependence of tunneling fit parameters.

MWCNT mean lenght	MWCNT concentration (wt. %)	$T_1, (K)$	$T_0 (K)$
328 nm	0.5	12	1
	1	36	19
	4	12	19
50 μm	2	47	40
	4	18	23
431 nm	1	58	19
	2	44	26
	4	25	35
335 nm	2	52	18
	4	35	12

The T_1/T_0 is proportional to the gap width w, which is approximately proportional to $p^{-1/3}$ [99]. Thus the ratio T_1/T_0 should decrease with the MWCNT concentration, and behaviour is observed in all investigated composites. Moreover, at the same nanotubes concentration this ratio is the highest in composites with "OX-medium" MWCNT inclusions, indicating the higher potential barrier for the electron tunneling.

Summary

The decrease in the length of the nanotubes improves the quality of their distribution in the polymer matrix. The strong adhesion between PMMA and the surface of the oxidized nanotubes decreases a number of nanotube interconnections. This, in turn, decreases the conductivity of the composite. Therefore, the percolation threshold is lower in the composites with the shortest nanotubes and the additionally oxidized nanotubes. The dielectric permittivity and the electrical conductivity are also higher in the composites with the shortest nanotubes. Below the percolation threshold the dielectric dispersion in composites is mainly related with the relaxation in the polymer matrix. The MWCNT type and the concentration have the huge influence on the polymer molecules dynamics - the relaxation time is shortest in composites with the higher nanotubes concentration. The conductivity of the composites

above the percolation threshold is governed by the electron tunneling between MWCNT clusters. At higher temperatures the electrical transport occurs also due to the finite electrical conductivity of the polymer matrix.

4.3 Graphite/epoxy composites

Carbon nanotubes based composites exhibit low percolation threshold and huge dielectric permittivity and electrical conductivity values in wide frequency range, including microwave and terahertz ranges. However, a drawback of carbon nanotubes is their higher cost in comparison with other carbon allotropes, such as carbon black or graphite. Another serious disadvantage is the possible toxicity of CNTs, which has been debated for long [100], and which is still controversial today. Such problem does not occur with considerably bigger carbon particles such as exfoliated graphite (EG) or other graphite forms.

The percolation threshold in EG-based composites can be very low, similar to that observed in polymer-CNT materials. Thus, EG can replace CNT in composites used as effective EMI shields [101, 102]. It means that exfoliated graphite, but maybe also other kinds of graphite such as artificial graphite particles with different particle sizes, could be interesting for electromagnetic (EM) applications in low and microwave frequency ranges.

At the present time, no consistent broadband dielectric investigations of EG and other graphite-based polymer composites exist in a wide temperature range. This motivated the present dielectric analysis along with microwave characterization of epoxy-graphite composites as an important step for manufacturing effective EM materials. The main idea was to systematize the experimental data in wide frequency range (20 Hz – 1 THz), including microwaves (26 – 37 GHz), at different temperatures (30 – 450 K), and to observe the influence of the graphite primary particle size, if any, on the dielectric properties of graphite-based composites.

Composite materials based on epoxy resin filled with various kinds of graphite particles: exfoliated graphite (EG), natural graphite (NG) artificial

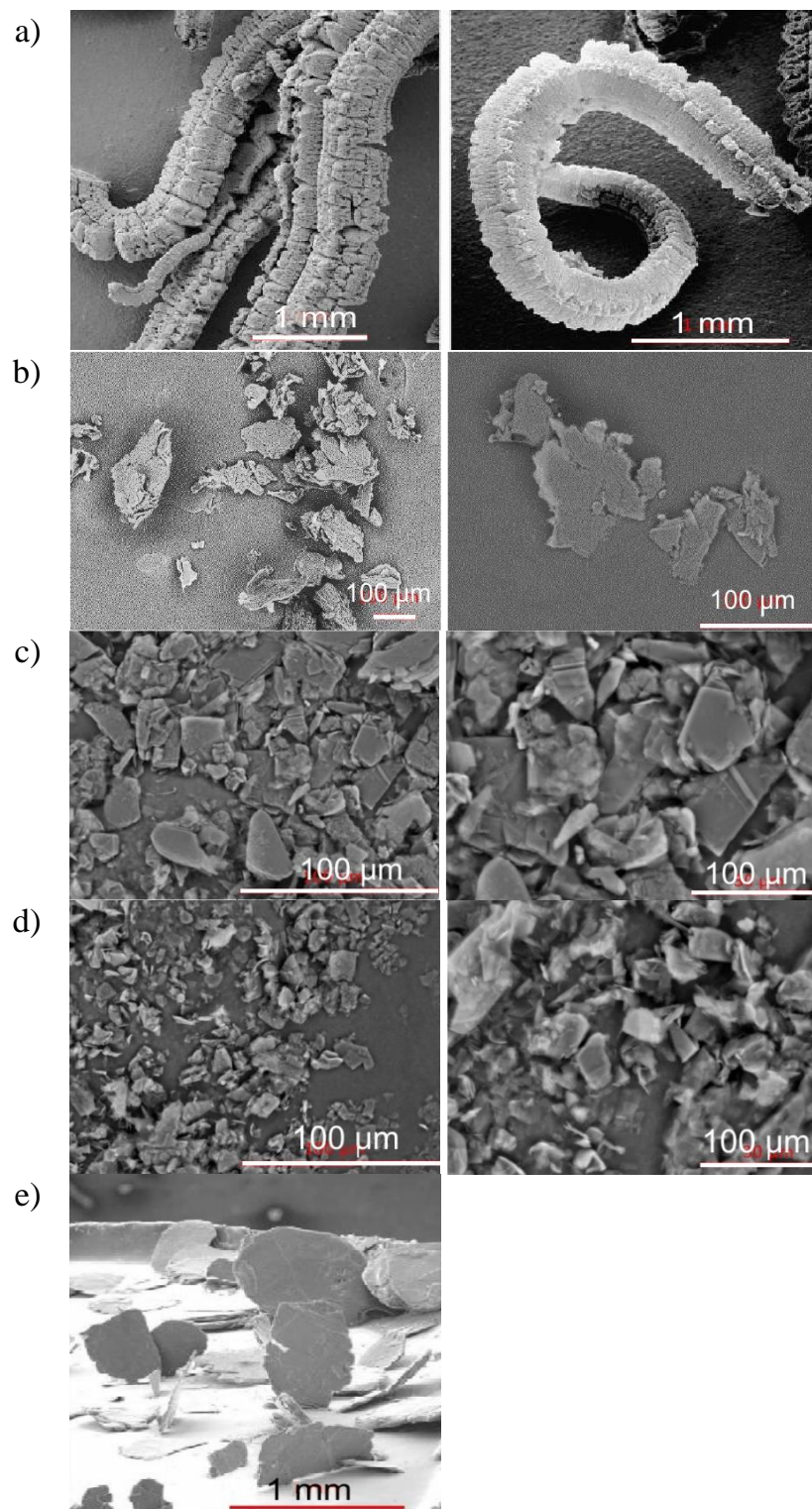graphite particles such as coarse (CG), medium (MG) and fine (FG) graphite were investigated (Fig. 4.29).

Fig. 4.29. SEM images of the graphite particles used as fillers in the present epoxy-graphite composites: (a) EG; (b) CG; (c) MG; (d) FG; (e) NG [103]

The graphite filler concentration is considered to be restricted to the range of relatively low concentration 0 – 2 wt. % at which the mechanical properties of graphite based composites are still high [104]. The homogeneity of composites was checked with scanning electron microscope (SEM) Helios NanoLab 650 [103]. For example, in Fig. 4.30 SEM image of composites with FG filler (concentration 2 wt. %) is presented in Fig. 4.30. Fabricated composite demonstrate good quality, with graphite inclusions being reasonably well dispersed.
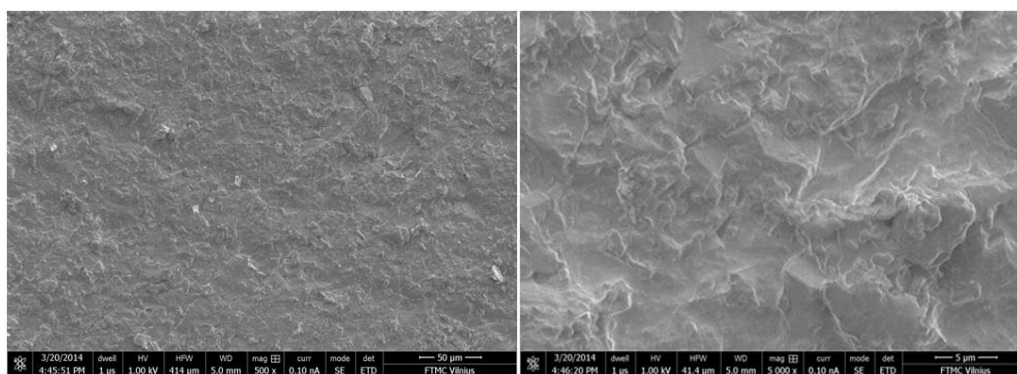

Fig. 4.30. SEM image of composites with FG filler (concentration 2 wt. %) [103]

The critical fraction or percolation threshold could be estimated from excluded volume theory[43] assuming that the filler particles are randomly dispersed in composite matrix getting the values from 22 wt. % to 32 wt. % depending on graphite particle size. The percolation threshold values are about one order of magnitude higher than the highest graphite loading used in composites, so that means that investigated composites are far below percolation threshold.

The percolation threshold of EG composites could be predicted assuming that EG are rod-like particles. However, it is uneasy due to particles' elongated shape and low density. EG particles do not behave as straight rods, they can be easily broken into several rod-like pieces 3 to 4 times smaller than their initial length during mixing with resin, and at the same time, their porosity is easily collapsed. In the present case, the EG particles were gently mixed with epoxy resin, so that only a fraction of the porosity was lost. EG particles behave as

small accordions [98], the loss of porosity corresponds to a decrease of length while the diameter remains constant. If x is the loss of porosity of EG particles, then particles' density is:

$$\rho_f' = \frac{\rho_G}{1 + (1 - x)\left(\frac{\rho_G}{\rho_f} - 1\right)}$$

$$\text{and } A' \approx (1 - x)A$$

where ρ_f' and ρ_f are the densities of the EG particles before and after having lost x % of porosity, respectively, ρ_G is the density of bulk graphite, 2.28 g/cm^3), and A and A' are the aspect ratio (length/diameter) of the EG particles before and after having lost x % of porosity, respectively. Thus, if for example 20, 50, 80 or 90% of the EG particles' porosity is lost during composite preparation, the critical concentrations of EG are 0.063, 0.201, 1.47 and 4.59 wt. %, respectively. As a final remark, the expected percolation threshold in EG based composites is much lower than the one obtained with other graphite particles mainly due to the very low density of the highly porous filler.

Frequency dependencies of complex dielectric permittivity of composites filled with 0.5 wt. % of different types of graphite particles at room temperature are presented in Fig. 4.31. The dielectric permittivity of graphite based composites increase with graphite particle size. A similar behaviour of dielectric permittivity is observed for all other concentrations. The effect is related to the lower percolation threshold for composites with bigger graphite particles. Indeed, according to percolation theory, ε' below the threshold [105] the universal critical exponent is close to 1.7 in three-dimensional systems.
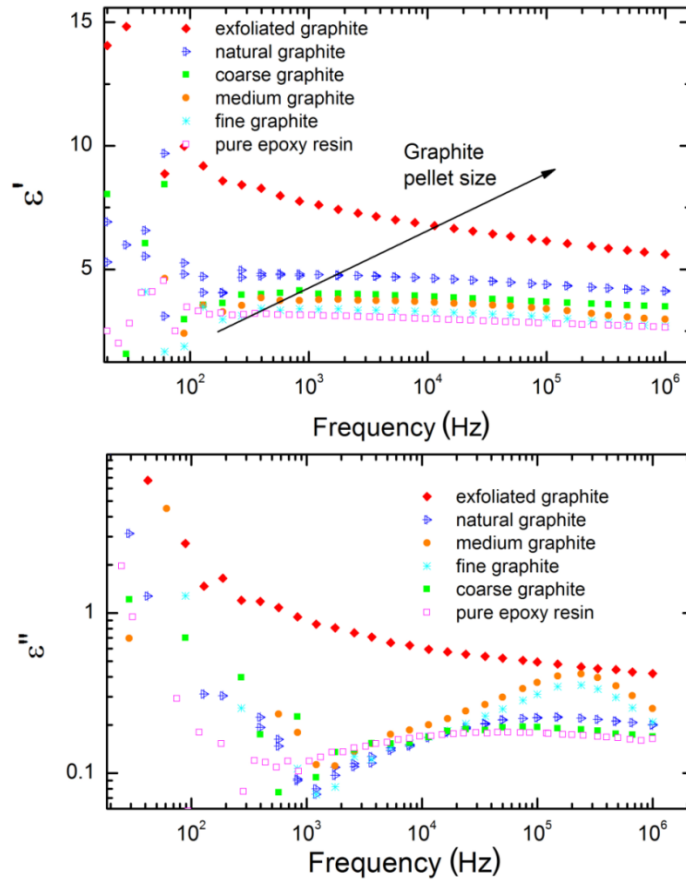
Fig. 4.31. Frequency dependences of complex dielectric permittivity of composites based on different graphite fillers at concentration 0.5 wt. % and at room temperature

The dielectric permittivity of composites also increases with increasing concentration of the filler. The frequency dependencies of complex dielectric permittivity of composites with different concentrations of NG and EG particles at room temperature are presented in Fig. 4.32 for the comparison.
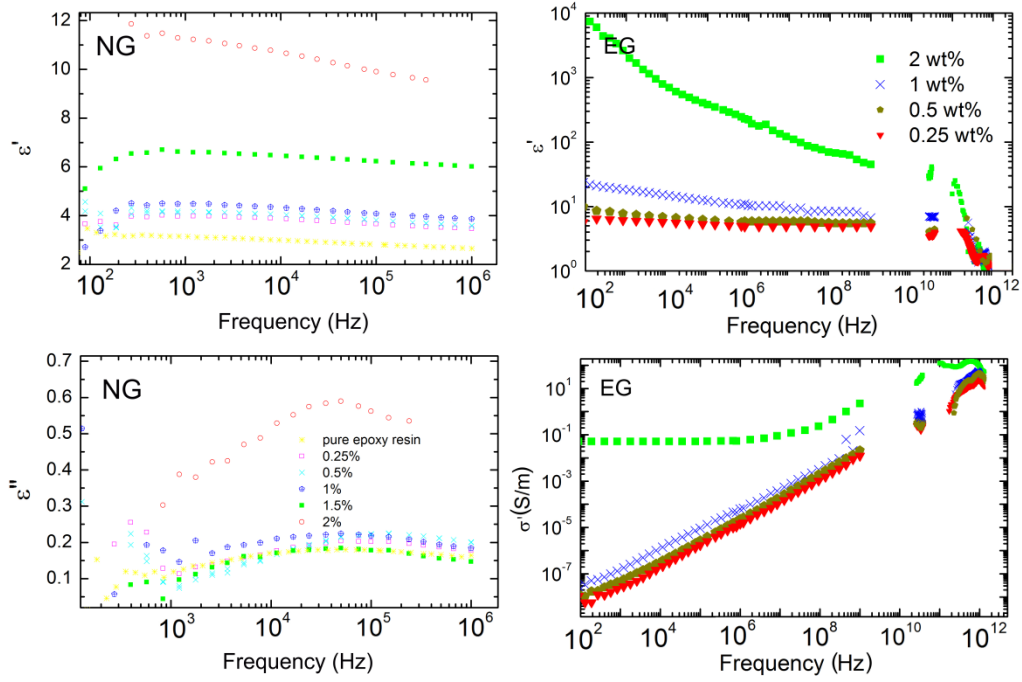
Fig. 4.32. Frequency dependencies of complex dielectric permittivity of composites with different concentrations of a) NG, b) EG fillers at room temperature (© 2015 IEEE)

The values of the real part of the complex dielectric permittivity for NG composites having filler concentrations up to 2 wt. % are low, as it does not exceed 12. Both real and imaginary parts of complex dielectric permittivity of composites are frequency-dependent, with a maximum of the imaginary part within the frequency range 10 – 100 kHz. A similar form of dielectric spectra with low values of complex dielectric permittivity at room temperature are observed for other composites with CG, MG, FG artificial graphites and also for the epoxy resin without carbon inclusions. Therefore, for these composites, the percolation threshold is also estimated to be higher than 2 wt. %. This finding also agrees with the expected percolation thresholds, which can be calculated either from percolation theory or from effective-medium theory, and are in the range 18 – 31 wt % depending on graphite particle size.

The values of complex dielectric permittivity of composites containing 1.5 wt. % and 2 wt. % of EG are very high (see Fig. 4.32). For example, below the frequency of 129 Hz, the dielectric permittivity of composites containing 2 wt. % of EG is almost 105 and the electrical conductivity is about 0.4 S/m. The

values of dielectric permittivity are very high even at microwave frequencies, for example, for composite filled with 2 wt. % of EG, $\varepsilon' = 45$ at 1 GHz. That indicates that the percolation threshold is between 1.0 and 1.5 wt. %. The obtained value of complex dielectric permittivity in microwave range is higher than the one previously reported for CNT composites above percolation threshold even with much higher nanotubes loading [106, 107]. This can be explained by the very flat frequency dependence of complex dielectric permittivity for EG composites and different nature of electrical transport in EG and carbon nanotubes composites. Microwave experiments show (Fig. 4.33) that the really effective additive for producing EMI shielding with epoxy resin – graphite composites is exfoliated graphite. Being embedded into epoxy at 2 wt. % (which is above percolation threshold), EG provides almost 100 % of EM attenuation due to 30 % absorption of microwave power and 70 % reflection.
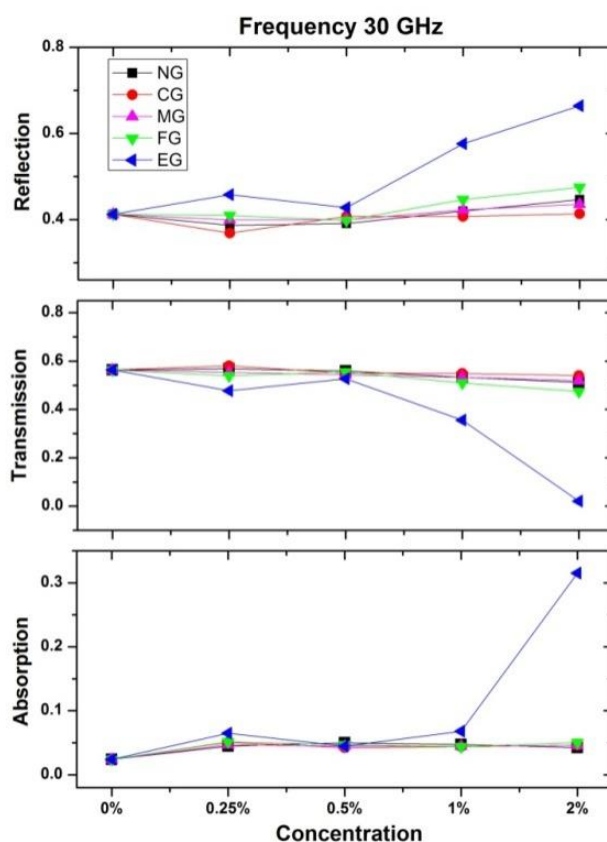

Fig. 4.33. Concentration dependencies of absorption-transmission-reflection of epoxy/graphite composites at 30 GHz. The thickness of free standing samples is 1.4 mm

For analysing more in-depth the dielectric dispersion in composites, the temperature dependencies of the complex dielectric permittivity has been investigated. The temperature dependencies of complex dielectric permittivity at different frequencies of the composite with 1.5 wt. % of NG filler is presented in Fig. 4.34. The imaginary part of complex dielectric permittivity exhibits a frequency-dependent maximum at low temperatures, which is progressively shifted towards higher temperatures when the frequency increases. At the same time, the real part of complex dielectric permittivity shows dispersion. The similar dielectric dispersion caused by polymer chain dynamics was observed in pure epoxy and is known to be related to α transition [108]. At temperatures above 350 K, the complex dielectric permittivity increases due to the onset of electrical conductivity.
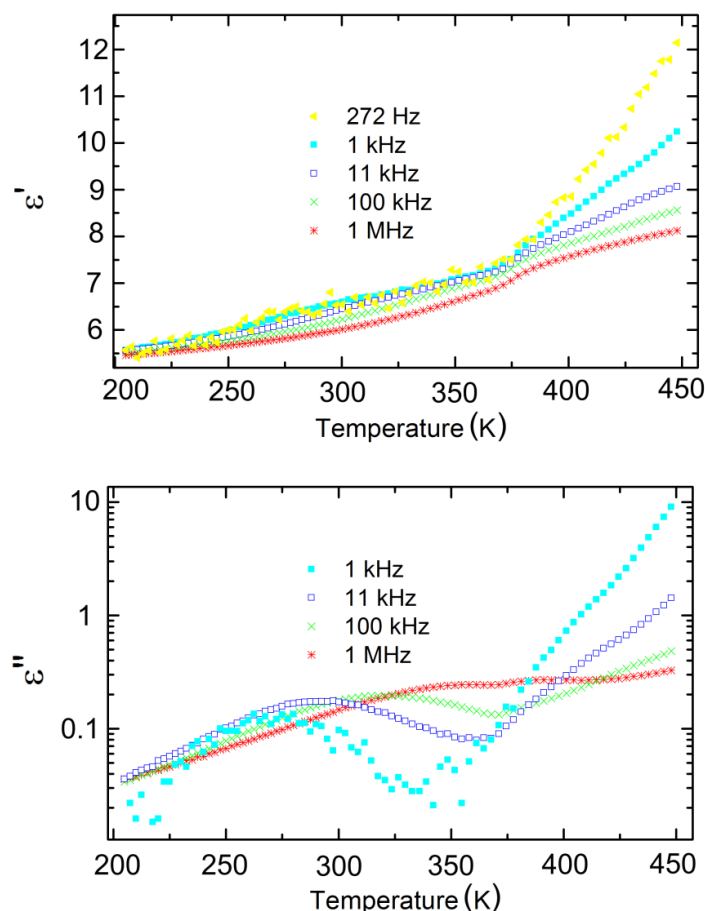

Fig. 4.34. Temperature dependence of complex dielectric permittivity of composites with NG filler (concentration 1.5 wt. %) at different frequencies

The frequency dependencies fit Havriliak-Negami equation (Fig. 4.35a), from which the mean relaxation time could be obtained. On cooling, the relaxation time increases according to Vogel-Fulcher law (Fig. 4.35 b).
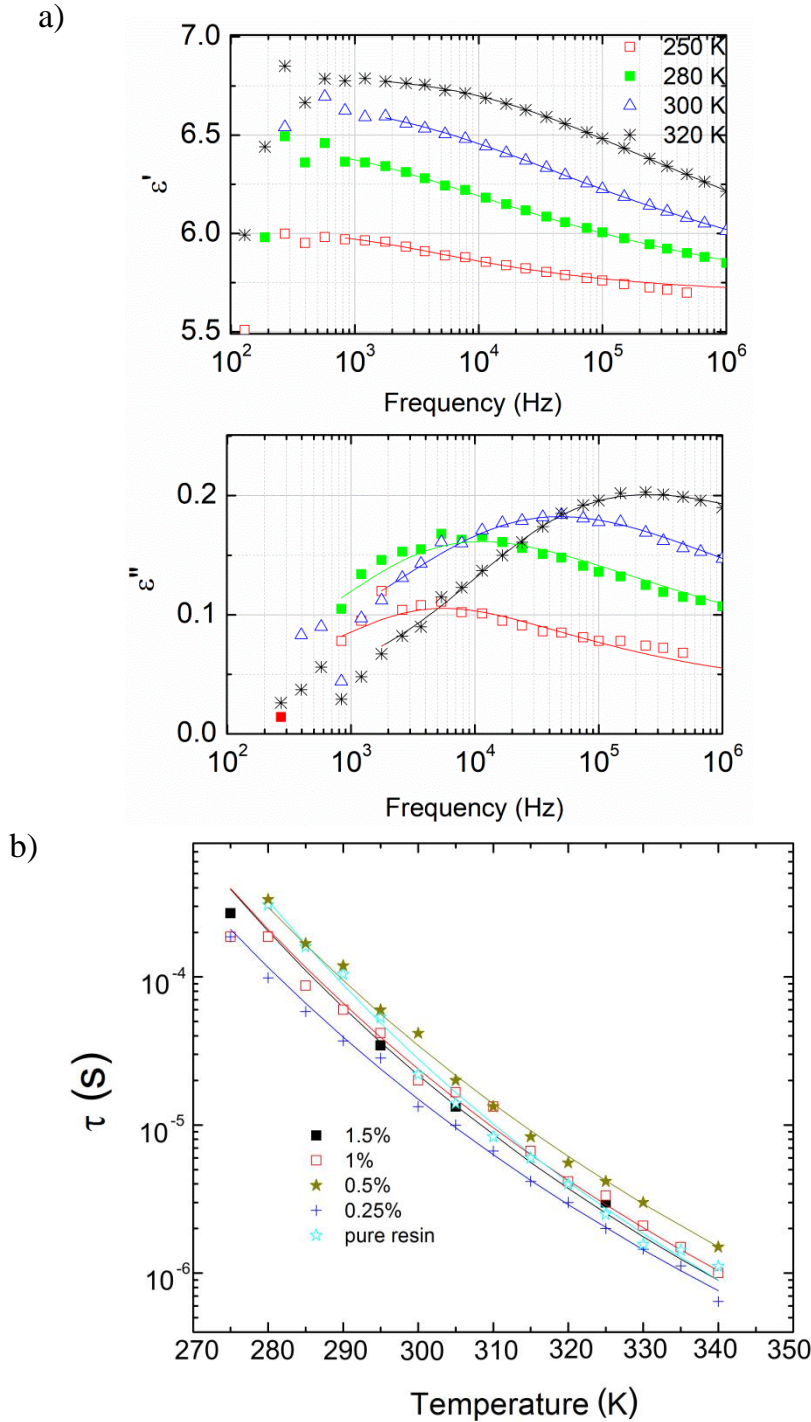

Fig.4.35. a) Frequency dependence of complex dielectric permittivity of composites with NG filler (concentration 1.5 wt. %) at different temperatures. Solid lines are the fits of Havriliak-Negami equation; b) Temperature dependence of relaxation time of composites based on NG filler. Solid lines are fits of Vogel-Fulcher equation

The best fits were obtained using the same $\tau_0 = 1.14$ ps value for all composites below the percolation threshold, the same value of τ_0 was also obtained for pure resin [109], and led to the parameters presented in Fig. 4.36. The concentration dependence of relaxation activation energy for artificial and natural graphite has a maximum for concentrations 0.5 wt. % - 1 wt. %. The glass transition temperature is lower in all composites than in pure polymer matrix and shows a pronounced minimum at 0.5 – 1 wt. % concentration, depending on the kind of graphite. Such a minimum, as well as a maximum in concentration dependence of relaxation activation energy, may be explained by the contribution of two antagonistic effects. On one hand, the graphite particles may adsorb macromolecules at their surface, thus hindering polymer mobility and hence decreasing the glass transition temperature, as usually observed in most composites [110]. On the other hand, glass transition temperature may have complex behaviours, for example if heterogeneous crosslinking around filler particles occurred [111], or depending on how the composite has been cured [112]. A decrease of T_0 may be related to the enhanced polymer dynamics due to the extra free volume at the polymer–filler interface. Thus, in composites with artificial graphite and NG fillers, T_0 presents a minimum in the medium concentration range 0.5 – 1 wt. %. At lower concentrations, the glass transition temperature decreases more rapidly in EG composites than in composites with smaller artificial graphite particles. It can be explained by a free volume at the polymer-graphite interface which is higher when the filler particles are bigger. At the same time, the concentration dependence of glass transition temperature shows the opposite tendency at higher graphite concentrations, which is obviously related with stronger interactions between polymer matrix and graphite particles.
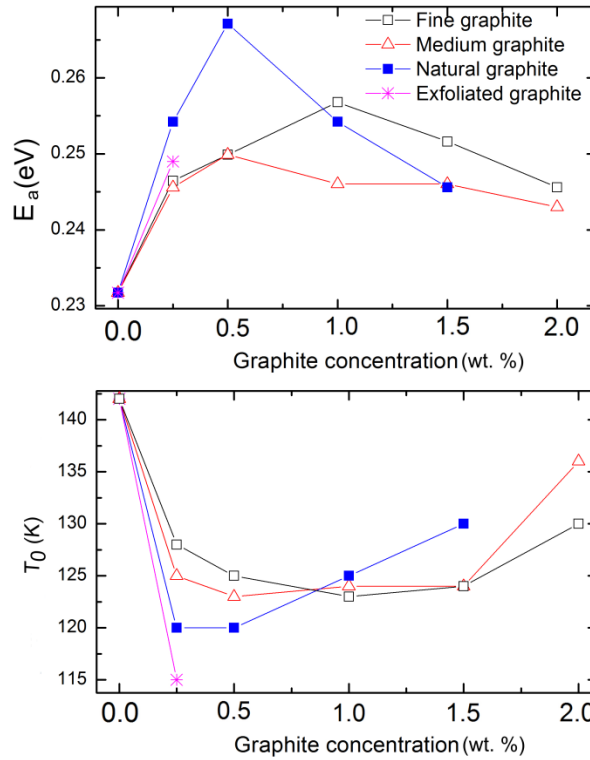
Fig. 4.36. Concentration dependence of dielectric relaxation activation energy and glass transition temperature for different graphite fillers

The DC conductivity has been obtained from frequency dependence of conductivity according to Jonscher's equation. The temperature dependence of DC conductivity for EG-based composites (except for the one at 0.25 wt. %, for which σ_{DC} occurs at frequencies below lower experimental frequency limit) is presented in Fig. 4.37 a. Three different temperature regions can be separated: I - below 150 K, in which the DC conductivity slowly decreases with temperature for composites above percolation threshold; II – between 150 K and 410 K, in which the DC conductivity decreases when temperature increases; III – above 410 K, in which DC conductivity increases with temperature in all composites, independently on whether they are below or above percolation threshold (except for the composite at 2 wt. % for which the increase of DC conductivity with temperature is expected to occur above 450 K). After annealing, the electrical conductivity decreases in all composites. However, the most significant effect was observed in composites with high EG

concentration, especially in the composite at 2 wt. %, whose DC conductivity decreases by 10 times.
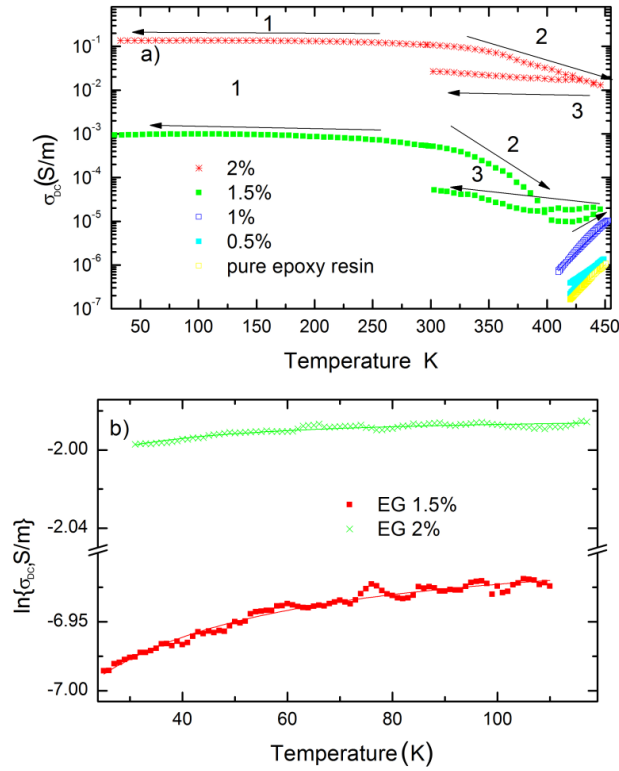

Fig. 4.37. Temperature dependencies of DC conductivity of composites based on EG filler: a) full temperature region; b) low-temperature region. Arrows indicate temperature change direction and numbers order

The temperature dependence of DC conductivity in temperature region I (Fig. 4.37 b) was fitted with fluctuation-induced tunneling model. The resultant fitting parameters are listed in Table 4.9. Very low values of T_1 and T_0 (Table 4.9) indicate very low potential barrier height for electrons to tunnel between EG clusters in comparison with what has been reported for CNTs- and carbon black-based composites even at much higher filler concentration [113, 114]. Thus, in temperature regions I and II, electrical conductivity is mainly governed by electron tunneling between EG particles. In the temperature region II, electrical conductivity increases when the temperature decreases due to shrinkage of polymer matrix.

Table 4.9. Tunneling fit parameters

	$ln(\sigma_0\ (S\ m^{-1}))$	$T_1\ (K)$	$T_0\ (K)$
EG 2 wt. %	-1.98	0.5	0.2
EG 1.5 wt. %	-6.88	4.2	16.6

At the higher temperatures (above 410 K), the temperature dependence of DC conductivity can be fitted with Arrhenius law (Fig. 4.37 a). The concentration dependence of the activation energy E_A for composites with different graphite fillers is presented in Fig. 4.38.
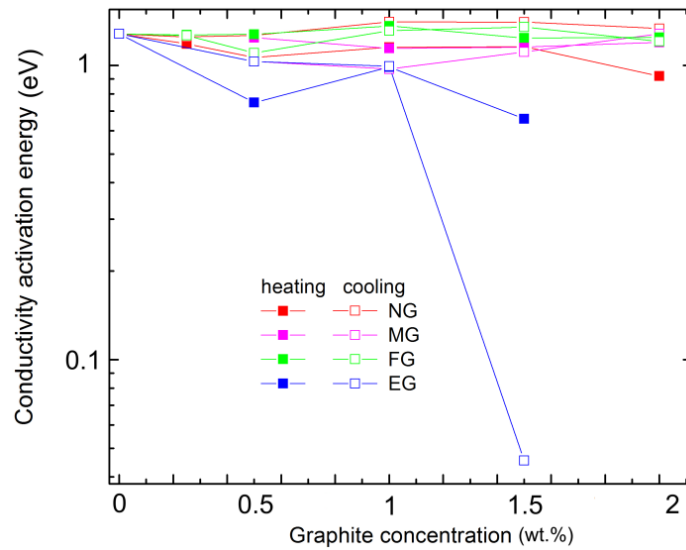

Fig. 4.38. Concentration dependence of the conductivity activation energy for different graphite fillers

Below percolation threshold, the conductivity activation energy E_A is almost concentration-independent. In contrast, for the composites with 1.5 wt. % of EG, its value is very low. The difference between heating and cooling data is clearly observed in composites with bigger graphite particles, for NG- and EG-based composites, since conductivity activation energy significantly increased after annealing in NG composites and decreases in EG composites. In contrast, the difference between heating and cooling conductivity activation energies is very small for composites based on smaller graphite particles (MG and FG). The lowest activation energy values were obtained in EG-based composites,

even below the percolation threshold. In composites below percolation threshold, electrical conductivity occurs due to finite epoxy resin conductivity. Graphite particles and boundary between graphite and polymer matrix can make disturbance for electron traveling in the polymer due to non-ohmic contacts or in contrary can provide additional channels for carrier traveling, due to their tunneling from polymer matrix to graphite particles. In the latter case, the conductivity activation energy should be lower in composites with higher filler concentration. This is clearly observed in the composites above percolation threshold. However, even below the percolation threshold, the conductivity activation energy is lower in most composites than in polymer matrix, except for NG-based composites after annealing. After annealing of epoxy resin composites, graphite conductive networks are partially destroyed and total composite conductivity is decreased [115]. Therefore, it can be concluded that the formation of conductive networks near and above percolation threshold significantly decreases the conductivity activation energy in composites.

Summary

Results of broadband (20 Hz – 1 THz) dielectric investigations of epoxy – graphite composites in wide temperature region are reported. The dielectric permittivity of composites at room temperature apparently increases with graphite particle size. Such a finding is explained by the decrease of the percolation threshold with microsized graphite particle size, which is confirmed theoretically.

All tested graphites could be interesting for applications which do not require the high DC conductivity, such as antistatic and electrostatic dissipation applications. The only but very promising candidate for producing effective EMI shielding material, out of all composites with graphite fillers investigated here, is exfoliated graphite (EG). Moreover, EG demonstrates relatively low electrical percolation threshold, between 1.0 and 1.5 wt. %. All

other graphite additives, both natural and artificial, have percolation thresholds much higher than 2 wt. %.

The electrical conductivity of EG-based composites above percolation threshold and at low temperatures (below glass transition temperature of pure polymer matrix) is mainly governed by electron tunneling between graphite particles. Such tunneling is characterised by very low potential barriers for carriers with respect to what has been reported for much higher concentrations of other carbon fillers such as carbon nanotubes or carbon blacks. Below the percolation threshold, the dielectric properties of graphite-based composites are mainly governed by alpha relaxation in pure epoxy resin matrix. The dependence of freezing temperature on graphite concentration shows a minimum at concentration 0.5 – 1 wt. %. At higher temperatures, electrical conductivity occurs in all composites whether they are below or above the percolation threshold, and such conductivity is strongly impacted by electron tunneling between graphite particles throughout polymer matrix.

4.4 MWCNT/GNP/epoxy composites

In this section the attempt combining MWCNT and GNP into a hybrid structure which could lead to a potentially new multifunctional material as the result of synergy effect of both fillers, improving electrical characteristics will be discussed. The small size of nanofillers with different shape results in a large surface area, thus increasing the amount of polymer in contact with the filler. When the volume content of the nanofiller is large enough, the inter-phase becomes the dominant phase in the composite. In addition, the use of different shape (1D – MWCNT and 2D – GNP) nanoparticles is able to increase the efficiency at smaller filler content. For the same filler content of particles with various geometrical arrangements of the chains, particles' lengths and shape different results can be achieved. Therefore, it is hard to predict theoretically the final results. Physical properties of composite filled with carbon nanoparticles in different filler content and combination should be experimentally investigated in order to determine the optimal nanoparticles'

content, the filler combination and the ratio which would maximally improve certain physical properties of composite, reduce production costs, enhance multifunctionality and application possibilities. As well as, the synergistic effect of carbon nanofillers in improving the electrical properties of the material is not clearly determined. Moreover, usually electrical properties of hybrid composites were investigated only at room temperature [116], while investigations in the wide temperature are needed to determine the electrical transport mechanism.

The aim of the investigations of hybrid filler nanocomposites at different MWNTs/GNPs ratios was to highlight synergic effects on the electrical conductivity. The electrical conductivity measurements were performed in a wide frequency and temperature range starting from cryogenic temperature (30 K) to room temperature (300 K) in order determine electrical transport mechanism at different temperatures.

The microscopy methods were used to characterize and determine the dispersion and interactions of carbon nanoparticles in the polymer matrix. Using optical microscopy analysis samples with MWCNT and GNP were characterized by nominal dimensions of 10×10 mm with a thickness varying in the range 200 ± 50 μm (Fig. 4.39).
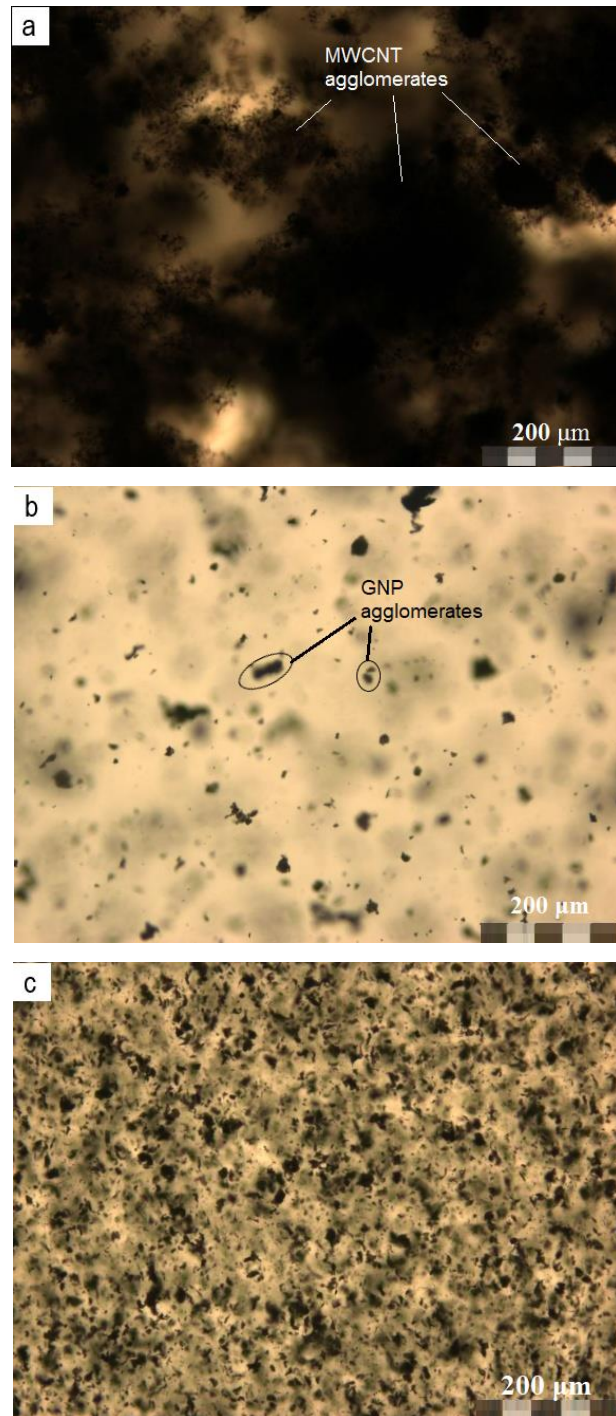
Fig. 4.39. Optical microscopy images of epoxy resin filled with: a) 0.03 wt.% of MWCNT; b) 0.03 wt.% of GNP; c) 1.00 wt.% of GNP, at 10x magnification [117]

The image Fig. 4.39 shows the uneven distribution of MWCNT in the epoxy resin. There are areas with high concentration and agglomerated of MWCNT and small areas with almost negligible concentration of carbon nanotubes. Agglomerates could be related to the strong van der Waals forces between carbon nanotubes. The images Fig. 4.39 b, c, of the GNP composites

99

shows large agglomerates of the GNP due to interactions between graphene nanoplatets sheets, smooth surface of the GNP could result weak interfacial bonding with the polymer [118]. For further structural investigations the SEM images are performed (Fig. 4.40).
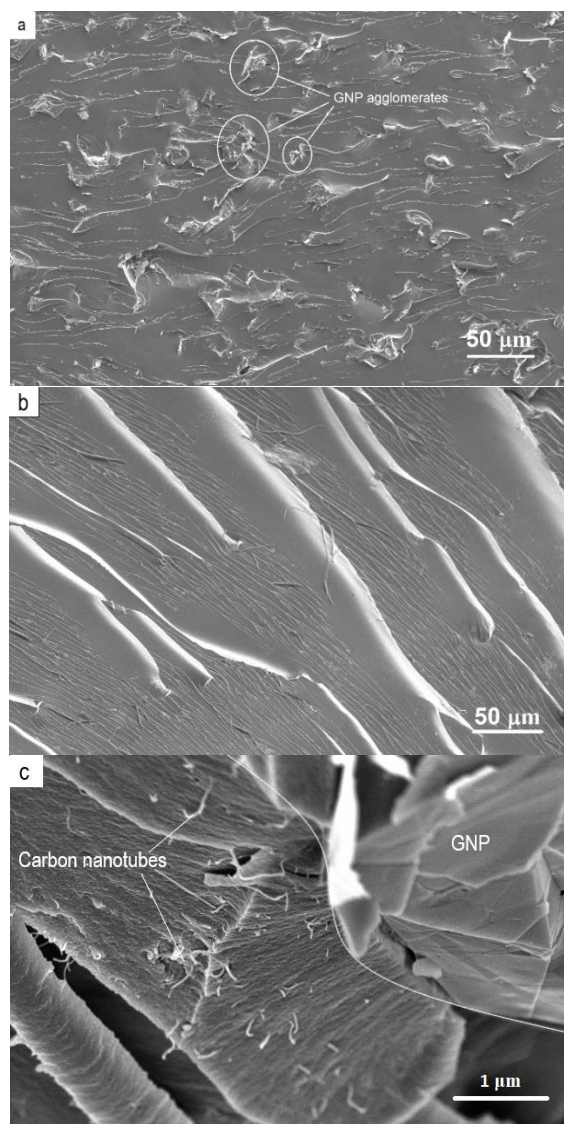
Fig. 4.40. SEM images of epoxy resin composites filled with a) 0.3 wt.% of GNP , magnification 500x, b) MWCNT/GNP (5:1)   magnification 500x, c) MWCNT/GNP (5:1) magnification 35 000x [117]

Fig. 4.40 a shows the surface of a composite containing 0.3 wt.% GNP. GNP agglomerates of varying size are randomly dispersed in polymer matrix. In contrast, the surface of hybrid filler composites is smoother with no visible large agglomerates of GNP or MWCNT, carbon nanotubes likely reduce the

size of GNP aggregates. The magnification of SEM images in Fig. 4.40 a and b is 500x. Fig. 4.40 c SEM image (magnification 35000x) shows that smaller agglomerates GNP still can be found, but the dispersion of MWCNT is much even.

The dielectric and the electrical properties of the composites containing MWCNT, GNP and hybrid nanocomposites with different combinations of MWCNT/GNP are compared in the wide frequency and temperature range. Frequency dependencies of dielectric permittivity and electrical conductivity at room temperature for composites containing only MWCNT and GNP fillers are presented in Fig 4.41. The values of dielectric permittivity and electrical conductivity increase sharply close to percolation threshold. Moreover, above the percolation threshold in the frequency dependence of the conductivity a frequency independent plateau is observed.

The theoretical percolation threshold for GNP, as for round shape particles calculated from excluded volume theory [43] is 1.41 vol. % or 3 wt. %, when the average aspect ratio value for GNP particles is A_{GNP}=1500. However, considering the experimental data Fig. 4.41, the dielectric permittivity and the electrical conductivity of GNP composites are low enough and similar to pure epoxy resin properties even with the highest available filler concentration (3 wt.%). It denotes that the percolation threshold in GNP composites is higher than 3 wt.% and somewhat higher than the value of percolation threshold calculated from excluded volume theory. Such high experimental percolation threshold value could be attributed to non-even distribution and large aggregates of GNP in the polymer matrix and similar percolation threshold values were already observed in GNP/epoxy composites [119, 120]. At low filler concentrations aggregated particles do not form the conductive path.

According to the excluded volume theory the theoretical percolation threshold for rod-like particles calculated from excluded volume theory is 0.1 vol.% or 0.14 wt. % [43], when aspect ratio for MWCNTs is A_{MWCNT}=505. The experimental percolation threshold for MWCNT composites is close to 0.03 wt. %.
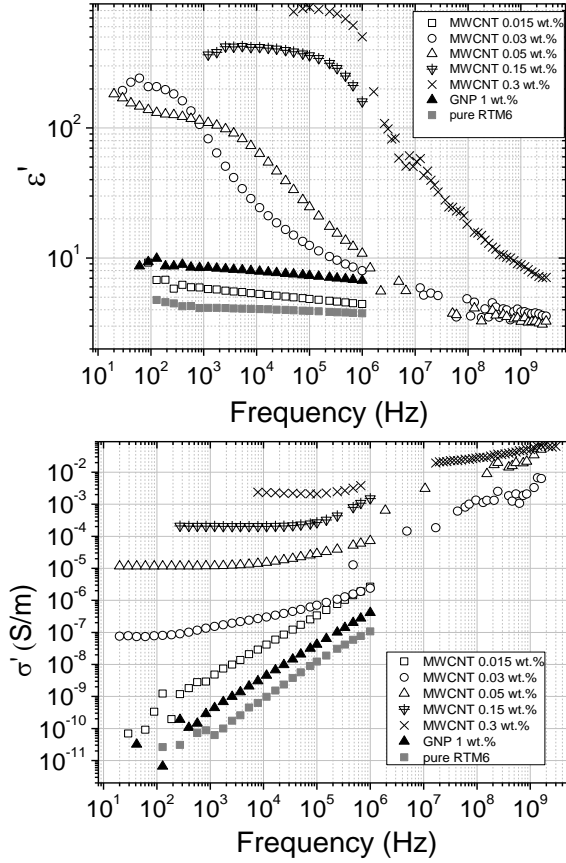
4.41. Frequency dependencies of real parts of complex dielectric permittivity and electrical conductivity of GNP and MWCNT composites.

The dielectric permittivity and the electrical conductivity of hybrid filler MWCNT/GNP composites with various proportions and total 0.3 wt.% concentration are presented in Fig. 4.42. All investigated composites with hybrid nanofillers are above the percolation threshold, and this is quite expected because for hybrid filler MWCNT/GNP composites according to excluded volume theory.

For hybrid filler composites the electrical conductivity and the dielectric permittivity increase with MWCNT concentration.
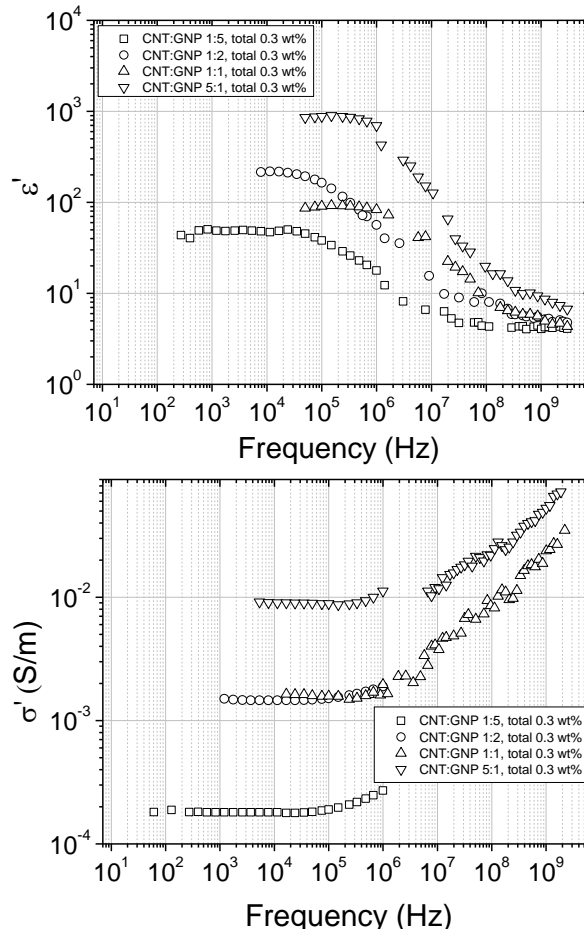
Fig.4.42. Frequency dependencies of real parts of complex dielectric permittivity and electrical conductivity of hybrid MWCNT/GNP composites.

Above the percolation threshold the frequency dependence of the electrical conductivity follows the Jonscher's equation. The values of electrical conductivity as a function of the filler concentration of single filler MWCNT and hybrid filler composites are presented in Fig. 4.43. Above percolation threshold the DC conductivity follows the power law.
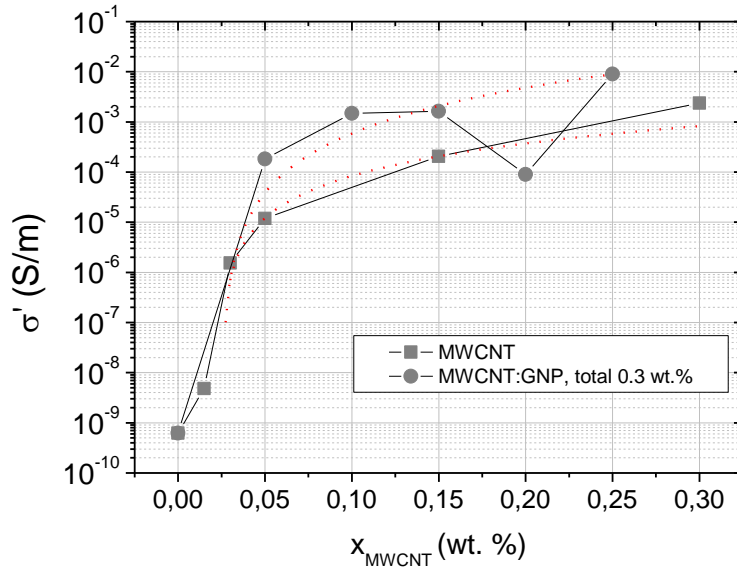
Fig. 4.43. Concentration dependence of real part of complex electrical conductivity for composites containing MWCNT only and hybrid filler MWCNT:GNP fillers. Dotted lines are the fits of the power law.

The highest DC conductivity value – 8.9 mS/m is observed in hybrid filler MWCNT:GNP composites with proportions 5:1 (total content 0.3 wt.%) and it is increased by four times of magnitude over of composites containing 0.3 wt.% MWCNT. Such high value clearly is higher than can be predicted by the simple rule of mixture (ROM) theory [121]:

$$\sigma = \frac{1}{\sum_{i=0}^{n} V_i} \sum_{i=0}^{n} \sigma_i V_i,$$

where V_i and σ_i is the volume and the conductivity of i-th component. Indeed, the conductivity of composites only with MWCNT is much higher than the conductivity of composites only with GNP, therefore the conductivity of hybrid filler composites clearly overcomes the values predicted by ROM theory all frequency range, including microwaves, while in other works the similar effect was observed only at low frequencies below 1 MHz [122]. An increase could be attributed to the formation of more effective conductive network due to combining 2D MWCNT and 1D GNP conductive particles.

The electrical transport in hybrid filler MWCNT/GNP composites can occur via 1) the hopping and the tunneling of electrons in the MWCNT

subsystem, 2) the hopping and the tunneling of electrons in the GNP subsystem and 3) the tunneling of electrons between the GNP and the MWCNT subsystems [123]. The increase of the conductivity with the MWCNT concentration for hybrid composites with total 0.3 wt.% concentration of nanofillers indicate that the second conductivity mechanism is negligible small in comparison with the first and third ones. Therefore, the electrical conductivity in hybrid filler composites increases because of the better distribution of MWCNT and the tunneling of electrons between the GNP and the MWCNT.

Temperature dependencies of the DC conductivity are presented in Fig. 4.44. Above percolation threshold the DC conductivity below room temperature fits the electrical tunneling model. Obtained tunneling model fit parameters are listed in Table 4.10.

Table 4.10. Tunneling model fit parameters

MWCNT (wt.%)	$Ln(\sigma_0, S/m)$	T_1 (K)	T_0 (K)
0.03	-13.3	63	34
0.05	-11.1	77	27
0.15	-8.5	22	15
0.3	-5.1	46	41
CNT:GNP (total 0.3 wt.%)			
1:5	-8.5	50	20
1:2	-6.3	61	37
2:1	-9.1	52	41
5:1	-4.5	36	27

The ratio T_1/T_0 decreases with MWCNT concentration in single and hybrid composites. Thus the interparticle distance and the potential barrier amplitude can decrease with MWCNT concentration for both single and hybrid composites. The gap width is approximately proportional to $p^{-1/3}$ in single filler composites [99]. The dependence T_1/T_0 is very similar in hybrid and single

composites. However the ratio T_1/T_0 is higher in single filler composites. According to SEM investigations the smallest distance between nanoparticles is in hybrid filler composites. Therefore the ratio T_1/T_0 is lower in hybrid composites due to the better distribution of nanoparticle.
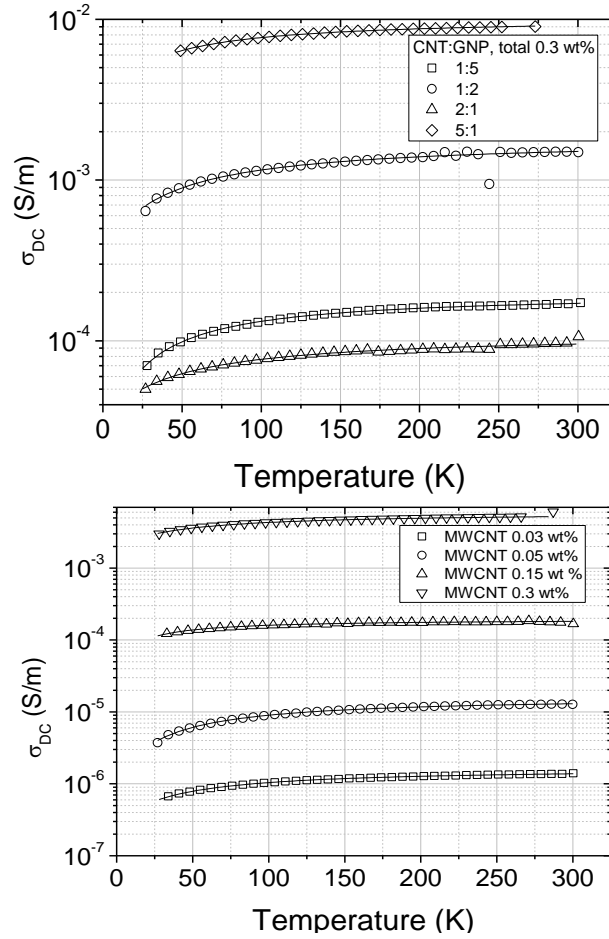

Fig. 4.44. Temperature dependencies of DC conductivity for composites filled with: a) MWCNT, b) MWCNT/GNP, total concentration is 0.3 wt.%. Solid lines are fits of the tunneling model.

Summary

MWCNT/epoxy and GNP/epoxy nanocomposites with different filler contents (0.015 – 0.3 wt. %) and hybrid epoxy nanocomposites filled with CNT/GNP in a total reinforcement of 0.3 wt.% were fabricated and the effects of varying individual CNT/GNP contents and combination on electrical properties were evaluated.

The lowest electrical percolation threshold is observed in MWCNT composites (0.03 wt. % concentration). Although the percolation threshold in hybrid filler MWCNT/GNP can be described by the excluded volume theory, the electrical conductivity of hybrid filler composites is substantially higher in comparison with single composites. The electrical conductivity of hybrid nanocomposite containing 0.3 wt.% MWCNT and GNP in ratio 5:1 exhibits the highest value of 0.009 S/m, which is more than 4 times higher than that composites containing only 0.3 wt.% MWCNT (0.002 S/m). The concurrent 1D and 2D particles did not affect the percolative behaviour of MWNTs but led to an outstanding increment in the final electrical conductivity. That could be considered as a synergistic effect between GNP and MWCNT due to the better distribution of MWCNT and the tunneling of electrons between the GNP and the MWCNT.

Conclusions

In this work the dielectric and electrical properties of carbon based/polymer composites were investigated in wide frequency (20 Hz – 1 THz) and temperature range (30 – 500 K). It could be concluded that:

- The electrical conductivity in all OLC composites above percolation threshold is governed by quasi-one dimensional hopping inside OLC clusters and tunneling between the clusters.

- The small-sized, 40 nm OLC aggregates, which are more easily deformable and form the elongated structure in polymer matrix lead to the lower percolation threshold. These values are 5.4 vol. % for OLC/PU composites and 6.8 vol. % for OLC/PDMS composites with 40 nm aggregates, and in comparison the percolation threshold with 100 nm aggregates is 7.1 vol.%. OLC composites have the electrical conductivity as high as MWCNTs composites, but higher percolation threshold values.

- In OLC/PDMS composites close to percolation threshold the transition into insulating state occurs at higher temperatures. The transition temperature is dependent from OLC aggregate size.

- The percolation threshold for MWCNTs composites is the lowest (0.5 wt. %) with the shortest (325 nm) carbon nanotubes that were investigated, but according to the percolation theory, the lowest percolation threshold is expected for composites with the longest carbon nanotubes. This could be explained by easier agglomeration, when the length of carbon nanotubes is higher.

- In composites with graphite inclusions below the percolation threshold the dielectric permittivity increases with graphite particle size. In contrary to other graphite forms, EG composites show relatively low percolation threshold, which is 1.5 wt. %, due to porous structure and is as low as in some composites with carbon nanotube inclusions. Micro-

sized carbon additives could compete with commercially available CNTs and provide, even at low concentration, high DC conductivity and EMI shielding ability.

- In hybrid filler OLC/MWCNT composites the electrical percolation threshold is substantially lower as is predicted by excluded volume theory due to the synergy effects.

- The combination of graphene nanoplatelets (1D) and multiwalled carbon nanotubes (2D) particles led to increment of electrical conductivity in comparison with single MWCNT filler composites with the same filler concentration (0.3 wt.%). That could be attributed to the synergy effect between different types of the particles due to better distribution of the filler particles and the incorporation of additional conductive pathways to the existing MWCNT network.

References

[1] T. Kuilla, S. Bhadra, D. Yao, N. H. Kim, S. Bose, J. H. Lee, *Prog. Polym. Sci.,* **35**, 11 (2010).

[2] R. J. Young, I. A. Kinloch, L. Gong ir K. S. Novoselov, *Compos. Sci. Technol.* **72**, 12 (2012).

[3] F. Qin, C. Brosseau, *J. Appl. Phys.,* **111**, 6 (2012).

[4] G. Inzelt, Conducting polymers: A new era in electrochemistry, Berlin: Springer (2008).

[5] S. Battacharya, Metal-Filled Polymers, New York: Dekker (1986).

[6] R. Strumpler, J. Glatz-Reichenbach, *J. Electrocer.,* **3**, 4 (1999).

[7] L. J. Adriaanse, J. A. Reedijk, P. A. A. Teunissen, H. B. Brom, M. A. J. Michels ir J. C. M. Brokken-Zijp, *Phys. Rev. Lett.*, **78**, 1755 (1997).

[8] W. Bauhofer, Z. Kovacs, *Compos. Sci. Technol.,* **69**, 1486 (2009).

[9] Z. Han, A. Fina, *Prog. Polym. Sci.,* **36**, 914 (2011).

[10] E. Ivanov, R. Kotsilkova, E. Krusteva, E. Logakis, A. Kyritsis, P. Pissis, C. Silvestre, D. Duraccio ir M. Pezzuto, *J. Polym. Sci. Part B: Polym. Phys.,* **49**, 431 (2011).

[11] T. Blyther, Electrical properties of polymers, Cambridge University Press (2005).

[12] J. R. Fried, Polymer Science and Technology, Pearson Education (2014).

[13] P. Flory, Principles of Polymer Chemistry, Ithaca: Cornell University Press (1953).

[14] R. Bird, C. Curtis, R. Armstrong ir O. Hassenger, Dynamics of Polymer Fluids, vol. 1 & 2, 2nd ed, New York: Wiley (1987).

[15] C. E. Wilkes, PVC Handbook, Hanser Verlag (2005).

[16] J. W. Nicholson, The Chemistry of Polymers, 4, Revised ed., Royal Society of

Chemistry (2011).

[17] C. C. Ibeh, Thermoplastic Materials: Properties, Manufacturing Methods, and Applications, CRC Press (2011).

[18] K. P. Menard, Dynamic mechanical analysis. A practical introduction, CRC press (1999).

[19] H. Block, *Adv Polym Sci,* **33**, 93 (1979).

[20] Debye, Polar molecules, New York: Chemical Catalog Co., Inc (1929).

[21] K. Cole ir R. Cole, *J. Chem. Phys.,* **9**, 341-351 (1941).

[22] S. Havriliak ir S. Negami, *Polym.,* **8**, 161–210 (1967).

[23] R. Zorn, *J. Chem. Phys.,* **116**, 8 (2002).

[24] H. O. Pierson, Handbook of Carbon, Graphite, Diamond and Fullerenes, New Jersey: Noyes Publications (1993).

[25] S. Iijima, *Nature*, **354**, 56–58 (1991).

[26] P. Calvert, *Nature,* **399**, 210-211 (1999).

[27] S. Subramoney, *Adv. Mater.,* **10**, 15 (1998).

[28] R. Che, L. Peng, X. F.Duan, Q. Chen, X. Liang, *Adv. Mater.,* **16**, 5, (2004).

[29] A. R. Hippel, Dielectrics and Waves, New York: Wiley (1954).

[30] A. K. Jonscher, Universal relaxation law, London: Chelsea Dielectrics Press (1992).

[31] J. C. Dyre, *J. Appl. Phys*, **64**, 5 (1988).

[32] J. Barton, *Verres Refract*., **20**, 328 (1966).

[33] T. Nakajima, Annual Report, Conference on Electric Insulation and Dielectric Phenomena, National Academy of Sciences, National Academy of Sciences, Washington,DC, 168-176 (1972).

[34] H. Namikawa, *J. Non-Cryst. Solids,* **18**, 173 (1975).

[35] Petzelt, I. Rychetsky, D. Nuzhnyy, *Ferroelectrics,* **426**, 171-193 (2012).

[36] G. Grimmett, Percolation and disordered systems, Springer-Verlag Berlin Heidelberg (1997).

[37] A. Bunde, *J. Electroceramics* **5**, 2 (2000).

[38] M. L. Clingerman, Development and Modelling of Electrically Conductive Composite Materials, Michigan Technological University, Houghton, Michigan (2001).

[39] F. Lux, *J. Mater. Sci.,* **28**, 2 (1993).

[40] S. Kirkpatrick, *Rev. Mod. Phys.,* **45**, 574-588 (1987).

[41] I. Balberg, *Phys. Rev. Lett.*, **59**, 12 (1987).

[42] E. J. Garboczi, K. A. Snyder, J. F. Douglas, M. F. Thorpe, *Phys. Rev. E*, 52, 819-828 (1995)

[43] I. Balberg, C. H. Anderson, S. Alexander, N. Wagner, *Phys. Rev. B,* **30**, 3933 (1984).

[44] A. Celzard, E. McRae, C. Deleuze, M. Dufort, G. Furdin, J. F. Marêché, *Phys. Rev. B,* **53**, 6209 (1996).

[45] N. F. Mott, E. A. Davis, Electronic processes in non-crystaline solids, London: Oxford University (1971).

[46] W. Y. Jang, N. N. Kulkarni, C. K. Shish, Z. Yao, *Appl. Phys. Lett.,* **84**, 1177 (2004).

[47] T.W. Ebbesen, *Annu Rev. Mater. Sci.*, **24**, 235 (1994)

[48] C. Gau, C.Y. Kuo, H.s. Ko, *Nantechnol,.* **20**, 395705 (2009)

[49] Z.H. Khan, M.Husain, T.P.Perng, N. Salah, S.Habib*, J. Phys. Condens. Matter* **20**, 475207 (2008)

[50] L. Wang, H. Wang, T. Datta, M. Yin, X. Tian, *J. Appl. Phys*., **116**, 173708

(2014)

[51] P. Sheng, E. K. Sichel, *Phys. Rev. Lett.*, **40**, 18 (1978).

[52] H. Deng, R. Zhang, E. Bilotti, J. Loos, T. Peijs, *J. Appl. Polym. Sci.,* **113**, 742-51 (2009).

[53] W. G. Weng, G. H. Chen, D. J. Wu, W. L. Yan, *Compos. Interface,* **11**, 2, (2004).

[54] I. Neitzel, V. Mochalin, Y. Gogotsi, Ultrananocrystalline Diamond, Elsevier, (2012).

[55] S. Liao, *J. Power Sources,***185**, 2 (2008).

[56] J. Li, J. K. Kim, *Compos. Sci. Technol.,* **67**, 10 (2007).

[57] J. Li, *Adv. Funct. Mater.,* **17**, 16 (2007).

[58] J. Sandler, *Polym.,* **40**, 21 (1999).

[59] D. H. Park, Y. K. Lee, S. S. Park, C. S. Lee, S. H. Kim, W. N. Kim, *Macromolecular Research*, **21**, 8 2013.

[60] J. Sumfleth, X. C. Adroher, K. Schulte, *J. Mater. Sci.,* **44**, 3241 (2009).

[61] C.Li, E.T. Thorstenson, T.W. Chou, Appl. Phys. Lett., 91, 223114 (2007).

[62] Y. Sun, H. D. Bao, Z. X. Guo, J. Yu, *Macromolecules,* **42**, 459 (2009).

[63] V. L. Kuznetsov, Y. V. Butenko, A. L. Chuvilin, A. I. Romanenko, A. V. Okotrub, *Chem. Phys. Lett ,* **336**, 397, (2001).

[64] V. Kuznetsov, D. V. Krasnikov, A. Schmakov, K. V. Elumeeva, *Phys. Stat. Sol. B,* **249**, 2390 (2012).

[65] M. S. Russ, S. S. Rahatekar, K. Koziol, B. Farmer ir H. X. Peng, *Compos. Sci. Technol. ,* **81**, 42 (2013).

[66] A. Celzard, J. F.Mareche, G. Furdin, *Prog. Mater. Sci.,* **50**, 93 (2005).

[67] F.Nobili, S.Dsoke, T.Mecozzi, R.Marassi, *Electrochim. Acta,* **51**, 536 (2005).

[68] J. Macutkevic, P. Kuzhir, D. Seliuta, G. Valusis, J. Banys, A. Paddubskaya, D. Bychanok, G. Slepyan, S. Maksimenko, V. Kuznetsov, S. Moseenkov, O. Shenderova, A. Mayer, Ph. Lambin, *Diam. Relat. Mater*, **19**, 91-99 (2010).

[69] R. Langlet, P. Lambin, A. Mayer, P. P. Kuzhir, S. A. Maksimenko, *Nanotech.* **19**, 115706 (2008).

[70] J. Macutkevic, D. Seliuta, G. Valušis, J. Banys, V. Kuznetsov, S. Moseenkov, O. Shenderova, *J. Appl. Lett,* **95**, 112901 (2009).

[71] P.P Kuzhir, A. G. Paddubskaya, S. A. Maksimenko, V. L. Kuznetsov, S. Moseenkov, A. I. Romanenko, O. A. Shenderova, J. Macutkevic, G. Valusis, P. Lambin, *IEEE Transactions on Electromagnetic Compatibility*, **54**, 6 (2012).

[72] J. Macutkevic, I. Kranauskaite, J. Banys, S. Moseenkov, V. Kuznetsov, O. Shenderova, *J. Appl. Phys.*, **115**, 21 (2014)

[73] T. Koga, M. Takenaka, K. Airawa, M. Nakamura, T. Hashimoto, *Langmuir*, **21**, 11409 (2005).

[74] Z. M. Dang, L. Wang, Y. Yin, Q. Zhang, Q. Q. Li, *Adv. Mater.,* **19**, 852 (2007).

[75] C. Brosseau, P. Queffelec, P. Talbot, *J. Appl. Phys.,* **89**, 4532 (2001).

[76] J. Liu, Ch. G. Duan, W. G. Yin, W. N. Mei, R. W. Smith, J. R. Hardy, *Phys. Rev. B*, **70**, 144106 (2004).

[77] B. J. P. Adohi, A. Mdarhri, C. Prunier, B. Haidar, C. Brosseau, *J. Appl. Phys.,* **108**, 074108 (2010).

[78] D. Bychanok, P. Kuzhir, S. Maksimenko, S. Bellucci, C. Brosseau, *J. Appl. Phys.,* **113**, 124113 (2013).

[79] A. Podzorov ir G. Gallot, *Chem. Phys. Lett.,* **495**, 46 (2010).

[80] J. Liang, Q. Yang, *J.Appl. Phys.,* **102**, 083508 (2007).

[81] C. W. Nan, *Prog. Mater. Sci.,* **37**, 1 (1993).

[82] A. Mdahari, F. Carmona, C. Brosseau, P. Delhaes, *J. Appl. Phys.,* **103**, 054303 (2008).

[83] A. Zylbersztejn, N. F. Mott, *Phys. Rev. B,* **11**, 4383 (1975).

[84] I. Kranauskaite, J. Macutkevic, J. Banys, V. Kuznetsov, M. Letellier, V. Fierro, A. Celzard, O. Shenderova, Polym. Compos., DOI 10.1002/pc.24816 (2018).

[85] D. J. Bergman, *Phys. Rev. Lett.,* **44**, 1285 (1980).

[86] I. Kranauskaite, J. Macutkevic, J. Banys, E. Talik, V. Kuznetsov, N. Nunn, O. Shenderova, *Phys. Status solidi B,* **252**, 8 (2015).

[87] H. M. Kim, M. S. Choi, J. Joo, J. J. Cho, H. S. Yoon, *Phys. Rev. B,* **74**, 054202 (2006).

[88] Z. F. Liu, G. Bai, Y. Huang, Y. F. Ma, F. Du, F. F. Li, T. Y. Guo, Y. S. Chen, *Carbon*, **45**, 821 (2007).

[89] P. Pötschke, S. M. Dudkin, I. Alig, *Polymer*, **44**, 17 (2003)

[90] I. Kranauskaite, J. Macutkevic, J. Banys, V. Kuznetsov, S. Moseenkov, N. Rudyna, D. Krasnikov, *Physica Status Solidi A*, **213**, 4 (2016).

[91] B. E. Kilbride, J. N. Coleman, J. Fraysse, P. Fournet, M. Cadek, A. Drury, S. Hutzler, S. Roth, W. J. Blau, *J. Appl. Phys,* **92**, 4024 (2002).

[92] F. Deng, Q. S. Zheng, L. F. Wang, C. W. Nan, *Appl. Phys. Lett.* **90**, 021914 (2007)

[93] F. Deng, Q. S. Zheng, *Appl. Phys. Lett.* **92**, 071902 (2008).

[94] H. Deng, L. Lin, M. Ji, S. Zhang, M. Yang, *Prog. Polym. Sci.,* **39**, 627 (2014).

[95] K. Schmidt-Rohr, A. S. Kulik, H. W. Becktran, A. Ohlemacher, U. Pawlzik, C. Boeffel, H. W. Spiess, *Macromolecules*, **27**, 17 (1994).

[96] G. Ceccorulli, M. Pizzoli, G. Ceccorulli; M. Pizzoli, *Polymer Bulletin,* **47**, 283 (2001).

[97] B. J. Ash, R. W. Siegel, L. S. Schadler, *J. of Polym. Sci. Part B: Polym. Phys.,* **42**, 4371, (2004).

[98] S. A. Khiar, R. Puteh, A. K. Arof, *Physica B*, **373**, 23 (2006).

[99] T. A. Ezquerra, M. Kulesza, F. J. Balta Calleja, *Synth. Met.*, 41-43, 915 (1991).

[100] R. K. Goyal, *Mater. Chem. Phys*. **142**, 195 (2013)

[101] P. Kuzhir, A. Paddubskaya, A. Plyushch, N. Volynets, S. Maksimenko, J. Macutkevic, I. Kranauskaite, J. Banys, E. Ivanov, R. Kotsilkova, A. Celzard, V. Fierro, J. Zicans, T. Ivanova, R. Merijs Meri, I. Bochkov, A. Cataldo, F. Micciulla, S. Bellucci, Ph. Lambin, J. *Appl. Phys.* **114**, 164304 (2013).

[102] S. Bellucci, Carbon Nanotubes Toxicity. Nanoparticles and nanodevices in Biological Applications, The INFN Lectures – Vol. 1.

[103] I. Kranauskaite, J. Macutkevic, P. Kuzhir, N. Volynets, A. Paddubskaya, D. Bychanok, S. Maksimenko, J. Banys, R. Juskenas, S. Bistarelli, A. Cataldo, F. Micciulla, S. Bellucci, V. Fierro, A. Celzard, *Physica status solidi A*, **211**, 7 (2014).

[104] P. Kuzhir et al, *J. Appl. Phys,* **114**, 164304 (2013).

[105] M. Sahimi, Applications of percolation theory, Taylor & Francis, Bristol PA (1994).

[106] D. Nuzhnyy, M. Savinov, V. Bovtun, M. Kempa, J. Petzelt, B. Mayoral, T. McNally, *Nanotechnology,* **24**, 055707 (2013).

[107] B. Wen, M. Cao, Z. Han, W. Song, L. Zhang, M. Lu, H. Jin, *Carbon,* **65**, 124 (2013).

[108] C. Brosseau, M. E. Achour*, J. Appl. Phys*. **105**, 124102 (2009).

[109] J. Macutkevic, P. Kuzhir, A. Paddubskaya, S. Maksimenko, J. Banys, A. Celzard, V. Fierro, E. Stefanutti, A. Cataldo, F. Micciulla, S. Bellucci, *J. Nanosci. Nanotechnol.,* **13**, 5434 , (2013).

[110] G.J. Howard, R.A. Shanks. J. Macromol. *Sci – Chem A*, **17**, 287 (1982).

[111] P. Bartlet, Y. Lin, J. Pascault ir H. Sautereau, *Polymer Bulletin,* **17**, 97, (1987).

[112] G. Fourche,L. Lafeychine, F. Carmona, *Macromol. Chem. Macromol. Symp*., **9**, 179 (1987)

[113] H. M. Kim, M. S. Choi, J. Joo, S. J. Cho, H. S. Yoon, *Phys. Rev. B,* **74**, 054202 (2006).

[114] P. Sheng, E. K. Sichel, and J. I. Gittleman, *Phys. Rev. B,* **18**, 5712, (1978).

[115] J. Macutkevic, P. Kuzhir, A. Paddubskaya, S. Maksimenko, J. Banys, A. Celzard, V. Fierro, S. Bistarelli, A. Cataldo, F. Micciulla, S. Bellucci, *J. App. Phys*. **114**, 033707 (2013).

[116] J. Mark, K. Ngai, W. Graessley, L. Mandelkern, E. Samulski, J. Koning, and G. Wignall, Physical Properties of Polymers, Cambridge University Press (2004).

[117] I. Kranauskaitė, J. Macutkevic, A. Borisova, A. Martone, M. Zarrelli, A. Selskis, A. Aniskevich, J. Banys, *Lithuanian J. Phys*., **57**, 4 (2017).

[118] J. N. Coleman, U. Khan, W. J. Blau, Y. K. Gun'ko, *Carbon,* **44** (2006).

[119] A. Li, C. Zhang, Y. F. Zhang, *Polym*., **9**, 9 (2017)

[120] A. Plyushch, J. Macutkevic, P. Kuzhir, J. Banys, Dz. Bychanok, Ph. Lambin, S. Bistarelli, A. Cataldo, F. Micciulla, S. Bellucci, *Compos. Sci. Technol*., **128**, 75 (2016).

[121] U. Szeluga, B. Kumanek, B. Trzebicka, *Compos.:Part A,* **73**, 204 (2015).

[122] Z. A. Ghaleb, M. Mariatti ir Z. M. Ariff, *J. Reinf. Plast. Compos*., **36**, 689 (2017).

[123] I. Balberg, *J. Phys. D: Appl. Phys*. **42**, 064003 (2009).

5 Santrauka lietuvių kalba

Nanotechnologijos – viena iš sparčiai besivystančių sričių, kurioje svarbią vietą užima nanokompozitų tyrimai ir praktiniai taikymai. Elektriškai laidūs kompozitai, kuriuos sudaro polimerinė matrica ir laidžios anglies dalelės tai nauja inžinerinių medžiagų klasė. Šios medžiagos potencialiai gali būti pritaikytos gaminti antistatines, radarų bangas absorbuojančias bei apsaugančias nuo elektromagnetinės spinduliuotės dangas [1-3], taip pat elektronikoje – gaminti elektronikos komponentus [4].

Vieni efektyviausių kompozitų užpildų yra anglies nanodalelės – nanovamzdeliai, grafenas, anglies nanosvogūnai, suteikiančios kompozitams unikalių mechaninių, terminių ir elektrinių savybių. Bet tuo pačiu metu gaminant kompozitus tenka susidurti su technologinėmis problemomis, kurioms spręsti reikalingi efektyvūs sprendimai. Nanodalelės, patalpintos polimero matricoje, dėl stiprių van der Vaalso jėgų jungiasi į aglomeratus, kurie didina perkoliacijos slenkstį. Siekiant išlaikyti mechanines kompozito savybes bei sumažinti gamybos kaštus, perkoliacijos slenkstis turi būti kiek įmanoma žemesnis. Žemiausios perkoliacijos slenksčio vertės yra stebimos kompozituose su anglies nanovamzdeliais, tačiau jos gali skirtis priklausomai nuo gamybos technologijos net ir esant tai pačiai polimerinei matricai [5]. Tai reiškia, kad perkoliacijos slenksčio vertei įtakos turi ne tik dalelių dydis bei forma, bet taip pat ir dalelių pasiskirstymas polimerinėje matricoje bei gamybos technologija.

Geras dalelių pasiskirstymas gali būti pasiektas anglies daleles chemiškai modifikuojant, legiruojant, oksiduojant ir t.t., tačiau tai gali turėti neigiamą poveikį fizikinėms kompozito savybėms [6]. Kitas galimas būdas pagerinti pasiskirstymą yra dviejų skirtingo tipo užpildų panaudojimas, kas leidžia sumažinti užpildo dalelių koncentraciją išlaikant tas pačias kompozito savybes ar net pagerinant jas. Tačiau šis efektas dar nėra iki galo ištirtas.

Taigi, šiuo metu vis dar nėra pakankamai žinių apie anglies nanokompozitų mikroskopinių savybių, dalelių dydžio ir elektrinių savybių

sąryšį, todėl dielektriniai šių kompozitų tyrimai galėtų praplėsti suvokimą apie šias medžiagas.

Darbo tikslai ir uždaviniai

Šios disertacijos tikslas – ištirti įvairaus anglies užpildo dalelių dydžio ir sinergijos įtaką kompozitų dielektrinėms ir elektrinėms savybėms.

Tikslui įgyvendinti išsikelti pagrindiniai darbo uždaviniai yra: ištirti kompozitų su skirtingo dydžio anglies nanosvogūnų agregatais, skirtingo ilgio nanovamzdeliais, skirtingo dydžio grafito dalelėmis ir mišraus tipo anglies nanosvogūnų-nanovamzdelių ir grafeno-nanovamzdelių užpildu dielektrines bei elektrines savybes plačiuose dažnių (20 Hz – 1 THz) ir temperatūros (30 K – 500 K) intervaluose.

Mokslinis naujumas

Kompozitų dielektrinės savybės pirmą kartą buvo ištirtos tokiame plačiame dažnių nuo 20 Hz iki 1 THz, ir temperatūros intervale nuo 30 K iki 500 K.

Pirmą kartą ištirta anglies nanosvogūnų dalelių dydžio įtaka elektrinėms kompozitų savybėms ir perkoliacijos slenksčiui, taip pat atrasti sinergijos efektai kompozituose su mišraus užpildo anglies nanosvogūnų-nanovamzdelių užpildu.

Pirmą kartą buvo ištirta kompozitų su nanovamzdeliais dalelių dydžio įtaka elektrinėms savybėms plačiuose dažnių bei temperatūros intervaluose.

Ginamieji teiginiai

1. Kompozitų su mažesnėmis anglies nanosvogūnų dalelėmis perkoliacijos slenkstis yra žemesnis.
2. Kompozitų su anglies nanovamzdeliais elektrinio laidumo ir perkoliacijos slenkčio vertės priklauso nuo nanovamzdelių pasiskirstymo polimerinėje matricoje, bet ne nuo nanovamzdelių ilgio kaip numato perkoliacijos teorija.

120

3. Kompozitų su grafito dalelėmis žemiau perkoliacijos slenksčio dielektrinės skvarbos vertė didėja didėjant dalelių dydžiui.

4. Kompozitų su mišriu anglies nanosvogūnų-nanovamzdelių poliuretano matricoje ir grafeno-nanovamzdelių užpildu epoksidinės dervos matricoje elektrinis laidumas žymiai didesnis nei vieno užpildo kompozituose dėl sinergijos efekto.

Disertacijos sandara

Disertaciją sudaro įvadas, literatūros apžvalga, tyrimų metodika, eksperimentiniai rezultatai ir jų aptarimas, išvados, literatūros sąrašas.

Įvade pristatoma disertacijos tema bei problematika, iškeliami darbo tikslai ir suformuluojami uždaviniai jiems įgyvendinti. Taip pat pateikiamas pranešimų konferencijose bei mokslinių publikacijų sąrašas.

Literatūros apžvalgoje aptariami polimeriniai kompozitai su anglies struktūromis, fizikinės teorijos bei modeliai skirti jiems nagrinėti. Nagrinėjamos kitų autorių publikacijos bei atlikti tyrimai šioje srityje.

Trečiajame skyriuje aprašomi skirtingų dažnių diapazonų dielektrinės spektroskopijos kompozitų tyrimo metodai.

Eksperimentinėje dalyje bei rezultatų aptarime aprašomi kompozitai su skirtingais anglies dalelių užpildais – anglies nanosvogūnais, anglies nanovamzdeliais, grafitu, mišriu anglies nanosvogūnų-nanovamzdelių ir grafeno-anglies nanovamzdelių užpildais. Aptariami gauti rezultatai pritaikant teorinius modelius – perkoliacijos teoriją, tuneliavimo modelį virš perkoliacijos slenksčio laidumo mechanizmui nustatyti, dielektrinės dispersijos modelius žemiau perkoliacijos slenksčio.

Penktajame skyriuje pateikiamos išvados, šeštajame – literatūros šaltiniai.

5.1 Apžvalga

Kompozitai – tai medžiagos, sudarytos iš dviejų ar daugiau cheminėmis ir fizikinėmis savybėmis besiskiriančių fazių, atskirtų aiškia riba. Sujungtos kartu skirtingos medžiagos sudaro unikaliomis savybėmis pasižymintį junginį. Kompozitų pagrindinės struktūrinės dalys yra matrica ir užpildas. Polimerinių anglies kompozitų atveju, kompozito matrica – tai polimeras, kuris užpildomas anglies dalelėmis.

Polimerinė kompozitų matrica

Polimerai gali būti skirstomi į termoelastinius ir termoreaktyvius plastikus. Termoelastiniai plastikai kambario temperatūroje yra kietos būsenos. Kaitinant šias medžiagas, vidutinis atstumas tarp molekulių grandinių didėja, polimero molekulės gali laisviau judėti tarpusavyje, o tam tikroje temperatūroje, vadinamoje stiklėjimo temperatūra (T_s arba T_α), jis pereina iš stikliškosios būsenos į elastinę. Polimerui pereinant iš vienos būsenos į kitą keičiasi jo savybės – šiluminė talpa, savitasis tūris, elektrinės ir mechaninės savybės [7].

Termoelastiniai plastikai naudojami dėl paprasto paruošimo, šios medžiagos pasižymi plastiškumu – lengvai galima suteikti norimą formą, taip pat gali būti pakartotinai išlydomos, tai reiškia, kad jos tinkamos perdirbimui. Termoreaktyvūs plastikai pasižymi dideliu tvirtumu ir yra atsparūs cheminiam bei temperatūros poveikiui, aukštoje temperatūroje nesilydo.

Dielektrinė dispersija polimeruose

Patalpinus polimerą kintamajame elektriniame lauke, įvyksta atomų ir molekulių krūvių persiskirstymas elektrinio lauko kryptimi – poliarizacija. Dielektrinė skvarba užrašoma kompleksine forma:

$$\varepsilon^*(\omega) = \varepsilon'(\omega) - i\varepsilon''(\omega) \tag{5.1}$$

ε', ε" – reali bei menama kompleksinės dielektrinės skvarbos dalys.

Polimerai – tai kompleksiškos, neidealios sistemos, turinčios platų, asimetrinį dielektrinį spektrą ir relaksacijos trukmių pasiskirstymą, todėl aprašomos empirinėmis Debajaus relaksacijos [8] modelio modifikacijomis.

β relaksacijos spektras dažniausiai platus ir simetriškas, todėl gali būti aprašytas Koulo – Koulo formule [9]:

$$\varepsilon^* = \varepsilon_\infty + \frac{\Delta\varepsilon}{1+(i\omega\tau_{CC})^\alpha} \qquad (5.2)$$

čia α - parametras nusakantis spektro plotį ($0 < \alpha \leq 1$), τ_{CC} – Koulo-Koulo relaksacijos trukmė ($\tau_{cc} = <\tau>$). β relaksacijos proceso vidutinė relaksacijos trukmė dažniausiai aprašoma Arenijaus dėsniu:

$$\tau = \tau_0 exp\left[-\frac{E_A}{k_B T}\right] \qquad (5.3)$$

τ_0 – priešeksponentinis daugiklis, E_A– aktyvacijos energija, k_B – Bolcmano konstanta.

Bendru atveju, α-relaksacijos spektras yra platus ir asimetriškas, tuomet dielektrinė dispersija gali būti aprašyta Havriliak – Negami formule [10]:

$$\varepsilon^* = \varepsilon_\infty + \frac{\Delta\varepsilon}{(1+(i\omega\tau_{HN})^\alpha)^\gamma} \qquad (5.4)$$

α, γ – parametrai nusakantys spektro plotį bei asimetriją, τ_{HN} – Havriliak – Negami relaksacijos trukmė. Kadangi $\tau_{HN} \neq <\tau>$, tai vidutinė relaksacijos trukmė apskaičiuojama [11]:

$$\langle\tau\rangle = ln\tau_{HN} + \frac{\Psi(\gamma)+Eu}{1-\alpha} \qquad (5.5)$$

Ψ(γ) - digama funkcija, Eu – Eulerio konstanta (Eu=0,5772).

α relakasacijos proceso relaksijos trukmės temperatūrinė priklausomybė stiklėjimo temperatūros aplinkoje aprašoma Vogel-Fulcher lygtimi:

$$\tau = \tau_0 exp\left[-\frac{E_A}{k_B(T-T_0)}\right] \qquad (5.6)$$

čia T_0 – Vogel-Fulcher temperatūra temperatūra.

Anglies užpildas kompozituose

Anglis – plačiai žinomas ir labai paplitęs elementas, nuo kitų elementų beskiriantis savo struktūrų įvairove bei cheminėmis ir fizikinėmis savybėmis, kurios priklauso nuo anglies atomų tarpusavio išsidėstymo. Kompozitų

gamyboje naudojamos anglies atmainos – grafitas, grafenas, anglies nanovamzdeliai, amorfinė anglis bei fulerenai. Šios medžiagos pasižymi dideliu elektriniu laidumu.

Laidumas

Laidumas gali būti užrašomas kompleksine forma ir yra susijęs su kompleksine dielektrine skvarba:

$$\sigma^*(\omega) = \sigma'(\omega) + i\sigma''(\omega) = i\omega\varepsilon_0\varepsilon^*(\omega) \tag{5.7}$$

σ', σ'' - laidumo reali bei menama dalys, ε_0 – elektrinė konstanta ($\varepsilon_0 = 8{,}85\cdot10^{-12}$ F/m). Kai laidumo priklausomybė nuo dažnio turi dvi komponentes: nuo dažnio nepriklausantį DC laidumą ir nuo dažnio priklausantį AC laidumą, didėjantį didėjant dažniui, tuomet laidumo priklausomybė nuo dažnio užrašoma Jonscher pasiūlyta formule [12]:

$$\sigma'(\omega) = \sigma_{DC} + A\omega^n \tag{5.8}$$

A ir n – koeficientai ($0 < n \leq 1$), σ_{DC} – nuo dažnio nepriklausantis laidumas.

Perkoliacijos teorija

Užpildžius nelaidžią polimerinę matricą laidžiomis anglies dalelėmis, egzistuoja tokia dalelių koncentracija, kuriai esant kompozitas iš elektriškai nelaidaus tampa laidžiu. Ši kritinė koncentracija yra vadinama perkoliacijos slenksčiu, o modelis aprašantis sistemos perėjimą iš vienos būsenos į kitą, šiuo atveju iš nelaidžios medžiagos į laidžią, yra vadinamas perkoliacijos teorija. Taigi, pagal perkoliacijos teoriją, laidumo ir užpildo koncentracijos sąryšis išreiškiamas [13]:

$$\sigma(\varphi) \sim (\varphi - \varphi_c)^t \tag{5.9}$$

Čia φ_c – perkoliacijos slenkstis, φ – užpildo koncentracija, t – eksponentė, kurios vertė (1.6 – 2) priklauso nuo gardelės dimensijos.

Teorinis perkoliacijos slenkstis, priklausomai nuo dalelių dydžio ir formos, gali būti nustatytas pasinaudojant išplėstinio tūrio teorija [14]. Kai kompozito užpildo dalelės yra elipsės formos, tuomet perkoliacijos slenkstis:

$$1 - exp\left(-\frac{2 \times 1{,}8}{\pi A}\right) \leq \Phi_C \leq 1 - exp\left(-\frac{2 \times 2{,}28}{\pi A}\right). \tag{5.10}$$

Kai užpildo dalelės yra pailgos strypelių formos:

$$1 - exp\left(-\frac{1.4 \times \left[\frac{A\pi}{4} + \frac{\pi}{6}\right]}{\frac{A^2}{2} + 2A\pi + \frac{4\pi}{3}}\right) \leq \Phi_c \leq 1 - exp\left(-\frac{2.8 \times \left[\frac{A\pi}{4} + \frac{\pi}{6}\right]}{\frac{A^2}{2} + 2A\pi + \frac{4\pi}{3}}\right) \tag{5.11}$$

Čia A – diametro ir aukščio santykis arba ilgio ir diametro santykis.

Laidumas kompozituose

Elektrinis laidumas kompozituose virš perkoliacijos slenksčio yra sąlygotas elektronų šokinėjimo per potencinį barjerą ir tuneliavimo reiškinių, kurie gali būti paaiškinti fliuktuacijas įskaitančiu tuneliavimo modeliu ir šokinėjimo per barjerą aprašančiu Moto dėsniu. Moto dėsnis, kuris apibūdina elektrines netvarkių medžiagų savybes yra išreiškiamas formule [15]:

$$\sigma_{DC}(T) = \sigma_0 exp\left[-\left(\frac{T_M}{T}\right)^\gamma\right] \tag{5.12}$$

čia σ_0 – priešeksponentinis daugiklis, T_M – Moto charakeringoji temperatūra, apibūdinanti termiškai aktyvuotą šokinėjimą lokalizuotoje būsenoje γ – parametras susijęs su krūvio pernašos dimensija d sąryšiu $\gamma = 1/(1 + d)$, kur d = 1,2,3.

Kompozituose, kuriuose elektriškai laidžios dalelės patalpintos nelaidžioje matricoje, laidumas yra sąlygotas elektronų tuneliavimo ir yra užrašomas formule [16]:

$$\sigma_{DC} = \sigma_0 exp\left[-\frac{T_1}{(T + T_0)}\right] \tag{5.13}$$

čia T_1 – nusako energiją, kuri reikalinga elektronui peršokti potencinį barjerą tarp dviejų laidžių elementų medžiagoje, T_0 – temperatūra, kuriai esant atsiranda termiškai aktyvuota krūvio pernaša. Tuneliavimo barjero aukštis yra apibūdinamas atstumu tarp laidžių dalelių.

Kompozitų laidumą ir perkoliacijos slenkstį lemiantys veiksniai

Pagal perkoliacijos teoriją, perkoliacijos slenkstis ir laidumas priklauso nuo dalelių dydžio ir formos, tačiau eksperimentiniai rezultatai atskleidžia, kad perkoliacijos slenkstis gali būti tiek didesnis, tiek mažesnis nei numatytas

teoriškai [17]. Taip yra dėl to, kad perkoliacijos slenkstis taip pat priklauso ir nuo kitų faktorių – geometrinio dalelių išsidėstymo bei kompozitų gamybos technologijos. Pavyzdžiui, didinant nanovamzdelių koncentraciją neišvengiama jų aglomeracijos, kas mažina laidumą ir didina perkoliacijos slenksčio vertę [18].

Elektrinis laidumas gali būti padidintas, o tuo pačiu sumažintas perkoliacijos slenkstis gerinant užpildo dalelių pasiskirtstymą - modifikuojant daleles, įterpiant papildomą užpildą į matricą. Papildomo užpildo įterpimas į matricą, pavyzdžiui, suodžių ir TiO_3 arba nelaidžių nanodeimantų kartu su anglies nanovamzdeliais, leidžia pagerinti užpildo tarpusavio pasiskirstymą ir sumažinti perkoliacijos slenkstį dėl sinergijos efekto. Pagal išplėstojo tūrio teoriją, kompozitai su mišriu dalelių užpildu turi tenkinti lygybę [19]:

$$\frac{m_1}{p_{c,1}} + \frac{m_2}{p_{c,2}} = 1 \qquad (5.14)$$

Čia m_1 ir m_2 – pirmojo ir antrojo užpildo masės dalis kompozite, $p_{c,1}$ ir $p_{c,2}$ perkoliacijos slenksčiai kompozituose, kai yra tik vieno tipo užpildas. Kai ši suma yra mažesnė negu 1, galima teigti, kad pasiektas sinergijos efektas. Sinergijos efektas reiškia, kad su mažesniu dalelių kiekiu galima pasiekti tas pačias laidumo vertes.

5.2 Tyrimų metodika

Tirtos medžiagos

Disertacijoje apžvelgiamos kelios skirtingos kompozitų grupės:

1. Kompozitai su skirtingo dydžio (40 nm, 100 nm, 250 nm) anglies nanosvogūnų užpildu, kai užpildo dalelių koncentracija yra 0 – 14 tūrio %. Kompozitų matrica – polidimetilsiloksanas (PDMS) ir poliuretanas (PU).
2. Kompozitai su mišriu anglies nanosvogūnų-nanovamzdelių užpildu, kai bendra dalelių koncentracija iki 7,5 masės %. Kompozitų matrica - poliuretanas (PU).

3. Kompozitai su skirtingo ilgio nanovamzdeliais, kai visų nanovamdelių skersmuo 9 nm, o dalelių koncentracija 0 – 4 masės %. Kompozitų matrica – polimetilmetakrilatas (PMMA).

4. Kompozitai su skirtingo dydžio grafito dalelėmis, kai dalelių koncentracija kompozite 0 – 2 masės %. Kompozitų matrica – bisfenolio A epoksidinė derva.

5. Kompozitai su grafenu, anglies nanovamzdeliais ir mišriu nanovamzdelių – grafeno dalelių užpildu. Kompozitų matrica – RTM 6 epoksidinė derva.

Matavimų metodai

Tiriamųjų kompozitų kompleksinės dielektrinės skvarbos $\varepsilon^* = \varepsilon' - i\varepsilon''$ matavimai atlikti plačiame temperatūros (nuo 30 K iki 500 K) ir dažnių (nuo 20 Hz iki 1 THz) intervale. Žemuose dažniuose, nuo 20 Hz iki 1 MHz matavimai atlikti LCR matuokliu (HP 4284A), kuriuo išmatuota bandinio talpa ir nuostolių kampas. Dažnių ruože nuo 1 MHz iki 3 GHz matavimai atlikti vektoriniu grandinių analizatoriumi (Agilent 8714ET) bendraašėje linijoje. Buvo išmatuoti signalo atspindys ir fazė. Mikrobangų diapazone, nuo 27 GHz iki 40 GHz, matavimai atlikti skaliariniu grandinių analizatorium (R2-408R, ELMIKA, Vilnius, Lietuva). Dažnių ruože nuo 100 GHz iki 3 THz matavimai atlikti terahercų spektrometru (EKSPLA, Vilnius, Lietuva).

5.3 Pagrindiniai rezultatai

Kompozitai su anglies nanosvogūnų užpildu

Šiame poskyryje pateikti tyrimų rezultatai ir jų aptarimas, kurie atskleidžia elektrinių savybių ir perkoliacijos slenksčio priklausomybę nuo anglies nanosvogūnų (OLC, *anglų k. onion like carbon*) agregatų dydžio. Anglies nanosvogūnų dalelės yra koncentriškai išsidėstę fulerenai, kurių laidumas kambario temperatūroje gali siekti iki kelių šimtų S/m [20]. Daugiausia su šių

dalelių intarpais užpildytų kompozitų tyrimų yra atlikta žemiau perkoliacijos slenksčio, kur kompleksinė dielektrinė skvarba nežymiai didėja didinant dalelių koncentraciją [21, 22]. Tikėtina, kad anglies nanosvogūnų dalelės, savo struktūra turinčios panašumų su suodžiais, gali jungtis į agregatus, nuo kurių dydžio priklauso dielektrinės ir elektrinės kompozitų savybės.

Buvo nustatyta, kad žemiausios perkoliacijos slenksčio vertės yra stebimos kompozituose su mažiausio dydžio (40 nm) anglies nanosvogūnų dalelėmis (5.1 pav.) nepriklausomai nuo polimerinės matricos – 5,4 tūrio % OLC/PDMS kompozituose ir 7,1 tūrio % OLC/PU kompozituose. Anglies nanosvogūnų dalelės, įterptos į polimerinę matricą, deformuojasi ir jungiasi į grandinę formuodamos pailgą struktūrą. Mažesnio dydžio dalelės deformuojasi žymiai lengviau, todėl perkoliacijos slenkstis yra žemesnis.
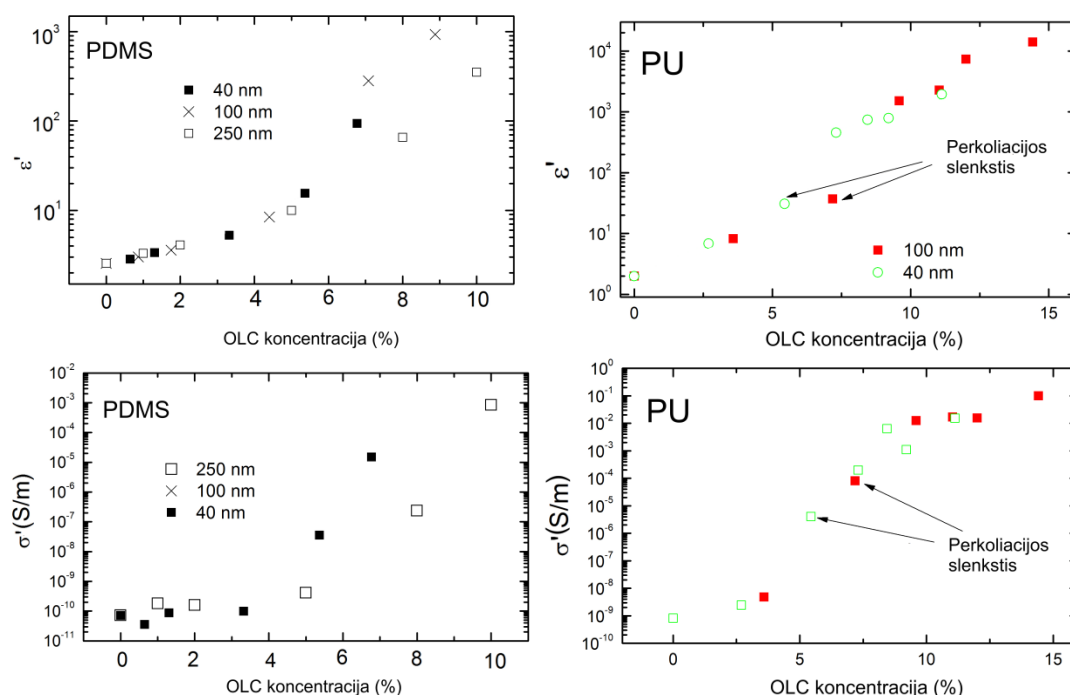

5.1 pav. PDMS ir PU kompozitų kompleksinės dielektrinės skvarbos realios dalies ir kompleksinio laidumo realios dalies priklausomybės nuo anglies nanosvogūnų dalelių koncentracijos kambario temperatūroje

PDMS kompozitai su anglies nanosvogūnų užpildu

PDMS kompozitų dielektrinės bei elektrinės savybės buvo tirtos plačiuose dažnių (20 Hz – 1 THz) ir temperatūros intervaluose nuo 30 K iki 500 K. Galima išskirti dvi elektrinio laidumo kitimo sritis – virš ir žemiau kambario

temperatūros. Virš kambario temperatūros elektrinis laidumas mažėja didėjant temperatūrai ir aukštesnėje negu 470 K temperatūroje išnyksta visuose tirtuose PDMS kompozituose.
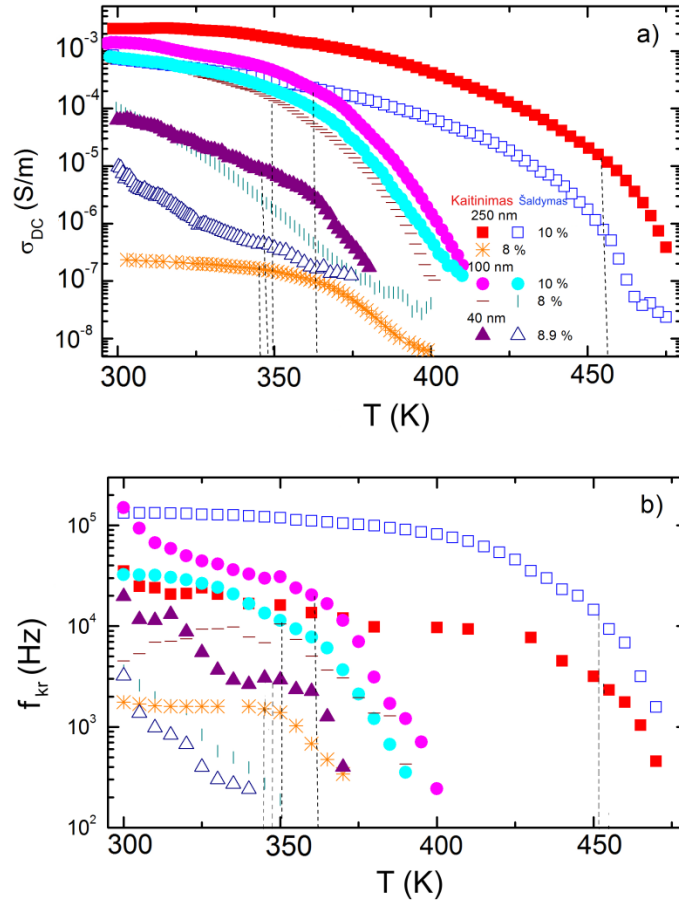
5.2 pav. PDMS kompozitų su anglies nanosvogūnų dalelėmis a) nuo dažnio nepriklausančio laidumo, b) kritinio dažnio priklausomybės nuo temperatūros

Iš temperatūrinių priklausomybių matyti (5.2 pav.), kad žemoje temperatūroje elektrinis laidumas ir kritinis dažnis beveik nepriklauso nuo temperatūros ir priklausomai nuo dalelių dydžio, tam tikroje kritinėje temperatūroje pereina iš laidininko būsenos į izoliatoriaus. Kritinės temperatūros pateiktos Lentelėje 5.1.
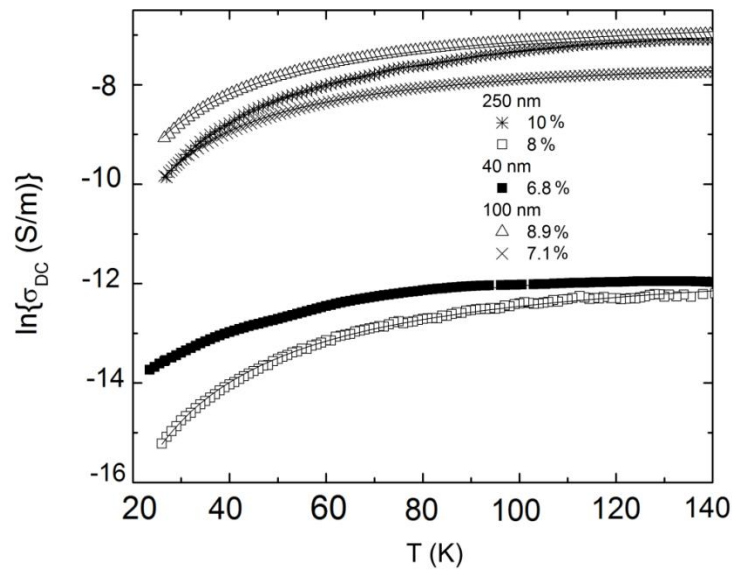
Lentelė 5.1. PDMS kompozitų su anglies nanosvogūnų dalelėmis kritinės temperatūros, kuriose kompozitai pereina iš laidininko būsenos į izoliatoriaus būseną

Agregatų dydis (nm)	Koncentracija (tūrio %)	T (K)
250	10	476
	8	382
100	8.9	413
	7.1	401
40	6.8	398

Kritinė temperatūra priklauso nuo dalelių dydžio ir koncentracijos. Ši temperatūra mažėja mažėjant dalelių dydžiui ir koncentracijai. Šis perėjimas iš laidininko būsenos į izoliatoriaus būseną gali būti paaiškintas skirtingu anglies nanosvogūnų ir PDMS matricos terminiu plėtimusi. PDMS matrica plečiasi žymiai sparčiau, todėl didėja tarpai tarp laidžių dalelių, kas lemia didėjantį barjerą elektronų tuneliavimui ir aukštoje temperatūroje laidumas išnyksta. Kai dalelių koncentracija nedidelė, didėjant temperatūrai suardomas laidus tinklas ir perėjimas iš laidininko į izoliatoriaus būseną yra negrįžtamas procesas. Panašus laidumo sumažėjimas didėjant temperatūrai buvo stebimas ir kituose kompozituose, tačiau izoliatoriaus būsena nebuvo pasiekta dėl pačios kompozito matricos laidumo [23].

Žemose temperatūrose elektrinis laidumas didėja didėjant temperatūrai ir gali būti aproksimuotas tuneliavimo modeliu arba Moto dėsniu (5.3 pav.).

5.3 pav. PDMS kompozitų su anglies nanosvogūnų dalelėmis nuo DC laidumo priklausomybės nuo temperatūros esant skirtingam dalelių dydžiui ir koncentracijai. Ištisinėmis kreivėmis pavaizduotos aproksimacijos tuneliavimo dėsniu

Iš aproksimavimo tuneliavimo dėsniu, energijos reikalingos elektronui tuneliuoti ber barjerą (T_1) ir temperatūros, kuriai esant atsiranda termiškai aktyvuotas laidumas (T_0), santykis T_1/T_0 mažėja mažėjant dalelių dydžiui. Santykis T_1/T_0 taip pat mažėja didinant dalelių koncentraciją (100 nm dalelės). Iš aproksimacijos Moto dėsniu, parametro vertė n yra lygi ~ 1, kuri yra tipiška anglies nanosvogūnų milteliams [20]. Taigi, elektrinis laidumas kompozituose su anglies nanosvogūnų dalelėmis gali būti sąlygotas elektronų šokinėjimo anglies dalelių klasterių viduje ir tuneliavimo tarp anglies dalelių.

PU kompozitai su anglies nanosvogūnų dalelėmis

Kompozitų su PU polimerine matrica ir anglies nanosvogūnų užpildu dielektrinės bei elektrinės savybės tirtos dažniuose nuo 20 Hz iki 1 THz ir temperatūros intervale nuo 30 K iki 300 K.

Virš perkoliacijos slenksčio kompozitų elektrinis laidumas nuo dažnio kinta pagal Jonscher dėsnį – žemuose dažniuose stebimas nuo dažnio nepriklausantis (DC) laidumas, o aukštuose dažniuose nuo dažnio priklausantis laidumas (AC). Šios dvi laidumo sritys atskirtos kritiniu dažniu (f_{kr}). DC

laidumas mažėja žemėjant temperatūrai ir žemose temperatūrose kinta pagal tuneliavimo ir Moto dėsnius.

Kaip ir PDMS kompozitų atveju, žemose temperatūrose temperatūrinės laidumo priklausomybės gali būti aproksimuotos tuneliavimo bei Moto dėsniais. Dimensija n yra apie 0.5, kas yra tipiška anglies nanosvogūnų dalelėms pagamintoms atkaitinus nanodeimantus 1600 K [20].

PU kompozitai su mišriu anglies nanosvogūnų – nanovamzdelių užpildu

Šiame poskyryje aptariamos elektrinės kompozitų su mišriu anglies nanosvogūnų – nanovamzdelių užpildu, kai nanovamzdelių (CNT, *anglų k. carbon nanotubes*) koncentracija kompozite 0,5 masės %, o anglies nanosvogūnų koncentracija 2, 5 ir 7 masės %. Elektrinio laidumo priklausomybės nuo dažnio pavaizduotos 5.4 pav.
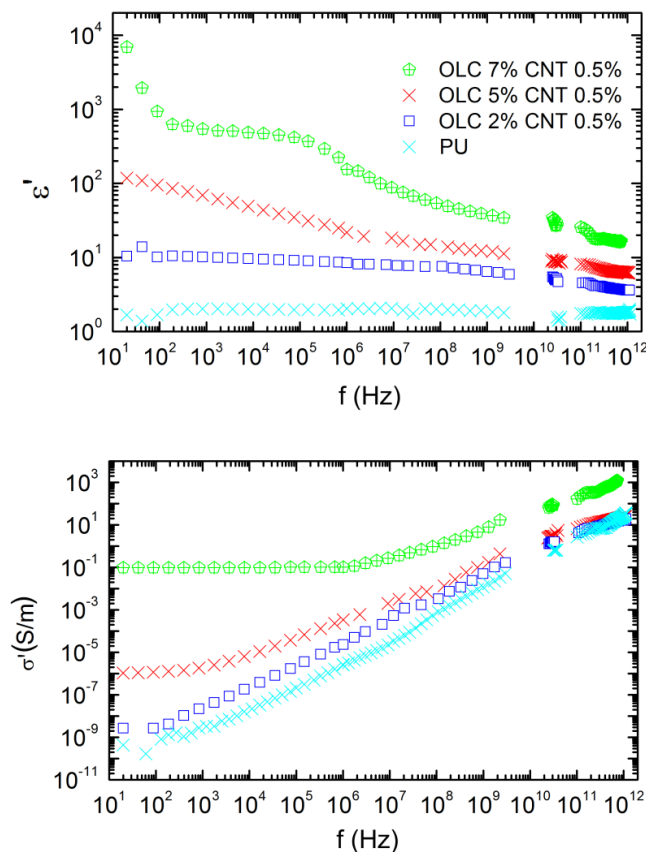

5.4 pav. PU kompozitų su mišriu anglies nanosvogūnų-nanovamzdelių užpildu kompleksinės dielektrinės skvarbos realios dalies ir kompleksinio laidumo realios dalies priklausomybės nuo dažnio kambario temperatūroje

Dielektrinės skvarbos vertė ir laidumas kompozitų su 2 masės % anglies nanosvogūnų užpildo ir 0,5 masės % nanovamzdelių yra artimos grynos PU matricos vertėms, tačiau šios vertės, didinant anglies nanosvogūnų koncentraciją, didėja ir žymiai išauga. Taip pat stebimas nuo dažnio nepriklausantis laidumas, o tai rodo, kad pasiekta elektrinė perkoliacija. Kompozituose su mišriu užpildu perkoliacijos slenkstis ~ 5 masės %, nors perkoliacija nei su 5 masės % anglies nanosvogūnų dalelėmis, nei su 0,5 masės % nanovamzdelių nebūtų stebima.

Kompozitai su anglies nanovamzdeliais

Priklausomai nuo daugiasienių anglies nanovamzdelių (MWCNT, *anglų k. multiwalled carbon nanotubes*) koncentracijos ir matmenų santykio dielektrinės skvarbos ir elektrinio laidumo vertės gali skirtis, todėl yra svarbu nustatyti šių savybių ir nanovamzdelių parametrų sąryšį dėl praktinės šių kompozitų pritaikymo galimybės [24]. Daugiausiai tyrimų atlikta kambario temperatūroje ir siauruose dažnių intervaluose [25], o plačiame temperatūros ir dažnių intervale atlikti tyrimai neatskleidė anglies nanovamzdelių dydžio (ilgio ir skersmens santykio) įtakos dielektrinėms ir elektrinėms kompozitų savybėms [26]. Kompozitų su anglies nanovamzdeliais dielektrinės skvarbos ir laidumo priklausomybė nuo dalelių koncentracijos pateikta 5.5 pav.
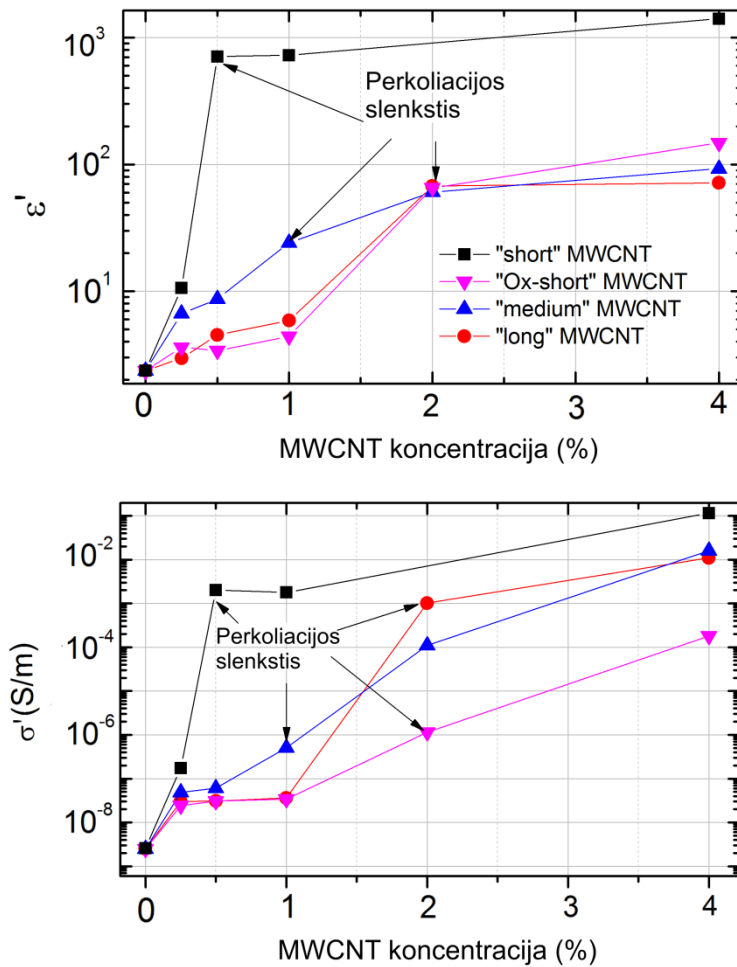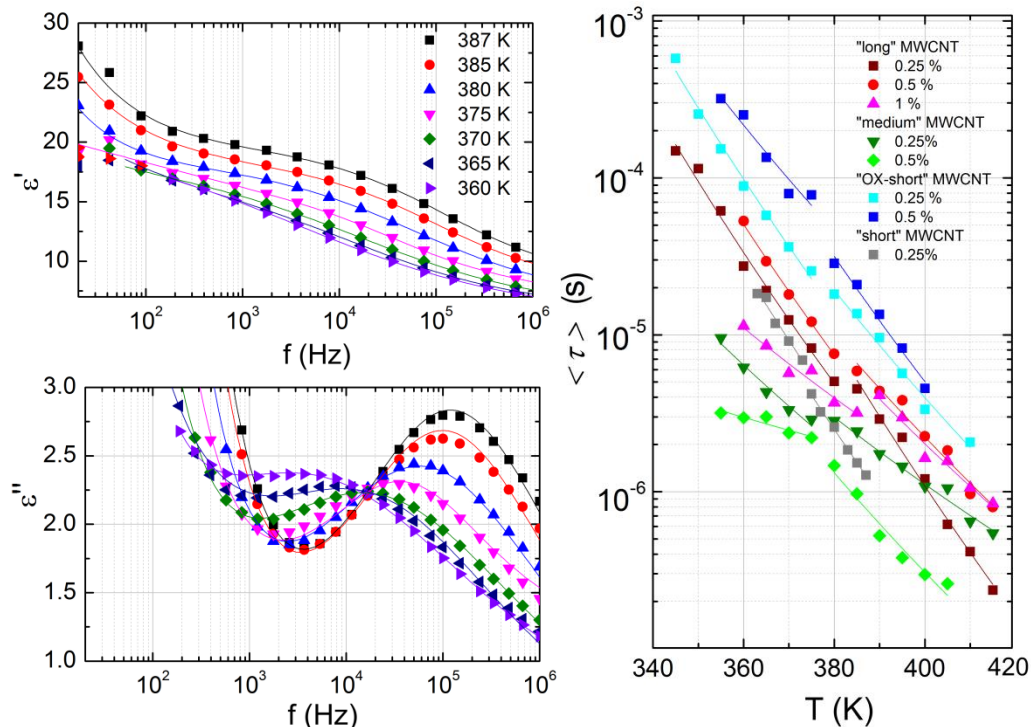
5.5 pav. Kompozitų su anglies nanovamzdeliais dielektrinės skvarbos ir laidumo priklausomybė nuo nanovamzdelių koncentracijos esant skirtingam nanovamzdelių ilgiui. Rodyklėmis pavaizduoti perkoliacijos slenksčiai

Pagal perkoliacijos teoriją perkoliacijos slenkstis yra atvirkščiai proporcingas dalelių dydžiui, tačiau iš eksperimentinių rezultatų matyti, kad šiuo atveju perkoliacijos slenkstis nepriklauso nuo nanovamzdelių ilgio. Žemiausias perkoliacijos slenkstis stebimas kompozituose su mažiausio ilgio nanovamzdeliais ir didžiausias – su didžiausio ilgio nanovamzdeliais. Tai galima paaiškinti netolygiu nanovamzdelių pasiskirtstymu polimerinėje matricoje ir aglomeratų formavimusi dėl stiprių van der Vaalso jėgų.
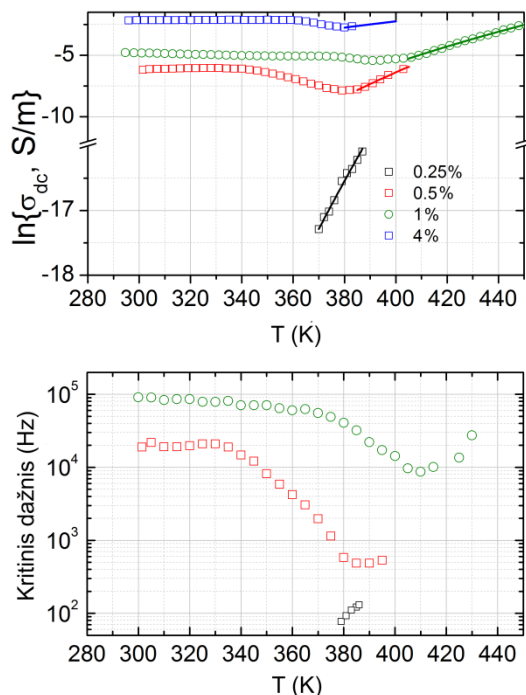
Kompozituose su anglies nanovamzdeliais žemiau perkoliacijos slenksčio kambario ir aukštesnėje temperatūroje, kaip ir PMMA, stebima dielektrinė dispersija, kuri gali būti siejama su polimero perėjimu iš stikliškosios būsenos į elastinę (5.6 pav.). Dielektriniai spektrai platūs ir simetriniai, todėl gali būti

aprašyti Havriliak-Negami formule. Vidutinis relaksacijos laikas yra mažiausias kompozitų su mažiausio ilgio nanovamzdeliais, tačiau vertės artimos polimerinės matricos be užpildo vertėms.

5.6 pav. Kompozitų su anglies nanovamzdeliais, kurių ilgis 438 nm, kompleksinės dielektrinės skvarbos realios bei menamos dalies priklausomybės nuo dažnio esant skirtingoms temperatūroms, kai nanovamzdelių koncentracija 0,25 % (ištisinėmis kreivėmis pavaizduota aproksimacija Havriliak-Negami formule) ir vidutinio relaksacijos laiko priklausomybės nuo temperatūros(ištisinėmis kreivėmis pavaizduota aproksimacija Arenijaus dėsniu)

Virš perkoliacijos slenksčio visuose tirtuose kompozituose visame temperatūros intervale yra stebimas nuo dažnio nepriklausantis DC laidumas (5.7 pav.). Laidumo kitimo pobūdis skiriasi priklausomai nuo temperatūros intervalo. Galima išskirti tris elektrinio laidumo sritis: 1) laidumas žemose temperatūrose kinta pagal tuneliavimo dėsnį, 2) temperatūros intervale nuo 340 K iki 380 K laidumas mažėja dėl skirtingų terminių PMMA matricos ir anglies nanovamzdelių savybių, PMMA matricai plečiantis, vidutinis atstumas tarp laidžių dalelių didėja, 3) aukštose temperatūrose laidumas didėja didėjant temperatūrai ne tik kompozituose virš perkoliacijos slenksčio, bet ir žemiau perkoliacijos slenksčio. Taigi šis didėjimas gali būti paaiškintas polimerinės matricos laidumo atsiradimu aukštoje temperatūroje.

5.7 pav. Kompozitų su 328 nm ilgio anglies nanovamzdeliais DC laidumo ir kritinio dažnio priklausomybės nuo temperatūros

Žemoje temperatūroje, žemesnėje negu 200 K, nuo dažnio nepriklausantis DC laidumas kinta pagal tuneliavimo dėsnį. Kadangi parametrų santykis T_1/T_0 yra proporcingas atstumui tarp laidžių dalelių, tai šis santykis turi mažėti nuo nanovamzdelių koncentracijos, kas ir yra stebima tirtuose kompozituose.

Epoksidinės dervos kompozitai su grafito dalelėmis

Kompozitai su anglies nanovamzdeliais turi žemą perkoliacijos slenkstį ir dideles dielektrinės skvarbos bei laidumo vertes įskaitant mikrobangų ir terahercų diapazonus. Tačiau pagrindiniai nanovamzdelių trūkumai yra palyginus didelė jų kaina, taip pat nanovamzdeliai yra galimai toksiški [27]. Kaip alternatyva anglies nanovamzdeliams iš dalies galėtų būti grafito dalelės, tokios kaip išplėstasis grafitas (EG, *anglų k. exfoliated graphite*), pasižymintis porėta struktūra ir dideliu laidumu.

Kompozitų su skirtingo dydžio grafito dalelėmis: FG (*anglų k. fine graphite*), NG (*anglų k. natural graphite*), CG (*anglų k. coarse graphite*), EG (*anglų k. exfoliated graphite*) ir grynos epoksidinės dervos kompleksinės

136

dielektrinės skvarbos priklausomybės nuo dažnio kambario temperatūroje pateiktos 5.8 pav.
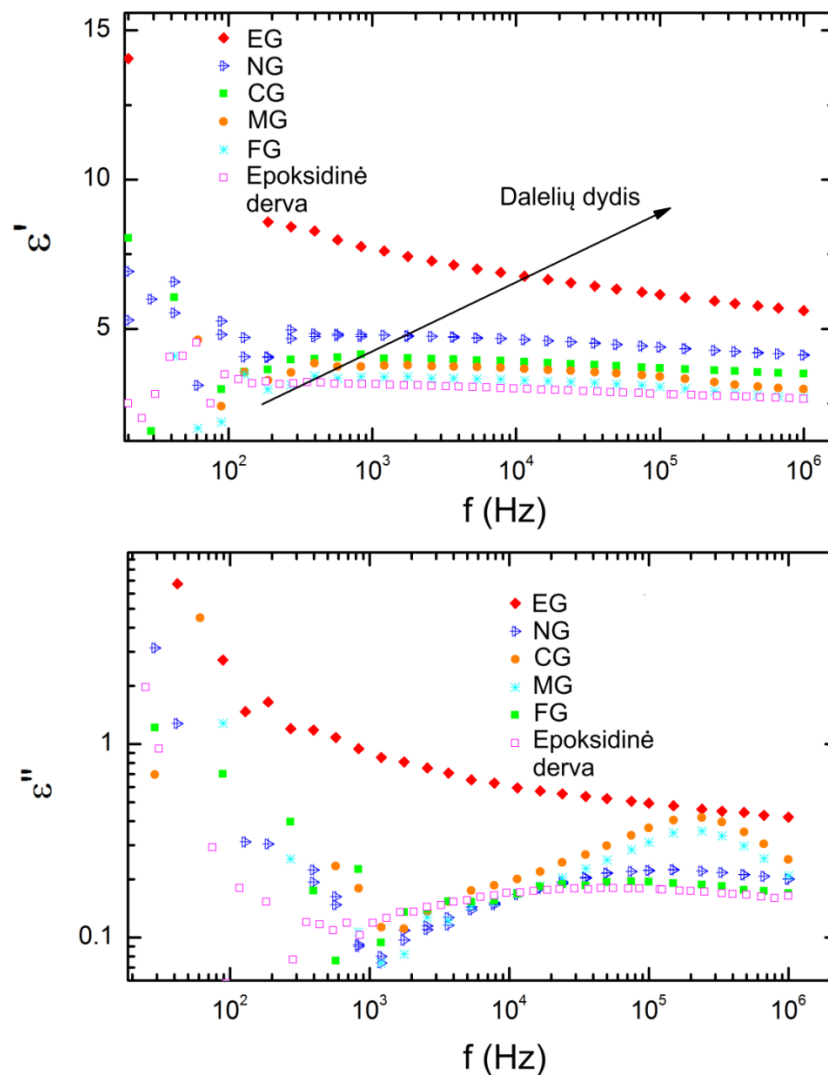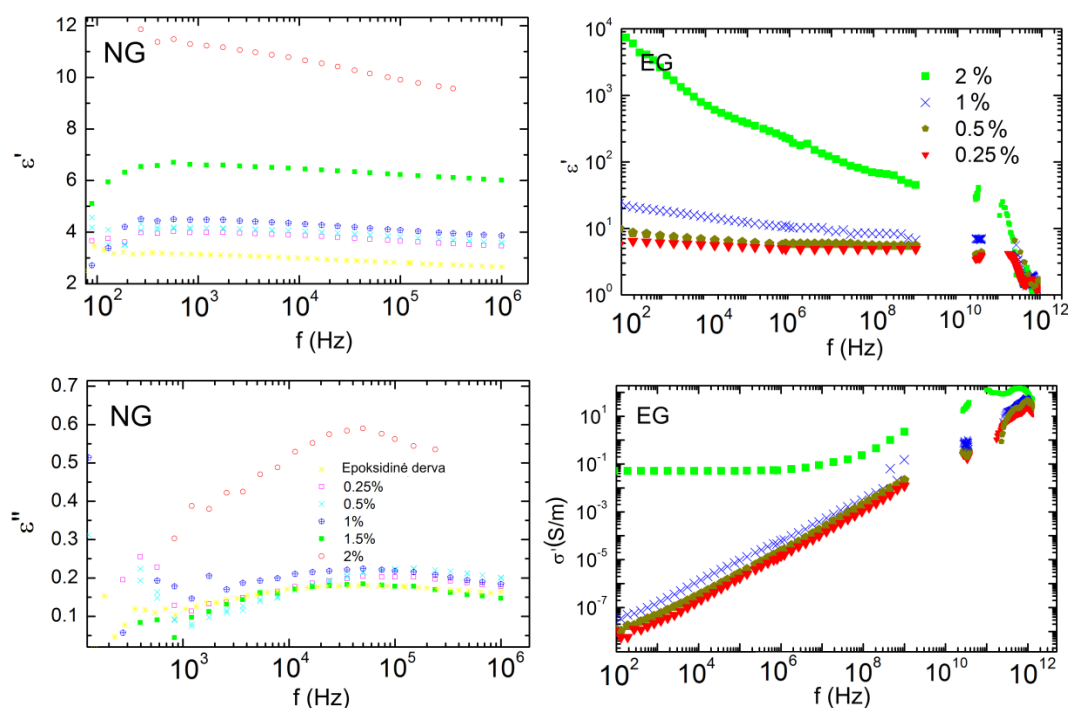

5.8 pav. Epoksidinės dervos kompozitų su grafito dalelėmis kompleksinės dielektrinės skvarbos priklausomybė nuo dažnio kambario temperatūroje, kai dalelių koncentracija 0,5 %

Dielektrinės skvarbos vertė didėja didėjant grafito dalelių dydžiui esant tai pačiai dalelių koncentracijai. Dielektrinės skvarbos didėjimą didėjant grafito dalelių dydžiui galima paaiškinti žemesniu perkoliacijos slenksčiu kompozituose su didesnėmis grafito dalelėmis.

Didinant dalelių koncentraciją, dielektrinės skvarbos vertė didėja (5.9 pav.), bet išlieka artima grynos epoksidinės dervos dielektrinės skvarbos vertei, išskyrus kompozitus su išplėstuoju grafitu. Dielektrinė dispersija stebima dažniuose nuo 10 kHz iki 100 kHz ir gali būti siejama su grynos epoksidinės

dervos α relaksacija polimerinėje matricoje. Tai reiškia, kad kritinė dalelių koncentracija, kuriai esant atsiranda elektrinė perkoliacija yra didesnė negu 2 %. Panašūs rezultatai buvo gauti tiriant kitus kompozitus su dirbtinio grafito dalelėmis (FG, MG, CG), kuriuose perkoliacijos slenkstis taip pat didesnis negu 2 %. Kompozitų su išplėstuoju grafitu perkoliacijos slenksčio vertė yra ~1,5 % užpildo dalelių koncentracijos (5.9 pav.). Aukščiau ir arti perkoliacijos slenksčio kompleksinės dielektrinės skvarbos vertės žymiai išauga. Žema perkoliacijos slenksčio vertė gali būti siejama su mažu išplėstojo grafito tankiu ir dideliu porėtumu.

5.9 pav. Kompozitų su naturaliu grafitu (NG) ir su išplėstuoju grafitu (EG) kompleksinės dielektrinės skvarbos priklausomybės nuo dažnio

Kompozituose su grafito dalelėmis žemesnėje negu 370 K temperatūroje stebima dielektrinė dispersija, dielektrinės skvarbos menamos dalies maksimumas didėjant dažniui slenka aukštesnių temperatūrų link (5.10 pav.). Aukštesnėje negu 370 K temperatūroje dispersija gali būti siejama su laidumu. Panašus dielektrinės dispersijos kitimo pobūdis dėl polimero molekulių dinamikos yra stebimas grynoje epoksidinėje dervoje.
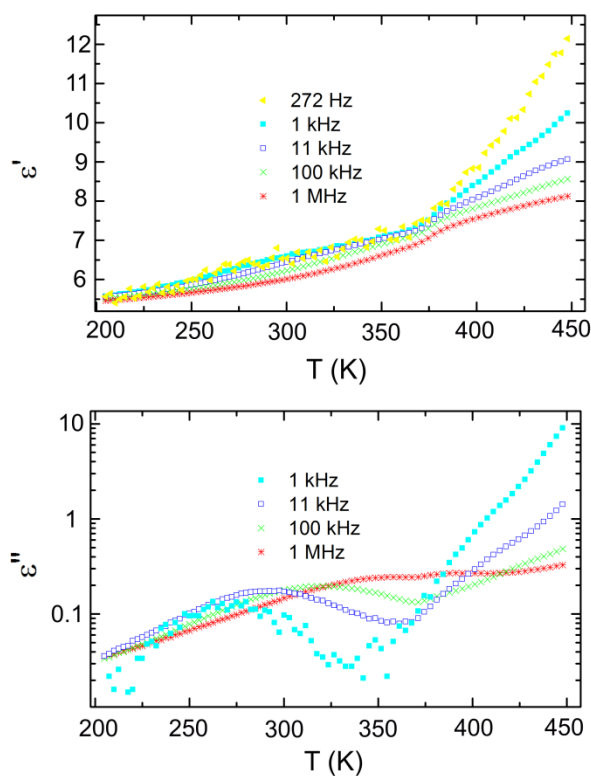
5.10 pav. Epoksidinės dervos kompozitų su natūraliu grafitu kompleksinės dielektrinės skvarbos realios ir menamos dalies priklausomybė nuo temperatūros skirtinguose dažniuose, kai dalelių koncentracija 1,5 %

Kompozitų su natūralaus grafito dalelėmis dielektrinės skvarbos priklausomybės nuo dažnio gali būti aprašytos Havriliak-Negami formule (5.11 pav.). Kompleksinės dielektrinės skvarbos menamos dalies maksimumo vertė didėjant temperatūrai didėja ir slenka aukštesnių dažnių link. Vidutinės relaksacijos priklausomybė nuo temperatūros kinta pagal Vogel – Fulcher dėsnį (5.11 pav.).

139
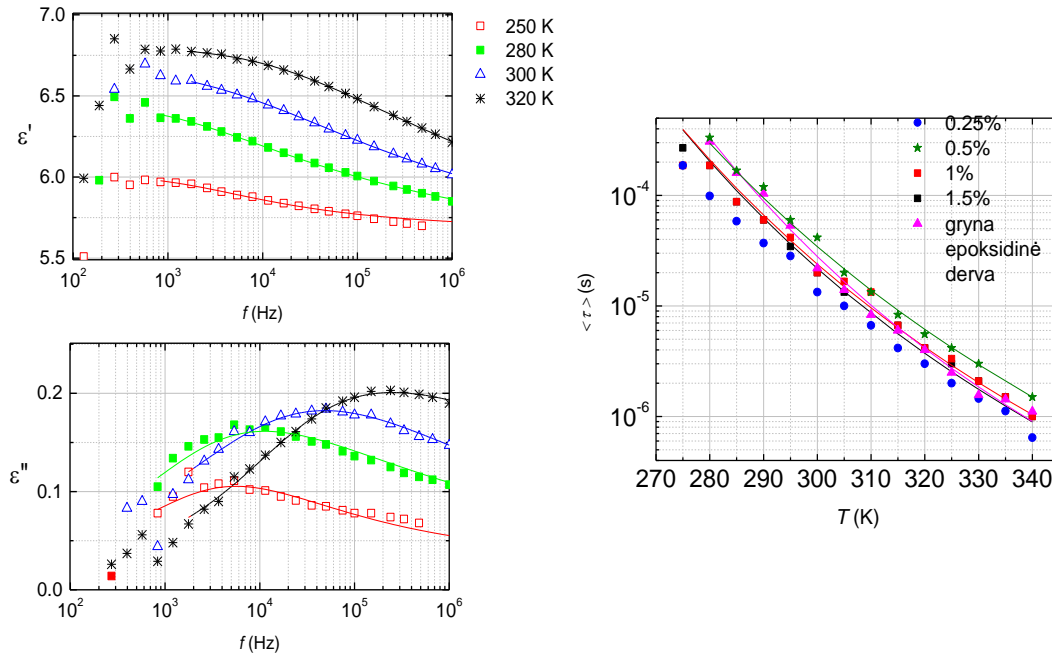
5.11 pav. Kompozitų su natūralaus grafito dalelėmis kompleksinės dielektrinės skvarbos priklausomybė nuo dažnio (ištisinėmis kreivėmis pavaizduota aproksimacija Havriliak-Negami formule) ir relaksacijos laiko priklausomybė nuo temperatūro (ištisinėmis kreivėmis pavaizduota aproksimacija Vogel-Fulcher dėsniu

Kompozitų su išplėstuoju grafitu perkoliacijos slenkstis yra ~1,5 %, virš perkoliacijos slenksčio stebimas nuo dažnio nepriklausantis laidumas visame tirtame temperatūros intervale nuo 30 K iki 450 K (5.12 pav.). Temperatūrines laidumo priklausomybes galima suskirstyti į tris kitimo sritis: 1 – žemesnėse negu 150 K temperatūrose, kuriose laidumas kinta pagal tuneliavimo dėsnį, 2 – temperatūros intervale nuo 150 K iki 410 K, kuriame laidumas mažėja didėjant temperatūrai, 3 – virš 410 K laidumas didėja didėjant temperatūrai pagal Arenijaus dėsnį (5.12 pav.).
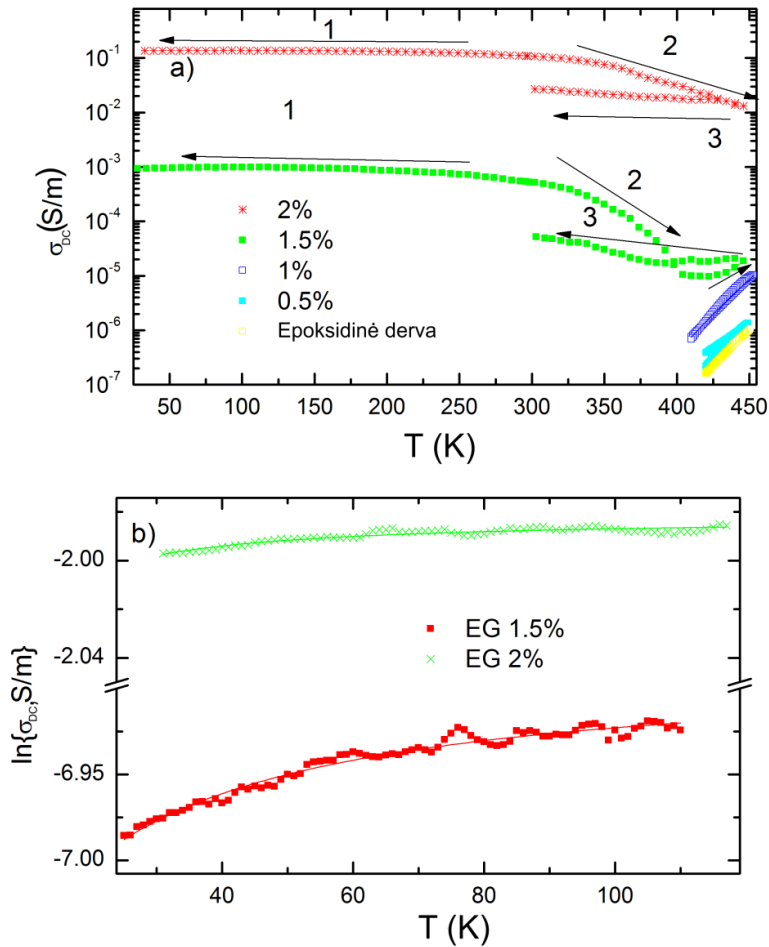
5.12 pav. Kompozitų su išplėstuoju grafitu DC laidumo priklausomybės nuo temperatūros a) visame tirtame temperatūros intervale, b) temperatūroje žemesnėje negu 150 K

Kompozitų su išplėstuoju grafitu elektrinis laidumas virš perkoliacijos slenksčio yra lemiamas elektronų tuneliavimo tarp grafito dalelių. Tuneliavimo reiškinys charakterizuojamas žemu potenciniu barjeru elektronų tuneliavimui. Tokios vertės buvo stebimos kompozituose su anglies nanovamzdeliais ir su suodžiais, tačiau esant didesnei dalelių koncentracijai.

Kompozitai su mišriu anglies nanovamzdelių-grafeno užpildu

Kompozitų su daugiasieniais anglies nanovamzdeliais (MWCNT, *anglų k. multiwalled carbon nanotubes*), grafeno dalelėmis (GNP, *anglų k. graphene nanoplatelets*) ir mišriu nanovamzdelių-grafeno dalelių (MWCNT/GNP) užpildu dielektrinės ir elektrinės savybės ištirtos plačiame dažnių (20 Hz – 30 GHz) ir temperatūros intervale (30 – 300 K) . Kompozitų su grafenu teorinis

141

pagal perkoliacijos teoriją apskaičiuotas perkoliacijos slenkstis yra 3 masės %, tačiau iš eksperimentinių rezultatų matyti, kad perkoliacijos slenkstis yra aukštesnis negu 3 masės %. Šiuo atveju dielektrinės skvarbos ir laidumo vertės yra artimos epoksidinės dervos vertėms. Visi tirti kompozitai su mišriu anglies nanovamzdelių-grafeno užpildu yra virš perkoliacijos slenksčio. Mišraus užpildo panaudojimas perkoliacijos slenksčio vertės nesumažino, tačiau žymiai išaugo laidumas esant tai pačiai nanovamzdelių koncentracijai.
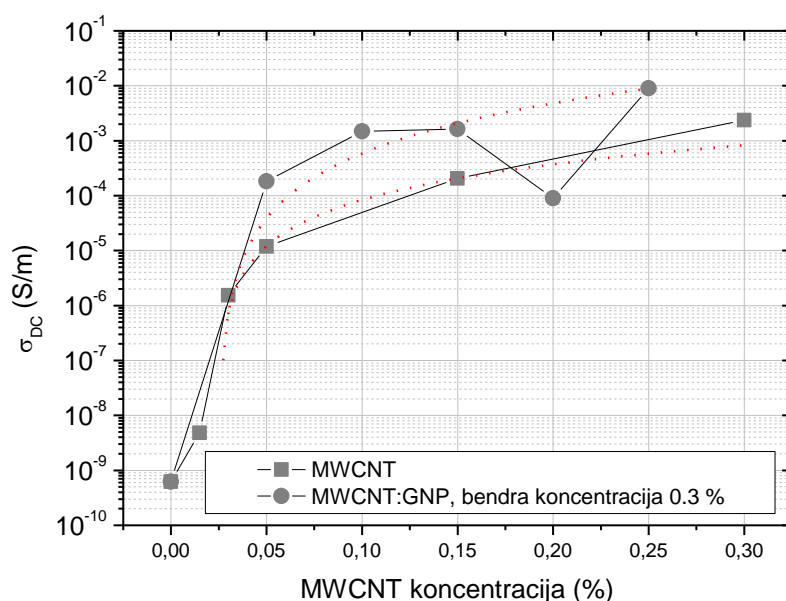
5.13 pav. DC laidumo priklausomybė nuo anglies nanovamzdelių koncentracijos

Didžiausia laidumo vertė (8,9 mS/m) gauta kompozitams su mišriu užpildu, kai nanovamzdelių koncentracija 0,25 %, grafeno dalelių 0,05 % (bendra užpildo koncentracija yra 0,3 masės %). Palyginimui, kompozitų tik su anglies nanovamzdelių užpildu ir 0,3 masės % koncentracija laidumas mažesnis 4 kartus (2 mS/m). Toks laidumo padidėjimas įterpus mišraus užpildo daleles gali būti siejamas su žymiai efektyvesnio laidaus tinklo formavimusi sąveikaujant 2D anglies nanovamzdeliams ir 1D GNP dalelėms.

Temperatūrinės laidumo priklausomybės žemiau kambario temperatūros gali būti aproksimuotos tuneliavimo dėsniu (5.14 pav.). Aproksimavimo tuneliavimo dėsniu parametrų vertės pateiktos Lentelėje 5.2.
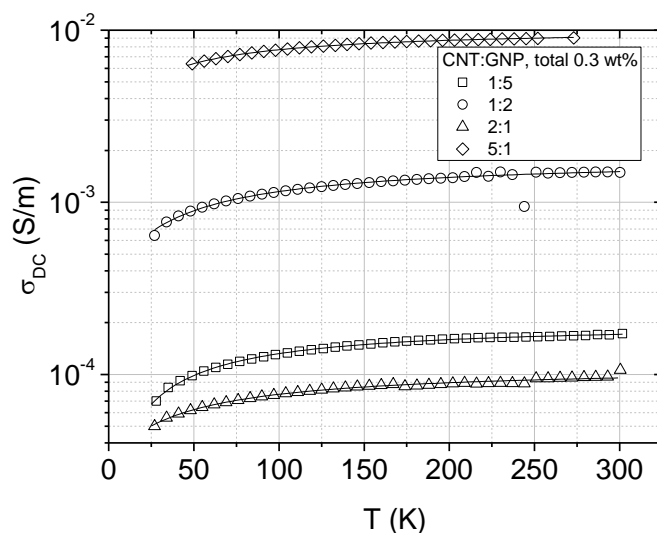
5.14 pav. Kompozitų su mišriu anglies nanovamzdelių-grafeno dalelių užpildu DC laidumo priklausomybės nuo temperatūros. Ištisinėmis linijomis pavaizduotas aproksimavimas tuneliavimo dėsniu

Lentelė 5.2. Aproksimavimo tuneliavimo dėsniu parametrų vertės

MWCNT (wt.%)	$\ln\sigma_0$ (S/m)	T_1 (K)	T_0 (K)
0.03	-13.3	63	34
0.05	-11.1	77	27
0.15	-8.5	22	15
0.3	-5.1	46	41
CNT:GNP (total 0.3 wt.%)			
1:5	-8.5	50	20
1:2	-6.3	61	37
2:1	-9.1	52	41
5:1	-4.5	36	27

Parametrų santykis T_1/T_0 mažėja didinant dalelių koncentraciją nepriklausomai nuo to ar užpildas yra tik anglies nanovamzdeliai ar mišrus, kadangi sumažėja atstumas elektronams tuneliuoti per barjerą. Taip pat šis santykis yra mažesnis kompozitų su mišriu užpildu dėl mažesnių atstumų tarp laidžių dalelių. Taigi, geresnis dalelių pasiskirstymas matricoje ir dėl to žymiai išaugęs elektrinis laidumas mišraus užpildo kompozituose gali būti laikomas sinergijos efektu.

5.4 Pagrindinės išvados

Šiame darbe buvo tirtos dielektrinės ir elektrinės kompozitų su anglies nanodalelėmis savybės plačiame dažnių bei temperatūros intervaluose. Buvo nustatyta, kad:

- Kompozitų su anglies nanosvogūnų užpildu virš perkoliacijos slenksčio laidumas lemiamas elektronų šokinėjimo anglies nanosvogūnų viduje ir tuneliavimo tarp dalelių agregatų.

- Mažesnio dydžio anglies nanosvogūnų agregatai žymiai lengviau deformuojasi sudarydami išilginę struktūrą, o tai leidžia sumažinti perkoliacijos slenksčio vertę. Šios kompozitų laidumo vertės panašios kaip ir kompozitų su anglies nanovamzdeliais, tačiau perkoliacijos slenkstis yra aukštesnis.

- PDMS kompozituose su anglies nanosvogūnais virš perkoliacijos slenksčio aukštoje temperatūroje stebimas perėjimas iš laidžios į izoliatoriaus būseną. Virsmo temperatūra priklauso nuo dalelių dydžio.

- Kompozitų su anglies nanovamzdeliais perkoliacijos slenkstis nepriklauso nuo nanovamzdelių ilgio, bet priklauso nuo jų pasiskirstymo polimerinėje matricoje.

- Kompozitų su grafito dalelėmis dielektrinė skvarba žemiau perkoliacijos slenksčio didėja nuo grafito dalelių dydžio. Kompozitų su išplėstuoju grafitu, skirtingai nuo kitų tirtų grafito dalelių tipo, dėl porėtos struktūros, perkoliacijos slenkstis žemas ir yra panašus kaip kai kurių kompozitų su anglies nanovamzdeliais.

- Kompozitų su mišraus užpildo anglies nanosvogūnų – nanovamzdelių užpildu perkoliacijos slenkstis yra žemesnis nei teorinis, nustatytas iš perkoliacijos teorijos, dėl sinergijos efekto.

- Dviejų tipų 1D ir 2D – grafeno ir anglies nanovamzdelių panaudojimas kompozitų užpildymui leido žymiai padidinti kompozitų elektrinį laidumą.

5.5 Literatūros šaltiniai

[1]   F. Qin, C. Brosseau, *J. Appl. Phys.,* **111**, 6 (2012).

[2]   G. Inzelt, Conducting polymers: A new era in electrochemistry, Berlin: Springer (2008).

[3]   S. Battacharya, Metal-Filled Polymers, New York: Dekker (1986).

[4]   R. Strumpler, J. Glatz-Reichenbach, *J. Electrocer.,* **3**, 4 (1999).

[5]   W. Bauhofer, Z. Kovacs, *Compos. Sci. Technol.,* **69**, 1486 (2009).

[6]   E. Ivanov, R. Kotsilkova, E. Krusteva, E. Logakis, A. Kyritsis, P. Pissis, C. Silvestre, D. Duraccio ir M. Pezzuto, *J. Polym. Sci. Part B: Polym. Phys.,* **49**, 431 (2011).

[7]   J. R. Fried, Polymer Science and Technology, Pearson Education (2014).

[8]   Debye, Polar molecules, New York: Chemical Catalog Co., Inc (1929).

[9]   K. Cole ir R. Cole, *J. Chem. Phys.,* **9**, 341-351 (1941).

[10] S. Havriliak ir S. Negami, *Polym.,* **8**, 161–210 (1967).

[11] R. Zorn, *J. Chem. Phys.,* **116**, 8 (2002).

[12] A. K. Jonscher, Universal relaxation law, London: Chelsea Dielectrics Press (1992)..

[13] F. Lux, *J. Mater. Sci.,* **28**, 2 (1993).

[14] A. Celzard, E. McRae, C. Deleuze, M. Dufort, G. Furdin, J. F. Marêché, *Phys*

Rev B, **53**, 6209 (1996).

[15] N. F. Mott, E. A. Davis, Electronic processes in non-crystaline solids, London: Oxford University (1971).

[16] P. Sheng, E. K. Sichel, *Phys. Rev. Lett.*, **40**, 18 (1978).

[17] H. Deng, R. Zhang, E. Bilotti, J. Loos, T. Peijs, *J. Appl. Polym. Sci.,* **113**, 742-51 (2009).

[18] S. Liao, *J. Power Sources,* **185**, 2 (2008).

[19] Y. Sun, H. D. Bao, Z. X. Guo, J. Yu, *Macromolecules,* **42**, 459 (2009).

[20] V. L. Kuznetsov, Y. V. Butenko, A. L. Chuvilin, A. I. Romanenko, A. V. Okotrub, *Chem. Phys. Lett ,* 336, 397, (2001).

[21] J. Macutkevic, P. Kuzhir, D. Seliuta, G. Valusis, J. Banys, A. Paddubskaya, D. Bychanok, G. Slepyan, S. Maksimenko, V. Kuznetsov, S. Moseenkov, O. Shenderova, A. Mayer, Ph. Lambin, *Diam. Relat. Mater*, **19**, 91-99 (2010).

[22] R. Langlet, P. Lambin, A. Mayer, P. P. Kuzhir, S. A. Maksimenko, *Nanotech.* **19**, 115706 (2008).

[23] A. Mdahari, F. Carmona, C. Brosseau, P. Delhaes, *J. Appl. Phys.,* **103**, 054303 (2008).

[24] Z. F. Liu, G. Bai, Y. Huang, Y. F. Ma, F. Du, F. F. Li, T. Y. Guo, Y. S. Chen, *Carbon,* **45**, 821 (2007).

[25] Z. M. Dang, L. Wang, Y. Yin, Q. Zhang, Q. Q. Li, *Adv. Mater.,* **19**, 852 (2007).

[26] P. Pötschke, S. M. Dudkin, I. Alig, *Polymer*, **44**, 17 (2003)

[27] S. Bellucci, Carbon Nanotubes Toxicity. Nanoparticles and nanodevices in Biological Applications, The INFN Lectures – Vol. 1

5.6 Informacija apie autorę

Vardas Pavardė   Ieva Kranauskaitė

Išsilavinimas

2008 m.   Klaipėdos Ąžuolyno gimnazija

2012 m.   VU, Fizikos fakultetas, Moderniųjų techologijų fizika ir vadyba, Fizikos bakalauras

2014 m.   VU, Fizikos fakultetas, Telekomunikacijų fizika ir elektronika

                   Elektronikos inžinerijos magistras

2014 - 2018 m.   VU, Fizikos fakultetas, Doktorantūros studijos, Fizika (02P)

Publications

I. J. Macutkevic, **I. Kranauskaite**, J. Banys, S. Moseenkov, V. Kuznetsov, O. Shenderova, Metal-insulator transition and size dependent electrical percolation in onion-like carbon/polydimethylsiloxane composites, *Journal of Applied Physics,* **115**, 213702 (2014).

II. **I. Kranauskaite**, J. Macutkevic, P. Kuzhir, N. Volynets, A. Paddubskaya, D. Bychanok, S. Maksimenko, J. Banys, R. Juskenas, S. Bistarelli, A. Cataldo, F. Micciulla, S. Bellucci, V. Fierro, A. Celzard, Dielectric properties of graphite-based epoxy composites, *Physica status solidi A*, **211** (7), 1623 – 1633 (2014).

III. **I. Kranauskaite**, J. Macutkevic, J. Banys, E. Talik, V. Kuznetsov, N. Nunn, O. Shenderova, Synergy effects in the electrical conductivity behavior of onion-like carbon and multiwalled carbon nanotubes composites, *Physica status solidi, B* **252** (8), 1799 – 1803 (2015).

IV. **I. Kranauskaite**, J. Banys, E. Talik, V. Kuznetsov, N. Nunn, O. Shenderova, Electric/dielectric properties of composites filled with onion-like carbon and multiwalled carbon nanotubes, *Lithuanian Journal of Physics,* **55** (2), 126 – 131 (2015).

V. **I. Kranauskaite**, J. Macutkevic, J. Banys, V. Kuznetsov, S. Moseenkov, N. Rudyna, D. Krasnikov, Length-dependent broadband electricproperties of PMMA composites filledwith carbon nanotubes, *Physica Status Solidi A,* **213** (4), 1025 – 1033 (2016).

VI. **I. Kranauskaitė**, J. Macutkevic, A. Borisova, A. Martone, M. Zarrelli, A. Selskis, A. Aniskevich, J. Banys, Enhancing electrical conductivity of MWCNT/epoxy composites by GNP particles, *Lithuanian Journal of Physics*, **57** (4), 195–203 (2017).

VII. **I. Kranauskaite**, J. Macutkevic, J. Banys, V. Kuznetsov, M. Letellier, V. Fierro, A. Celzard, O. Shenderova, Size-dependent electrical and thermal properties of onion-like carbons/polyurethane composites, *Polymer composites*, DOI 10.1002/pc.24816 (2018).

I

Metal-insulator transition and size dependent electrical percolation in onion-like carbon/polydimethylsiloxane composites

J. Macutkevic, I. Kranauskaite, J. Banys, S. Moseenkov, V. Kuznetsov,

O. Shenderova

Metal-insulator transition and size dependent electrical percolation in onion-like carbon/polydimethylsiloxane composites

J. Macutkevic, I. Kranauskaite, J. Banys, S. Moseenkov, V. Kuznetsov, and O. Shenderova

---

Articles you may be interested in

High dielectric permittivity of percolative composites based on onion-like carbon
Applied Physics Letters 95, 112901 (2009); 10.1063/1.3224187

A review and analysis of microwave absorption in polymer composites filled with carbonaceous particles
Journal of Applied Physics 111, 061301 (2012); 10.1063/1.3688435

General equation for the determination of the crystallite size L_a of nanographite by Raman spectroscopy
Applied Physics Letters 88, 163106 (2006); 10.1063/1.2196057

A morphological and structural approach to evaluate the electromagnetic performances of composites based on random networks of carbon nanotubes
Journal of Applied Physics 115, 154311 (2014); 10.1063/1.4871670

Percolation threshold and electrical conductivity of graphene-based nanocomposites with filler agglomeration and interfacial tunneling
Journal of Applied Physics 118, 065101 (2015); 10.1063/1.4928293

Epoxy composites filled with high surface area-carbon fillers: Optimization of electromagnetic shielding, electrical, mechanical, and thermal properties
Journal of Applied Physics 114, 164304 (2013); 10.1063/1.4826529

Metal-insulator transition and size dependent electrical percolation in onion-like carbon/polydimethylsiloxane composites

J. Macutkevic,[1,a)] I. Kranauskaite,[1] J. Banys,[1] S. Moseenkov,[2] V. Kuznetsov,[2,3] and O. Shenderova[4]

[1]*Vilnius, Sauletekio al. 9, LT-00122 Vilnius, Lithuania*
[2]*Boreskov Institute of Catalysis SB RAS, Lavrentiev Ave. 5, Novosibirsk 630090, Russia*
[3]*National Tomsk State University, Tomsk, Russia*
[4]*International Technology Center, Raleigh, North Carolina 27715, USA*

Dielectric/electric properties of onion-like carbon (OLC)/polydimethylsiloxane composites were investigated over very wide frequency (20 Hz–3 THz) and temperature (26–500 K) ranges. The percolation threshold in these composites strongly dependents on the OLC aggregate sizes and was lowest for the composites with the smallest OLC aggregate sizes (∼40 nm). Interestingly, the transition into the insulator state of the composites occurred at higher temperatures. The transition temperature increases with OLC aggregate concentration. Above the percolation threshold, the electrical conductivity in the composites occurs mainly due to electron tunneling between OLC clusters and quasi-one-dimensional hopping inside the clusters. The hopping almost vanishes at frequencies above 100 GHz where the phonon contribution dominates. © 2014 AIP Publishing LLC.
[http://dx.doi.org/10.1063/1.4880995]

INTRODUCTION

Electrically percolative polymer-based composites have been attracting much attention because of their potential applications, such as electroactive materials, sensitive materials, and electromagnetic coatings.[1] In these composites, electrical percolation occurs at some critical concentration (called the percolation threshold) of fillers.[2] It is an important task to reach as low as possible percolation threshold in order to preserve optimal mechanical properties of polymers and to use minimal concentration of expensive fillers. Probably, the lowest percolation threshold was observed in carbon nanotubes (CNTs) composites due to their high aspect ratio.[3] Nevertheless, the percolation threshold in other composites, for example, in carbon black composites, can be also very low.[4] On the other hand, the percolation threshold in nominally the same polymer matrix and for the same carbon nanotubes can very significantly.[3] Moreover, a drawback of carbon nanotubes is their higher cost in comparison with other carbon allotropes, such as carbon black or graphite. Another serious disadvantage is a possible toxicity of CNTs, which has been long debated[5] and is still controversial.

Onion-like carbons (OLCs), consisting of stable defected multishell fullerenes, exhibit high conductivity similar to carbon nanotubes.[6] However, most investigations of the dielectric properties of OLC-based composites, both theoretical and experimental, were performed below the percolation threshold, where the complex effective permittivity of composites increases slowly with OLC concentration, according to the Maxwell Garnett theory.[7] In this case, it was demonstrated that the electrical polarizability is weakly dependent on the geometry of OLC molecules and chiefly proportional to the volume of the whole cluster.[8]

Nevertheless, these investigations did not take into account the electrical conductivity of OLC and Maxwell-Wagner polarization effects, which usually appear in the conductive composites.[9] Therefore, these conclusions are valid mainly below the percolation threshold. It was also found that the percolation threshold in OLC composites is 10 vol. % for polyurethane composites with mean aggregate size about 130 nm.[10] Thus, the percolation threshold in OLC composites is lower than predicted by Monte-Carlo calculations in three dimensional space, ∼31.2 vol. %.[11,12] The aggregate structure of conductive particles has a strong impact on the composite dielectric/electric properties and the percolation threshold;[13–17] and for some carbon black composites, the effect was explained by the aggregate structure model.[18] Onion-like carbons, similar to carbon black, have a complex aggregate structure,[6] however its influence on the composite dielectric properties up to now have not been investigated.

In order to analyse the behavior of the complex permittivity in the composites at the microscopic scale, several models have been proposed, such as percolation theory,[19] effective-medium theory of Maxwell Garnett,[20] McLachlan's[21] generalised effective-medium theory combining most of the features of both percolation and effective-medium theories, and generalised McLachlan-Jonscher theory,[22] which is enabled to describe the frequency and concentration dependence of complex effective permittivity. Moreover, nowadays computer simulations methods are very popular in order to predict the dielectric properties of composites. Many researchers have examined this subject by performing *ab initio* calculations, for example, with density functional theory (DFT),[23] or finite element method (FEM),[24,25] or combining FEM and Monte-Carlo calculations.[26,27] The FEM has considerable flexibility because arbitrary shapes can be modeled. However, these calculations were performed mainly for the dielectric properties at room

---

a)jan.macutkevic@gmail.com

temperature; while by changing the composite temperature, many more effects can be observed in composites.[28]

The temperature dependence of the electric properties of polymer composites was investigated mainly at low temperatures (below room temperature) and there was observed a decrease of conductivity according to Mott's law or the tunneling model.[29–33] Investigations at higher temperatures are rather rare. At high temperature, the resistivity may increase or decrease with temperature.[33,34]

Polydimethylsiloxane (PDMS) is a non-conducting silicone-based elastomer that has been of widespread interest due to its flexibility and ease of micromolding for rapid prototyping of microdevices and systems. PDMS has played an important role in lab-on-a-chip systems, serving not only as a stamp for pattern transfer via soft lithography[35,36] but also as an unique material in chip fabrication because of its properties such as transparency, biocompatibility, and excellent flexibility. Polydimethylsiloxane (PDSM) is a semicrystalline polymer. It exhibits a glass transition between elastomeric and vitreous phases close to 150 K.[37]

In this work, we have investigated the possibility for further reduction of the percolation threshold in onion-like carbon composites. OLCs were obtained by a phase transformation of detonation nanodiamonds (DNDs) annealed at high temperature in vacuum.[6] Since DNDs consist of tight aggregates of primary 5 nm diamond particles, this structure is inherited by OLC, also consisting of aggregates of primary carbon onion particles ($\sim$7 nm in diameter). The study of electrical percolation was performed in a PDMS matrix with different sizes of OLC aggregates. It will be demonstrated that the lowest percolation threshold was obtained in the OLC/PDMS composite with small size OLC aggregates ($\sim$40 nm), however a transition into an insulator state occurred at higher temperatures. The transition temperature is strictly dependent on the OLC aggregate size and concentration.

EXPERIMENTAL

The OLC samples used to fabricate OLC/PDSM composite films were prepared as follows. Detonation nanodiamonds were obtained by detonation of a mixture of trinitrotoluene (TNT) and 1,3,5–trinitroperhydro–1,3,5–triazine (RDX) in CO_2 atmosphere, followed by oxidation of sp^2 carbon in the mixture of concentrated sulfuric acid and chromic anhydride at 110 °C, washed with water, and dried. It is known that DND exists in the form of strong aggregates (up to few hundred nanometers in size) with coherent and incoherent interfaces between primary ND particles of 4–7 nm in size.[6] Polydispersed DND material was fractionated by centrifugation into fractions with average aggregate size of 40 nm, 100 nm, and 250 nm, correspondingly. Volumetric aggregate sizes were measured by a dynamic light scattering technique in water suspensions of DNDs. Fractions of the DNDs were heated in vacuum (10^{-4} Torr) at 1650 °C for 3 h providing fractions of the OLC with aggregate sizes corresponding to the sizes of the starting DND fractions (approximately 250 nm, 100 nm, and 40 nm, correspondingly). The polydimethylsiloxane, Sylgard, was

purchased from Dow-Corning as a two part material. When forming PDMS-OLC composites, an intermediate solvent (isopropanol (IPA)) was employed that served as a dispersion medium for the nanoparticles prior to mixing with the polymer matrix. The nanoparticles were dispersed in the solvent and sonicated to break up large agglomerates, then the suspension was combined with uncured PDMS and the IPA solvent subsequently removed by vacuum. Curing of the PDMS-nanoparticle mixture at 60 °C for 2 h and 40 °C overnight resulted in films with good nanoparticle dispersion.

Scanning electron microscopy (SEM) and transmission electron microscopy (TEM) images were obtained with JSM 6460 LV and JEM 2010 electron microscopes, correspondingly. We used low concentration suspensions of OLC in N, N–dimethylformamide (DMF) for the deposition on TEM grids to get possibility to estimate distribution of aggregates.

Complex effective permittivity was measured as a function of frequency and temperature using a HP4284A precision *LCR* meter in the frequency range 20 Hz–1 MHz. For the low temperature measurements, a helium closed cycle cryostat was used; while for the high temperature measurements, a home-made furnace was used. Each measurement was started at room temperature. In the frequency range 1 MHz–3 GHz, dielectric measurements were performed using a vector network analyzer Agilent 8714ET. In the microwave frequency range from 8 to 53 GHz, a home-made waveguide spectrometer was used. The method of a thin rod in the waveguide was used.[38] In the frequency range from 1 MHz to 53 GHz, the measurement accuracy was $\sim$10%. Silver paste has been used for creating the contacts. In the terahertz frequency range (from 100 GHz to 3 THz), a terahertz time domain spectrometer (Ekspla Ltd) based on a femtosecond laser was used for the measurements. The spectrometer is based on the femtosecond laser fiber (wavelength 1 μm, pulse duration less than 150 fs) and GaBiAs photoconductive terahertz emitter and detector.[39] The signal to noise ratio was as high as 60 dB at frequency 0.5 THz. The complex effective permittivity was calculated according to the Fresnel equation.[40] The measurements accuracy was better than 1% at frequency 0.5 THz (where a signal to noise ratio is the highest).[41] The real part σ' of the complex electrical conductivity was calculated as $\sigma' = \omega \varepsilon_0 \varepsilon''$, where ω is the angular frequency, ε_0 is the permittivity of vacuum, and ε'' is the imaginary part of complex effective permittivity.

RESULTS AND DISCUSSION

Room temperature dielectric properties and composites structure

TEM images of OLC particles used in the study with 40 nm, 100 nm, and 250 nm average aggregate sizes are presented in Fig. 1. The left part of Fig. 1 illustrates low magnification TEM images of the aggregates while the right part presents their high resolution images. One can see that the primary OLC particles consist of enclosed defective fullerene-like shells, which in turn are combined into tight aggregates with joint graphene layers.

SEM images of OLC/PDSM composites with up to 10 vol. % OLC are presented in Fig. 2. Films with small
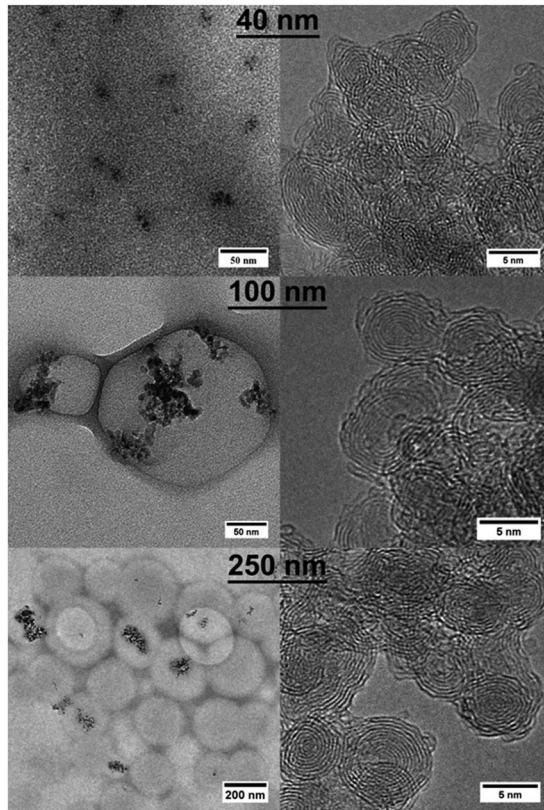
FIG. 1. TEM images of OLC with 40 nm, 100 nm, and 250 nm average aggregate size. Left part—low magnification images of aggregates deposited on the amorphous carbon layer of TEM grid. Right part presents of HR TEM images of OLC aggregates.

content of OLC are very soft and flexible while increasing OLC loading (more than 5 vol. %) results in formation of brittle films. It can be assumed that the broken surfaces are spread along the direction with diminished strength and with

highest concentration of OLC agglomerates, revealing the distribution of the aggregates in these regions. In samples with lowest OLC, content secondary agglomerates (of micron size) can be observed as well as individual primary aggregates of OLC. Increases OLC content up to 5 vol. % and more results in increased sizes of clustered aggregates, however small aggregates also can be observed. Thus, OLC/PDSM composites exhibit a fractal structure of the aggregates similar to carbon black composites.[42]

The frequency dependence at room temperature of the effective permittivity (ε') and the electrical conductivity (σ') of PDSM composites with different loadings of 250 nm OLC is shown in Fig. 3. The values of the effective permittivity and conductivity for composites with p $\leq$ 5 vol. % (where *p* is OLC volume fraction) are very low, similar to pure PDMS values. However, the effective permittivity starts to increase for composites with 8 vol. % inclusions. At low frequencies (below 1 kHz), DC electrical conductivity plateau is clearly expressed in conductivity spectra of composites with 8 vol. % inclusions, indicating that the percolation threshold in OLC/PDMS composites with 250 nm OLC inclusions is 8 vol. %.

The effective permittivity and the electric conductivity are very high for composites with 10 vol. % of OLC at low frequencies, the effective permittivity is of the order of 10^3, and the electric conductivity is about 0.001 S/m. Nevertheless, the electric conductivity value at low frequencies is as small as the corresponding value of the pure OLC of the order of 10^2 S/m.[6] The value of complex effective permittivity is very similar to the values of complex effective permittivity of functionalized carbon nanotubes composites near the percolation threshold.[43] In the microwave frequency range, the value of complex effective permittivity for the presented composites is higher in comparison with the carbon black composites.[44] Three different trends are observed in the
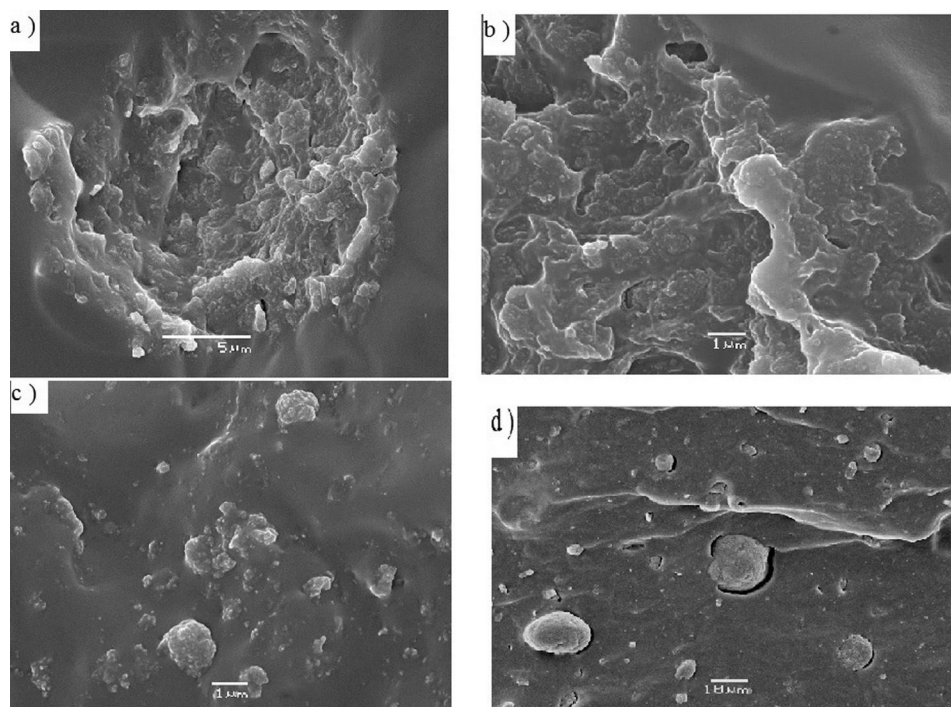

FIG. 2. SEM images of OLC/PDSM composites (a) 1 vol. %, (b) 5 vol. %, (c) 10 vol. %, OLC aggregates 250 nm; (d) 6.8 vol. % OLC aggregates 40 nm).
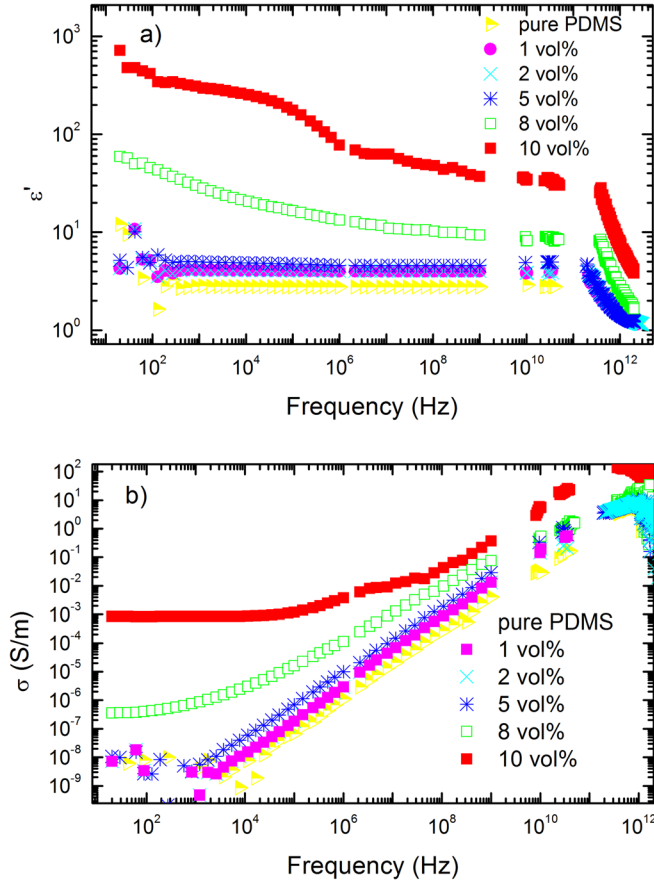
FIG. 3. Frequency spectra of effective permittivity (a) and electrical conductivity (b) for OLC/PDSM (with 250 nm OLC inclusions) composites at room temperature.

frequency spectra of the effective permittivity: in the frequency below 129 Hz, in the frequency range 10 kHz–1 MHz, and in the frequency range 1 MHz–1GHz. In these frequency ranges, the effective permittivity decreases according to the Jonscher universal power law with different exponents.[45] The different dispersions are related with the Maxwell–Wagner contribution to the effective permittivity.[9] In the middle frequency range 129 Hz–10 kHz, the effective permittivity and the electric conductivity are almost frequency independent. The loss tangent is also very high at low frequencies, indicating a high absorbtion ability of electromagnetic waves by composite with 10 vol. % of OLC. A flat frequency dependence of the effective permittivity observed in the frequency range 8–53 GHz is in good agreement with carbon black and carbon nanotubes composites.[46,47]

A rapid decrease with frequency of the effective permittivity and a maximum of electrical conductivity above 100 GHz is typical for phonon related dielectric dispersions (Fig. 3). The part of the spectra above 100 GHz obtained for pure PDSM is in good agreement with results presented in Ref. 48. Thus, the origin of dielectric spectra above 100 GHz is related to the continuous distribution of phonon modes in OLC/PDMS.[48]

In order to reveal the influence of the OLC concentration and aggregate size, the effective permittivity and the electrical conductivity at the frequency 129 Hz and room temperature for all investigated composites are plotted as a

function of concentration (Fig. 4). Note that in the frequency spectra of composites with 250 nm (at concentrations 10 vol. % and 8 vol. %), 100 nm (at concentrations 8.9 vol. % and 7.1 vol. %), and 40 nm aggregate size (at concentration 6.8 vol. %), a frequency-independent DC plateau can be observed at low frequencies, so that the conductivity at 129 Hz for these composites coincide with the DC conductivity. Therefore, the percolation threshold is close to 10 vol. % for composites with 250 nm, 7.1 vol. %—with 100 nm and 6.8 vol. %—with 40 nm OLC aggregates, correspondingly. Thus, the lowest percolation threshold is observed in the composites with small size OLC aggregates. Below the percolation threshold, the effective permittivity ε' at 129 Hz was fitted according to the classical law[18]

$$\varepsilon' = \varepsilon_m \left(\frac{p_c - p}{p_c} \right)^{-q}, \qquad (1)$$

where ε_m is the dielectric permittivity of polymer matrix, p_c is the critical volume fraction, and q is the critical index. Obtained parameters are $\varepsilon_m = 2.55$ for all types of OLC, while $p_c = 8$ vol. % and $q = 1.35$ were obtained for 250 nm OLC, $p_c = 7.1$ vol. % and $q = 1.25$ for 100 nm OLC, $p_c = 6.7$ vol. % and $q = 1.04$ for 40 nm OLC aggregates, correspondingly. At concentrations close to the percolation threshold, the percolation theory predicts the value of the exponent close to 2 in any three-dimensional medium.[49] So, obtained values of the critical index are in agreement with
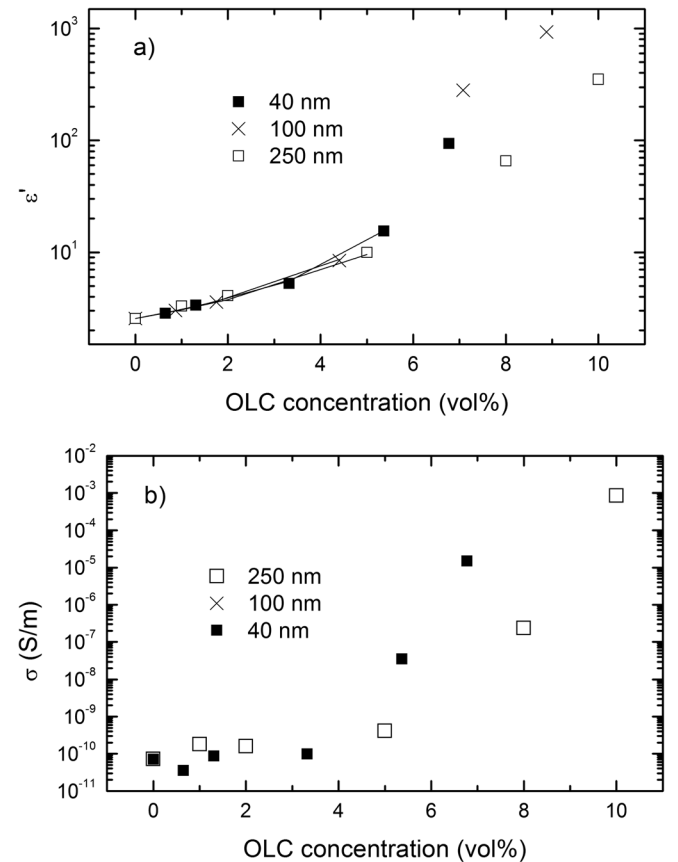

FIG. 4. The effective permittivity (a) and the electrical conductivity (b) of OLC/PDSM composites vs OLC concentration and aggregate size at frequency 129 Hz and room temperature.

the percolation theory. In order to increase the determination accuracy of p_c and q, many more samples with different OLC concentrations should be investigated at concentrations close to the critical value. Nevertheless, the critical volume fraction is lower than should be expected from theory. Indeed, according to the percolation theory for the two phase random composite whose fillers are spherical, the percolation threshold should be about 0.16 (volume fraction).[49]

Metal-insulator transition in OLC/PDSM composites

Temperature dependence of the effective permittivity and the electrical conductivity of OLC/PDSM composites with 250 nm OLC inclusions at 10 vol. % is presented in Fig. 5 at different frequencies from room temperature up to 500 K. Both the effective permittivity and the electrical conductivity decreases during heating; however, the most pronounced decrease occurs at temperatures above 450 K and at lower frequencies (below 11 kHz). In order to understand the phenomena, the electrical conductivity was plotted as a function of frequency at various representative temperatures in Fig. 6. During heating, not only was the electrical conductivity decreased but also substantially changes in the shape of the conductivity spectrum took place. A frequency independent conductivity (DC conductivity) is observed at lower frequencies and at lower temperatures. Above 470 K, no DC conductivity is observed in

FIG. 6. Frequency dependence of the effective permittivity and the electrical conductivity of OLC/PDSM composites (with 250 nm OLC 10 wt. % inclusions) at different temperatures (high temperature region).

the conductivity spectra of the investigated composites. The frequency spectra of the conductivity was fitted with the fundamental equation[50]

$$\sigma = \sigma_{DC} + A\omega^s, \qquad (2)$$

where σ_{DC} is the DC conductivity and $A\omega^s$ is the AC conductivity. Equation (2) is consistent with the Jonscher universal dielectric response and the parameter s has the same physical meaning as the Jonscher exponent.[45] DC conductivity values for all composites above the percolation threshold are presented in Fig. 7(a). From this fit, it is possible to calculate the critical frequency f_{cr} at which the value of the conductivity $\sigma(\omega)$ deviates from the DC plateau. The experimental value for f_{cr} has been defined as the frequency at which the value of the conductivity is 10% higher than the DC conductivity value. The results are plotted in Fig. 7(b). It can be clearly seen that both the DC conductivity and the critical frequency f_{cr} are almost temperature independent at lower temperatures and rapidly decrease close to the specific temperature, which depends on the OLC aggregate size and concentration. Above this temperature, no DC conductivity occurs in the composites; therefore, a metal-insulator phase transition is observed. Note that the complex effective permittivity of a pure PDSM polymer matrix only very slowly increases with temperature, no anomaly is revealed and its value remains quite low ($\varepsilon' < 5$ and $\varepsilon'' < 1.5$) in the temperature region 300–500 K. The transition temperature was obtained as a temperature at which DC conductivity disappears and the results are presented in Table I. The transition temperature increases with OLC concentration and OLC aggregate size. DC conductivity and the static effective permittivity ε_s are connected with the critical frequency f_{cr} according to the relations

$$f_{cr} = \sigma_{DC}/\varepsilon_0\varepsilon_s, \qquad (3)$$

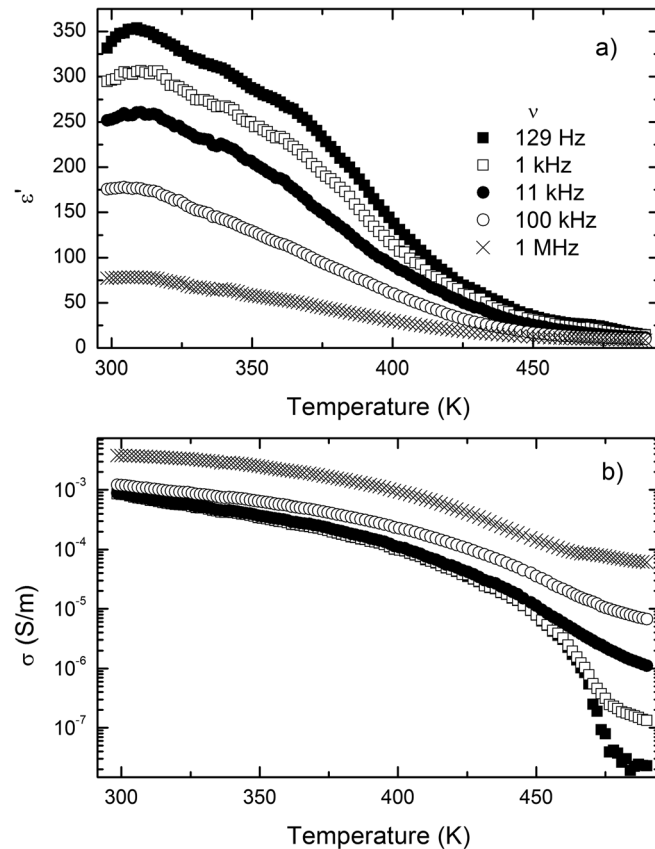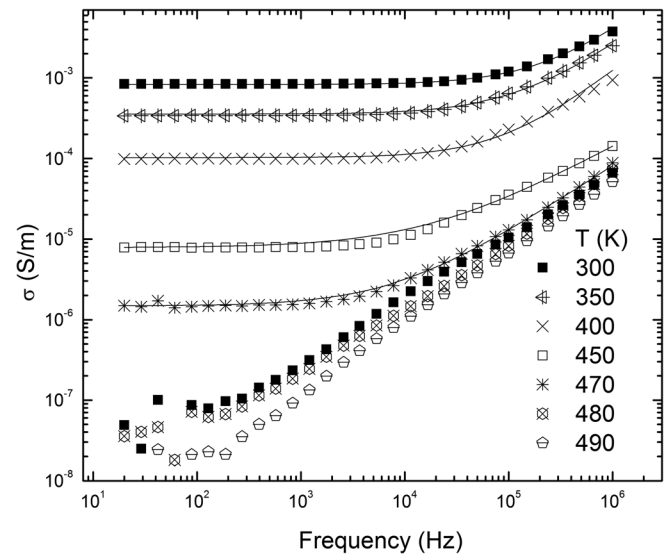$$\sigma_{DC} \sim f_{cr}^z, \qquad (4)$$

FIG. 5. Temperature dependence of the effective permittivity (a) and the electrical conductivity (b) of OLC/PDSM composites (with 250 nm OLC 10 wt. % inclusions) at different frequencies (high temperature region).
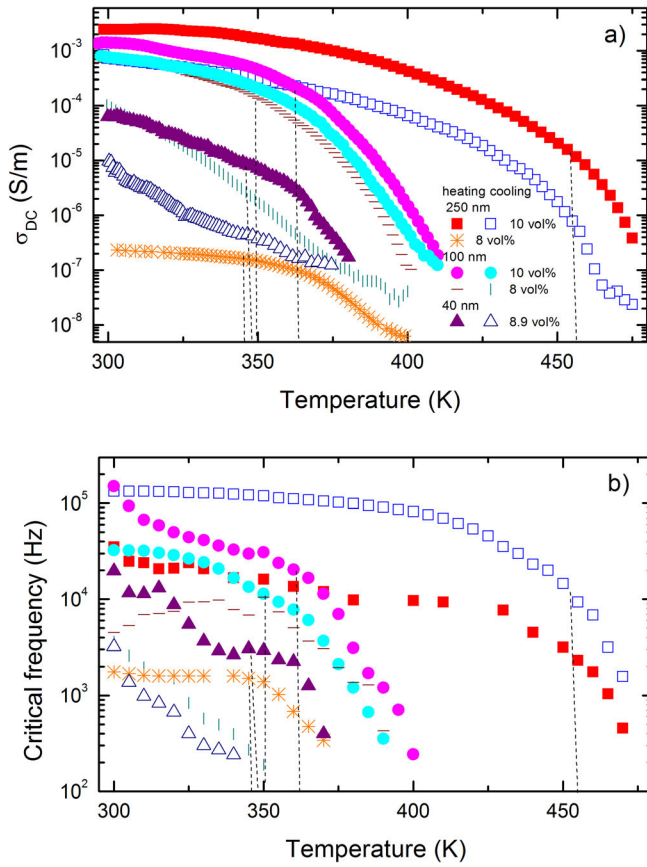
FIG. 7. Temperature dependence of OLC/PDSM composites DC conductivity (a) and critical frequency (b) (high temperature region). The dotted lines indicate a limit between a "slow" decreasing of DC conductivity and critical frequency with temperature and a "rapid" decreasing of these parameters.

where z is an exponent, which characterizes the relation between the capacitive and conductive networks in the composite. For the composites under study, σ_{DC} and f_{cr} are almost temperature independent at temperatures far from the metal-insulator transition temperature; thus in this temperature region, z is almost zero. Close to the metal-insulator transition temperature, both DC conductivity and critical frequency rapidly decreases and the critical exponent is ∼1.5 in this temperature region for all composites. This indicates a strong dependence on the gaps (the distances between OLC clusters) of both effective permittivity and electrical conductivity close to the metal-insulator transition temperature.[32]

Upon heating, both the electrical conductivity and the effective permittivity decrease due to very different thermal expansion properties of the pure PDSM polymer matrix and OLC. The volume of OLC clusters remains almost the same,

TABLE I. The metal-insulator transition temperatures for OLC/PDSM composites.

OLC type	Concentration, vol. %	Transition temperature, K
250 nm	10	476
	8	382
100 nm	8.9	413
	7.1	401
40 nm	6.8	398

while the polymer matrix volume increases rapidly with heating. At low frequencies, the electrical conductivity in the investigated composites can occurs via several mechanisms: (1) electron hopping in the infinite OLC clusters, (2) serial transport by hopping in finite clusters and a tunneling between these finite clusters, (3) tunneling between finite and infinite clusters. Due to the rapid polymer matrix expansion, only tunneling conductivity decreases because the distance for electron tunneling is increased. At higher temperatures (above the metal-dielectric transition temperature), the DC electrical conductivity disappears when the mean distance between the OLC clusters exceeds a critical value at which no more tunneling is possible. Thus, electrical transport in the OLC/PDSM composites is governed by a 2d mechanism.

With increasing OLC concentration or aggregate size, the mean distance between the OLC clusters decreases; and therefore, the electrical conductivity is increased (Fig. 2). The volume concentration of OLC clusters φ_i can be calculated as

$$\varphi_i = V_{OLC}/(V_{OLC} + V_{PDSM}), \qquad (5)$$

where V_{OLC} is the volume of OLC in the composite and V_{PDSM} is the volume of matrix in the composite. Assuming that V_{OLC} is almost temperature independent, φ_i could be proportional to $1/V_{PDMS}$. Thus, the volume concentration decreases upon heating and when it reaches a critical value, a transition into the insulator state occurs, which is followed by vanishing of both DC conductivity and critical frequency. This is clearly seen in Fig. 7 where a slow decrease of both conductivity and critical frequency is observed on heating, as well as a rapid decrease close to the metal-insulator temperature. Moreover, the rapid decrease of the conductivity, which occurs close to the transition temperature, (Fig. 7) is similar to the concentration dependence of the conductivity close to the percolation threshold (Fig. 4). Therefore, the transition into an insulator state can be explained by the decrease of OLC volume concentration below some critical concentration. The critical volume concentration depends on the OLC type; therefore, the metal-insulator transition occurs at higher temperatures for bigger OLC aggregates (Table I).

For low OLC concentrations (8 vol. % of 250 nm OLC aggregates), the metal-insulator transition is irreversible, i.e., after annealing above the transition temperature the value of composite effective permittivity remains low upon cooling (Fig. 7). In this case, the destroyed OLC network does not recover with polymer matrix shrinkage upon cooling and the composite is an isolator at room temperature after annealing. At higher OLC concentrations, the behavior of the DC conductivity and the critical frequency is reversible (Fig. 7), i.e., upon cooling the values of DC conductivity and critical frequency are partially recovered.

A decrease in conductivity of percolative composites during heating was observed in other composites;[32] however in these composites, no metal-insulator transition occurred due to finite matrix conductivity at higher temperature. In contrast, no DC conductivity and any electric or dielectric anomaly was observed in the PDMS polymer up to 500 K. Above room temperature, the metal-insulator transition

usually occurs in vanadium oxide related compounds;[51] however in our case, the phase transition temperature can be easily changed by changing the OLC filler concentration and type. Moreover, in vanadium oxide related materials, the high temperature phase is conductive and low temperature is non-conductive;[51] while in our composites, the high temperature phase is not conductive. This is due to the fact that in OLC/PDMS composites at higher temperatures, the distances between the OLC clusters is too big and tunneling electrical conductivity does not occur in the composite. Thus, the OLC/PDMS composites can be useful in various applications, where a temperature dependent behavior is required.

Electrical conductivity at low temperatures

At low temperatures, effective permittivity and electrical conductivity increase during cooling and reach a maximum close to the glass transition temperature (150 K) of pure PDMS matrix (Fig. 8). The behavior can be explained by a rapid shrinkage of the PDMS matrix upon cooling down to the glass transition temperature. A similar behavior was observed also in other polymer composites.[12]

At low temperatures (below 170 K), both the effective permittivity and the electrical conductivity decrease upon cooling. Not only the DC conductivity changes upon cooling but also the shape of the conductivity spectra is changed (Fig. 9). Therefore, conductivity spectra $\sigma(\nu)$ were fitted with the Eq. (2). Obtained parameters are presented in Figs. 10 and 11.
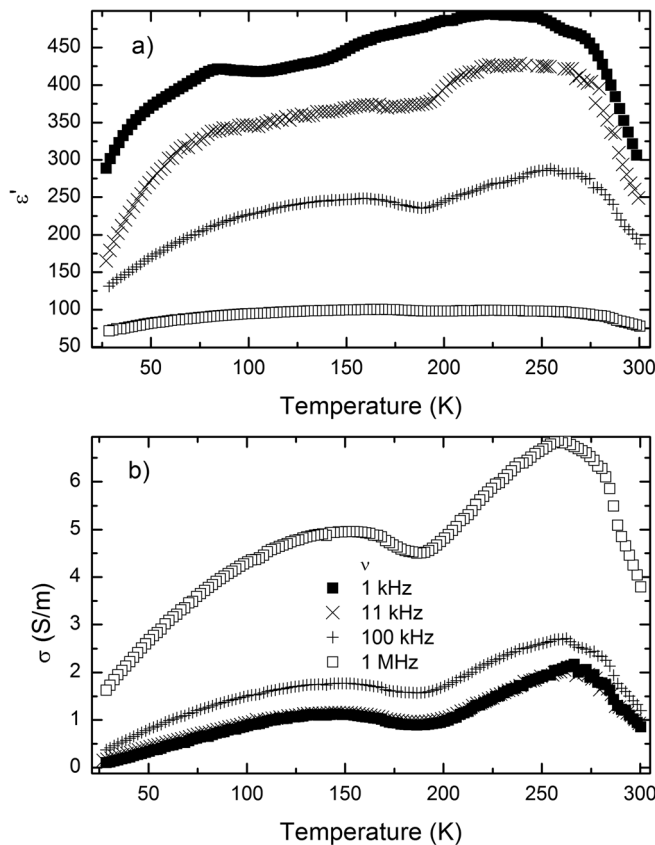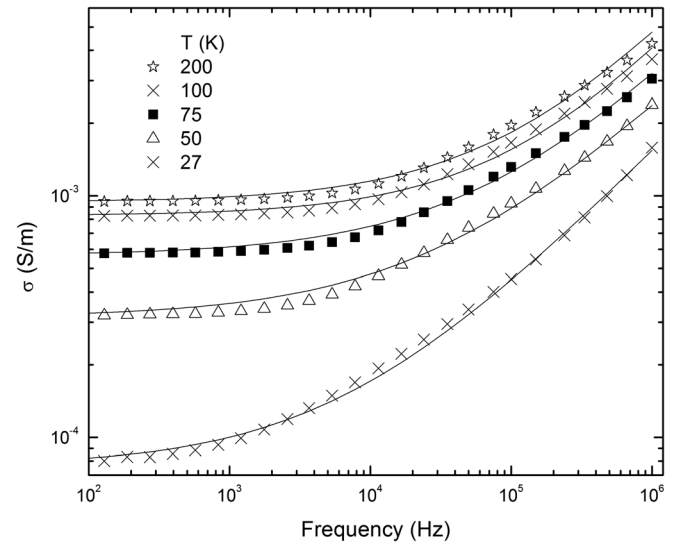

FIG. 9. Frequency dependence of the electrical conductivity of OLC/PDSM (with 250 nm OLC inclusions 10 wt. % inclusions) at different frequencies (low temperature region).

For temperatures below 170 K, the DC conductivity data fit well to the fluctuation induced tunneling model, as one can see in Fig. 10[30]

$$\sigma_{dc} = \sigma_0 \exp\left(-\left(T_1/(T + T_0)\right)\right), \qquad (6)$$

where T_1 represents the energy required for an electron to cross the insulator gap between the conductive particles aggregates, and T_0 is the temperature above which thermally activated conduction over the barriers begins to occur. According to the tunneling model,[31,32]

$$T_1 = wA\beta_0/8\pi k, \qquad (7)$$

$$T_0 = 2T_1/\pi\chi w, \qquad (8)$$

where $\chi = (2mV_0)^{0.5}/h$ and $\beta_0 = 4V_0/ew$, m and e being the electron mass and charge, respectively, V_0 is the potential

FIG. 8. Temperature dependence of the effective permittivity (a) and the electrical conductivity (b) of OLC/PDSM composites (with 250 nm OLC 10 wt. % inclusions) at different frequencies (low temperature region).
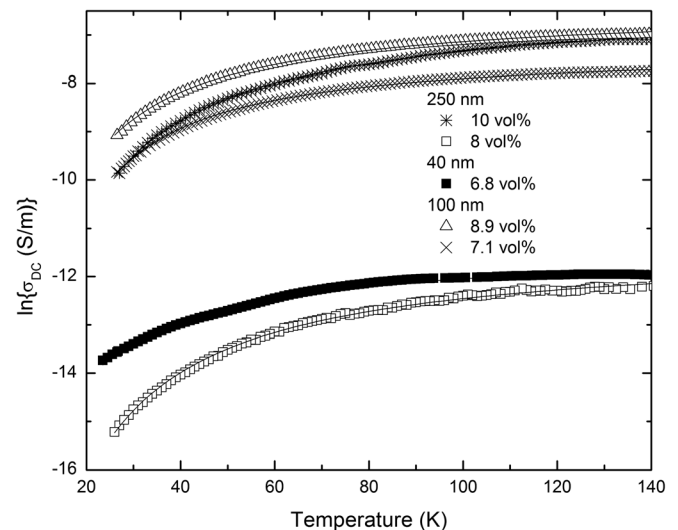

FIG. 10. Temperature dependence of OLC/PDSM composites DC conductivity with tunneling law fit (low temperature region).
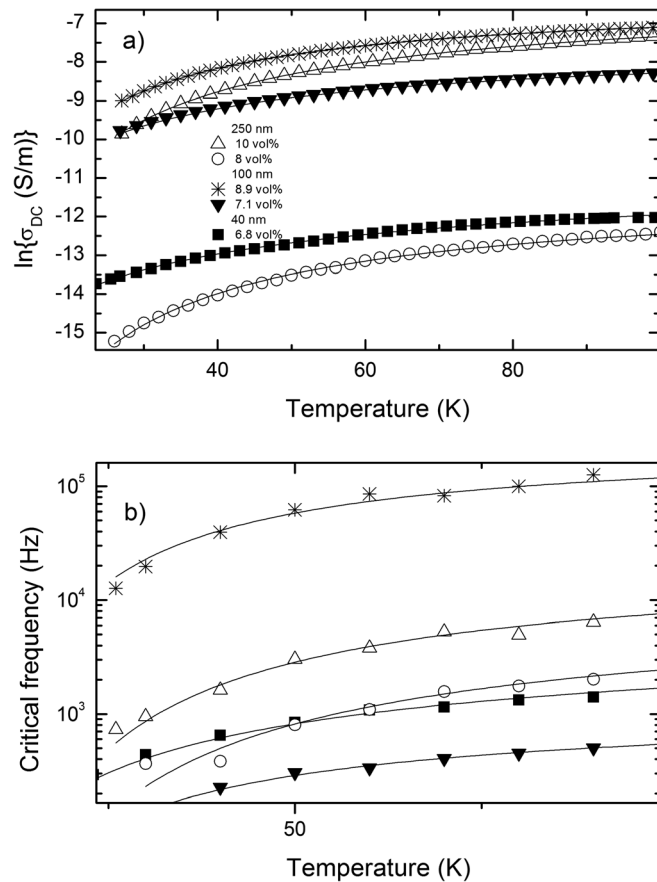
FIG. 11. Temperature dependence of OLC/PDSM composites DC conductivity (a) and critical frequency (b) with Mott law fit (low temperature region).

barrier height, w is the interparticle distance (gap width), and A is the area of capacitance formed by the junction. Obtained parameters are listed in Table II. From Eqs. (7) and (8), it follows that T_1/T_0 is proportional to the gap width w, which is approximately proportional to $p^{-1/3}$.[52] Thus, the ratio T_1/T_0 should decrease with the OLC concentration, as it was observed in the composites with 100 nm OLC aggregates.

However, below 100 K, not only the DC conductivity but also the shape of the conductivity spectra is temperature dependent (Fig. 9). This means that the critical frequency is also temperature dependent. We assumed that the temperature dependence of the DC conductivity at lower temperatures (below 100 K) can be fitted by the general Mott expression for variable range hopping (Fig. 11(a))[53]

$$\sigma_{dc} = \sigma_0 \exp(-(T_M/T)^{1/n}), \tag{9}$$

TABLE II. Tunneling model fit parameters for DC conductivity at low temperatures.

OLC type	Concentration, vol. %	σ_{dc0}, mS/m	T_1, K	T_0, K
250 nm	10	1.86	110	4.2
	8	0.0068	38	8.3
100 nm	8.9	1.66	75	2
	7.1	0.81	83	5
40 nm	6.8	0.011	70	5.2

TABLE III. Mott law fit parameters for DC conductivity at low temperatures.

OLC type	Concentration, vol. %	σ_{dc0}, mS/m	T_M, K	n	f_∞, kHz
250 nm	10	2.13	122	1.15	25
	8	0.01	117	1.09	0.89
100 nm	8.9	1.45	61	0.9	224
	7.1	0.43	57	1.02	67
40 nm	6.8	0.012	69	1.16	3.1

where T_M is a constant depending on the density of state and localization length of the system, $n = 1 + d$ (d is dimensionality of the system). A similar behavior is also valid for the critical frequency f_{cr} (Fig. 11(b))[53]

$$f_{cr} = f_{cr\infty} \exp(-(T_M/T)^{1/n}), \tag{10}$$

where $f_{cr\infty}$ is the frequency at very high temperatures. Obtained parameters are summarized in Table III. The value of n is close to 1 for all investigated composites; this is typical for pure OLC powder.[6] Thus, electrical transport in OLC/PDMS composites occurs via electron tunneling between OLC aggregates and a quasi-one-dimensional hopping inside the OLC clusters.

CONCLUSIONS

Electromagnetic properties of the OLC/PDMS percolative composites were investigated in a very wide frequency (20 Hz–3 THz) and temperature (26 K–500 K) ranges for the composites prepared with different sizes of OLC aggregates. The lowest percolation threshold (~6.8%) was observed in composites with smallest size of the OLC aggregates (~40 nm). The value of the effective permittivity and the electrical conductivity of the composites above the percolation threshold is very high, similar to the values for carbon nanotubes or carbon black composites. The electrical percolation occurs mainly due to electron tunneling between OLC clusters. The electromagnetic and electric properties of the composites above the percolation are mainly governed by electron tunneling between OLC clusters and electron hopping in quasi-one-dimensional chains inside clusters. At higher temperatures, the transition into the insulator state occurs, due to the very different thermal properties of the polymer matrix and OLC. The transition temperature increases with the OLC aggregate size and concentration. The presented composites can be useful in various electronic applications as a soft flexible material with high effective permittivity and electrical conductivity values in a wide frequency range. In addition, tunable metal-insulator transition taking place upon heating can be also useful for different electronic applications where temperature dependent metal-insulator properties are required.

ACKNOWLEDGMENTS

Rudina and A. V. Ishchenko for SEM and TEM study of OLC based samples.

[1] F. Qin and C. Brosseau, J. Appl. Phys. **111**, 061301 (2012).

[2] S. Kirkpatrick, Rev. Mod. Phys. **45**, 574 (1973).

[3] W. Bauhofer and Z. Kovacs, Compos. Sci. Technol. **69**, 1486 (2009).

[4] L. J. Adriaanse, J. A. Reedijk, P. A. A. Teunissen, H. B. Brom, M. A. J. Michels, and J. C. M. Brokken-Zijp, Phys. Rev. Lett. **78**, 1755 (1997).

[5] K. Kostarelos, Nat. Biotechnol. **26**, 774 (2008).

[6] V. L. Kuznetsov, Yu. V. Butenko, A. L. Chuvilin, A. I. Romanenko, and A. V. Okotrub, Chem. Phys. Lett. **336**, 397 (2001).

[7] J. Macutkevic, P. Kuzhir, D. Seliuta, G. Valusis, J. Banys, A. Paddubskaya, D. Bychanok, G. Slepyan, S. Maksimenko, V. Kuznetsov, S. Moseenkov, O. Shenderova, A. Mayer, and Ph. Lambin, Diamond Relat. Mater. **19**, 91–99 (2010).

[8] R. Langlet, P. Lambin, A. Mayer, P. P. Kuzhir, and S. A. Maksimenko, Nanotechnology **19**, 115706 (2008).

[9] J. Liu, Ch. G. Duan, W. G. Yin, W. N. Mei, R. W. Smith, and J. R. Hardy, Phys. Rev. B **70**, 144106 (2004).

[10] J. Macutkevic, D. Seliuta, G. Valusis, J. Banys, V. Kuznetsov, S. Moseenkov, and O. Shenderova, Appl. Phys. Lett. **95**, 112901 (2009).

[11] S. Kirkpatrick, Phys. Rev. Lett. **36**, 69 (1976).

[12] Y. J. Deng and H. W. J. Blote, Phys. Rev. E **72**, 016126 (2005).

[13] J. Ch. Huang, Adv. Polym. Technol. **21**, 299 (2002).

[14] C. Brosseau, F. Boulic, P. Queffelec, C. Bourbigot, Y. Le. Mest, J. Loaec, and A. Beroual, J. Appl. Phys. **81**, 882 (1997).

[15] C. Brosseau, P. Molinie, F. Boulic, and F. Carmona, J. Appl. Phys. **89**, 8297 (2001).

[16] C. Brosseau and M. E. Achour, J. Appl. Phys. **105**, 124102 (2009).

[17] S. El. Bouazzaoui, A. Droussi, M. E. Achour, and C. Brosseau, J. Appl. Phys. **106**, 104107 (2009).

[18] J. Liang and Q. Yang, J. Appl. Phys. **102**, 083508 (2007).

[19] A. L. Efros and B. I. Shklovskii, Phys. Status Solidi B **76**, 475 (1976).

[20] J. G. Maxwell Garnett, Philos. Trans. R. Soc. London, Ser. A **203**, 385 (1904).

[21] D. S. McLachlan, M. Blaszkiewicz, and R. Newnham, J. Am. Ceram. Soc. **73**, 2187 (1990).

[22] C. Brosseau, J. Appl. Phys. **91**, 3197 (2002).

[23] J. W. Evans, Rev. Mod. Phys. **65**, 1281 (1993).

[24] V. Myroshnychenko and C. Brosseau, J. Appl. Phys. **97**, 044101 (2005).

[25] V. Myroshnychenko and C. Brosseau, Phys. Rev. E **71**, 016701 (2005).

[26] V. Myroshnychenko and C. Brosseau, J. Phys. D: Appl. Phys. **41**, 095401 (2008).

[27] V. Myroshnychenko and C. Brosseau, J. Appl. Phys. **103**, 084112 (2008).

[28] J. Macutkevic, D. Seliuta, G. Valusis, J. Banys, S. Hens, V. Borjanovic, V. Kuznetsov, and O. Shenderova, Compos. Sci. Technol. **70**, 2298 (2010).

[29] D. van der Putten, J. T. Moonen, H. B. Brom, J. C. M. Brokken-Zijp, and M. A. J. Michels, Phys. Rev. Lett. **69**, 494 (1992).

[30] P. Sheng, E. K. Sichel, and J. I. Gettleman, Phys. Rev. Lett. **40**, 1197 (1978).

[31] V. K. Ksenevich, V. B. Odzaev, Z. Martunas, D. Seliuta, G. Valusis, J. Galibert, A. A. Melnikov, A. D. Wieck, D. Novitski, M. E. Kozlov, and V. A. Samuilov, J. Appl. Phys. **104**, 073724 (2008).

[32] A. Mdahari, F. Carmona, C. Brosseau, and P. Delhaes, J. Appl. Phys. **103**, 054303 (2008).

[33] K. M. Jager, D. H. McQueen, and J. Vilcakova, J. Phys. D: Appl. Phys. **35**, 1068 (2002).

[34] P. J. Mather and K. M. Thomas, J. Mater. Sci. **32**, 401 (1997).

[35] Y. Xia and G. M. Whitesides, Annu. Rev. Mater. Sci. **28**, 153 (1998).

[36] A. Khosla and B. L. Gray, Mater. Lett. **63**, 1203 (2009).

[37] S. J. Clarson, Polymer **26**, 930 (1985).

[38] J. Grigas, *Microwave Dielectric Spectroscopy of Ferroelectrics and Related Materials* (Gordon and Breach Science Publications, OPA, Amsterdam, 1996).

[39] K. Bertulis, A. Krotkus, G. Aleksejenko, V. Pacebutas, R. Adomavicius, G. Molis, and S. Marcinkevicius, Appl. Phys. Lett. **88**, 201112 (2006).

[40] I. Pupeza, R. Wilk, and M. Koch, Opt. Express **15**, 4335 (2007).

[41] S. R. Tripathi, M. Aoki, M. Takeda, T. Asahi, I. Hosako, and N. Hiromoto, Jpn. J. Appl. Phys., Part 1 **52**, 042401 (2013).

[42] T. Koga, M. Takenaka, K. Airawa, M. Nakamura, and T. Hashimoto, Langmuir **21**, 11409 (2005).

[43] Z. M. Dang, L. Wang, Y. Yin, Q. Zhang, and Q. Q. Li, Adv. Mater. **19**, 852 (2007).

[44] C. Brosseau, P. Queffelec, and P. Talbot, J. Appl. Phys. **89**, 4532 (2001).

[45] A. K. Jonscher, *Universal Relaxation Law* (Chelsea Dielectric, London, 1996).

[46] B. J. P. Adohi, A. Mdarhri, C. Prunier, B. Haidar, and C. Brosseau, J. Appl. Phys. **108**, 074108 (2010).

[47] D. Bychanok, P. Kuzhir, S. Maksimenko, S. Bellucci, and C. Brosseau, J. Appl. Phys. **113**, 124103 (2013).

[48] A. Podzorov and G. Gallot, Chem. Phys. Lett. **495**, 46 (2010).

[49] C. W. Nan, Prog. Mater. Sci. **37**, 1 (1993).

[50] D. Almond, G. K. Duncan, and A. R. West, Solid State Ion. **8**, 159 (1983).

[51] A. Zylbersztejn and N. F. Mott, Phys. Rev. B **11**, 4383 (1975).

[52] T. A. Ezquerra, M. Kulesza, and F. J. Balta-Galleja, Synth. Met. **41**, 915 (1991).

[53] N. F. Mott and E. A. Davis, *Electronic Processes in Non-Crystaline Solids* (Oxford University, London, 1971).

II

Dielectric properties of graphite-based epoxy composites

I.Kranauskaite, J. Macutkevic, P. Kuzhir, N. Volynets, A. Paddubskaya, D. Bychanok, S. Maksimenko, J. Banys, R. Juskenas, S. Bistarelli, A. Cataldo, F. Micciulla, S. Bellucci, V. Fierro, A. Celzard

Dielectric properties of graphite-based epoxy composites

Ieva Kranauskaite[1], Jan Macutkevic[*,1], Polina Kuzhir[2], Nadeja Volynets[2], Alesia Paddubskaya[2], Dzmitry Bychanok[2], Sergey Maksimenko[2], Juras Banys[1], Remigijus Juskenas[3], Silvia Bistarelli[4], Antonino Cataldo[4], Federico Micciulla[4], Stefano Bellucci[4], Vanessa Fierro[5], and Alain Celzard[5]

[1] Department of Radiophysics, Vilnius University, Sauletekio 9, 10022 Vilnius, Lithuania
[2] Research Institute of Nuclear Problems of Belarusian State University, Bobruiskaya str. 11, 220030 Minsk, Belarus
[3] Center for Physical Sciences and Technology, Savanoriu ave. 231, 02300 Vilnius, Lithuania
[4] Frascati National Laboratory, National Institute of Nuclear Physics, via E. Fermi 40, 00044 Frascati, Italy
[5] IJL-UMR Université de Lorraine, CNRS 7198, ENSTIB, 27 rue Philippe Séguin, CS 60036, 88026 Épinal Cedex, France

* Corresponding author: e-mail jan.macutkevic@gmail.com, Phone: +370 52366077, Fax: +370 52366003

Composite materials based on epoxy resin filled with various kinds of graphite particles: exfoliated graphite, natural graphite, and coarse, medium and fine artificial graphites have been prepared. Results of broadband dielectric investigations of such materials in wide temperature (25–450 K) and frequency (20 Hz–3 THz) ranges are presented. The dielectric permittivity strongly increases with graphite particle size. The graphite particle size and shape also have a strong impact on freezing temperature, conductivity activation energy and composite electromagnetic absorption properties at room temperature. The lowest percolation threshold is observed for exfoliated graphite (EG)-based composites. At low temperatures (below glass transition temperature of pure polymer matrix), the electrical conductivity in composites above the percolation threshold is mainly governed by electron tunnelling between graphite particles. At higher temperatures, electrical conductivity due to finite electrical conductivity of polymer matrix and by electron tunnelling from polymer matrix to graphite particles occurs in all composites. Microwave experiments show that EG is the only really effective additive, out of all investigated graphite particles, for producing electromagnetic interference shielding composite materials: 2 wt% of EG in epoxy is indeed not transparent for the electromagnetic radiation at 30 GHz.

1 Introduction Conductor–insulator composites exhibit a variety of phenomena, some of them having important commercial applications. Conductive polymer composites have been extensively used in resistors, over-current and over-temperature circuit protection devices, supercapacitors, organic solar cells, biosensors, flexible transparent displays, antistatic materials and materials for electromagnetic interference (EMI) shielding [1]. In order to analyse the conductive behaviour in such systems at the microscopic scale, several models have been proposed, such as percolation theory [2], effective-medium theory of Maxwell-Garnett [3], aggregate structure model which overcomes the disadvantages of effective-medium theory, and McLachlan's [4] generalised effective-medium (GEM) theory combining most of the features of both percolation and effective-medium theories.

Nowadays, composites made with carbon nanotubes (CNTs) are very popular [5]. Indeed, CNT-based composites exhibit low percolation threshold and huge dielectric permittivity and electrical conductivity values at all frequencies, including microwave and terahertz ranges [5, 6]. However, a drawback of carbon nanotubes is their higher cost in comparison with other carbon allotropes, such as carbon black or graphite. Another serious disadvantage is the possible toxicity of CNTs, which has been debated for long [7], and which is still controversial today. Such problem does not occur with considerably bigger carbon particles such as exfoliated graphite (EG) or other graphite forms.

EG is derived from intercalation compounds of natural graphite that have been suddenly heated at high temperature [8]. The percolation threshold in EG-based composites can be very low, similar to that observed in polymer-CNT

materials [9–12]. Thus, EG can replace CNT in composites used as effective EMI shields [11, 12]. It means that exfoliated graphite, but may be also other kinds of graphites such as graphite nanosheets [13, 14] or artificial graphite particles with different particle sizes [15], can be interesting for electromagnetic (EM) applications in low- and microwave (MW)-frequency ranges.

At the present time, and as far as we know, no consistent broadband dielectric investigations of EG- and other graphite-based polymer composites exist in a wide temperature range. This motivated the present dielectric analysis along with MW characterisation of epoxy–graphite composites as an important step for manufacturing effective EM materials. The main idea was to systematise the experimental data in wide frequency range (20 Hz–3 THz), including microwaves (26–37 GHz), at different temperatures (25–450 K), and to observe the influence of the graphite primary particle size, if any, on the dielectric

properties of graphite-based composites. We restricted our consideration to the range of relatively low graphite concentrations (i.e. lower or equal to 2 wt%) at which the mechanical properties of graphite-based composites are still high [12].

2 Experimental The following graphite particles were used as filler in epoxy resin. Exfoliated graphite (EG) was purchased from Mersen (France), and was obtained by intercalation of natural graphite flakes with sulphuric acid followed by a very fast heating. Accordion-like particles were thus produced, leading to a material of low packing density, around $0.003 \, \mathrm{g \, cm^{-3}}$ [16]. Typically, the diameter of the EG particles is in the range 0.3–0.5 mm, and their aspect ratio is around 20. Three types of artificial graphites flakes, kindly supplied by Timcal G + T (Switzerland) under the name TIMREX® KS, were also used: coarse graphite (CG), medium graphite (MG), and fine
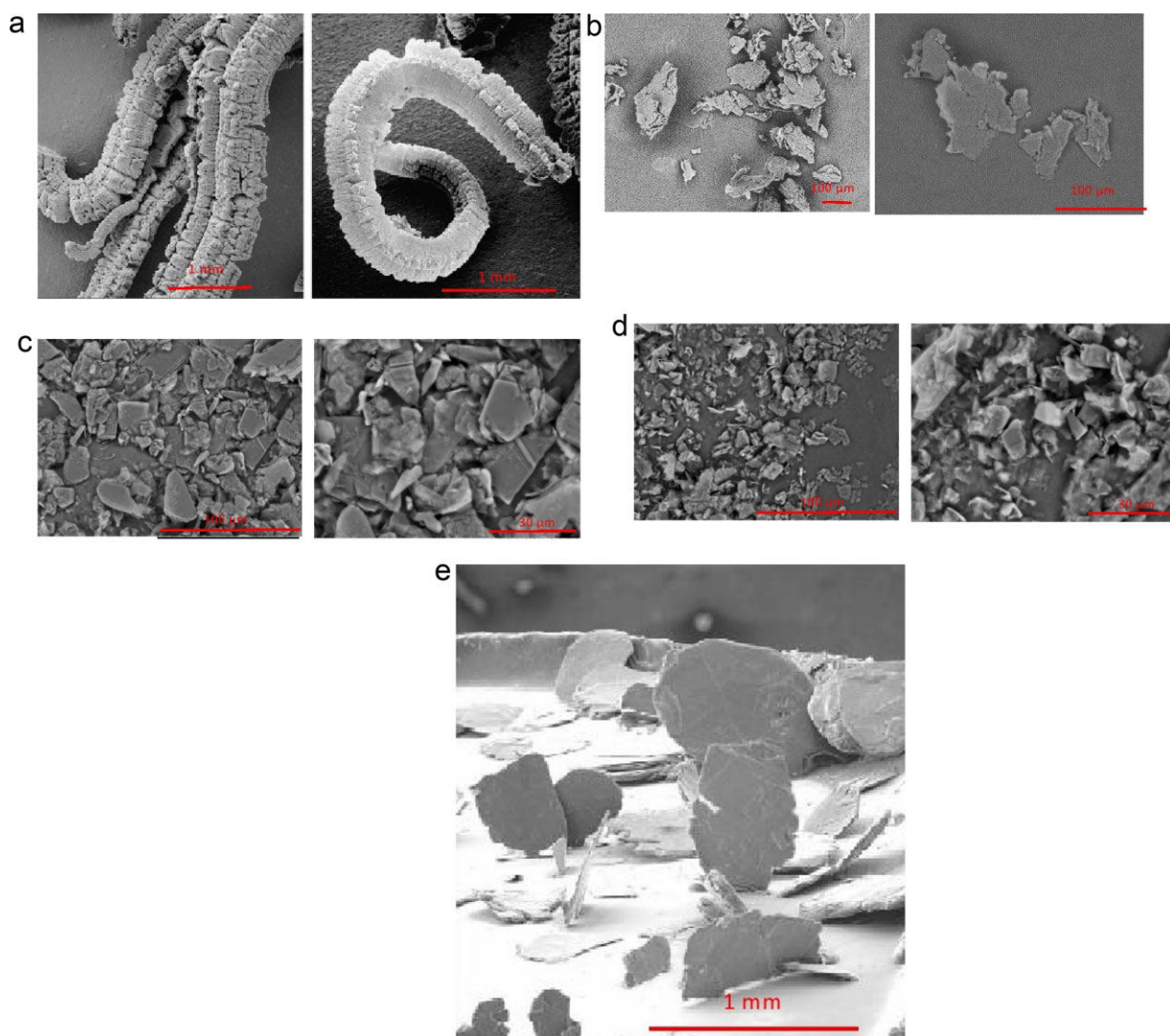
Figure 1 Scanning electron microscope images of the graphite particles used as fillers in the present epoxy–graphite composites: (a) EG; (b) CG; (c) MG; (d) FG; (e) NG.

Original Paper

Phys. Status Solidi A 211, No. 7 (2014) 1625

graphite (FG), having mean flake diameters between 100 and 200 μm, between 44 and 75 μm, and between 15 and 44 μm, respectively.

TIMREX® KS grades are synthetic graphites commercialised for being used as conductive additives up to 10% in the positive electrode of secondary lithium batteries [17]. They have relatively small single crystal domains in the particle, resulting in a relatively high isotropic electrical conductivity. Their particles are flattened spheroids giving excellent processability and rheological behaviour in liquid dispersions.

The aspect ratio of artificial graphites (ratio of the major to the minor axes of the ellipsoidal particles) is in the range 6.1–6.5, the higher the diameter, the higher the aspect ratio as the dimension of the minor axis changes much less.

The effect of all these graphites on the composites properties was compared to that obtained by using natural graphite from Madagascar (NG) as filler. The latter is composed of shiny, rather large, flakes having typical diameters within the range 500–750 μm, and a typical aspect ratio of 10–11. All the graphites used in the present study are shown in Fig. 1.

EPIKOTE™ Resin 828 was used as composite matrix. EPIKOTE Resin 828 is a medium viscosity liquid epoxy resin produced from bisphenol A resin and epichlorhydrin. It contains no diluent. EPIKOTE 828 provides good pigment wetting and good resistance to filler settling and a high level of mechanical and chemical resistance properties in cured state. Several series of composite samples, using Epikote 828, a curing agent called A1 (i.e. a modified TEPA) and 0.25, 0.5, 1, 1.5 and 2 wt% of various graphite fillers were fabricated as follows.

The resin was degassed under vacuum (1–3 mbar) for 12–14 h, then was put into an oven at 65 °C. In the meantime, the graphite was dispersed in propanol, and the suspension was submitted to an ultrasonic bath for 1.5 h. Afterwards, the alcoholic suspension of graphite was mixed with the resin. The obtained mixture was placed inside an oven at 130–150 °C for evaporating the alcohol. The curing agent A1 was added to the mixture of resin and filler through slow manual mixing for about 7 min. The blend was then poured into moulds of dimensions 1 cm × 1 cm × 7 cm, and left as such for 20 h for the curing process at room temperature, and finally 4 h in an oven at 80 °C. When the process was completed, the samples were removed from the moulds.

The homogeneity of composites was checked with scanning electron microscope (SEM) Helios NanoLab 650. For example, in Fig. 2 SEM image of composites with FG filler (concentration 2 wt%) is presented. Fabricated composites demonstrate good quality, with graphite inclusions being reasonably well dispersed.

The complex dielectric permittivity $\varepsilon^* = \varepsilon' - i\varepsilon''$ was measured by a LCR meter HP4284A in the frequency range 20 Hz–1 MHz. Each measurement started by heating the samples from room temperature up to 450 K, then cooling was performed down to 200 K. Low-temperature measurements were carried out by cooling in closed-cycle helium
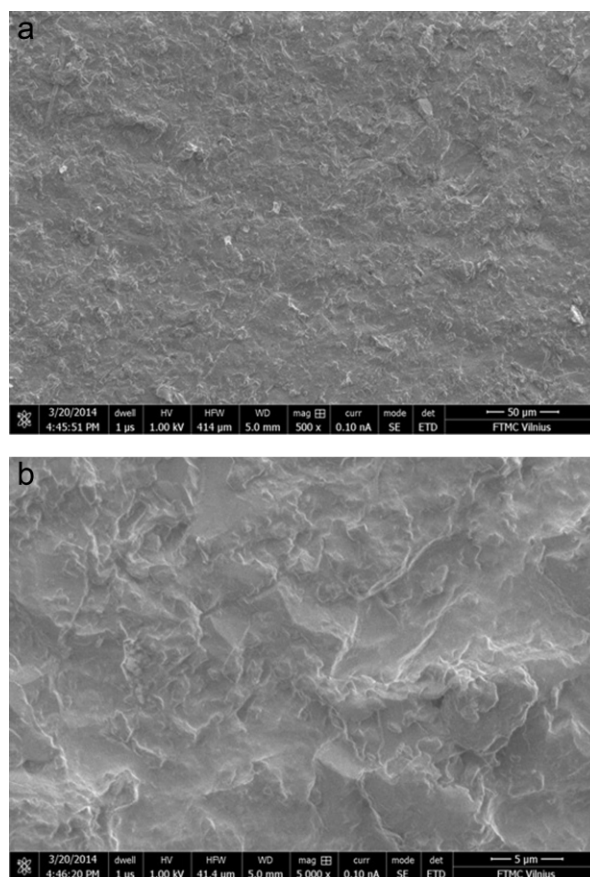
Figure 2 SEM image of composites with FG filler (concentration 2 wt%).

cryostat. In the frequency region from 1 MHz to 3 GHz, measurements were performed by a coaxial dielectric spectrometer with vector network analyser Agilent 8714ET. Microwave measurements were carried out with a scalar network analyser R2-408R (ELMIKA, Vilnius, Lithuania). In the frequency range from 100 GHz to 3 THz, measurements were performed by Time domain terahertz spectrometer (EKSPLA, Vilnius Lithunia) based on femtosecond laser (wavelength 1 μm, pulse duration less than 150 fs) and GaBiAs photoconductive switch as THz emitter and detector.

3 Results and discussion
3.1 Percolation thresholds
The critical weight fraction of graphite particles above which non-vanishing dc conductivity can be measured has not been determined from the experiments. The reason is related to the series of prepared composites which did not comprise enough different filler contents. A huge amount of different materials would have indeed allowed to build the full percolation curve and therefore observe the insulating – conducting transition. However, as the average aspect ratio A of the filler particles is known for each kind of graphite, being determined as the ratio of the major axis to the minor axis

for a prolate ellipsoid or a rod, or as the ratio diameter to thickness for a flake (and so that $A \geq 1$ in all cases), the critical fraction of conducting particles can be estimated. This can be achieved either from percolation theory (PT) or from effective-medium theory (EMT), provided that the filler particles are randomly dispersed in the matrix. According to PT, the percolation threshold Φ_c of disoriented thin discs of aspect ratio A reads [18]:

$$1 - \exp\left(-\frac{2 \times 1.8}{\pi A}\right) \leq \Phi_c \leq 1 - \exp\left(-\frac{2 \times 2.8}{\pi A}\right). \tag{1}$$

Assuming graphite flakes as flattened (oblate) ellipsoids, the critical volume fraction Φ_c can also be calculated from EMT [19]:

$$\Phi_c = \frac{9L_c(1 - L_c)}{2 + L_c(15 - 9L_c)}, \tag{2}$$

where L_c is the depolarisation factor, related to the eccentricity e of the (oblate) ellipsoids according to the following equations [20]:

$$L_c = \frac{1 + e^2}{e^3}(e - \arctan e), \quad e = \sqrt{A^2 - 1}. \tag{3}$$

From Eqs. (1) or (2), the (volume) percolation threshold Φ_c can be calculated, which must be converted into critical weight fractions ϕ_c, i.e. corresponding to the experimental quantities used in this work. Volume and weight critical concentrations are related to each other through the following equation:

$$\phi_c = \frac{1}{1 + (\rho_m/\rho_f)((1 - \Phi_c)/\Phi_c)}, \tag{4}$$

where ρ_m and ρ_f are the densities of matrix and filler, respectively.

The density of cured epoxy is $1.25 \,\text{g cm}^{-3}$, whereas that of bulk graphite is $2.28 \,\text{g cm}^{-3}$. The flaky graphite filler having the highest aspect ratio in the present study is NG. Introducing $A = 10$ in Eqs. (1) and (2), one gets $10.8 \,\text{vol\%} \leq \Phi_c \leq 16.3 \,\text{vol\%}$ and $\Phi_c = 13.1 \,\text{vol\%}$, respectively. The agreement between these two sets of values is quite satisfactory. From Eq. (4), one now gets $18.1 \,\text{wt\%} \leq \phi_c \leq 26.2 \,\text{wt\%}$ and $\phi_c = 21.5 \,\text{wt\%}$. This value is close to percolation threshold obtained in acrylonitrile butadiene rubber – poly(vinylchloride)/graphite composites [21]. These values are one order of magnitude higher than the highest graphite loading used in these composites, so the latter are clearly far below the percolation threshold. The same conclusion obviously applies to artificial graphites, whose particle aspect ratio is lower and therefore their corresponding percolation threshold is even higher.

The case of EG is different, due to the elongated shape and the extremely low density of its wormlike particles.

Estimating the critical volume fraction of elongated, rod-like, particles is also possible. PT predicts that Φ_c reads [22]:

$$1 - \exp\left(-\frac{1.4 \times [(A\pi/4) + (\pi/6)]}{(A^2\pi/2) + 2A\pi + (4\pi/3)}\right) \leq \Phi_c$$
$$\leq 1 - \exp\left(-\frac{2.8 \times [(A\pi/4) + (\pi/6)]}{(A^2\pi/2) + 2A\pi + (4\pi/3)}\right), \tag{5}$$

where A is again the aspect ratio, i.e. the length/diameter ratio in this case. EMT predicts that Φ_c also obeys Eq. (2), but using now the following definitions of the depolarisation factor L_c and of the eccentricity e of the (prolate) ellipsoids [23]:

$$L_c = \frac{1 - e^2}{2e^3}\left(\ln\frac{1 + e}{1 - e} - 2e\right) \quad\text{and}\quad e = \sqrt{1 - \left(\frac{1}{A}\right)^2}. \tag{6}$$

However, estimating the percolation threshold of composites made of EG filler is uneasy, as the wormlike particles do not behave as straight rods, and are extremely deformable due to their huge porosity. Indeed, and as suggested by the picture at the right of Fig. 1a, EG particles can be easily broken into several rod-like pieces of length three to four times smaller than their initial length during mixing with resin, and at the same time, their porosity is easily collapsed. As a result, their extremely low initial density, typically $0.015 \,\text{g cm}^{-3}$, can increase by two orders of magnitude when severely compressed [15]. In the present case, the EG worms were gently mixed with resin so that only a fraction of the porosity was lost, but such fraction is impossible to calculate. Therefore, only rough assumptions can be made. Given the anisotropy of EG particles, which behave as small accordions [15], the loss of porosity corresponds to a decrease of the length whereas the diameter remains constant. If x is the loss of porosity of EG particles, then aspect ratio and particle density are both related to x according to

$$\rho'_f = \frac{\rho_G}{1 + (1 - x)((\rho_G/\rho_f) - 1)} \quad\text{and}\quad A' \approx (1 - x)A, \tag{7}$$

where ρ_f and ρ'_f are the densities of the EG particles before and after having lost $x\%$ of porosity, respectively, ρ_G is the density of bulk graphite ($2.28 \,\text{g cm}^{-3}$), and A and A' are the aspect ratio (length/diameter) of the EG particles before and after having lost $x\%$ of porosity, respectively. Thus, if for example 20%, 50%, 80% or 90% of the EG particles' porosity is lost during composite preparation, combining Eqs. (7), (6), (2) and (4) leads to critical weight fractions of EG of 0.063, 0.201, 1.47 and 4.59 wt%, respectively. As a conclusion, the expected percolation threshold in EG-based composites is much lower than the one obtained with other graphite particles. Only the last value is indeed above 2 wt%, but corresponds to poorly realistic conditions in which 90%

Original

Paper

Phys. Status Solidi A 211, No. 7 (2014)

1627

of the porosity would be lost during the preparation process. The use of Eq. (5) leads to similar results, as shown in previous works which compared the results of Eqs. (2) and (5) for a broad range of aspect ratios [24].

As a final remark, so low percolation thresholds in EG-based composites are mainly due to the very low density of the highly porous filler. Indeed, Eq. (4) shows that $\Phi_c < \phi_c$ as long as $\rho_f > \rho_m$, which is the case for all non-porous graphites (NG, CG, MG and FG), whereas $\phi_c \ll \Phi_c$ as soon as $\rho_f \ll \rho_m$, which is the case for EG.

3.2 Room temperature dielectric properties The frequency dependence of complex dielectric permittivity of composites with different concentrations of NG particles at room temperature is presented in Fig. 3. The values of complex dielectric permittivity for these composites having filler concentrations up to 2 wt% is low, as it does not exceed 12, which is similar to that of pure epoxy resin. Therefore, the percolation threshold in the composites is higher than 2 wt%. Both real and imaginary parts of complex dielectric permittivity of composites are frequency-dependent, with a maximum of the imaginary part within the frequency range 10–100 kHz. A similar form of dielectric dispersion is also observed in pure epoxy resin, and it is related to alpha

relaxation in the polymer matrix [25]. The position of maximal dielectric losses is strictly dependent on NG concentration.

Similar form of dielectric spectra with low value of complex dielectric permittivity (as low as 12) at room temperature were observed (not shown) for all other composites made with artificial graphite fillers: CG, MG and FG. Therefore, for these composites, the percolation threshold is also estimated to be higher than 2 wt%. This finding also agrees with the expected percolation threshold which can be calculated either from percolation theory or from effective-medium theory, given the lower aspect ratios of such fillers, around 6, against around 10 for NG. As $\Phi_c \propto 1/A$ in the case of thin discs [26], then the percolation threshold of composites made with artificial graphites is thus roughly 10/6 times higher than those made with NG.
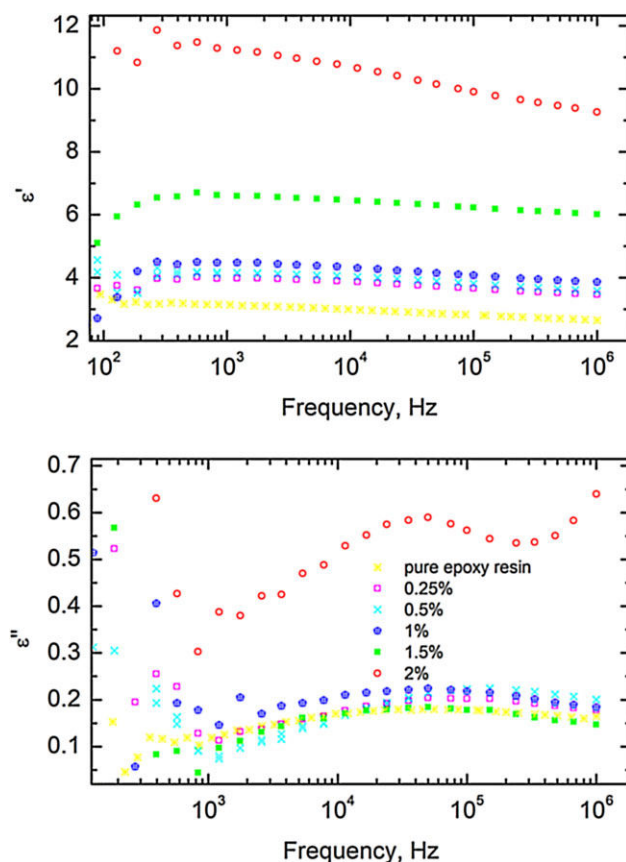
The value of complex dielectric permittivity of composites containing 1.5 and 2 wt% of EG is very high, see Fig. 4. For example, below the frequency of 129 Hz, the dielectric permittivity of composites containing 2 wt% of EG is almost 10^5 and the electrical conductivity is about $0.4\,S\,m^{-1}$. Such high values indicate that the percolation threshold is between 1.0 and 1.5 wt%. According to Bergman and Imry [27], close to percolation threshold:

$$\sigma(\omega) \sim \omega^x \ \text{and} \ \varepsilon'(\omega) \sim \omega^{-y}. \tag{8}$$

These critical exponents, x and y, are usually supposed to satisfy the following equation:

$$x + y = 1. \tag{9}$$

Obtained parameters are summarised in Table 1, but only for composites having graphite concentrations below the percolation threshold. Indeed, x could be determined only for these materials leading to straight lines of $\log \sigma$ versus $\log \omega$ in a sufficiently broad frequency range. Equation (9) is obeyed, as shown by Table 1. However, the individual values of x and y are different from those predicted by percolation theory, i.e. $x = t/(t + s)$ and $y = s/(t + s)$, where t and s are the usual conductivity exponents above and below the percolation threshold, respectively, leading to $x \approx 0.75$ and $y \approx 0.25$. Instead, x was found to take higher values and to decrease when the graphite concentration increased. Such behaviour was also reported by Chung et al. [28] in carbon black – PVC composites. Close to the percolation threshold, i.e. at a concentration of 1 wt%, the value of x, 0.86, is the same as that found by Song et al. [29] in carbon – Teflon® composites or similar to that obtained in EG/polyvinylidene fluoride composites [30].

Table 1 Parameters obtained by fitting Eq. (8) to the data of Fig. 4.

	x	y
EG 1 wt%	0.86	0.09
EG 0.5 wt%	0.93	0.05
EG 0.25 wt%	0.94	0.03

Figure 3 Frequency dependence of complex dielectric permittivity of composites with different concentrations of NG filler at room temperature.

The values of dielectric permittivity are very high even at microwave frequencies. For example, for the sample loaded at 2 wt% of EG, $\varepsilon' = 45$ at 1 GHz. Obtained results are in agreement with previously published results on microwave dielectric investigations of EG/epoxy composites [31]. The obtained value of microwave complex dielectric permittivity (Fig. 4) is higher than the one previously reported for carbon nanotube composites above percolation threshold even with much higher nanotubes loading [6, 32–33]. This can be explained by the very flat frequency dependence of complex dielectric permittivity for EG composites and different nature of electrical transport in EG and carbon nanotubes composites, which will be discussed below.

Moreover, a low frequency dielectric dispersion, related to Maxwell–Wagner relaxation of EG clusters, appears in composites with 2 wt% of filler, below 10 kHz (Fig. 4). However, its contribution to the static dielectric permittivity is lower in comparison with carbon nanotubes composites [6].

Microwave experiments (see Fig. 5) show that the only but really effective additive for producing EMI shielding with graphite–epoxy resin composites is exfoliated graphite. Being embedded into epoxy at 2 wt% (which is above percolation threshold), EG provides almost 100% of EM attenuation due to 30% absorption of microwave power and

70% reflection. All other functional fillers (NG, CG, MG and FG) do not demonstrate any EMI shielding ability, and the optical parameters (A, T, R) inherent to their composites in microwave range are controlled by the EM response of the neat epoxy resin matrix.

At higher frequencies (above 200 GHz), electrical conductivity due electron hopping almost vanishes and dielectric dispersion is mostly caused by phonon contribution, similarly as in pure epoxy resin matrix (Fig. 4).

Frequency dependence at room temperature of complex dielectric permittivity of composites filled with 0.5 wt% of different types of graphite particles is presented in Fig. 6. The real part ε' seems to increase strongly with graphite particle size at all frequencies. A similar behaviour of dielectric permittivity is observed for all other concentrations. The effect is related to the lower percolation threshold for composites with bigger graphite particles. Indeed, according to percolation theory, ε' below the threshold [34]:

$$\varepsilon' = \varepsilon_m \left(\frac{\Phi_c - \Phi}{\Phi_c} \right)^{-s}, \tag{10}$$

where ε_m is the dielectric permittivity of the matrix, Φ is the volume fraction of filler in the composite and s is the same
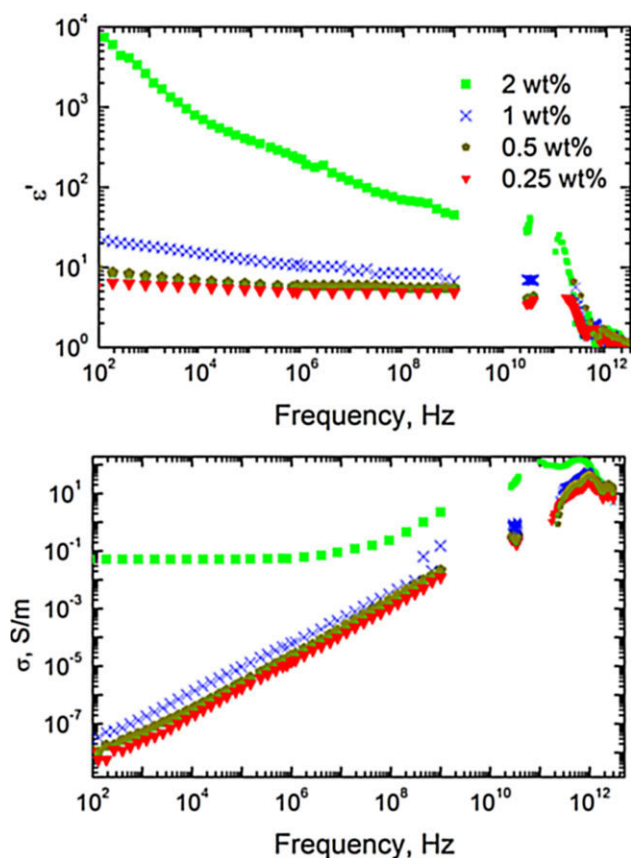
Figure 4 Frequency dependence of real parts of complex dielectric permittivity and electrical conductivity for composites with different concentrations of EG filler at room temperature.
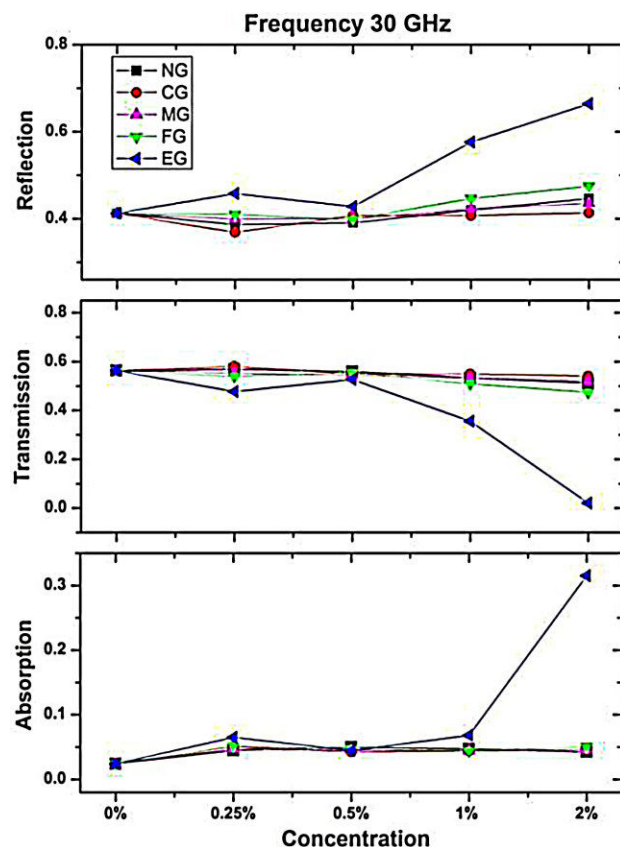

Figure 5 Concentration dependence of absorption–transmission–reflection of epoxy–graphite composites at 30 GHz. The thickness of free standing samples is 1.4 mm.

Phys. Status Solidi A 211, No. 7 (2014)

1629

universal critical exponent as above, close to 1.7 in three-dimensional systems [34]. In different composites having the same matrix and constant s, the dielectric permittivity thus increases when the critical concentration Φ_c decreases. Indeed, the lowest percolation threshold corresponds to EG-based composites, such that $1.0\,\text{wt\%} < \phi_c < 1.5\,\text{wt\%}$. NG leads to a much higher value, around 20 wt% (see again previous section), whereas CG, MG and FG lead to increasingly, even higher thresholds, typically ranging from 28 to 29 wt%, respectively, by application Eqs. (2)–(4).

The position of the maximum of the imaginary part for the same concentration of graphite filler is strictly dependent on the graphite particle size (Fig. 6). The maximum is observed at higher frequencies with smaller graphite particles. For MG and FG composites, it is close to the frequency of $2 \times 10^5\,\text{Hz}$.

At the same time, for the bigger particles NG and CG, the position of losses maximum is close to the position of maximum for pure epoxy resin. This effect is more pronounced than the shift of imaginary part of complex permittivity with graphite concentration.

3.3 Dielectric relaxation For analysing more in-depth the dielectric dispersion in composites, the temperature dependencies of both ε' and ε'' have been investigated.
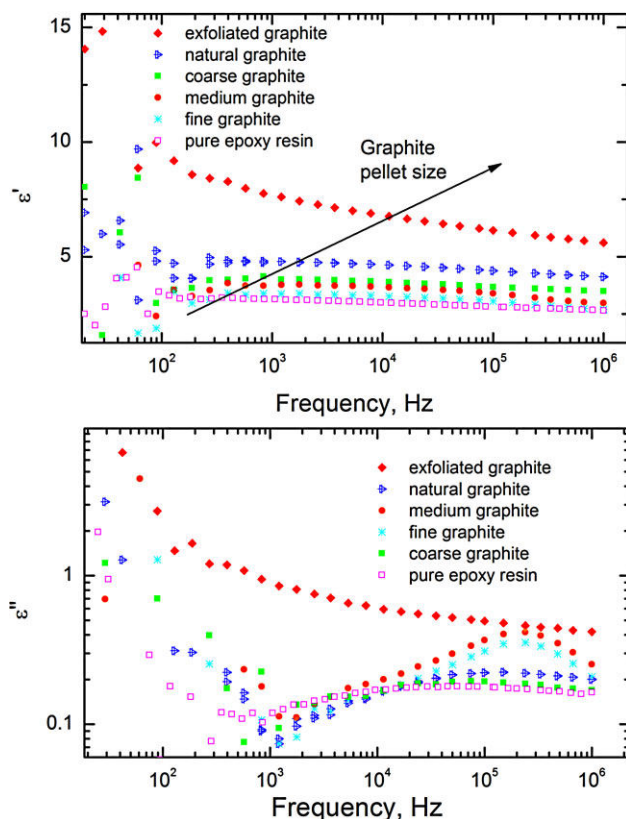
The temperature dependence of complex dielectric permittivity at different frequencies of the composite with 1.5 wt% of NG filler is presented in Fig. 7. The imaginary part of permittivity ε'' versus temperature exhibits a maximum at low temperatures. The position of such maximum is frequency-dependent, and is progressively shifted towards higher temperatures when the frequency increases. At the same time, the permittivity ε' shows dispersion (see top part of Fig. 7). The similar dielectric dispersion caused by polymer dynamics was observed in pure epoxy and is known to be related to α transition [25]. At temperatures above 350 K, the complex dielectric permittivity ε^* increases due to the onset of electrical conductivity. The mean relaxation time was obtained from the frequency dependence of ε^* (Fig. 8) as $\tau = 1/\nu_m$, where ν_m is the frequency corresponding to the maximal dielectric losses. On cooling, the relaxation time increases according to Vogel–Fulcher law (Fig. 9):

$$\tau = \tau_0 \exp[E/(k_B(T - T_0))], \tag{13}$$

where τ_0 is the relaxation time at very high temperatures, E_B is the relaxation activation energy, and T_g is the freezing temperature of the matrix.

The best fits were obtained using the same $\tau_0 = 1.14\,\text{ps}$ value for all composites below the percolation threshold, the
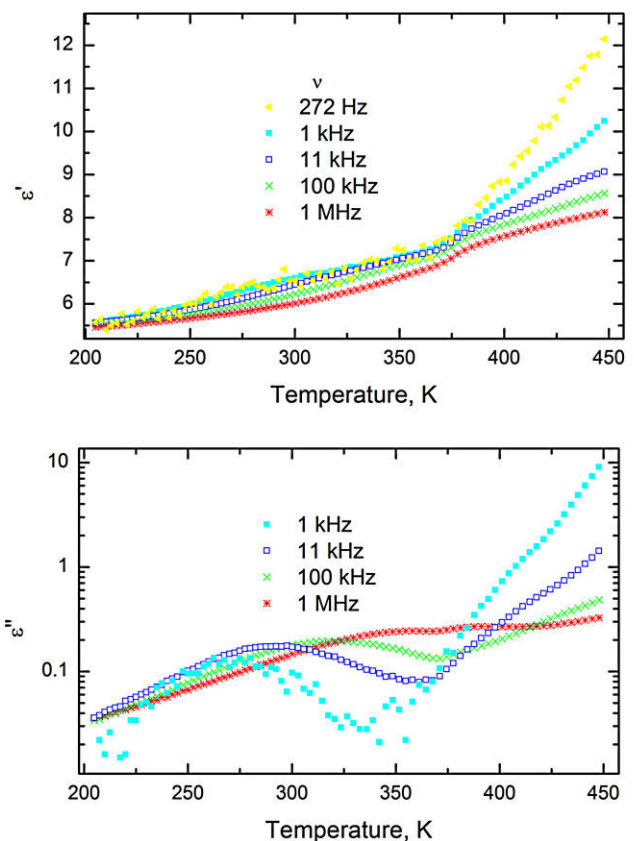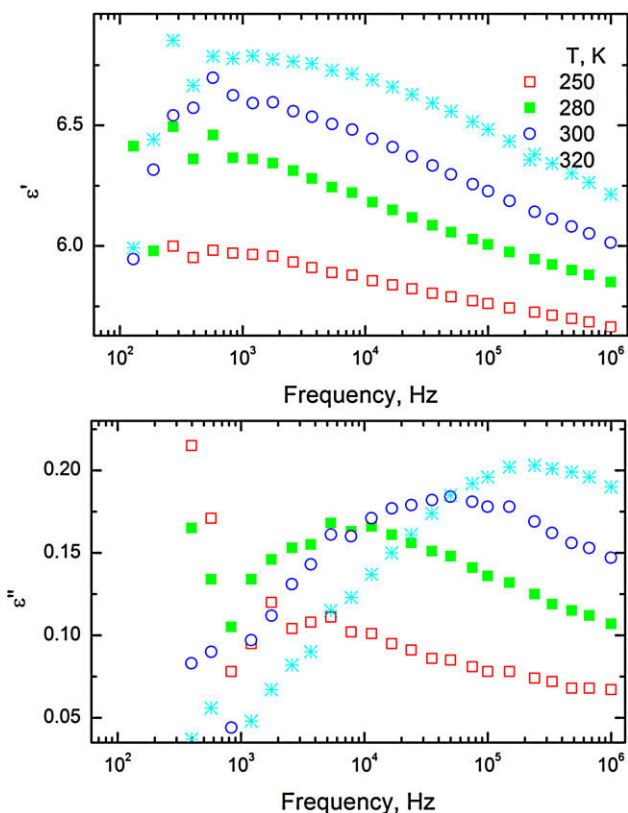

Figure 6 Frequency dependence of complex dielectric permittivity of composites based on different graphite fillers at concentration 0.5 wt% and at room temperature.
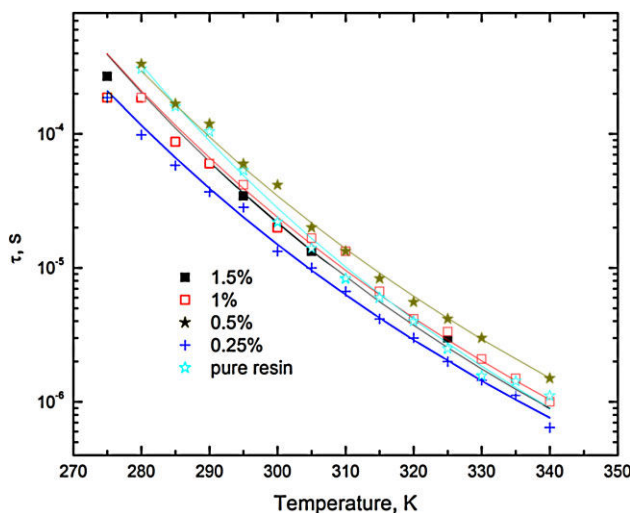

Figure 7 Temperature dependence of complex dielectric permittivity of composites with NG filler (concentration 1.5 wt%) at different frequencies.

Figure 8 Frequency dependence of complex dielectric permittivity of composites with NG filler (concentration 1.5 wt%) at different temperatures.

Figure 9 Temperature dependence of relaxation time of composites based on NG filler.

same value of τ_0 was also obtained for pure resin [35] (except for samples at 2 wt% NG and 0.5 and 1 wt% EG, for which maximum of imaginary part of complex dielectric permittivity related to the alpha relaxation was not observed), and led to the parameters presented in Fig. 10. The concentration dependence of relaxation activation energy for artificial and natural graphites has a maximum for concentrations 0.5–1 wt%. The freezing temperature T_g is lower in all composites than in pure polymer matrix and shows a pronounced minimum at 0.5–1 wt% concentration, depending on the kind of graphite. Such a minimum, as well as a maximum in the concentration dependence of relaxation activation energy, may be explained by the contribution of two antagonistic effects. On one hand, the graphite particles may adsorb macromolecules at their surface, thus hindering polymer mobility and hence decreasing the freezing temperature, as usually observed in most composites [36]. On the other hand, T_g may have complex behaviours, for example if heterogeneous crosslinking around filler particles occurred [37], or depending on how the composite has been cured [38]. A decrease of T_g may be related to the enhanced polymer dynamics due to the extra free volume at the polymer–filler interface. Thus, in composites with artificial graphite and NG fillers, T_g presents a minimum in the medium concentration range 0.5–1 wt%. At lower concentrations, the freezing

temperature decreases more rapidly in EG composites than in composites with smaller artificial graphite particles. It can be explained by a free volume at the polymer–graphite interface which is higher when the filler particles are bigger. At the same time, the concentration dependence of freezing temperature shows the opposite tendency at higher graphite concentrations, which is obviously related with stronger interactions between polymer matrix and graphite particles.

3.4 Electrical transport at different temperatures

The dc conductivity has been obtained from frequency dependence of conductivity according to Almond–West law [39]. The temperature dependence of dc conductivity for EG-based composites (except for the one at 0.25 wt%, for which σ_{dc} occurs at frequencies below our lower frequency limit) is presented in Fig. 11. Three different temperature regions can be separated: (I) below 150 K, in which the dc conductivity slowly decreases with temperature for composites above percolation threshold; (II) between 150 and 410 K, in which the dc conductivity decreases when temperature increases; (III) above 410 K, in which dc conductivity increases with temperature in all composites, independently on whether they are below or above percolation threshold (except for the composite at 2 wt% for which the increase of dc conductivity with temperature is expected to occur above 450 K). After annealing, the electrical conductivity decreases in all composites. However, the most significant effect was observed in composites with high EG concentration, especially in the composite at 2 wt%, whose dc conductivity decreases by 10 times.

The temperature dependence of dc conductivity in temperature region I (Fig. 11b) was fitted with fluctuation-induced tunnelling model [40]:

$$\sigma_{dc} = \sigma_0 \exp\left[-\frac{T_1}{T + T_0}\right], \qquad (14)$$

Original

Paper

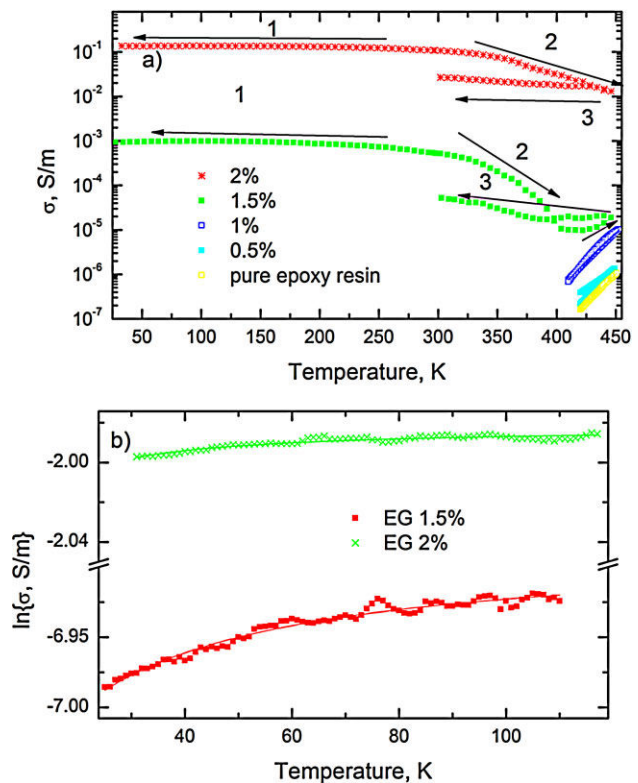Phys. Status Solidi A 211, No. 7 (2014)   1631
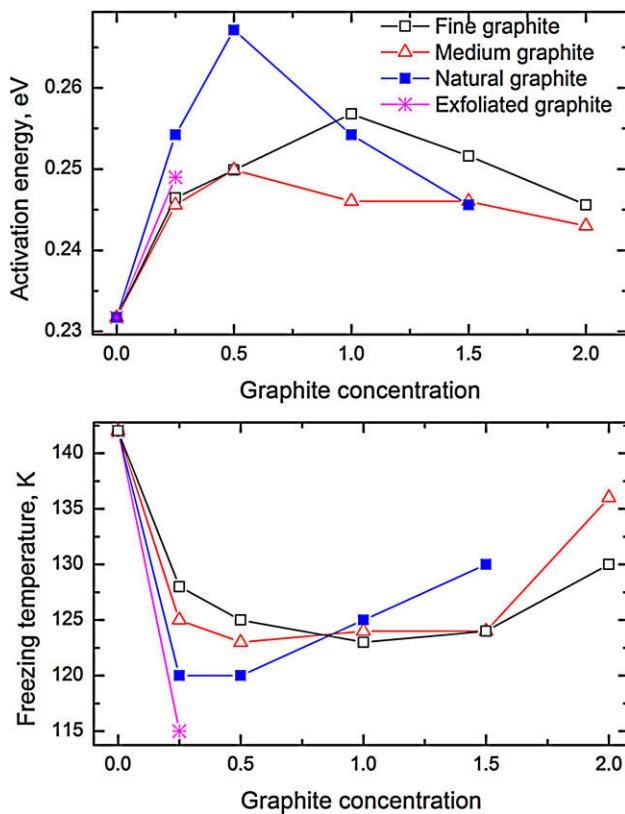
Figure 10 Concentration dependence of dielectric relaxation activation energy and freezing transition temperature for different natures and concentrations of graphite fillers.

Figure 11 Temperature dependence of dc conductivity of composites based on EG filler: (a) full temperature region; (b) low-temperature region. Arrows indicate temperature change direction and numbers order.

where T_1 represents the energy required for an electron to cross the insulator gap between conductive particles, and T_0 is the temperature above which thermally activated conduction over the barriers becomes significant. According to the tunnelling model [40],

$$T_1 = \frac{wa\beta_0}{8\pi k}, \tag{15}$$

$$T_0 = \frac{2T_1}{\pi \chi w}, \tag{16}$$

where $\chi = (2mV_0)^{0.5}/h$ and $\beta_0 = 4V_0/ew$, m and e being the electron mass and charge, respectively, V_0 the potential barrier height, w the interparticle distance, and a the area of the capacitance formed by the junction. The resultant fitting parameters are listed in Table 2. Very low values of T_1 and T_0, such as those obtained here, indicate the very low potential barrier height for electrons tunnelling between EG clusters in comparison with what has been reported for CNTs- and carbon black-based composites even at much higher filler concentration [41, 42]. Thus, in temperature regions I and II, electrical conductivity is mainly governed by electron tunnelling between EG particles. In the temperature region II, electrical conductivity increases when

the temperature decreases due to shrinkage of polymer matrix.

At higher temperatures (above 410 K), the temperature dependence of dc conductivity can be fitted very satisfactorily with Arrhenius law (Fig. 11a):

$$\sigma = \sigma_0 \exp\left[-\frac{E_A}{k_B T}\right]. \tag{17}$$

The concentration dependence of the activation energy E_A for composites with different graphite fillers is presented in Fig. 12. Below percolation threshold, the conductivity activation energy E_A is almost concentration-independent. In contrast, for the composites with 1.5 wt% of EG, its value is very low. The difference between heating and cooling data is clearly observed in composites with bigger graphite particles, for NG- and EG-based composites, since conductivity

Table 2 Parameters obtained by fitting Eq. (14) to the data of Fig. 11b.

	$\ln \sigma_0$ (S m^{-1})	T_1 (K)	T_0 (K)
EG 2 wt%	−1.98	0.5	0.2
EG 1.5 wt%	−6.88	4.2	16.6
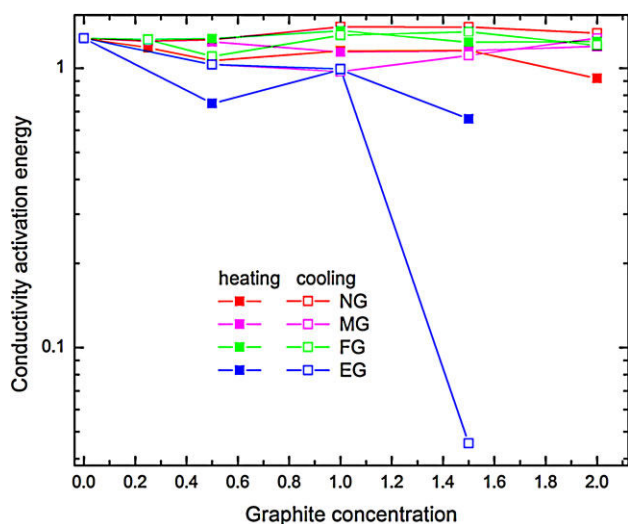
Figure 12 Concentration dependence of the conductivity activation energy for different graphite fillers.

activation energy significantly increased after annealing in NG composites and decreases in EG composites. In contrast, the difference between heating and cooling conductivity activation energies is very small for composites based on smaller graphite particles (MG and FG).

The lowest activation energy values were obtained in EG-based composites, even below the percolation threshold. In composites below percolation threshold, electrical conductivity occurs due to finite epoxy resin conductivity. Graphite particles and boundary between graphite and polymer matrix can make disturbance for electron travelling in the polymer due to non-ohmic contacts or in contrary can provide additional channels for carrier travelling, due to their tunnelling from polymer matrix to graphite particles. In the latter case, the conductivity activation energy should be lower in composites with higher filler concentration. This is clearly observed in composites above percolation threshold (see again Fig. 12). However, even below the percolation threshold, conductivity activation energy is lower in most composites than in pure polymer matrix, except for NG-based composites after annealing. After annealing of epoxy resin composites, graphite conductive networks are partially destroyed and total composite conductivity is decreased, as also found elsewhere [43] and as suggested by Fig. 11. Therefore, it can be concluded that the formation of conductive networks near and above percolation threshold significantly decreases the conductivity activation energy in composites.

In EG-based composites at 1.5 wt% loading, dc conductivity appears at lower temperatures than in pure epoxy resin or in composites with lower filler concentration (Fig. 11). The effect can be explained by temperature-dependent percolation threshold. The percolation threshold is lower in composite slightly below the pure epoxy glass transition temperature [44]. Close and above this temperature, the redistribution of graphite clusters is possible. A

decrease of percolation threshold indicates a possibility of forming a more conductive graphite network at higher temperatures.

4 Conclusions Results of broadband (20 Hz–3 THz) dielectric investigations of epoxy–graphite composites in wide temperature region are reported. The dielectric permittivity of composites at room temperature apparently increases with graphite particle size. Such a finding is explained by the decrease of the percolation threshold with microsized graphite particle size, which is confirmed theoretically.

All tested graphites could be interesting for applications which do not require high dc conductivity, such as antistatic and electrostatic dissipation applications. The only but very promising candidate for producing effective EMI shielding material, out of all graphite fillers investigated here, is exfoliated graphite (EG). Moreover, EG demonstrates relatively low percolation threshold in dc conductivity, between 1.0 and 1.5 wt%. All other graphite additives, both natural and artificial, have percolation thresholds much higher than 2 wt%.

The electrical conductivity of EG-based composites above percolation threshold and at low temperatures (below glass transition temperature of pure polymer matrix) is mainly governed by electron tunnelling between graphite particles. Such tunnelling is characterised by very low potential barriers for carriers with respect to what has been reported for much higher concentrations of other carbon fillers such as carbon nanotubes or carbon blacks. Below the percolation threshold, the dielectric properties of graphite-based composites are mainly governed by alpha relaxation in pure epoxy resin matrix. The dependence of freezing temperature on graphite concentration shows a minimum at concentration 0.5–1 wt%. At higher temperatures, electrical conductivity occurs in all composites whether they are below or above the percolation threshold, and such conductivity is strongly impacted by electron tunnelling between graphite particles throughout polymer matrix.

References

[1] G. Inzelt, Conducting Polymers. A New Era in Electrochemistry (Springer-Verlag, Heidelberg, 2008).
[2] M. B. Isichenko, Rev. Mod. Phys. **64**, 961 (1992).
[3] J. G. Maxwell Garnett, Philos. Trans. R. Soc. Lond. **203**, 385 (1904).
[4] D. S. McLachlan, M. Blaszkiewicz, and R. Newnham, J. Am. Ceram. Soc. **73**, 2187 (1990).
[5] F. Quin and C. Brosseau, J. Appl. Phys. **111**, 061301 (2012).

Phys. Status Solidi A 211, No. 7 (2014)

Original

Paper

1633

[6] D. Nuzhnyy, M. Savinov, V. Bovtun, M. Kempa, J. Petzelt, B. Mayoral, and T. McNally, Nanotechnology **24**, 055707 (2013).

[7] S. Bellucci, in: Nanoparticles and Nanodevices in Biological Applications, The INFN Lectures, Vol. 1, edited by S. Bellucci (Springer, Germany, 2009), ISBN 978-3-540-70943-5.

[8] D. D. L. Chung, J. Mater. Sci. **22**, 4190 (1987).

[9] W. Zheng, S. Ch. Wong, and H. J. Sue, Polymer **73**, 6767 (2003).

[10] S. Paszkiewicz, A. Szymczyk, Z. Spitalsky, M. Soccio, J. Mosnacek, T. A. Ezquerra, and Z. Roslaniec, J. Polymer Sci. B **50**, 1645 (2012).

[11] R. K. Goyal, Mater. Chem. Phys. **142**, 195 (2013).

[12] P. Kuzhir, A. Paddubskaya, A. Plyushch, N. Volynets, S. Maksimenko, J. Macutkevic, I. Kranauskaite, J. Banys, E. Ivanov, R. Kotsilkova, A. Celzard, V. Fierro, J. Zicans, T. Ivanova, R. Merijs Meri, I. Bochkov, A. Cataldo, F. Micciulla, S. Bellucci, and Ph. Lambin, J. Appl. Phys. **114**, 164304 (2013).

[13] G. Chen, W. Weng, D. Wu, and C. Wu, Europ. Polymer J. **39**, 2329 (2003).

[14] S. E. Lee, O. Choi, and H. T. Hahn, J. Appl. Phys. **104**, 033705 (2008).

[15] T. Ezquerra, M. Kulescza, and F. Balta-Calleja, Synth. Met. **41-43**, 915 (1991).

[16] A. Celzard, J. F. Mareche, and G. Furdin, Prog. Mater. Sci. **50**, 93 (2005).

[17] F. Nobili, S. Dsoke, T. Mecozzi, and R. Marassi, Electrochim. Acta **51**, 536 (2005).

[18] A. Celzard, C. Deleuze, M. Dufort, G. Furdin, J. F. Marêché, and E. McRae, Phys. Rev. B **53**, 6209 (1996).

[19] A. Celzard, J. F. Marêché, and F. J. Payot, J. Phys. D: Appl. Phys. **33**, 1556 (2000).

[20] K. S. Mendelson and M. H. Cohen, Geophysics **47**, 257 (1982).

[21] S. A. Mansour, M. E. Al-ghoury, E. Shalaan, M. H. I. El Eraki, and E. M. Abdel-Bary, J. Appl. Polymer Sci. **122**, 1226 (2011).

[22] A. Celzard, C. Deleuze, M. Dufort, G. Furdin, J. F. Marêché, and E. McRae, Phys. Rev. B **53**, 6209 (1996).

[23] L. D. Landau and E. M. Lifshitz, Electrodynamics of Continuous Media (Pergamon, New York 1980).

[24] A. Celzard, V. Fierro, and A. Pizzi, Cellulose **15**, 803 (2008); A. Celzard, V. Fierro, R. Kerekes, Cellulose **16**, 983 (2009).

[25] C. Brosseau and M. E. Achour, J. Appl. Phys. **105**, 124102 (2009).

[26] A. Celzard, C. Deleuze, M. Dufort, G. Furdin, J. F. Marêché, and E. McRae, Phys. Rev. B **53**, 6209 (1996).

[27] D. J. Bergman and Y. Imry, Phys. Rev. Lett. **39**, 1222 (1977).

[28] K. T. Chung, A. Sabo, and A. P. Pica, J. Appl. Phys. **53**, 6867 1982.

[29] Y. Song, T. W. Noh, S. I. Lee, and J. R. Gaines, Phys. Rev. B **33**, 904 (1986).

[30] Y. C. Li, R. K. Y. Li, and S. H. Tjong, J. Nanomater. **2010**, 261748 (2010).

[31] L. Vovchenko, L. Matzui, V. Oliynyk, and V. Launetz, Phys. Status Solidi C **7**, 1260 (2010).

[32] B. Wen, M. Cao, Z. Han, W. Song, L. Zhang, M. Lu, H. Jin, X. Fang, W. Wang, and J. Yuan, Carbon **65**, 124 (2013).

[33] D. Bychanok, P. Kuzhir, S. Maksimenko, S. Bellucci, and C. Brosseau, J. Appl. Phys. **113**, 124103 (2013).

[34] M. Sahimi, Applications of Percolation Theory (Taylor & Francis, Bristol PA, 1994,).

[35] J. Macutkevic, P. Kuzhir, A. Paddubskaya, S. Maksimenko, J. Banys, A. Celzard, V. Fierro, E. Stefanutti, A. Cataldo, F. Micciulla, and S. Bellucci, J. Nanosci. Nanotechnol. **13**, 5434 (2013).

[36] G. J. Howard and R. A. Shanks, J. Macromol. Sci. Chem. A **17**, 287 (1982).

[37] P. Bartlet, Y. G. Lin, J. P. Pascault, and H. Sautereau, Polymer Bull. **17**, 97 (1987).

[38] G. Fourche, L. Lafeychine, and F. Carmona, Macromol. Chem. Macromol. Symp. **9**, 179 (1987).

[39] D. P. Almond, G. K. Duncan, and A. R. West, Solid State Ion. **8**, 159 (1983).

[40] P. Sheng, E. K. Sichel, and J. I. Gittleman, Phys. Rev. Lett. **40**, 1197 (1978).

[41] H. M. Kim, M. S. Choi, J. Joo, S. J. Cho, and H. S. Yoon, Phys. Rev. B **74**, 054202 (2006).

[42] E. K. Sichel, J. I. Gittleman, and P. Sheng, Phys. Rev. B **18**, 5712 (1978).

[43] J. Macutkevic, P. Kuzhir, A. Paddubskaya, S. Maksimenko, J. Banys, A. Celzard, V. Fierro, S. Bistarelli, A. Cataldo, F. Micciulla, and S. Bellucci, J. App. Phys. **114**, 033707 (2013).

[44] J. Mark, K. Ngai, W. Graessley, L. Mandelkern, E. Samulski, J. Koning, and G. Wignall, Physical Properties of Polymers (Cambridge University Press, Cambridge, United Kingdom, 2004).

III

Synergy effects in the electrical conductivity behavior of onion-like carbon and multiwalled carbon nanotubes composites

I.Kranauskaite, J. Macutkevic, J. Banys, E. Talik, V. Kuznetsov, N. Nunn, O. Shenderova

Physica status solidi B 252 (8), 1799 – 1803 (2015)

Reprinted with permission from *Physica status solidi B*

Synergy effects in the electrical conductivity behavior of onion-like carbon and multiwalled carbon nanotubes composites

Ieva Kranauskaite[1], Jan Macutkevic[*,1], Juras Banys[1], Ewa Talik[2], Vladimir Kuznetsov[3,4], Nicholas Nunn[5], and Olga Shenderova[5]

[1] Vilnius University, Sauletekio al. 9, Vilnius 00122, Lithuania
[2] Institute of Physics, University of Silesia, ul. Uniwersytecka 4, Katowice 40-007, Poland
[3] Boreskov Institute of Catalysis SB RAS, Lavrentiev Ave. 5, Novosibirsk 630090, Russia
[4] National Research Tomsk State University, Lenina Street 36, 634050 Tomsk, Russia
[5] International Technology Center, Raleigh, NC 27715, USA

* Corresponding author: e-mail jan.macutkevic@gmail.com, Phone: +37052366077, Fax: +37052366003

The dielectric/electric properties of polyurethane composites filled with carbon nanotubes (CNT), onion-like carbon (OLC), and mixed OLC/CNT are compared across a wide frequency range from hertz to terahertz. The dielectric/electric properties of composites filled with OLC are very attractive and can be improved by addition of small amounts of CNTs due to a strong synergism between the two carbon allotropes. More-over, in composites with mixed OLC/CNT inclusions, the value of the percolation threshold is lower than the value predicted by the excluded-volume theory. In composites with mixed OLC/CNT inclusions, the dielectric permittivity and electrical conductivity increase due to a decrease in the average distance between nanocarbon clusters.

1 Introduction Nowadays, electrically percolative polymer-based composites with various nanocarbon inclusions are very popular due to their outstanding electrical, electromagnetic, mechanical, and thermal properties in comparison with the polymer matrix material [1]. Many investigations of such composites were performed within a narrow frequency range and at room temperature in order to find the percolation threshold (the minimum concentration of nanofillers at which composites are conductive) [2]. An important task is to obtain a low percolation threshold in order to preserve (or reach) optimal mechanical properties of polymers and to use a minimal concentration of expensive fillers. The lowest percolation threshold was observed in carbon nanotubes (CNT) composites due to their high aspect ratios [3]. However, CNT usually agglomerate within the polymer matrix because of the high Van der Waals force between CNT, and this leads to an increase of the percolation threshold. Therefore, the

percolation threshold in the same polymer matrix and for the same CNT can vary significantly [3]. Moreover, the percolation threshold in other composites, for example, in carbon black (CB) composites, can also be very low [4]. Thus, investigations of composites with other less expensive inclusions are very promising.

Onion-like carbon (OLC), consisting of stable, defected, multishell fullerenes, exhibits high conductivity similar to CNTs [5]. The percolation threshold in OLC composites is strictly dependent on aggregate size, and it is lowest for composites with the smallest aggregate size [6]. In particular, in OLC/polyurethane composites with an average aggregate size of $\sim$120 nm, the percolation threshold is 10 vol% [7]. Thus, the percolation threshold in OLC composites is lower than predicted by Monte-Carlo calculations $\sim$31.2 vol% [8] and can be lowered with improved composite preparation procedures [9]. Moreover, the dielectric permittivity of OLC-based composites is very high (more than 10^6 at low

frequencies), and these composites are very attractive for various applications [7]. However, the percolation threshold in OLC-based composites is still much higher in comparison with CNT composites.

Multiphase composites with several different fillers in the matrix are very interesting due to the potential synergy between the different components [10]. Often, the distribution of different fillers within the polymer matrix can be favorable, and electrical transport can occur in different fillers network together. When this occurs, the percolation threshold can decrease dramatically in comparison with single-filler composites [10]. Also, when the synergy effect is observed, the electrical conductivity of hybrid composites is higher than a simple sum of the conductivities of corresponding binary systems [11]. Many investigations of synergy effects were performed in CNT/CB composites, and a significant decrease in the percolation threshold, in comparison with CB composites, was observed [10–12]. Usually, this synergistic effect was investigated only at room temperature.

In this paper, we compare the broadband dielectric/electric properties of composites filled with CNT, OLC, and mixed CNT/OLC composites at temperatures starting from room down to 26 K. It was demonstrated that the dielectric and electrical properties with OLC inclusions can be substantially improved with the addition of CNT.

2 Experimental Polyurethane films with nanoadditives were prepared using Clear Gloss MINWAX® Fast-Drying Polyurethane. Nanoadditives included multi-walled CNT (20 nm diameter, 5–10 μm length) purchased from Amorphous Carbon Materials, Inc. and OLC derived by vacuum annealing of detonation nanodiamonds (DND) [5–7]. Aggregates of DND consisting of 5 nm primary particles were heated in vacuum (10^{-4} Torr) at 1650 °C for 3 h, providing aggregates of OLC with aggregate sizes corresponding to the sizes of the starting DND fractions (approximately 100 nm). Stock suspensions of nanoadditives (∼0.5–1.0% w/v) were prepared in an alcohol solvent and sonicated with a horn-based sonicator for 30 min. Seven grams of polyurethane (PU) was heated on a hot plate at 60 °C under magnetic stirring. The alcohol-based suspension containing the desired amount and type of the nanoadditives was added dropwise to the PU while maintaining stirring. After the alcohol suspension was combined with the PU, the alcohol was evaporated from the PU–nanoadditive mixture. The samples were then cast on a teflon substrate and cured at 40 °C for 24 h. After curing, the samples were annealed at 180 °C for 0.5 h in order to homogenize the nanofiller distribution. In this paper, composites containing up to 2 wt% inclusions of CNTs, up to 7 wt% of OLC, and mixed CNT/OLC containing up to 7 wt% of OLC, and a constant concentration of CNT—0.5 wt% were investigated. Microstructural characterization of the composites was performed using a JEOL-7600F scanning electron microscope.
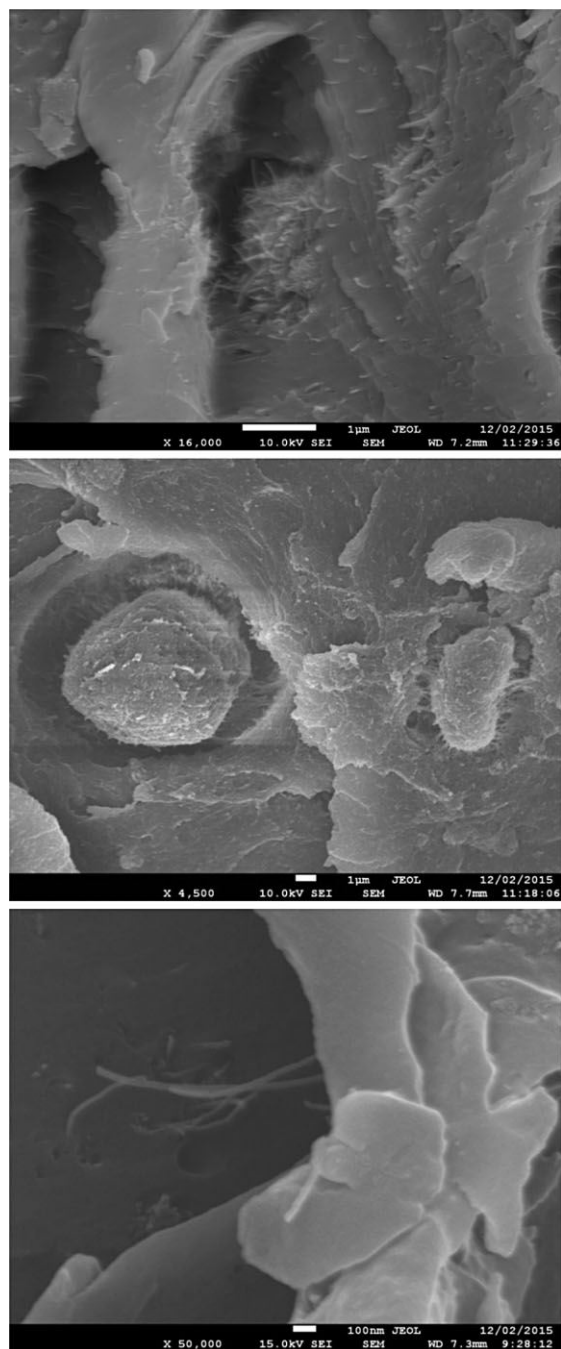
The complex dielectric permittivity was measured as a function of frequency and temperature using a HP4284A precision LCR meter in the frequency range from 20 Hz to 1 MHz. For the low-temperature measurements, a helium closed-cycle cryostat was used. In the frequency range from 1 MHz to 3 GHz, dielectric measurements were performed using a vector network analyzer (Agilent 8714ET). In the microwave frequency range from 8 to 53 GHz, a home-made waveguide spectrometer was used. The method of a thin rod in the waveguide was used [13]. In the frequency range from 1 MHz to 53 GHz, the measurements accuracy was ∼10%. Silver paste was used for creating the contacts. In the terahertz frequency range (from 100 GHz to 3 THz), a terahertz time-domain spectrometer (Ekspla Ltd) based on a femtosecond laser was used for the measurements. The spectrometer is based on the femtosecond fiber laser (wavelength 1 μm, pulse duration less than 150 fs) and a GaBiAs photoconductive terahertz emitter and detector. The complex effective permittivity was calculated according to the Fresnel equation. All measurements above 1 MHz were performed only at room temperature. The real part of the complex electrical conductivity (σ') was calculated as $\sigma' = \omega\epsilon_0\epsilon''$, where ω is the angular frequency, ϵ_0 is the permittivity of vacuum, and ϵ'' is the imaginary part of the complex effective permittivity.

3 Results and discussion Scanning electron microscopy images of composites filled with various inclusions are presented in Fig. 1. All composites demonstrate good quality, with carbon inclusions being reasonably well dispersed. However, the best dispersion of particles is observed in mixed CNT/OLC composites.

The frequency dependence of the dielectric permittivity and electrical conductivity of mixed composites with 0.5 wt % of CNT and different concentrations of OLC and pure PU (at room temperature) are presented in Fig. 2. The value of the dielectric permittivity of pure PU is very low (about 2), and it is almost frequency-independent for all frequency ranges. At low frequencies, the AC electrical conductivity of pure PU is very low (about 10^{-9} S m^{-1}), and no frequency independent conductivity plateau—typical of DC conductivity—is observed. The dielectric/electric properties of composites filled with 2 wt% of OLC and 0.5 wt% CNT inclusions are similar to pure PU properties; however, the values of dielectric permittivity and electrical conductivity for composites filled with 5 wt% of OLC and 0.5 wt% of CNT are considerably higher (at low frequencies the value of dielectric permittivity is 100× higher, and the value of electrical conductivity is as high as 1 μS m^{-1}) and a frequency-independent DC conductivity plateau is observed in the conductivity spectra. Thus, the percolation threshold in mixed OLC/CNT composites is close to 5 wt% OLC and 0.5 wt% of CNT. In contrast, for the composites with only 5 wt% of OLC $\epsilon' = 16$, $\sigma = 6.5 \times 10^{-9}$ S m^{-1} and for the composites with only 0.5 wt% CNT $\epsilon' = 4.5$, $\sigma = 2.5 \times 10^{-9}$ S m^{-1} at room temperature and a frequency of 129 Hz. Therefore, the synergy effect is clearly observed in the composite containing a mixture of 5 wt% of OLC and 0.5 wt% of CNT. The value of the percolation threshold in

Original
Paper

Phys. Status Solidi B 252, No. 8 (2015)   1801

Figure 2 Room-temperature frequency dependence of dielectric permittivity and electrical conductivity for composites with mixed CNT/OLC inclusions.
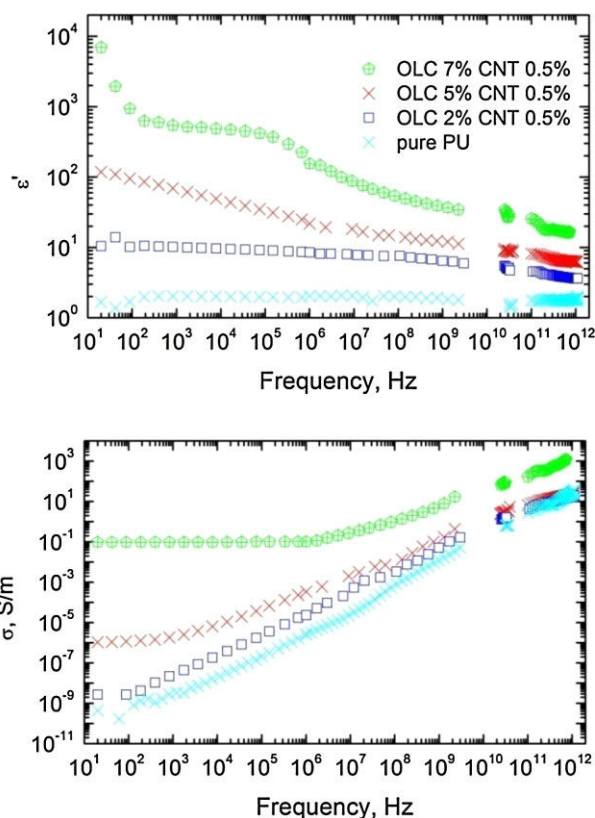

Figure 1 Scanning electron microscopy images of composites filled with 2 wt% of CNT (top), 2 wt% of OLC (middle), and mixed 2 wt% of OLC and 0.5 wt% of CNT (bottom).

PU filled with OLC inclusions was obtained by fitting the concentration dependence of conductivity and dielectric permittivity at the same frequency and at room temperature by the power law (not shown); it is substantially higher (7 wt%).

In composites filled with CNT inclusions, no electrical percolation was observed up to the highest available filler concentration (2 wt%), thus the percolation threshold is substantially higher than 2 wt%. According to the excluded-volume theory, the mixed OLC/CNT composites should obey the following relation [14]:

$$\frac{m_{\mathrm{OLC}}}{P_{\mathrm{c,OLC}}} + \frac{m_{\mathrm{CNT}}}{P_{\mathrm{c,CNT}}} = 1, \tag{1}$$

where m_{OLC} and m_{CNT} are the mass fraction of OLC and CNTs, respectively, and $P_{\mathrm{c,OLC}}$ and $P_{\mathrm{c,CNT}}$ are the mass percolation threshold in composites filled with OLC and CNTs, respectively. The synergy effect is observed in ternary composites where the percolation threshold occurs at the concentrations lower than predicted by Eq. (1) and percolation threshold values of binary composites [14]. In our case, for composites with 5 wt% of OLC and 0.5 wt% inclusions, Eq. (1) transforms into the inequality
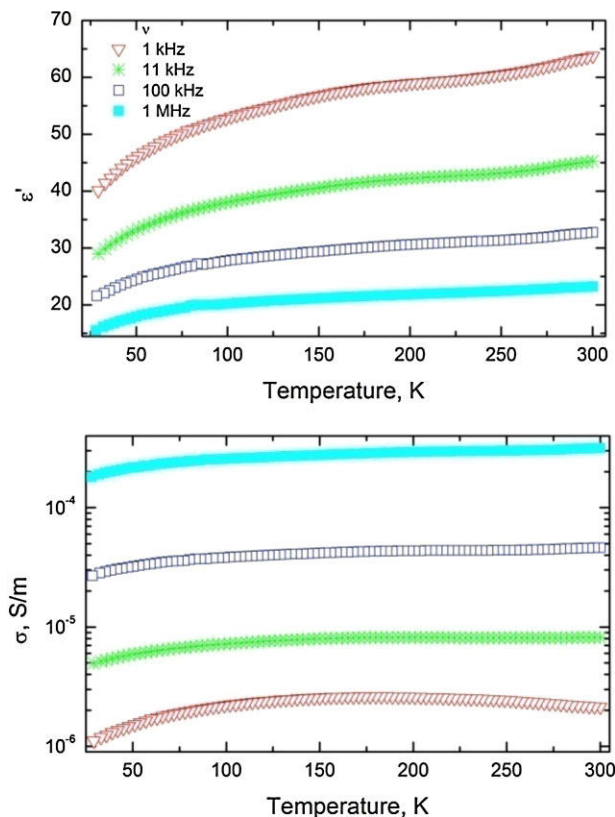
$$\frac{5}{7} + \frac{0.5}{x} < 1,$$

where x is greater than 2. Thus, the percolation threshold in mixed OLC/CNT composites is lower than the value predicted by Eq. (1), and the synergy effect is evident.

At low temperatures, both the dielelectric permittivity and the electrical conductivity decrease in CNT/OLC/PU composites (Fig. 3).
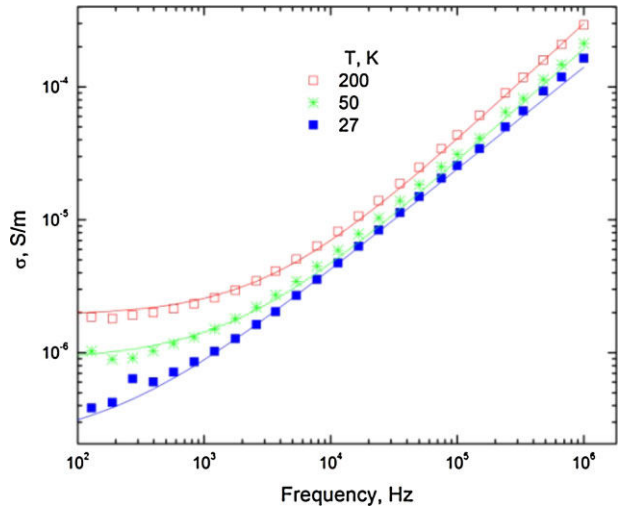
However, the most pronounced reduction occurs at temperatures below 100 K. A similar behavior was observed in other CNT/OLC/PU and OLC/PU composites and is in good agreement with the data presented in the literature for composites with nanocarbon inclusions [15]. For composites with low concentrations of inclusions (although still above the percolation threshold), not only the DC conductivity changes upon cooling, but the shape of the conductivity spectra is also changed (Fig. 3). Therefore, conductivity spectra, $\sigma(\nu)$, were fitted with the Almond–West equation [16]

$$\sigma = \sigma_{DC} + A\omega^s, \qquad (2)$$

where σ_{DC} is the DC conductivity and $A\omega^s$ is the AC conductivity. From this fit (cf. Fig. 4), it is possible to calculate the critical conductivity frequency (ω_{cr}) at which the value of the frequency-independent conductivity becomes higher than the DC conductivity. The critical frequency of composites with 7 wt% of OLC and 0.5 wt% of CNT inclusions is higher than 1 MHz (our upper frequency limit in low-temperature measurements); therefore, the


Figure 4 Frequency dependence of electrical conductivity at different temperatures for composites with 5 wt% of OLC and 0.5 wt% of CNT inclusions.

critical frequency values were calculated only for composites with lower concentrations of inclusions. The obtained parameters are summarized in Fig. 5.

The DC conductivity data fit well to the fluctuation induced tunneling model, as can be seen in Fig. 5 [17]:

$$\sigma_{dc} = \sigma_0 \exp[-(T_1/(T + T_0))], \qquad (3)$$
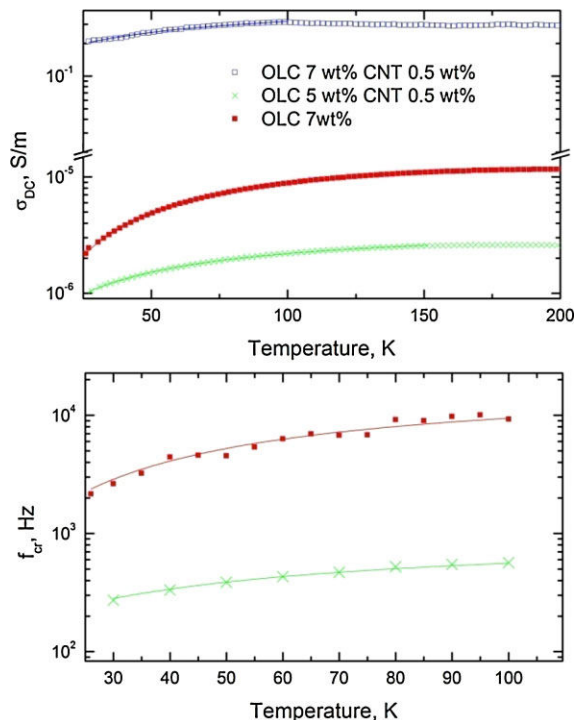
Figure 3 Temperature dependence of dielectric permittivity and electrical conductivity for composites with 5 wt% of OLC and 0.5 wt% of CNT inclusions.

Figure 5 Temperature dependence of DC conductivity and critical frequency of composites with various nanocarbon inclusions.

Phys. Status Solidi B 252, No. 8 (2015)

Original

Paper

1803

Table 1 Tunneling model parameters.

inclusions	T_1 (K)	T_0 (K)	σ_0 (S m^{-1})	$\omega_{cr\infty}$ (kHz)
7 wt% of OLC	88.4	15.2	1.9×10^{-5}	20.13
5 wt% of OLC and 0.5 wt% of CNT	76.7	29.9	3.99×10^{-6}	1
7 wt% of OLC and 0.5 wt% of CNT	63.5	44.7	0.49	–

where T_1 represents the energy required for an electron to cross the insulator gap between the conductive particle aggregates, and T_0 is the temperature above which thermally activated conduction over the barriers begins to occur. The tunneling model is represented by Eqs. (4) and (5) [17]:

$$T_1 = wA\beta_0/8\pi k, \tag{4}$$

$$T_0 = 2T_1/\pi \chi w, \tag{5}$$

where $\chi = (2mV_0)^{0.5}/h$ and $\beta_0 = 4V_0/ew$, m and e are the electron mass and charge, respectively, V_0 is the potential barrier amplitude, w is the interparticle distance (gap width), and A is the area of capacitance formed by the junction. Obtained parameters are listed in Table 1. From Eqs. (4) and (5) it follows that T_1/T_0 is proportional to the gap width w and the potential barrier V_0 amplitude. The best distribution of carbon inclusions is in OLC/CNT mixed composites (Fig. 1); thus, the interparticle distance is lowest in OLC/CNT mixed composites.

The critical frequency (ω_{cr}) is related to DC conductivity according to the Barton–Nakajima–Namikawa relation:

$$\sigma_{dc} = \Delta\epsilon\epsilon_0\omega_{cr}, \tag{6}$$

where $\Delta\epsilon$ is the dielectric strength.

Thus, for the critical frequency, we have assumed similar temperature dependence as for DC conductivity:

$$\omega_{cr} = \omega_{cr\infty}\exp[-(T_1/(T + T_0))]. \tag{7}$$

The best fit was obtained with the same parameters for the critical frequency and DC conductivity (Table 1).

4 Conclusions The dielectric/electric properties of CNT, OLC, and mixed OCL/CNT PU composites are presented across a wide frequency range from hertz to terahertz. The dielectric properties of composites with OLC inclusions are also very attractive and can be improved by addition of small amounts of CNTs due to the strong synergy effect. In composites with mixed OLC/CNT inclusions, the dielectric permittivity and the electrical conductivity increase due to the reduction of the average distance between nanocarbon clusters.

References

[1] F. Qin and C. Brosseau, J. Appl. Phys. **111**, 061301 (2012).
[2] M. J. Jiang, Z. M. Dang, and H. P. Xu, Appl. Phys. Lett. **90**, 042912 (2007).
[3] W. Bauhofer and Z. Kovacs, Compos. Sci. Technol. **69**, 1486 (2009).
[4] L. J. Adriaanse, J. A. Reedijk, P. A. A. Teunissen, H. B. Brom, M. A. J. Michels, and J. C. M. Brokken-Zijp, Phys. Rev. Lett. **78**, 1755 (1997).
[5] V. L. Kuznetsov, Yu. V. Butenko, A. L. Chuvilin, A. I. Romanenko, and A. V. Okotrub, Chem. Phys. Lett. **336**, 397 (2001).
[6] J. Macutkevic, I. Kranauskaite, J. Banys, S. Moseenkov, V. Kuznetsov, and O. Shenderova, J. Appl. Phys. **115**, 213702 (2014).
[7] J. Macutkevic, D. Seliuta, G. Valusis, J. Banys, V. Kuznetsov, S. Moseenkov, and O. Shenderova, Appl. Phys. Lett. **95**, 112901 (2009).
[8] S. Kirkpatrick, Phys. Rev. Lett. **36**, 69 (1976).
[9] J. Macutkevic, D. Seliuta, G. Valusis, J. Banys, S. Hens, V. Borjanovic, V. Kuznetsov, and O. Shenderova, Compos. Sci. Technol. **70**, 2298 (2010).
[10] J. Chen, X. Ch. Du, W. B. Zhang, J. H. Yang, N. Zhang, T. Huang, and Y. Wang, Compos. Sci. Technol. **81**, 1–8 (2013).
[11] J. Sumfleth, X. C. Adroher, and K. Shulte, J. Mater. Sci. **44**, 3241 (2009).
[12] E. Bilotti, H. Zhang, H. Deng, R. Zhang, Q. Fu, and T. Peijs, Compos. Sci. Technol. **74**, 84 (2013).
[13] J. Grigas, Microwave Dielectric Spectroscopy of Ferroelectrics and Related Materials (Gordon and Breach Science Publ., OPA, Amsterdam, 1996).
[14] Y. Sun, H. D. Bao, Z. X. Guo, and J. Yu, Macromolecules **42**, 459 (2009).
[15] H. M. Kim, M. S. Choi, J. Joo, J. J. Cho, and H. S. Yoon, Phys. Rev. B **74**, 054202 (2006).
[16] D. Almond, G. K. Duncan, and A. R. West, Solid State Ionics **8**, 159 (1983).
[17] P. Sheng, E. K. Sichel, and J. I. Gittleman, Phys. Rev. Lett. **40**, 1197 (1978).

IV

Electric/dielectric properties of composites filled with onion-like carbon and multiwalled carbon nanotubes

I.Kranauskaite, J. Banys, E. Talik, V. Kuznetsov, N. Nunn, O. Shenderova

ELECTRIC/DIELECTRIC PROPERTIES OF COMPOSITES FILLED WITH ONION-LIKE CARBON AND MULTIWALLED CARBON NANOTUBES

I. Kranauskaitė [a], J. Banys [a], E. Talik [b], V. Kuznetsov [c], N. Nunn [d], and O. Shenderova [d]

[a] *Vilnius University, Saulėtekio 9, LT-00122 Vilnius, Lithuania*
E-mail: ieva.kranauskaite@ff.vu.lt
[b] *Institute of Physics, University of Silesia, ul. Uniwersytecka 4, PL-40-007 Katowice, Poland*
[c] *Boreskov Institute of Catalysis SB RAS, Lavrentiev Ave. 5, Novosibirsk, 630090, Russia*
[d] *International Technology Center, Raleigh, NC 27715, USA*

The dielectric/electric properties of polyurethane composites filled with carbon nanotubes (CNTs), onion-like carbon (OLC) and mixed onion-like carbon/carbon nanotubes are compared across a wide frequency range from hertz to terahertz. The highest value of dielectric permittivity and electrical conductivity is observed in composites with carbon nanotubes. However, the dielectric/electric properties of composites filled with onion-like carbon are also very attractive and can be improved by addition of small amounts of carbon nanotubes due to the strong synergy effect. In composites with inclusions of mixed onion-like carbon/carbon nanotubes, the dielectric permittivity and electrical conductivity increase due to the decreasing of both the potential barrier for carrier tunneling and the average distance between nanocarbon clusters.

Keywords: carbon nanotubes, onion-like carbon, synergy, composites

PACS: 72.80.Tm, 77.22.Ch, 81.05.ub, 81.07.De

1. Introduction

Nowadays, investigations of electrically percolative polymer-based composites with various nanocarbon inclusions are very popular due to their outstanding electric, electromagnetic, mechanical and thermal properties in comparison with the polymer matrix material [1]. Conductive polymer composites find large-scale applications as antistatic materials, in printed electronics, supercapacitors, organic solar cells, biosensors, flexible transparent displays, etc. [2]. In spite of some practical limitations due to their limited processability and their manufacturing cost, DC and AC conductive composites are rapidly gaining attention in new applications such as packaging for electronics and chemical industry, metal replacement, heating elements and fuel cells, for electromagnetic shielding and for radar wave absorbing applications in wide frequency ranges [3]. The major field of applications for electrically conductive composites depends on the magnitude of their volume electrical resistivity. For antistatic applications the range should be at the level of 10^9–10^{14} Ωcm, whereas for electrostatic dissipation applications the range is expected to be 10^5–10^9 Ωcm.

Many investigations of such composites were performed within a narrow frequency range and at room temperature in order to find the percolation threshold (the minimum concentration of nanofillers at which composites are conductive) [4]. An important task is to obtain a low percolation threshold to preserve (or reach) optimal mechanical properties of polymers and to use a minimal concentration of expensive fillers. The lowest percolation threshold was observed in carbon nanotube (CNT) composites due to their high aspect ratios [5]. However, CNTs usually exhibit large agglomerates within the polymer matrix because of the high van der Waals force between CNTs, and this leads to an increase of the percolation threshold. Therefore, the percolation threshold in the same polymer matrix and for the same CNTs can vary significantly [6]. Moreover, the percolation threshold in other composites, for example, in carbon black (CB) composites, can also be very low [7]. Thus, investigations of composites with other less expensive inclusions are very promising.

Onion-like carbon (OLC), consisting of stable defected multishell fullerenes, exhibits high conductivity similar to CNTs [8]. The percolation threshold in OLC composites is strictly dependent on the aggregate

size, and it is lowest for composites with the smallest aggregate size [9]. Particularly, in OLC/polyurethane composites with an average aggregate size of ~120 nm, the percolation threshold is 10 vol% [10]. Thus, the percolation threshold in OLC composites is lower than predicted by Monte-Carlo calculations ~31.2 vol% [11] and can be lowered with optimal composite preparation procedures [12]. Moreover, the dielectric permittivity of OLC based composites is very high (more than 10^6 at low frequencies), and these composites are very attractive for various applications [10]. However, the percolation threshold in OLC based composites is still much higher in comparison with CNT composites.

Multiphase composites with several different fillers in the matrix are very interesting in order to find the so-called synergy effect [13]. Often, the distribution of different fillers within the polymer matrix can be favourable, and electrical transport can occur in different filler network together. When this occurs, the percolation threshold can decrease dramatically [13]. Many investigations of synergy effects were performed in CNT/CB composites, and a significant decrease in the percolation threshold, in comparison with CB composites, was observed [13–15]. Usually, this synergistic effect was investigated only at room temperature.

In this paper we compare the broadband dielectric/electric properties of composites filled with 12 wt% of CNT, OLC and mixed CNT/OLC composites at temperatures starting from room temperature down to 26 K. It was demonstrated that the dielectric and electric properties with OLC inclusions can be substantially improved with the addition of CNT.

2. Experiment

Polyurethane films with nanoadditives were prepared using Clear Gloss MINWAX® Fast-Drying Polyurethane. Nanoadditives included multi-walled CNT (20 nm diameter, 5–10 micrometre length) purchased from *Amorphous Carbon Materials, Inc.* and OLC delivered vacuum anealing of detonation nanodiamonds (DND) [8–10]. Aggregates of DNDs consisting of 5 nm primary particles were heated in vacuum (10^{-4} Torr) at 1650 °C for 3 h providing aggregates of OLC with aggregate sizes corresponding to the sizes of the starting DND fractions (approximately 100 nm). Stock suspensions of nanoadditives (~0.5–1.0% w/v) were prepared in an alcohol solvent and sonicated with a horn-based sonicator for 5 minutes. 7 g of polyurethane (PU) were measured out and added to a hot-plate at 120 °C with magnetic stirring. The alcohol based suspension containing the desired amount and type nanoadditive was then added to the polyurethane. The PU had a volatile mass of 50%, so 7 g of starting PU provided 3.5 g of solid upon cur-

ing; thus, the amount of the alcohol-nanoadditive suspension that was added corresponded to the desired amount of nanoadditve. After the alcohol suspension was combined with the PU, the alcohol was evaporated from the PU-nanoadditive mixture. The samples were then cast on a teflon substrate and cured at 40 °C. After curing, the samples were annealed at 180 °C for 0.5 h in order to obtain better homogeneity. In this paper, composites containing 12 wt% inclusions of CNT, OLC and mixed CNT/OLC (30–70% by wt.) were investigated.

The microstructural observations of the composites were conducted using the JEOL-7600F scanning electron microscope.

Complex dielectric permittivity was measured as a function of frequency and temperature using an HP4284A precision *LCR* meter in the frequency range 20 Hz – 1 MHz. For the low temperature measurements, a helium closed cycle cryostat was used. In the frequency range 1 MHz–3 GHz, dielectric measurements were performed using a vector network analyzer (*Agilent 8714ET*). In the microwave frequency range from 8 to 53 GHz, a home-made waveguide spectrometer was used. The method of a thin rod in the waveguide was used [19]. Cylindrically shaped samples where used for these measurements. Dimensions of the samples were with different radius: in 20 Hz – 1 MHz frequency range, the radius of samples was about 3 mm, in the 1 MHz – 3 GHz frequency range it was about 0.5 mm, while in the 8–53 GHz frequency range the radius was about 0.1 mm.

In the frequency range from 1 MHz to 53 GHz, the measurement accuracy was ~10%. Silver paste was used for creating the contacts. In the terahertz frequency range (from 100 GHz to 3 THz), a terahertz time domain spectrometer (*Ekspla Ltd*) based on a femtosecond laser was used for the measurements. The spectrometer is based on the femtosecond laser fiber (wavelength 1 μm, pulse duration less than 150 fs) and the GaBiAs photoconductive terahertz emitter and detector. The complex effective permittivity was calculated according to the Fresnel equation. For terahertz measurements plate-like thin samples were used (thickness about 0.5 mm). All measurements above 1 MHz were performed only at room temperature. The real part of the complex electrical conductivity was calculated as $\sigma' = \omega \varepsilon_0 \varepsilon''$, where ω is the angular frequency, ε_0 is the permittivity of vacuum, and ε'' is the imaginary part of complex effective permittivity.

3. Results and discussion

The scanning electron microscopy images of the composites filled with OLC, CNT and OLC/CNT inclusions are presented in Fig. 1. The dispersion of
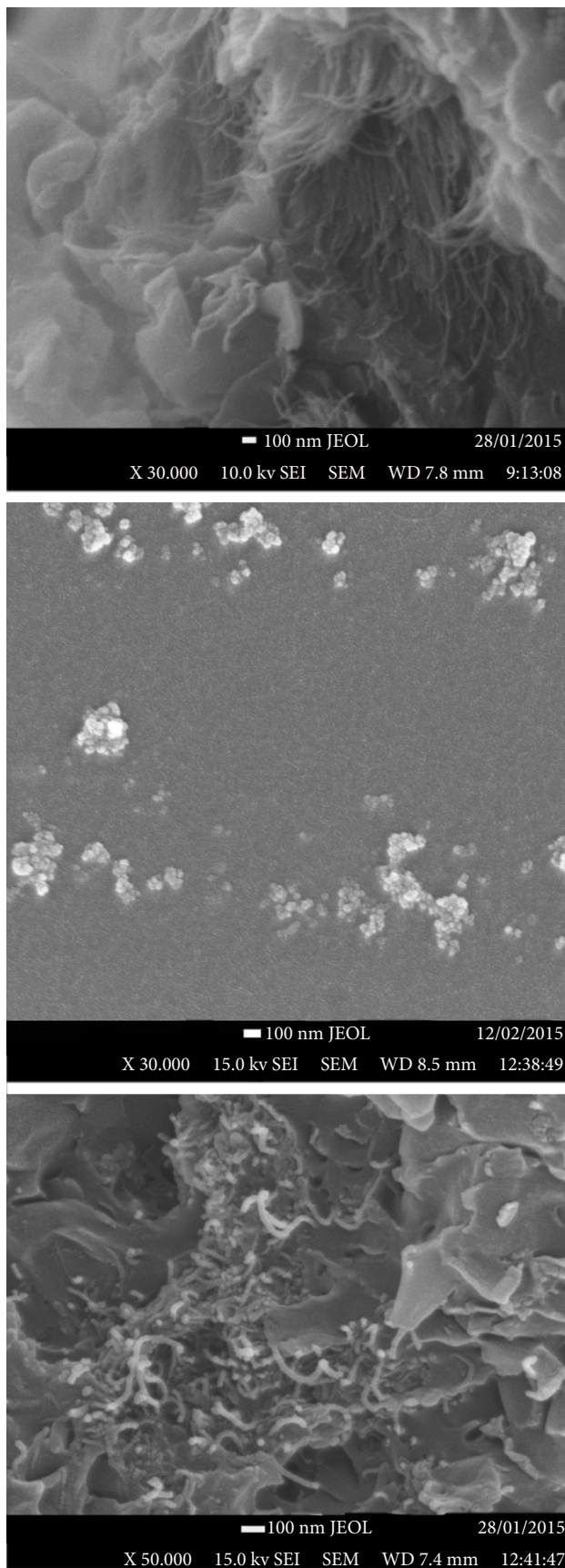
Fig. 1. Scanning electron microscopy image of composites with CNT (top), OLC (middle) and mixed CNT/OLC (bottom).

nano-inclusions in all composites is good enough, however, the best dispersion of nanoparticles is in the mixed OCL/CNT composites.

Frequency dependences of dielectric permittivity and electrical conductivity of all investigated composites and pure polyurethane are presented in Fig. 2.
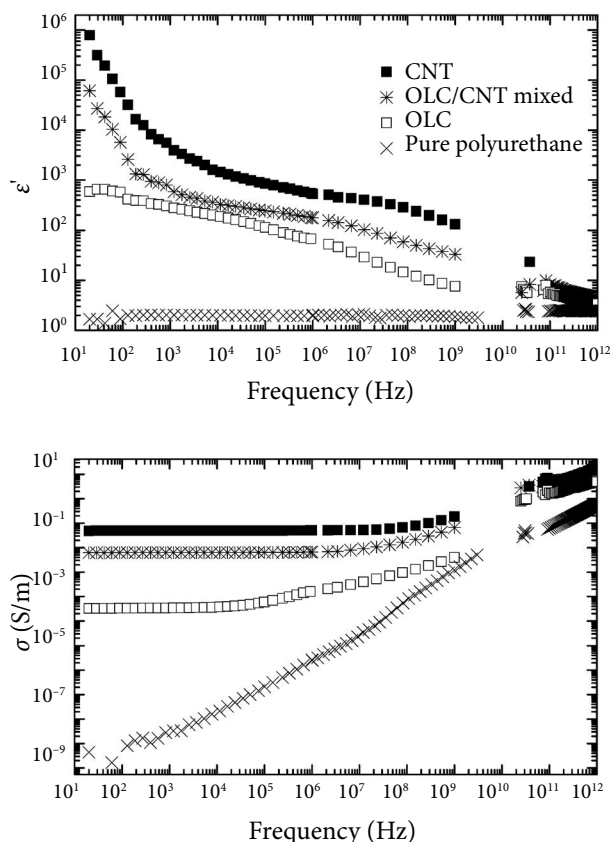

Fig. 2. Frequency dependence of dielectric permittivity and electrical conductivity for composites with various nanocarbon inclusions at room temperature.

The value of the dielectric permittivity of pure polyurethane is very low (about 2), and it is almost frequency independent for all frequency ranges. At low frequencies, the AC electrical conductivity of pure polyurethane is very low (about 10^{-9} S/m), and no frequency independent conductivity plateau – typical for DC conductivity – is observed. In all composites (with OLC, CNT and CNT/OLC inclusions) the dielectric permittivity is very high (at low frequencies, its value is higher than several hundred). Moreover, at low frequencies the highest value of dielectric permittivity is observed in the CNT based composites ($>10^5$). At low frequencies, all composites display a frequency independent conductivity plateau; thus, all composites are above the percolation threshold. Nevertheless, we can expect that the lowest percolation threshold value is in the composites with CNT, while the highest value is

in the composites with OLC inclusions because both the dielectric permittivity and electrical conductivity increase above the percolation threshold in the power law fashion [2]. So, the synergy effect is evident in the system. Thus, even a small part of CNT (30%) in the mixed OLC/CNT composites can substantially increase the value of the dielectric permittivity and electrical conductivity. For the composites with CNT and OLC/CNT inclusions a frequency independent plateau of dielectric permittivity in the frequency range 1 kHz – 1 MHz separates two different dispersions related with the Maxwell–Garnett relaxation (Fig. 2).

At low temperatures, both the dielelectric permittivity and the electrical conductivity decrease in the OLC/PU composites (Fig. 3).
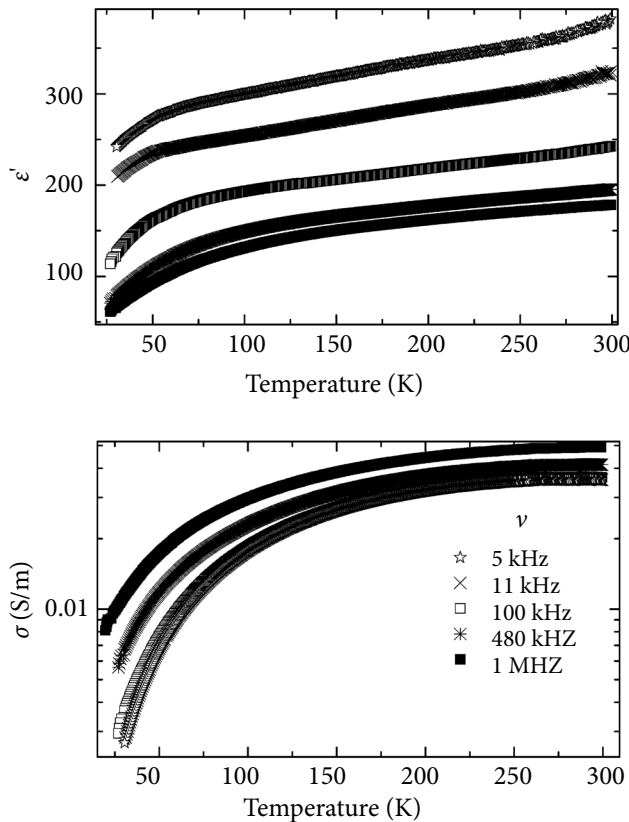

Fig. 3. Temperature dependence of dielectric permittivity and electrical conductivity for composites with OLC inclusions.

However, the most pronounced reduction occurs at temperatures below 100 K. A similar behaviour was observed in the CNT/PU and mixed CNT/OLC/PU composites and is in good agreement with the data presented in literature for composites with nanocarbon inclusions [17, 18]. For the composites with OLC inclusions, not only the DC conductivity changes upon cooling, but the shape of the conductivity spectra is also

changed (Fig. 4). Therefore, the conductivity spectra, $\sigma(v)$, were fitted with the Almond-West equation [18]:

$$\sigma = \sigma_{DC} + A\omega^s, \tag{1}$$

where σ_{DC} is the DC conductivity and $A\omega^s$ is the AC conductivity. From this fit, it is possible to calculate the critical conductivity frequency (ω_{cr}) at which the value of frequency dependent conductivity becomes higher than DC conductivity. Experimentally, the value for ω_{cr} has been defined as the frequency at which the value of conductivity is 10% higher than the DC conductivity value.

The critical frequency of the composites with CNT and CNT/OLC inclusions is higher than 1 MHz (Fig. 4) (our upper frequency limit in low temperature measurements); therefore, the critical frequency values were calculated only for the composites with OLC inclusions.
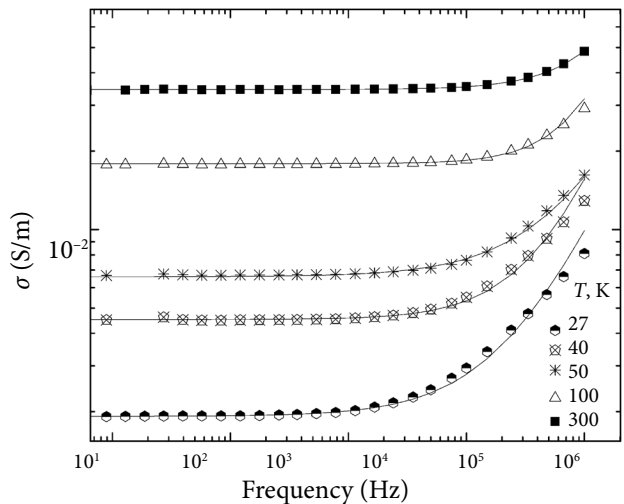

Fig. 4. Frequency dependence of electrical conductivity at different temperatures for composites with OLC inclusions.

The DC conductivity data fit well to the fluctuation induced tunneling model, as can be seen in Fig. 5 [19]:

$$\sigma_{dc} = \sigma_0 \exp[-[T_1/k(T+T_0)]], \tag{2}$$

where T_1 represents the energy required for an electron to cross the insulator gap between the conductive particle aggregates, and T_0 is the temperature above which thermally activated conduction over the barriers begins to occur. The tunneling model is represented by Eqs. (3) and (4) [19]:

$$T_1 = wA\beta_0/8\pi k, \tag{3}$$

$$T_0 = 2T_1/\pi\chi w, \tag{4}$$

where $\chi = (2\,mV_0)^{0.5}/h$ and $\beta_0 = 4\,V_0/ew$, m and e are the electron mass and charge, respectively, V_0 is the potential barrier height, w is the interparticle distance (gap width), and A is the area of capacitance formed by the junction. The obtained parameters are listed in Table 1. From Eqs. (3) and (4) it follows that T_1/T_0 is proportional to the gap width w and the potential barrier V_0. Thus, they both decrease in the composites filled with mixed CNT/OLC inclusions. The critical frequency (ω_{cr}) is related with DC conductivity according to the Barton–Nakajima–Namikawa relation:

$$\sigma_{DC} = \Delta\varepsilon\varepsilon_0\omega_{cr}, \tag{5}$$

where $\Delta\varepsilon$ is the dielectric strength and ε_0 is the dielectric permittivity of vacuum.

Table 1. Tunneling model fit parameters.

	$\ln\{\sigma_0,\text{S/m}\}$	T_1, K	T_0, K
OLC, 12 wt%	−2.8	134	12
OLC/CNT, 12 wt%	−2.5	92.9	37
CNT, 12 wt%	−0.6	33.2	32.8

Thus, for the critical frequency, we have assumed similar temperature dependence as for DC conductivity:

$$\omega_{cr} = \omega_{cr\infty}\exp[-[T_1/(T+T_0)]]. \tag{6}$$
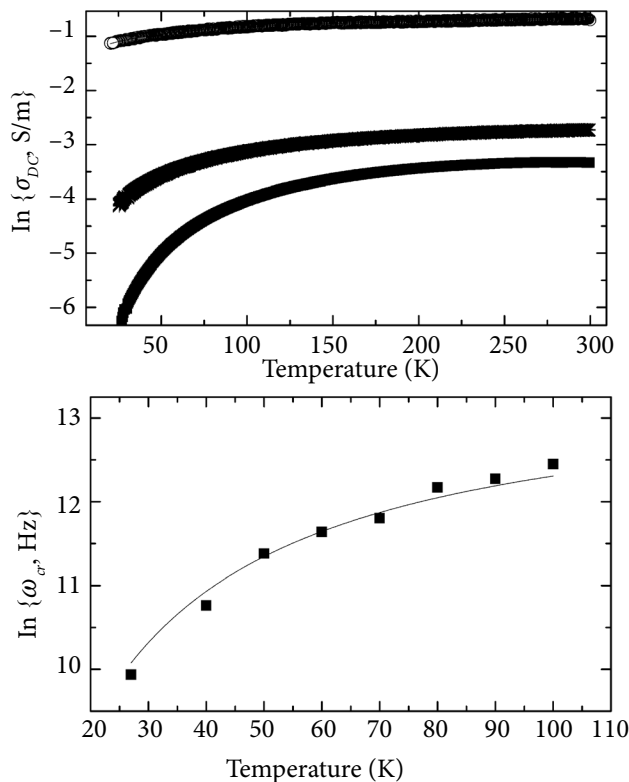

Fig. 5. Temperature dependence of DC conductivity of composites with various nanocarbon inclusions.

For the composites with OLC inclusions, the best fit was obtained with the same values of parameters T_1 and T_0 as for DC conductivity and $\omega_{cr\infty} = 729$ kHz (Fig. 5).

4. Conclusions

The dielectric/electric properties of carbon nanotube (CNT), onion-like carbon (OLC), and mixed onion-like carbon/carbon nanotube (OLC/CNT) polyurethane composites are presented across a wide frequency range from hertz to terahertz. Although the highest dielectric permittivity value is observed in the composites with CNT inclusions, the dielectric properties of composites with OLC inclusions are also very attractive and can be improved by addition of small amounts of CNTs due to the strong synergy effect. In the composites with mixed OLC/CNT inclusions, the dielectric permittivity and electrical conductivity increase due to the reduction of both the potential barrier for carrier tunneling and the average distance between nanocarbon clusters.

Acknowledgements

References

[1] F. Qin and C. Brosseau, A review and analysis of microwave absorption in polymer composites filled with carbonaceous particles, J. Appl. Phys. **111**, 061301 (2012).

[2] G. Inzelt, *Conducting Polymers: A New Era in Electrochemistry* (Springer, Berlin, 2008).

[3] K.J. Vinoy and R.M. Jha, *Radar Absorbing Materials from Theory to Design and Characterization* (Kluwer Academic Publishers, Boston, 1996).

[4] M.J. Jiang, Z.M. Dang, and H.P. Xu, Giant dielectric constant and resistance-pressure sensitivity in carbon nanotubes/rubber nanocomposites with low percolation threshold, Appl. Phys. Lett. **90**, 042912 (2007).

[5] W. Bauhofer and Z. Kovacs, A review and analysis of electrical percolation in carbon nanotube polymer composites, Compos. Sci. Technol. **69**, 1486 (2009).

[6] L.J. Adriaanse, J.A. Reedijk, P.A.A. Teunissen, H.B. Brom, M.A.J. Michels, and J.C.M. Brokken-Zijp, High-dilution carbon-black/polymer composites: Hierarchical percolating network derived from Hz to THz ac conductivity, Phys. Rev. Lett. **78**, 1755 (1997).

[7] V.L. Kuznetsov, Yu.V. Butenko, A.L. Chuvilin, A.I. Romanenko, and A.V. Okotrub, Electrical

resistivity of graphitized ultra-disperse diamond and onion-like carbon, Chem. Phys. Lett. **336**, 5–6 (2001).

[8] J. Macutkevic, I. Kranauskaite, J. Banys, S. Moseenkov, V. Kuznetsov, and O. Shenderova, Metal-insulator transition and size dependent electrical percolation in onion-like carbon/polydimethyl-siloxane composites, J. Appl. Phys. **115**, 213702 (2014).

[9] J. Macutkevic, D. Seliuta, G. Valusis, J. Banys, V. Kuznetsov, S. Moseenkov, and O. Shenderova, High dielectric permittivity of percolative composites based on onion-like carbon, Appl. Phys. Lett. **95**, 112901 (2009).

[10] S. Kirkpatrick, Percolation phenomena in higher dimensions: Approach to the mean-field limit, Phys. Rev. Lett. **36**, 69 (1976).

[11] J. Macutkevic, D. Seliuta, G. Valusis, J. Banys, S. Hens, V. Borjanovic, V. Kuznetsov, and O. Shenderova, Effect of thermal treatment conditions on the properties of onion-like carbon based polymer composite, Compos. Sci. Technol. **70**, 2298 (2010).

[12] J. Chen, X. Ch. Du, W.B. Zhang, J.H. Yang, N. Zhang, T. Huang and Y. Wang, Synergistic effect of carbon nanotubes and carbon black on electrical conductivity of PA6/ABS blend, Compos. Sci. Technol. **81**, 1–8 (2013).

[13] E. Bilotti, H. Zhang, H. Deng, R. Zhang, Q. Fu, and T. Peijs, Controlling the dynamic percolation of carbon nanotube based conductive polymer composites by addition of secondary nanofillers: The effect on electrical conductivity and tuneable sensing behaviour, Compos. Sci. Technol. **74**, 84 (2013).

[14] J. Sumfleth, X.C. Adroher, and K. Shulte, Synergistic effects in network formation and electrical properties of hybrid epoxy nanocomposites containing multi-wall carbon nanotubes and carbon black, J. Mater. Sci. **44**, 3241 (2009).

[15] J. Grigas, *Microwave Dielectric Spectroscopy of Ferroelectrics and Related Materials* (Gordon and Breach Science Publishers, Amsterdam, 1996).

[16] H.M. Kim, M.S. Choi, J. Joo, J.J. Cho, and H.S. Yoon, Complexity in charge transport for multiwalled carbon nanotube and poly(methyl methacrylate) composites, Phys. Rev. B **74**, 054202 (2006).

[17] J. Macutkevic, R. Adomavicius, A. Krotkus, J. Banys, V. Kuznetsov, S. Moseenkov, A. Romanenko, and O. Shenderova, Localization and electrical transport in onion-like carbon based composites, J. Appl. Phys. **111**, 103701 (2012).

[18] D. Almond, G.K. Duncan, and A.R. West, The determination of hopping rates and carrier concentrations in ionic conductors by a new analysis of ac conductivity, Solid State Ionics **8**, 159 (1983).

[19] P. Sheng, E.K. Sichel, and J.I. Gittleman, Fluctuation-included tunneling conduction in carbon-polyvinylchloride composites, Phys. Rev. Lett. **40**, 1197 (1978).

KOMPOZITŲ SU SVOGŪNINĖS ANGLIES IR DAUGIASIENIŲ ANGLIES NANOVAMZDELIŲ UŽPILDU ELEKTRINĖS IR DIELEKTRINĖS SAVYBĖS

I. Kranauskaitė [a], J. Banys [a], E. Talik [b], V. Kuznetsov [c], N. Nunn [d], O. Shenderova [d]

[a] *Vilniaus universitetas, Vilnius, Lietuva*
[b] *Silezijos universiteto Fizikos institutas, Katovicai, Lenkija*
[c] *Rusijos MA Sibiro skyriaus Boreskovo katalizės institutas, Novosibirskas, Rusija*
[d] *Tarptautinis technologijos centras, Rolis, Šiaurės Karolina, JAV*

Santrauka

Straipsnyje aptariamos kompozitų su anglies nanovamzdelių, svogūninės anglies, mišriu nanovamzdelių ir svogūninės anglies užpildu plačiame dažnių diapazone elektrinės bei dielektrinės savybės.

Kompozituose su anglies nanovamzdeliais yra stebimos didesnės dielektrinės skvarbos ir laidumo vertės nei kompozituose su svogūninės anglies užpildu. Kompozitų su svogūninės anglies užpildu elektrinės savybės gali būti pagerintos įterpiant nedidelį kiekį anglies nanovamzdelių. Mišriuose kompozituose dėl sumažėjusio atstumo tarp anglies intarpų mažėja potencinis barjeras elektronams tuneliuoti, todėl padidėja kompozitų dielektrinė skvarba ir elektrinis laidumas.

V

Length-dependent broadband electricproperties of PMMA composites filledwith carbon nanotubes

I.Kranauskaite, J. Macutkevic, J. Banys, V. Kuznetsov, S. Moseenkov, N. Rudyna, D. Krasnikov

Length-dependent broadband electric properties of PMMA composites filled with carbon nanotubes

Ieva Kranauskaite[1], Jan Macutkevic*,[1], Juras Banys[1], Vladimir L. Kuznetsov[2,3,4], Sergey I. Moseenkov[2], Nina A. Rudyna[2], and Dmitriy V. Krasnikov[2,3]

[1] Vilnius University, Sauletekio ave. 9, 10222 Vilnius, Lithuania
[2] Boreskov Institute of Catalysis SB RAS, Lavrentieva ave. 5, Novosibirsk, Russia
[3] Novosibirsk State University, Pirogova str. 2, Novosibirsk, Russia
[4] Tomsk State University, Tomsk, Lenina Avenue 36, 634050 Tomsk Oblast, Russia

* Corresponding author: e-mail jan.macutkevic@gmail.com, Phone: +37052366077, Fax: +37052366003

Broadband dielectric/electric properties of multiwalled carbon nanotubes (MWCNT) polymethylmetacrylate composites were studied in a wide temperature range (25–400 K). It was established that the percolation threshold is lower in composites with the shortest MWCNT, due to the better distribution of the MWCNT in the polymer matrix. The value of the dielectric permittivity and the electrical conductivity below the percolation threshold is also higher in composites with the shortest MWCNT. Below the percolation threshold the dielectric dispersion in composites is mainly related with the β relaxation in the polymer matrix. The length of the MWCNT and its concentration have also the huge influence on polymer matrix molecular dynamics, the relaxation time is shortest in composites with the higher MWCNT concentration and in composites with the shortest MWCNT. At low temperatures the conductivity of composites above the percolation threshold is governed by an electron tunneling between MWCNT clusters. At higher temperatures the electrical transport occurs also due to the finite electrical conductivity of the polymer matrix.

1 Introduction Carbon nanotube (CNT) is a very popular object for investigations and various applications, due to their high aspect ratio, the high electrical conductivity and the excellent thermal and mechanical properties [1–3]. Moreover, the properties of the CNT can be easy controlled. For example, it was demonstrated that the absorbtion peak position of single wall carbon nanotubes films is length-dependent [4]. Polymer composites reinforced with nano-carbon inclusions are very popular in various applications, such as aviation, protective coatings, synthetic metals, solar cells, and others [5–7]. The percolation threshold of composites filled with the CNT can be extremely low [8]. Depending from the CNT concentration and the type the values of the dielectric permittivity, the electrical conductivity and the loss tangent of the composites filled with the CNT can be very different, that is very important for composite applications, for example, as electromagnetic shielding or dissipation coatings [9]. Nevertheless, the most

investigations of composites filled with the CNT are performed only at room temperature and in some narrow frequency range [10].

Close to the percolation threshold the dielectric permittivity and the electrical conductivity of the CNT based composites increases with the concentration in a power law fashion [11]. However, this law does not take into account the influence of the CNT length and the diameter on composite dielectric/electric properties. According to the excluded volume theory the percolation threshold is inversely proportional to the CNT aspect ratio [12]. Although, such a relation is claimed in the review papers [13, 14], however, experimentally, it was very often observed that the percolation threshold is substantially higher or sometimes even lower than the reciprocal aspect ratio, mainly due to the fact that the dielectric properties of composites are strongly dependent from the composite preparation technology and various additional CNT

parameters, such as the CNT waviness, which are different in different works [13–16]. Moreover, recent investigations of composites filled with the commercially available CNT of the different aspect ratio did not demonstrate any clear impact of the CNT aspect ratio on the percolation threshold [17]. This is also particularly due to the fact that the commercially available CNT often have a broad distribution of lengths and diameters [16–18]. A simple way to overcome the influence of the composite preparation technology and hardly controlled CNT parameters is to reduce the CNT length in the part of nanotubes and to compare dielectric properties of composites filled with the reduced length CNT and the primary CNT [19]. However, in the work of Russ et al. [19], only the dc conductivity of composites filled with two different length nanotubes were compared. So, that the impact of the CNT aspect ratio on composite broadband dielectric properties is still unclear.

Moreover, it was clearly demonstrated that the distribution of CNT is crucial for the electrical properties of the composites [14]. The distribution of CNT in the polymer matrix can be changed by the thermal annealing above the glass transition temperature [20], by the shear force [21], by the composite preparation technology [22], and others [14]. Naturally, that additionally the distribution of the CNT in the matrix could be dependent from their aspect ratio.

Therefore, it very important to study the composites produced under the same preparation conditions with the difference only in the nanotubes length. Our paper is exactly focused on the study of such samples. The aim of this paper is to investigate the influence of the carbon nanotubes length on composite broadband (20 Hz–3 THz) dielectric/electric properties in a wide temperature range.

2 Experimental All of nanotubes used were synthesized by CVD technique (670 °C, Ar/C_2H_4 1:1, 400 sccm) with $Fe–Co/Al_2O_3$ catalyst [23]. This catalyst possesses the high activity ($>120 \, g_{MWCNT}/g_{cat}h$) and provides MWCNT of a high purity (no amorphous carbon) and a narrow diameter distribution ($d_{mean} = 9 \, nm$). Traces of the catalyst were removed by refluxing with HCl (1:1) for 6 h with subsequent rinsing with distilled water and drying at 60 °C. Oxidized MWCNTs were produced by refluxing with nitric acid (conc.) for 2 h with subsequent rinsing with distilled water and drying at 60 °C. This procedure provides formation of 1.5-2 oxygen-containing groups on the MWCNT surface [19]. To obtain the MWCNT of a small length, carbon nanotubes were subjected to mechanical activation in a high-power planetary ball mill APF (the acceleration of the balls was $200 \, m \, s^{-2}$, the ball/powder weight ratio was 900:10 and 900:20, the ball diameter – 5 mm, the milling time was of 2 min; mill was designed by ISSC SB RAS (Russia). Thereby, there were four forms of the MWCNTs:

(i) the MWCNT which were only refluxed with HCl (the mean length $\sim$50 μm (according to TEM statistics) – the "long" MWCNT. These nanotubes in majority consist of a tangle agglomerate (the nanotubes length 20–50 μm),

(ii) the MWCNT which were refluxed with HCl and then grinded in the APF mill with the ball/powder weight ratio of 900:10 (the mean length $328 \pm 20 \, nm$) –the "short" MWCNT,

(iii) the MWCNT which were refluxed with HCl and then grinded in the APF mill with the ball/powder weight ratio of 900:20 (the mean length $438 \pm 20 \, nm$) –the "medium" MWCNT, and

(iv) the MWCNT which were refluxed with HCl, oxidized with HNO_3 and then grinded in the APF mill with the ball/powder ratio of 900:20 (the mean length $335 \pm 20 \, nm$) –the "OX-short" MWCNT.

PMMA/MWCNT composites were produced via the coagulation precipitation technique [23]. PMMA (MW = 1 20 000, Sigma–Aldrich) solution in N-methylpyrrolidone (NMP) was ultrasonicated with the MWCNT hinge. The dispersion produced was then introduced to an excessive amount of water (1.5 L, 318 K). Due to the immediate dissolution of NMP in water, the precipitation of the PMMA/MWCNT composites results in spongy species with gray/black color (depending on the MWCNT loading). Composites then were filtered, washed from NMP residuals, and dried in the air at 333 K. The composite powder was hot pressed at 453 K with subsequent cooling into the press for 30 min ($T\sim$313–323 K). The films with the thickness of 0.4–0.5 mm and different MWNCT content (0.25, 0.5, 1.0, 2.0, 4.0 wt.%) were obtained for the following microscopy and the broadband dielectric spectroscopy studies. JSM6460LV and JEM-2010 were employed for scanning and transmission electron microscopy studies, correspondingly. For SEM analysis composite films were broken at 77 K in order to decrease the PMMA elasticity. In order to avoid charging effects, composites were gold coated with the layer thickness of 6–8 nm. For TEM analysis powder samples were deposited on the copper grid from the ethanol suspension employing the ultrasonicator. The complex dielectric permittivity $\varepsilon^* = \varepsilon' - i\varepsilon''$ was measured by a LCR meter HP4284A in the frequency range 20 Hz–1 MHz. Each measurement started by heating the samples from the room temperature up to 450 K, then cooling was performed down to the room temperature. Low-temperature measurements were carried out by cooling in the closed-cycle helium cryostat. In the frequency region from 1 MHz to 3 GHz, measurements were performed by a coaxial dielectric spectrometer with a vector network analyzer Agilent 8714ET. Microwave measurements were carried out with a scalar network analyzer R2-408R (ELMIKA, Vilnius, Lithuania). In the frequency range from 100 GHz to 3 THz, measurements were performed by time domain terahertz spectrometer (EKSPLA, Vilnius Lithunia) based on the femtosecond laser (the wavelength 1 μm, the pulse duration less than 150 fs) and GaBiAs photoconductive switch as THz emitter and detector.

Phys. Status Solidi A 213, No. 4 (2016)

Original

Paper

1027

3 Results and discussion

3.1 Composite structure The interaction of the polymer matrix with the nanotube surface and the nanotube distribution in the PMMA/MWCNT composite were characterized with TEM and SEM.

TEM study of the composite powders produced with of "long" MWCNT before hot pressing demonstrates non uniform distribution of PMMA on nanotube surface. Polymer nanotubes are not fully covered with the polymer as it was previously mentioned in Ref. [23].

Both covered and "naked" nanotube surface areas are observed. The diffusion of polymer species inside the nanotube tangle is also limited. MWCNT agglomerates of several microns in size, which were not disintegrated by ultrasonication, and areas of the nanotube surface without any polymer species were observed (Fig. 1A and B). Melting of the PMMA/MWCNT powder allows the polymer molecules penetrate inside the MWCNT aggregates. Nevertheless, a non-uniform distribution of MWCNT was obtained. Thus, SEM study of composite breaks demonstrates areas of high and almost negligible concentration of the nanotubes (Fig. 2B, marked with dotted lines).

On the contrary, PMMA/"short" MWCNT and PMMA "OX-short" composites do not contain any considerable agglomerates of the nanotubes (Fig. 1C–F) and demonstrate the uniform wetting of the nanotube surface with the polymer. The almost homogeneous distribution of the nanotubes in the PMMA matrix was observed (Fig. 2A).
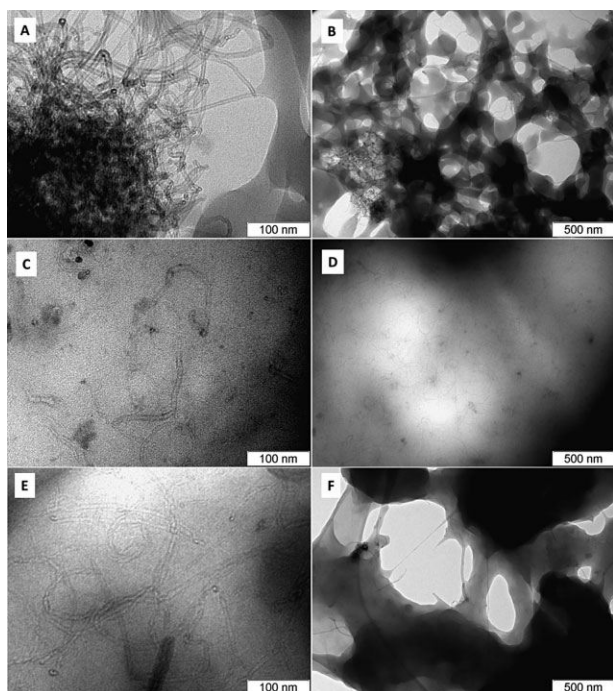
Figure 1 TEM images of composite powders: (A) and (B) "long" MWCNT/PMMA 1.0%, (C) and (D) "short" MWCNT/PMMA 1.0%, (E) and (F) "OX-short" MWCNT/PMMA 1.0%.
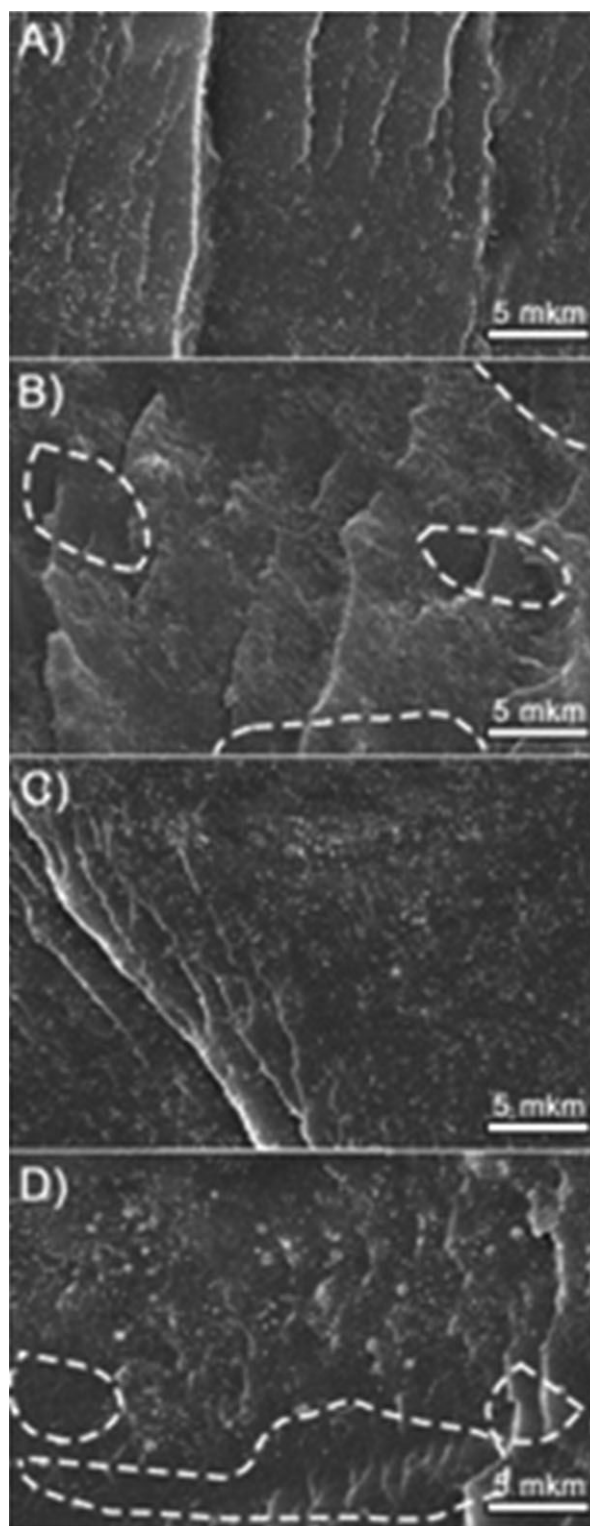
Figure 2 SEM images of the composite film breaks obtained after cracking at liquid nitrogen temperature. Brigth fragments (dots or villus are attributed to nanotubes): (A) "short" MWCNT/PMMA 2.0%, (B) "long" MWCNT/PMMA 2.0%, (C) "OX-short" MWCNT/PMMA 2.0%, (D) "medium" MWCNT/PMMA 2%. Dotted lines demonstrate the regions with the negligible concentration of the nanotubes.

Composites with "medium" MWCNT inclusions demonstrate the intermediate nanotubes distribution in polymer. On the one hand, any big agglomerate structures were observed. On the other hand, areas with the almost negligible concentration of nanotubes were observed in the composite breaks (Fig. 2D, marked with dotted lines).
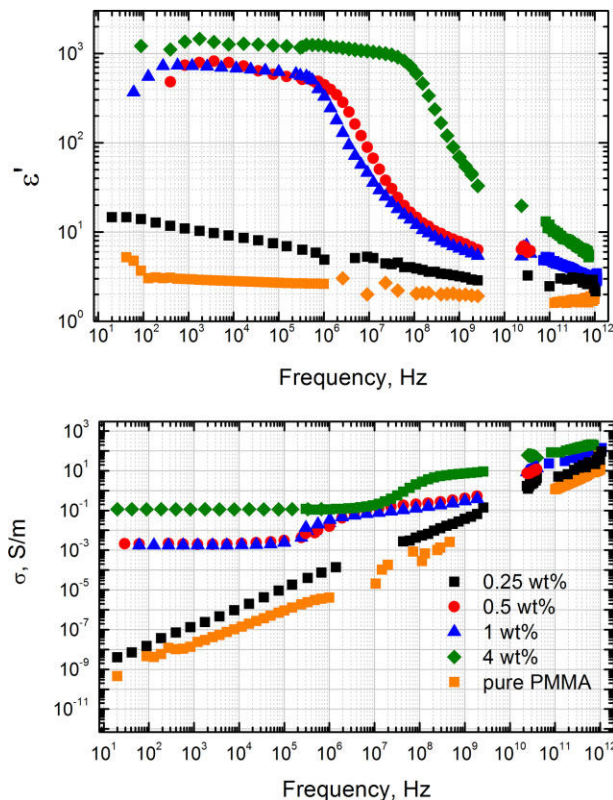
3.2 Room temperature properties The frequency dependence of the real parts of the complex dielectric permittivity and the complex electrical conductivity with different concentrations of "short" MWCNT at room temperature is presented in Fig. 3. The values of the dielectric permittivity and the electrical conductivity of composites with 0.25 wt.% inclusions are quite low and are similar to the pure polymer matrix properties. In contrast, at higher MWCNT concentrations the value of the dielectric permittivity is high enough (higher as 10^3 for composite with 4 wt.% inclusions) and the frequency independent conductivity plateau is observed in the frequency dependence of the electrical conductivity.

Thus in composites with "short" MWCNT the percolation threshold is close to 0.5 wt.%. In all other studied composites at different MWCNT concentrations th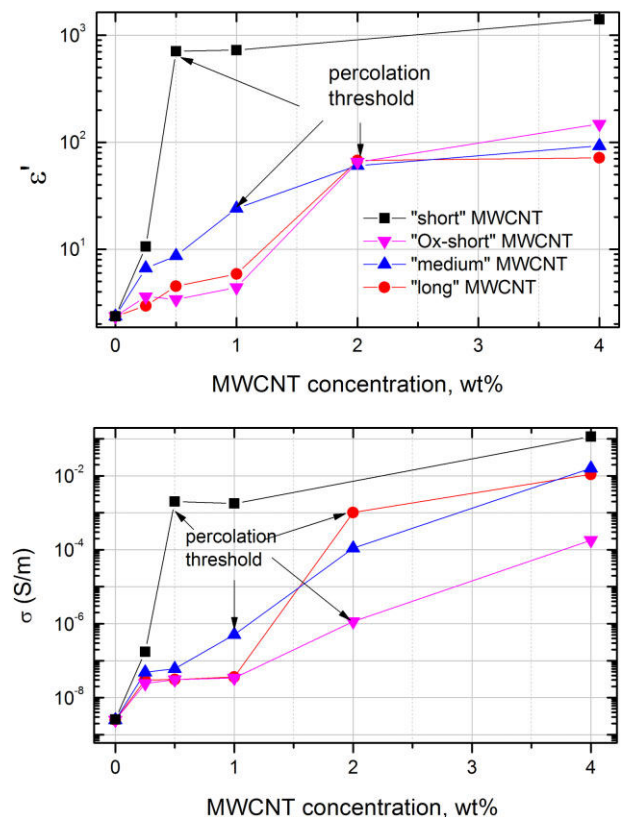e electrical percolation also occurs. The percolation threshold can be easily established from the concentration dependence of the dielectric permittivity and the electrical conductivity, indeed close to the percolation threshold the values of both parameters increase rapidly (Fig. 4) and a typical dc conductivity plateau is observed in the frequency dependence of the conductivity (not shown). By this way it was established that the percolation threshold in composites with the "Ox-short" and "long" MWCNT is 2 wt.%, in composites with "medium" MWCNT is 1 wt.%. The small decrease in the dc conductivity and the dielectric permittivity when the concentration of the "shortest" MWCNT increases from 0.5–1 wt.% is related with the local fluctuation of the CNT distributions (Fig. 4) [24]. Thus the percolation threshold decreases with the mean MWCNT length. Firstly, it should be admitted that the percolation threshold values for composites with the threaded MWCNT are close to the values predicted by the excluded volume theory [14].

Secondly, for the short MWCNT another model for the percolation threshold is proposed [25, 26]:

$$f_c = \frac{9H(1-H)}{-9H^2 + 15H + 2}, \tag{1}$$

Figure 3 Frequency dependence of the real parts of the complex dielectric permittivity and electrical conductivity for composites with different concentrations of "short" MWCNT inclusions at room temperature.

Figure 4 Concentration dependence of real parts of the complex dielectric permittivity and the electrical conductivity for all composites at room temperature and frequency 1 kHz.

Phys. Status Solidi A 213, No. 4 (2016)

1029

Original

Paper

where H is related with the aspect ratio in the following way:

$$H(p) = \frac{1}{p^2 - 1}\left[\frac{p}{\sqrt{p^2 - 1}}\ln(p + \sqrt{p^2 - 1}) - 1\right].$$

(2)

According to Eqs. (1) and (2) the percolation threshold is almost independent from the aspect ratio when the aspect ratio is in the range [20–100], so it should be for composites with not threaded MWCNT.

However, usually composites comprise individual, perfectly dispersed, the MWCNT and the MWCNT agglomerates. The percolation threshold of these composites can be estimated by Ref. [27]

$$f_c = v\varphi\pi/6 + (1 - v)27\pi/4p^2,$$

(3)

where φ is the localized volume content of MWCNT in an agglomerate, and v is the volume fraction of agglomerated MWCNT. Therefore, if the volume fraction of agglomerated MWCNT is different in composites with different aspect ratio MWCNT, the percolation threshold can be lower in composites with short MWCNT, as it is observed in our case. This assumption is also supported by SEM investigations (Fig. 2). Moreover, below the percolation threshold the values of the dielectric permittivity and the electrical conductivity are also highest for composites with the "short" nanotubes and decrease with the mean MWCNT length. The effect is related with the fact that the dielectric permittivity and the electrical conductivity close to the percolation threshold increases according to the power law [14]. Thus, in all composites below the percolation threshold, the lower percolation threshold value is accompanied by the higher value of the dielectric permittivity and the electrical conductivity. In contrast above the percolation threshold the dielectric permittivity value of all composites is very similar, except composites with the "short" MWCNT where the dielectric permittivity and the electrical conductivity values are highest.

3.3 Dielectric relaxation The temperature dependence of the complex dielectric permittivity for the composite with the "short" MWCNT inclusions at different frequencies is presented in Fig. 5. The dielectric permittivity is temperature dependent and has a maximum close to 337 K. The position of the maximum is frequency independent. Nevertheless, a broad dielectric dispersion is observed below and above the dielectric permittivity maximum temperature, the dielectric dispersion is related with the β relaxation in the PMMA matrix [28]. Therefore, the maximum of the dielectric permittivity is also related with the β relaxation in the PMMA matrix, not with the ferroelectric phase transition [28]. At higher temperatures (above 370 K) an increase in the complex dielectric permittivity is related with the electrical conductivity effects.

For all other composites below the percolation threshold the values of the complex dielectric permittivity are similar to pure PMMA matrix properties.

Frequency dependencies were analyzed with the Havriliak–Negami formula (Fig. 6)

$$\varepsilon^* = \varepsilon_\infty + \frac{\Delta\varepsilon}{(1 + (i\omega\tau_{HN})^\alpha)^\gamma},$$

(4)

where ε_∞ is the permittivity at the high frequency, $\Delta\varepsilon = \varepsilon_s - \varepsilon_\infty$, ε_s is the static dielectric permittivity; the exponents α and γ describe the asymmetry and the broadness of the dielectric spectra, τ_{HN} is the relaxation time. For $\gamma = 1$ the Havriliak–Negami equation reduces to the Cole–Cole equation [29]. A mean relaxation was calculated according to the equation [30]

$$\langle\tau\rangle = \tau_{HN} + \frac{\Psi(\gamma) + Eu}{\alpha},$$

(5)

where $\Psi(\gamma)$ is the digamma function, Eu is the Euler constant (Eu = 0.5772...).

The value of the mean relaxation time is lowest in the composites with the shortest nanotubes and for the composites with the higher MWCNT concentration
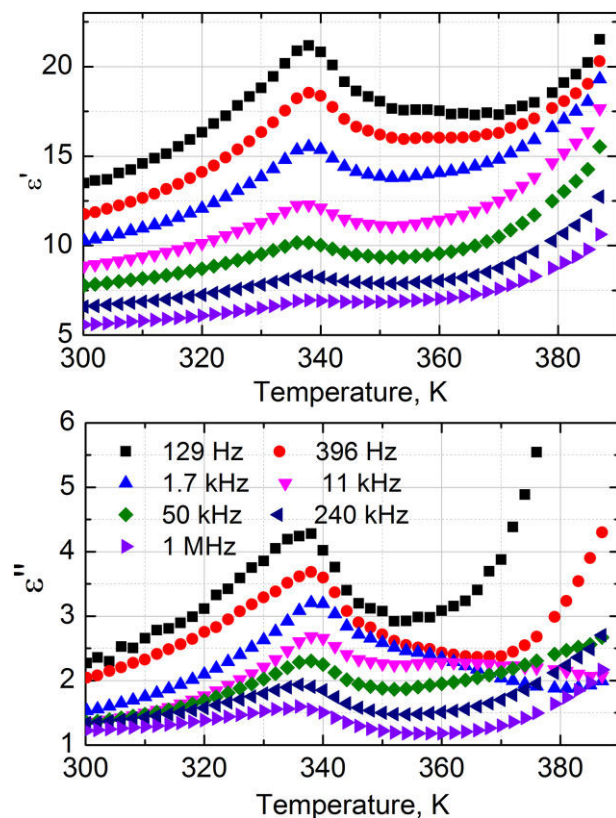
Figure 5 Temperature dependence of the complex dielectric permittivity for the composites with the "short" MWCNT inclusions at different frequencies. The MWCNT concentration is 0.25 wt.%.
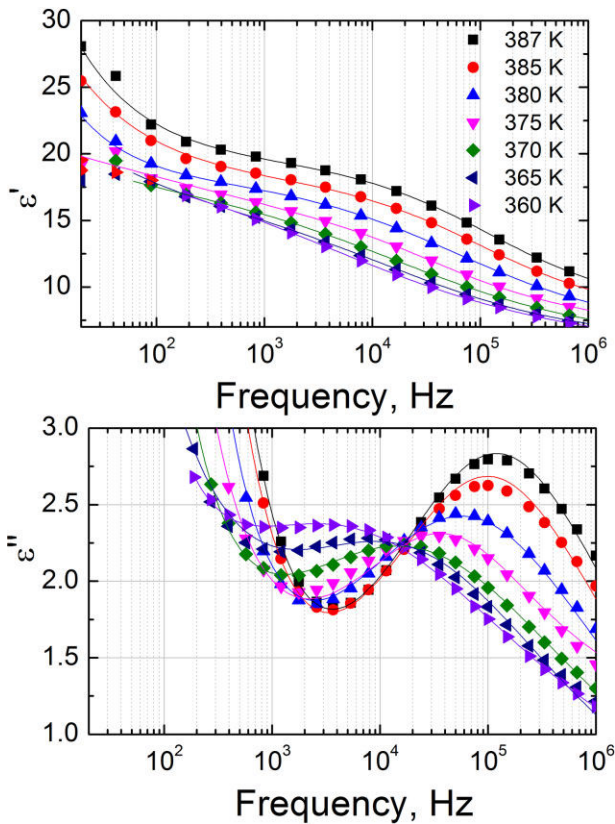
Figure 6 Frequency dependence of the complex dielectric permittivity for the composites with the "short" MWCNT inclusions at different temperatures. The MWCNT concentration is 0.25 wt.% (below the percolation threshold). Solid lines are fits of the Havriliak–Negami equation (Eq. (4)).

Figure 7 Temperature dependence of the mean relaxation time for all investigated composites below the percolation threshold. Solid lines are fits of the Arrhenius law.

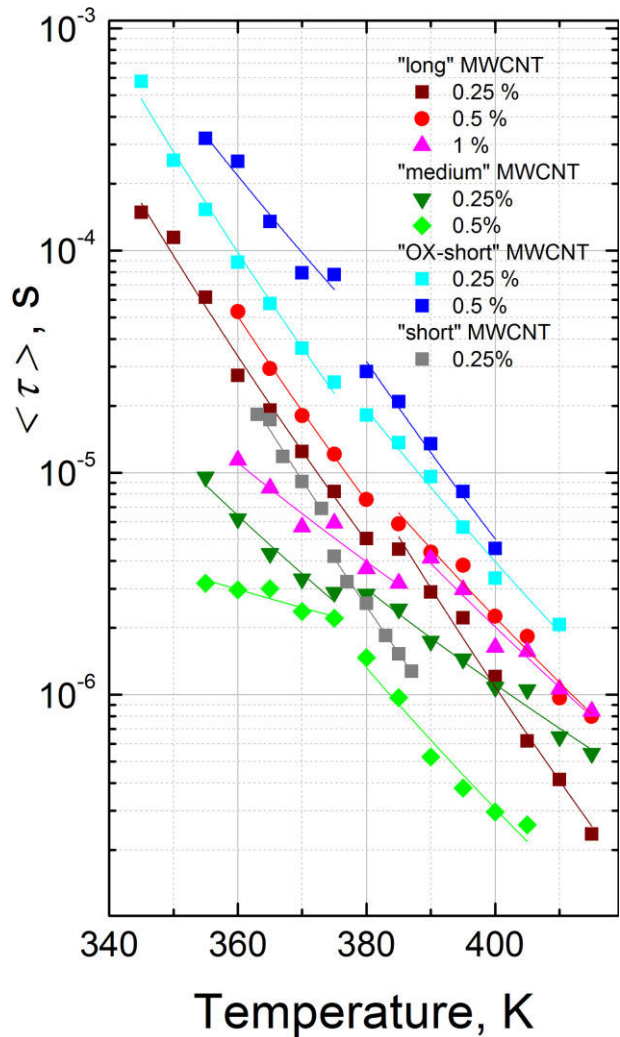(Fig. 7). The temperature dependence of the mean relaxation time was fitted with the Arrhenius law

$$\tau = \tau_0 e^{U/k_B T}. \tag{6}$$

The mean relaxation time have a change in the slope close to the glass transition temperature ($\sim$380 K) [31].

Therefore, the mean relaxation time was fitted with the Arrhenius law separately below and above the glass transition temperature. The obtained parameters are presented in Table 1. Obtained values of parameters for pure PMMA are in good agreement with the data presented in Refs. [31, 32]. In composites with non-treated MWCNT the activation energy strongly decreases with the MWCNT concentration.

In other composites the concentration dependence of the activation energy is less expressed.

3.4 Electrical transport Above the percolation threshold all composites exhibit non-zero dc conductivity in the whole temperature range. The frequency dependence of the electrical conductivity for composites with the

shortest MWCNT (the concentration 0.5 wt.%) at different temperatures is presented in Fig. 8.

At low frequencies the conductivity is frequency independent (the dc conductivity) and at higher frequencies the conductivity increases according to the power law (the ac conductivity). The frequency dependence of the electrical conductivity was fitted with the Jonscher equation [33]

$$\sigma = \sigma_{dc} + A\omega^n, \tag{7}$$

where σ_{dc} is the dc conductivity, $A\omega^n$ is the ac conductivity, A and n are parameters. The dc conductivity exhibit the different behavior at low temperatures (below the room temperature) and at high temperatures (above the room temperature). Above the room temperature the temperature dependence of the dc conductivity and the critical frequency have three different area (Fig. 9): (i) the dc conductivity and the critical frequency are almost temperature independent
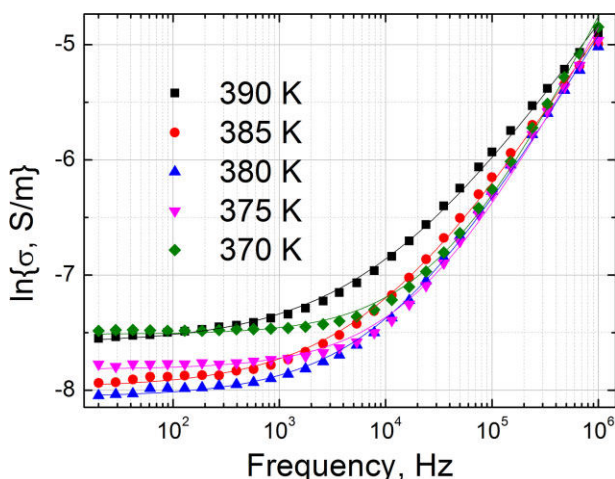
Original

Paper

Phys. Status Solidi A 213, No. 4 (2016)
1031

Table 1 Arrhenius fit parameters for the temperature dependence of the mean relaxation time.

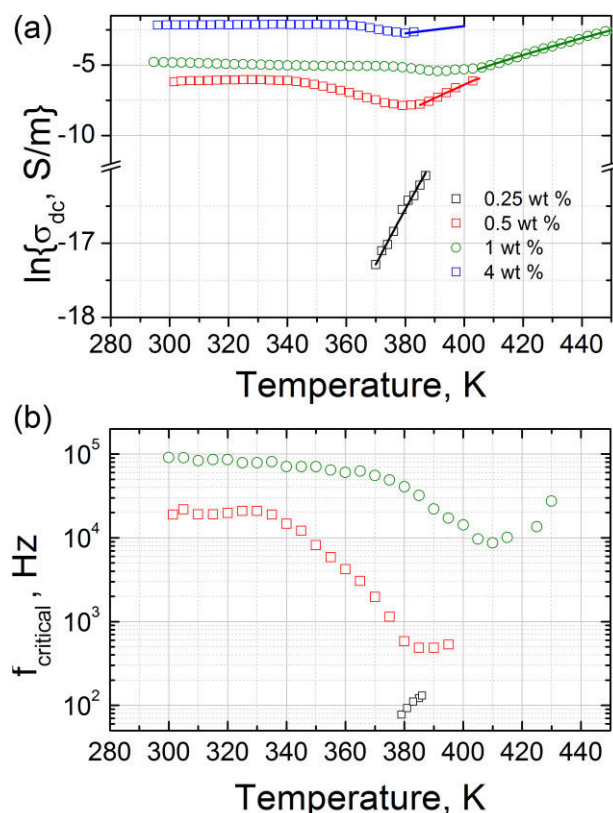| MWCNT mean length	MWCNT concentration (wt.%)	temperature region	τ_0 (s)	U (eV)
pure PMMA		$T < T_g$	8.5×10^{-17}	0.95
		$T > T_g$	2.86×10^{-20}	1.2
50 μm	0.25	$T < T_g$	4.9×10^{-21}	1.1
		$T > T_g$	4.9×10^{-24}	1.3
	0.5	$T < T_g$	8.2×10^{-21}	1.1
		$T > T_g$	1.9×10^{-18}	0.9
	1	$T < T_g$	3.8×10^{-14}	0.6
		$T > T_g$	1.4×10^{-17}	0.9
438 nm	0.25	$T < T_g$	1.3×10^{-15}	0.7
		$T > T_g$	8.1×10^{-15}	0.6
	0.5	$T < T_g$	2.7×10^{-9}	0.6
		$T > T_g$	2.8×10^{-19}	0.9
335 nm	0.25	$T < T_g$	1.3×10^{-20}	1.1
		$T > T_g$	3.7×10^{-19}	1
	0.5	$T < T_g$	3.4×10^{-17}	0.9
		$T > T_g$	3.5×10^{-21}	1.2
328 nm	0.25	$T < T_g$	3.4×10^{-22}	1.2
		$T > T_g$	1.4×10^{-22}	1.2

at low temperatures (below 340 K for composites with 0.5 wt.% MWCNT inclusions), (ii) the dc conductivity and the critical frequency decreases with the temperature in intermediate temperature range (from 340 to 380 K for composites with 0.5 wt.% MWCNT inclusions), (iii) the dc conductivity and the critical frequency increases with the temperature at higher temperatures (above 380 K for composites with 0.5 wt.% MWCNT inclusions). The decrease of the conductivity and the critical frequency is related with very different thermal properties of the PMMA matrix and the MWCNT.

On heating the PMMA matrix suddenly expands, while the volume of MWCNT remains the same. In this way the average distance for charge carriers increase and the electrical conductivity decrease. However, at higher temperatures the electrical conductivity effects were observed even in the composites below the percolation

Figure 9 Temperature dependence of the dc conductivity (a) and the critical frequency (b) of composites with the "short" MWCNT inclusions (the high temperature region).

Figure 8 Frequency dependence of the electrical conductivity of the composites with "short" MWCNT inclusions at different temperatures, the high temperature region. The filler concentration is 0.5 wt.% (above the percolation threshold). Solid lines are fits of the Jonscher equation.

threshold and also in pure PMMA. At these higher temperatures the conductivity of the composites above the percolation threshold increases due to the finite polymer matrix conductivity. However, for pure PMMA we cannot determine the dc electrical conductivity because it occurs below our low frequency limit (20 Hz). The dc conductivity at these higher temperatures follow the Arrhenius law

$$\sigma = \sigma_0 e^{E/k_B T}. \qquad (8)$$

Obtained activation energy values are summarized in Table 2. One can be concluded that the activation energy decreases with the MWCNT concentration above the percolation threshold. At higher temperatures the electrical transport occurs due to the finite PMMA matrix conductivity and due to the tunneling between MWCNT clusters. These conductivities are connected parallel.

The conductivity related with the electrical transport in the MWCNT network is weakly temperature dependent, at the same time the electrical conductivity of the PMMA matrix follows the Arrhenius law, similarly as in other polymers [34]. With increasing the MWCNT concentration the contribution of the matrix conductivity to the total conductivity decreases and together the temperature dependence of the total electric conductivity becomes more flat.

At low temperatures (below 200 K) the dc conductivity decreases according to the electrical tunneling model (Fig. 10) [35]
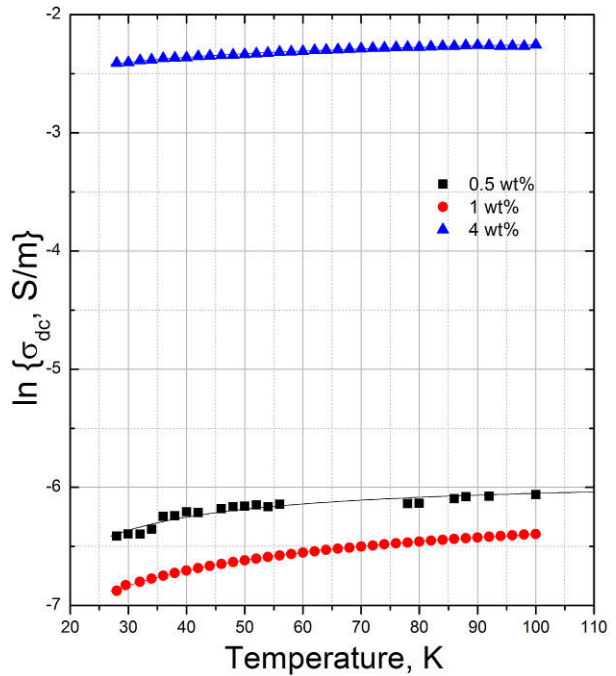
$$\sigma_{DC} = \sigma_{DC0} \exp(T_1/(T + T_0)), \qquad (9)$$

where T_1 represents the energy required for an electron to cross the insulator gap between conductive particle aggregates and T_0 is the temperature above which the thermally activated conduction over the barriers begins to occur. According to the tunneling model [35],

$$T_1 = wA\beta_0/8\pi k, \qquad (10)$$

Figure 10 Temperature dependence of the dc conductivity of composites with the "short" MWCNT inclusions (the low temperature region).

$$T_0 = 2T_1/\pi\chi w, \qquad (11)$$

where $\chi = (2mV_0)^{0.5}/h$ and $\beta_0 = 4V_0/ew$, m and e being the electron mass and the charge, respectively, V_0 is the potential barrier height, w is the interparticle distance (gap width), and A is the area of the capacitance formed by the junction. Obtained parameters are listed in Table 3. From Eqs. (7) and (8) it follows that T_1/T_0 is proportional to the gap width w, which is approximately proportional to $p^{-1/3}$ [36]. Thus, the ratio T_1/T_0 should decrease with the MWCNT concentration, indeed such behavior is observed in all our investigated composites. Moreover, at same nanotubes concentration this ratio is highest in composites

Table 2 Concentration dependence of the dc conductivity activation energy.

MWCNT mean length	MWCNT concentration (wt.%)	E_a (eV)
50 μm	2	0.92
	4	0.2
438 nm	1	1
	2	0.66
	4	0.21
335 nm	2	0.1
	4	0.33
328 nm	0.25	0.9
	0.5	1.3
	1	0.95
	4	0.33

Table 3 Concentration dependence of tunneling fit parameters.

MWCNT mean length	MWCNT concentration (wt.%)	T_1 (K)	T_0 (K)
328 nm	0.5	12	1
	1	36	19
	4	12	19
50 μm	2	47	40
	4	18	23
431 nm	1	58	19
	2	44	26
	4	25	35
335 nm	2	52	18
	4	35	12

Phys. Status Solidi A 213, No. 4 (2016)

1033

Original

Paper

with "OX-short" MWCNT inclusions, indicating the higher potential barrier for the electron tunneling.

4 Conclusions The influence of the nanotube length and the surface compound on the dielectric and the electrical properties of the PMMA/MWCNT composites were studied. The decrease in the length of the nanotubes improves the quality of their distribution in the polymer matrix. The strong adhesion between PMMA and the surface of the oxidized nanotubes decreases a number of nanotube interconnections. This, in turn, decreases the conductivity of the composite. Therefore, the percolation threshold is lower in the composites with the shortest nanotubes and the additionally oxidized nanotubes. The dielectric permittivity and the electrical conductivity are also higher in the composites with the shortest nanotubes. Below the percolation threshold the dielectric dispersion in composites is mainly related with the β relaxation in the polymer matrix. The MWCNT type and the concentration have the huge influence on the polymer molecules dynamics, the relaxation time is shortest in composites with the higher nanotubes concentration and in composites with the shortest nanotubes. The conductivity of the composites above the percolation threshold is governed by the electron tunnelling between MWCNT clusters. At higher temperatures the electrical transport occurs also due to the finite electrical conductivity of the polymer matrix.

References

[1] R. H. Baughman, A. A. Zakhidov, and W. A. De Heer, Science **297**, 787 (2002).

[2] S. Iijima and T. Ichihashi, Nature **363**, 603 (1993).

[3] M. M. J. Treacy, T. W. Ebbesen, and J. M. Gibson, Nature **381**, 678 (1996).

[4] M. V. Shuba, A. G. Paddubskaya, P. P. Kuzhir, G. Ya. Slepyan, S. A. Maksimenko, V. K. Ksenevich, P. Buka, D. Seliuta, I. Kasalynas, J. Macutkevic, G. Valusis, C. Thomsen, and A. Lakhtakia, Phys. Rev. B **85**, 165435 (2012).

[5] N. Li, Y. Huang, F. Du, X. B. He, X. Lin, H. J. Gao, Y. F. Ma, F. F. Li, Y. S. Chen, and P. C. Eklund, Nano Lett. **6**, 1141 (2006).

[6] M. F. L. De Volder, S. H. Tawfick, R. H. Baughman, and A. J. Hart, Science **339**, 553 (2013).

[7] C. G. Granqvist, Sol. Energ. Mater. Sol. Cells **91**, 1529 (2007).

[8] J. K. W. Sandler, J. E. Kirk, I. A. Kinloch, M. S. P. Shaffer, and A. H. Windle, Polymer **44**, 5893 (2003).

[9] Z. F. Liu, G. Bai, Y. Huang, Y. F. Ma, F. Du, F. F. Li, T. Y. Guo, and Y. S. Chen, Carbon **45**, 821 (2007).

[10] Z. M. Dang, L. Wang, Y. Yin, Q. Zhang, and Q. Q. Lei, Adv. Mater. **19**, 852 (2007).

[11] L. Wang and Z. M. Dang, Appl. Phys. Lett. **87**, 042903 (2005).

[12] I. Balberg, C. H. Anderson, S. Alexander, and N. Wagner, Phys. Rev. B **30**, 3933 (1984).

[13] W. Baunhofer and J. Z. Kovacs, Comp. Sci. Technol. **69**, 1486 (2009).

[14] H. Deng, L. Lin, M. Ji, Sh. Zhang, M. Yang, and Q. Fu, Prog. Polym. Sci. **39**, 627 (2014).

[15] C. A. Martin, J. K. W. Sandler, M. S. P. Shaffer, M. K. Schwarz, W. Bauhofer, K. Schulte, and A. H. Windle, Comp. Sci. Technol. **64**, 2309 (2004).

[16] P. Musto, P. Russo, F. Cimino, D. Acierno, G. Lupo, and C. Petrarca, Europ. Polym. J. **64**, 170 (2015).

[17] A. S. Abu-Surrach, E. Al-Ramahi, S. A. Jawad, A. B. Hallak, and Z. Khattari, Physica B **463**, 76 (2015).

[18] K. Shehzad, M. N. Ahmad, T. Hussain, M. Mumtaz, A. T. Shach, A. Mujahid, C. Wang, J. Elingsen, and Z. M. Dang, J. Appl. Phys. **116**, 064908 (2014).

[19] M. S. Russ, S. S. Rahatekar, K. Koziol, B. Farmer, and H. X. Peng, Comp. Sci. Technol. **81**, 42 (2013).

[20] V. Alig, P. Potschke, D. Lellinger, T. Skipa, S. Pegel, G. R. Kasaliwal, and T. Villmow, Polymer **53**, 4 (2012).

[21] H. Deng, R. Zhang, E. Bilotti, J. Loos, and T. Peijs, J. Appl. Polym. Sci. **113**, 742 (2009).

[22] A. Ch. Baudouin, D. Auhl, F. F. Tao, J. Devaux, and C. Baily, Polymer **52**, 149 (2011).

[23] V. L. Kuznetsov, D. V. Krasnikov, A. N. Schmakov, and K. V. Elumeeva, Phys. Status Solidi B **249**, 2390 (2012).

[24] B. E. Kilbride, J. N. Coleman, J. Fraysse, P. Fournet, M. Cadek, A. Drury, S. Hutzler, S. Roth, and W. J. Blau, J. Appl. Phys. **92**, 4024 (2002).

[25] F. Deng, Q. S. Zheng, L. F. Wang, and C. W. Nan, Appl. Phys. Lett. **90**, 021914 (2007).

[26] F. Deng and Q. S. Zheng, Appl. Phys. Lett. **92**, 071902 (2008).

[27] J. Li, P. Ma, W. Chow, C. To, B. Tang, and J. K. Kim, Adv. Funct. Mater. **17** (16), 3207 (2007).

[28] K. Schmidt-Rohr, A. S. Kulik, H. W. Becktran, A. Ohlemacher, U. Pawlzik, C. Boeffel, and H. W. Spiess, Macromolecules **27**, 4733 (1994).

[29] S. Cole and R. H. Cole, J. Chem. Phys. **9**, 341 (1941).

[30] R. Zorn, J. Chem. Phys. **116**, 3204 (2002).

[31] R. Bergman, F. Alvarez, A. Alegria, and J. Colmenero, J. Chem. Phys. **109**, 7546 (1998).

[32] R. Bergman, F. Alvarez, A. Alegria, and J. Colmenero, J. Noncryst. Solids **235–237**, 580 (1998).

[33] A. K. Jonsher, IEEE T. Electr. **27**, 407 (1992).

[34] S. A. Khiar, R. Puteh, and A. K. Arof, Physica B **373**, 23 (2006).

[35] P. Sheng, E. K. Sichel, and J. I. Gettleman, Phys. Rev. Lett. **40**, 1197 (1978).

[36] T. A. Ezquerra, M. Kulesza, and F. J. Balta Galleja, Synth. Met. **41–43**, 915 (1991).

VI

Enhancing electrical conductivity of MWCNT/epoxy composites by GNP particles

I. Kranauskaitė, J. Macutkevic, A. Borisova, A. Martone, M. Zarrelli, A. Selskis, A. Aniskevich, J. Banys

ENHANCING ELECTRICAL CONDUCTIVITY OF MULTIWALLED CARBON NANOTUBE/EPOXY COMPOSITES BY GRAPHENE NANOPLATELETS

I. Kranauskaitė [a], J. Macutkevič [a], A. Borisova [b], A. Martone [c], M. Zarrelli [c], A. Selskis [d],

A. Aniskevich [b], and J. Banys [a]

[a] *Faculty of Physics, Vilnius University, Saulėtekio 3, 10257 Vilnius, Lithuania*
[b] *Institute for Mechanics of Materials, University of Latvia, 23 Aizkraukles iela, 1006 Riga, Latvia*
[c] *Institute for Polymers, Composites and Biomedical Materials, National Research Council, P.le E. Fermi 1, 80155 Portici, Naples, Italy*
[d] *National Center for Physical Sciences and Technology, Saulėtekio 3, 10222 Vilnius, Lithuania*
Email: ieva.kranauskaite@ff.vu.lt

The need of high performance integrated circuits and high power density communication devices drives the development of materials enhancing the conductive performances by carbon nanoparticles. Among nanocomposites, the ternary hybrid carbon nanotubes/graphene nanoplatelets/polymer composites represent a debatable route to enhance the transport performances.

In this study hybrid ternary nanocomposites were manufactured by direct mixing of multiwalled carbon nanotubes (MWCNTs) and graphene nanoplatelets (GNPs) at a fixed filler content (0.3 wt.%), but different relative combination, within an epoxy system. MWNT/epoxy nanocomposites were manufactured for comparison. The quality of dispersion was evaluated by optical and scanning electron microscopy (SEM). The electrical properties of hybrid composites were measured in the temperature range from 30 up to 300 K.

The synergic combination of 1D/2D particles did not interfere with the percolative behaviour of MWCNTs but improved the overall electrical performances. The addition of a small amount of GNPs (0.05 wt.%) led to a strong increment of the sample conductivity over all the temperature range, compared to that of mono filler systems.

Keywords: graphene nanoplatelets, multiwalled carbon nanotubes, epoxy resin, hybrid nanocomposites, electrical conductivity

PACS: 72.80.Tm

1. Introduction

Epoxies are an indispensable class of thermosetting polymers widely used in modern industry. These materials are ubiquitous, due to the fact that scientists and engineers from a wide range of disciplines use them in various applications. Carbon nanomaterials such as carbon nanotubes (CNTs) and graphene nanoplatelets (GNPs) are among the most utilized nanomaterials due to their electrical, mechanical and thermal properties. The result of combining the insulating epoxy as a host matrix and conducting carbon nanomaterials as fillers is the material with a whole new set of properties that are not found in individual components [1, 2]. Conducting polymer composites are mainly applied as electromagnetic coatings, radar waves absorbing materials, and as antistatic materials [3–5]. In electronics, conductive polymer composites find applications as adhesives and circuit elements [6].

Electrical conductivity of polymer composites depends on the filler concentration. For a low filler content the distance between conductive particles is large and the conductivity is limited in an insulating polymer matrix. Increasing the content of filler composites evokes a non-linear increase of the electrical conductivity as a function of the filler concentration. At a certain filler concentration, known as the percolation threshold (φ_c), the electrical conductivity suddenly increases by several orders leading

a composite from an insulator to a conductor. Sometimes addition of a very small amount of conducting particles makes a filler to form an effective conducting path thus making the whole composite conductive. CNTs and GNPs, as effective fillers, could be used to produce a conductive polymer composite with a very low percolation threshold [7]. The typical percolation threshold values that were reported in literature vary from 0.002 to over 2 wt.% [8–10] for MWCNT composites and from 1 to 8 wt.% for GNP composites [11, 12]. Such large variations of percolation threshold values show that the nanofiller content, aspect ratio, dimensions and geometrical arrangement, and also composite processing conditions are important [13, 14].

The main problems limiting the expected improvement of epoxy resin are that such nanoparticles increase viscosity and form agglomerates due to van der Waals forces [2, 15, 16], and the sufficient network is not created in the polymer matrix which leads to a higher percolation threshold. The agglomeration could be decreased by improving the dispersion state of the filler in the polymer matrix. One of the most promising solutions is to attempt combining two carbon fillers into a hybrid structure which could lead to a potentially new multifunctional material in research and application as the result of synergy effect of both fillers, improving mechanical [17, 18], thermal [13] and electrical [14] characteristics. A small size of nanofillers with a different shape results in a large surface area, thus increasing the amount of the polymer in contact with the filler. When the volume content of the nanofiller is large enough, the inter-phase becomes the dominant phase in the composite. In addition, the use of different shape (1D – CNT and 2D – GNP) nanoparticles allows one to increase the efficiency at a smaller filler content. For the same filler content of particles with various geometrical arrangements of the chains, different results of particle lengths and shape can be achieved. Therefore, it is hard to predict theoretically the final results. Physical properties of a composite filled with carbon nanoparticles in a different filler content and combination should be experimentally investigated in order to determine the optimal nanoparticle content, the filler combination and the ratio which would maximally improve certain physical properties of the composite, reduce production costs, enhance multifunctionality and application possibilities. The synergistic effect of carbon nanofillers on improving the thermomechan-

ical and electrical properties of the material is not clearly determined as well. Moreover, usually electrical properties of hybrid composites were investigated only at room temperature [19], while investigations in a wide temperature range are needed to determine the electrical transport mechanism [20].

The aim of this work is to systematically investigate hybrid nanocomposites at different MWNTs/GNPs ratios to highlight synergic effects on the electrical conductivity. In this paper electrical conductivity measurements were performed in a wide frequency and temperature range starting from cryogenic temperature (30 K) to room temperature (300 K) in order to determine the electrical transport mechanism at different temperatures.

2. Materials and methods

Composites were prepared with multiwalled carbon nanotubes (MWCNTs) and graphene nanoplatelets in an epoxy resin matrix. The epoxy resin is a mono-component thermosetting resin RTM6 (HexFlow®), which is already degassed. It is a premixed epoxy-amine system for service temperatures from –60 up to 180 °C, specifically developed to fulfill the requirements of aerospace industries in the advanced resin transfer moulding process. This resin is characterized by a high ultimate glass transition temperature (200 °C) and a low viscosity (50 MPa) within the range 100–120 °C.

MWCNTs N7000 were purchased from *Nanocyl* (Belgium) and they were produced via the catalytic carbon vapour deposition process. The mean length of a MWCNT is 0.1–10 μm, the diameter 10 nm. The MWCNT filler content is 0.015–0.30 wt.%. Graphene nanoplatelets (GNPs) were purchased from *PuntoQuantico* (Italy). The average particle (lateral) size is 20–50 μm, the specific surface area is 60–80 m^2/g, and the average density is 2.43 g/cm^3. Filler contents 0.015–3.0 wt.% were chosen. According to the data sheet, the electrical conductivity of particles is $\approx 5 \cdot 10^{-5}$ W·cm, but the thermal conductivity is 3000 W/m·K. Using both carbon nanofillers, hybrid nanocomposites with the filler content 0.30 wt.%, the ratio of MWCNTs and GNPs being selected as 1:1, 1:2, 1:5, 2:1, 5:1, were produced.

Epoxy resin/carbon nanofiller nanocomposites were prepared using 150 g of resin mixed with carbon particles in different contents for a constant time (70 min) at 85 °C temperature with a nominal

speed of 6000 rpm. The mixer used in this work was a T 25 digital ULTRA-TURRAX high-performance disperser by *IKA* with the output power 500 W and the frequency 50 Hz. A disperser horn was directly put into a resin and MWCNT mixture warmed up to 60 °C. The disperser used produces extremely strong shear and thrust forces due to high accelerations acting on the material, and additionally a high turbulence occurs in the shear gap between the rotor and the stator, which provides an optimum mixing of the components.

The structure and dispersion of the filler in the polymer matrix were determined using microscopic methods – optical microscopy and scanning electron microscopy (SEM). Optical microscopy analysis was carried out by using an *Olympus* system type BX51 in transmitted light configuration. The homogeneity of composites was checked with a scanning electron microscope *Helios* NanoLab 650.

Dielectric properties of the composites were measured in a wide frequency range (from 20 Hz to 3 GHz) at room temperature and at low frequencies (20 Hz – 1 MHz) in the temperature range from 30 to 300 K. In the frequency range from 20 Hz to 1 MHz measurements were performed using a LCR meter (HP4284) measuring the capacitance and the loss tangent. For low temperature measurements a helium closed cycle cryostat was used. In the frequency range from 1 MHz to 3 GHz reflection and phase were measured using the coaxial line technique with a vector network analyzer (*Agilent* 8714 ET). The samples were of a cylindrical shape with different thickness and diameter for different technique. In the frequency range 20 Hz – 3 GHz the height and radius were 3 and 6 mm and in the frequency range 1 MHz – 3 GHz they were 3 and 1 mm, respectively. Silver paste was used for contacts. The real part of the electrical conductivity is calculated using the formula $\sigma' = \varepsilon_0 \varepsilon'' \omega$, where ε_0 is the vacuum permittivity, ε'' is the imaginary part of the dielectric permittivity and ω is the frequency.

3. Results and discussion

3.1. Structure characterization

Microscopy methods were used to characterize and determine the dispersion and interactions of carbon nanoparticles in the polymer matrix. Using the optical microscopy analysis the samples with MWCNTs

and GNPs were characterized by nominal dimensions of 10 × 10 mm with a thickness varying in the range 200±50 μm (Fig. 1).

The image in Fig. 1(a) shows an uneven distribution of MWCNTs in the epoxy resin. There are areas with a high concentration and agglomerated MWCNTs and small areas with an almost negligible
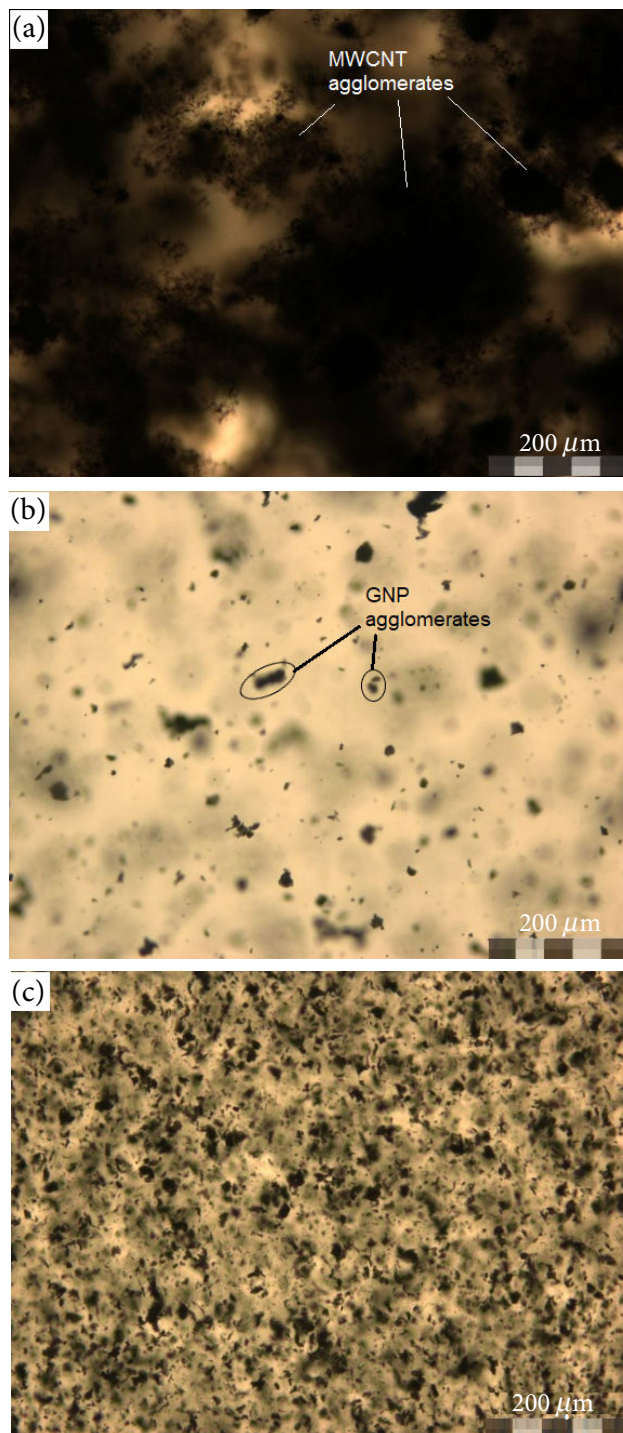

Fig. 1. Optical microscopy images of epoxy resin filled with (a) 0.03 wt.% of MWCNTs; (b) 0.03 wt.% of GNPs; (c) 1.00 wt.% of GNPs, at 10× magnification.

concentration of the carbon nanotubes. The agglomerates could be related to strong van der Waals forces between the carbon nanotubes. The images of the GNP composites in Fig. 1(b) and (c) of the GNP composites show large agglomerates of the GNPs due to interactions between the sheets of graphene nanoplatets. A smooth surface of the GNPs could result in a weak interfacial bonding with the polymer [7]. For further structural investigations the SEM images are performed (Fig. 2).
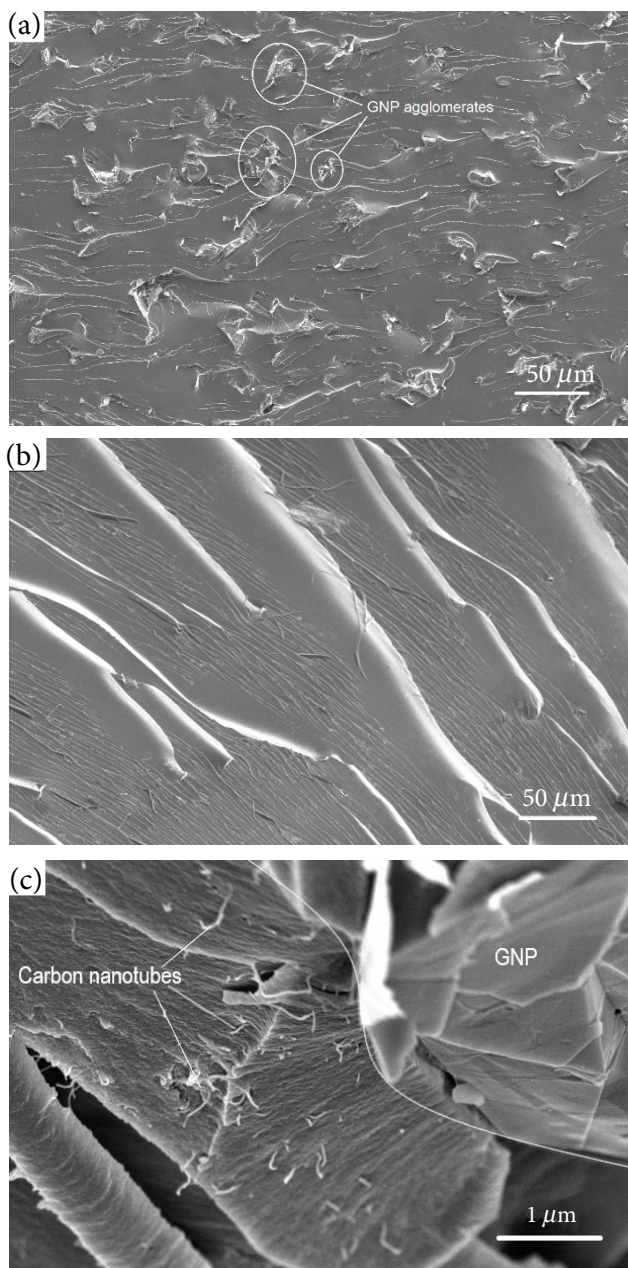

Fig. 2. SEM images of epoxy resin composites filled with (a) 0.3 wt.% of GNPs, magnification 500×; (b) MWCNTs/GNPs (5:1), magnification 500×; (c) MWCNTs/GNPs (5:1), magnification 35000×.

Figure 2(a) shows the surface of a composite containing 0.3 wt.% GNPs. GNP agglomerates of varying size are randomly dispersed in the polymer matrix. In contrast, the surface of hybrid filler composites is smoother with no visible large agglomerates of GNPs or MWCNTs, and carbon nanotubes likely reduce the size of GNP aggregates. The magnification of the SEM images in Fig. 2(a) and (b) is 500×. The SEM image (magnification 35000×) in Fig. 2(c) shows that smaller GNP agglomerates can still be found, but the dispersion of MWCNTs is much more even.

3.2. Electrical properties

The dielectric and electrical properties of the composites containing MWCNTs, GNPs and hybrid nanocomposites with different combinations of MWCNTs/GNPs are compared in a wide frequency and temperature range.

The frequency dependences of the dielectric permittivity and the electrical conductivity at room temperature for the composites containing only MWCNT and GNP fillers are presented in Fig. 3. The values of dielectric permittivity and electrical conductivity increase sharply close to the percolation threshold. Moreover, above the percolation threshold in the frequency dependence of the conductivity a frequency independent plateau is observed.

The theoretical percolation threshold for GNP particles could be calculated from the excluded volume theory [21, 22]

$$\varphi_c = \frac{21.2}{A_{\mathrm{GNP}}}, \tag{1}$$

where A_{GNP} is an aspect ratio of round shape particles. As the average aspect ratio value for GNP particles is $A_{\mathrm{GNP}} = 1500$, the percolation threshold is 1.41 volume % or 3 wt.%. However, considering the experimental data (Fig. 3), the dielectric permittivity and the electrical conductivity of GNP composites are low enough and similar to pure epoxy resin properties even with the highest available filler concentration (3 wt.%). It indicates that the percolation threshold in GNP composites is higher than 3 wt.% and somewhat higher than the value of percolation threshold calculated from the excluded volume theory. Such high
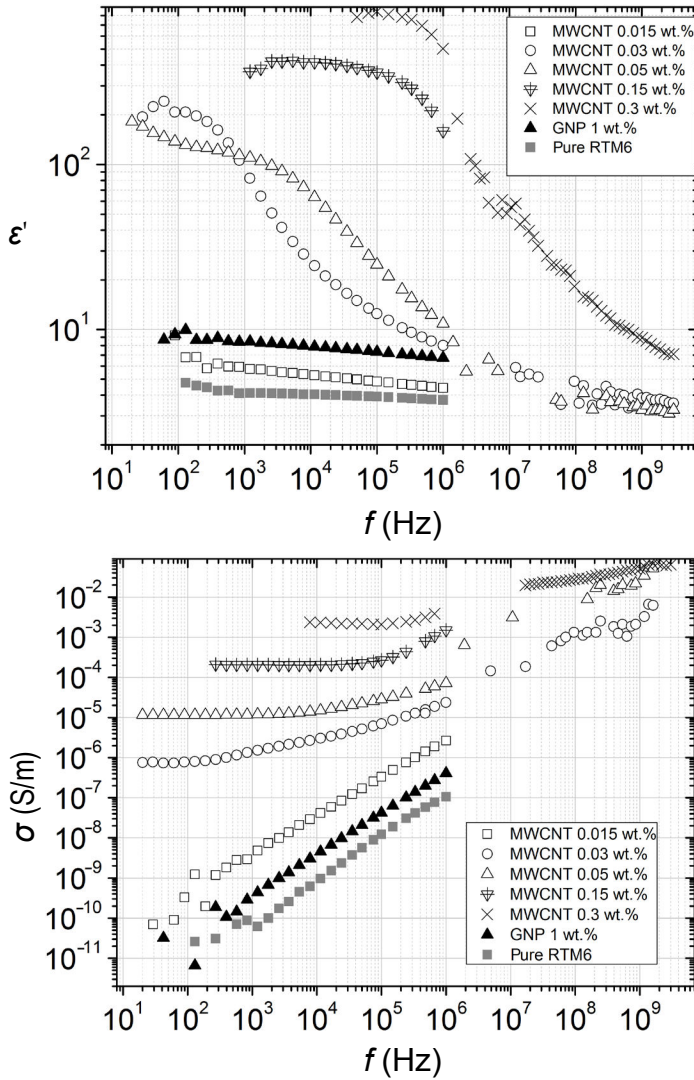
Fig. 3. Frequency dependence of the dielectric permittivity and the electrical conductivity of GNP and MWCNT composites.

experimental percolation threshold value could be attributed to the uneven distribution and large aggregates of GNPs in the polymer matrix. Similar percolation threshold values were already observed in GNP/epoxy composites [23, 24]. At low filler concentrations aggregated particles do not form a conductive path.

According to the excluded volume theory, the theoretical percolation threshold for rod-like particles could be calculated by the formula [21, 22]

$$\varphi_c = \frac{0.5}{A_{\mathrm{MWCNT}}}, \qquad (2)$$

where A_{MWCNT} is the aspect ratio, and the average aspect ratio for MWCNT is $A_{\mathrm{MWCNT}} = 505$. The percolation threshold for MWCNT composites is 0.1 volume % or 0.14 wt.%. Moreover, the experimental percolation threshold for MWCNT composites is close to 0.03 wt.%.

The dielectric permittivity and the electrical conductivity of mixed MWCNT/GNP composites with various proportions and the total 0.3 wt.% concentration are presented in Fig. 4. All investigated composites with hybrid nanofillers are above the percolation threshold because the frequency independent conductivity plateau is very well expressed in conductivity spectra. This is quite expected because according to the excluded volume theory the following relation should be valid for mixed MWCNT/GNP composites:

$$\frac{m_{\mathrm{MWCNT}}}{p_{c,\mathrm{MWCNT}}} + \frac{m_{\mathrm{GNP}}}{p_{c,\mathrm{GNP}}} = 1. \qquad (3)$$

Here m_{MWCNT} and m_{GNP} are mass fractions of MWCNTs and GNPs, respectively, and $p_{c,\mathrm{MWCNT}}$ and $p_{c,\mathrm{GNP}}$ are mass percolation thresholds in composites filled with MWCNTs and GNPs, respectively.
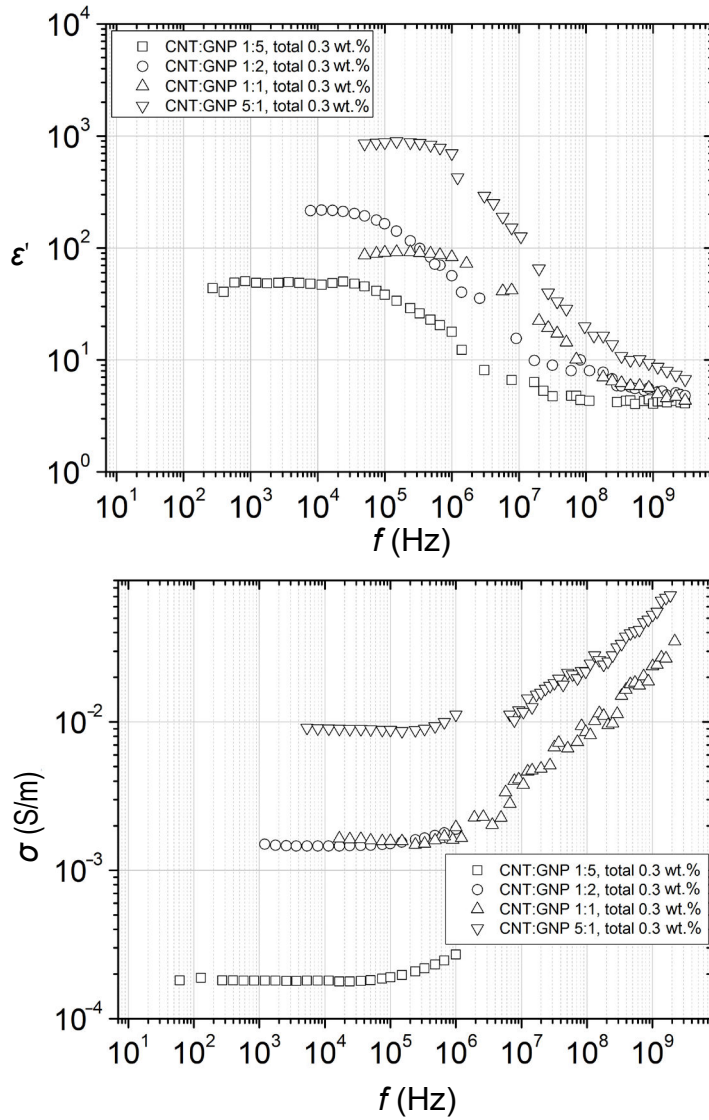
Fig. 4. Frequency dependence of the dielectric permittivity and the electrical conductivity of hybrid MWCNT/GNP composites.

$m_{\mathrm{MWCNT}} > p_{c,\mathrm{MWCNT}}$ composites will be above the percolation threshold for any m_{GNP}.

For mixed composites the electrical conductivity and dielectric permittivity increase with the increase of the MWCNT concentration.

Above the percolation threshold the frequency dependence of electrical conductivity could follow the Jonscher equation [25]

$$\sigma'(\omega) = \sigma_{\mathrm{DC}} + A\omega^n, \qquad (4)$$

where σ_{DC} is the DC conductivity and $A\omega^n$ is the AC conductivity. The values of electrical conductivity as a function of the filler concentration of single filler MWCNT and hybrid filler composites are presented in Fig. 5. Above the percolation threshold the DC conductivity follows the power law [26]

$$\sigma(p) \propto (p-p_c)^t, \qquad (5)$$

where p_c is the percolation threshold and t is the critical exponent.

The highest DC conductivity value 8.9 mS/m is observed in MWCNT:GNP mixed filler composites with proportions 5:1 (total content 0.3 wt.%) and it is increased by four orders of magnitude over that of composites containing 0.3 wt.% MWCNTs. Such high value is clearly higher than can be predicted by a simple rule of mixtures (ROM) theory [27]

$$\sigma = \frac{1}{\Sigma_{i=0}^n V_i} \Sigma_{i=0}^n \sigma_i V_i, \qquad (6)$$

where V_i and σ_i are the volume and the conductivity of the ith component. Indeed, the conductivity of composites only with MWCNTs is much higher than the conductivity of composites only with
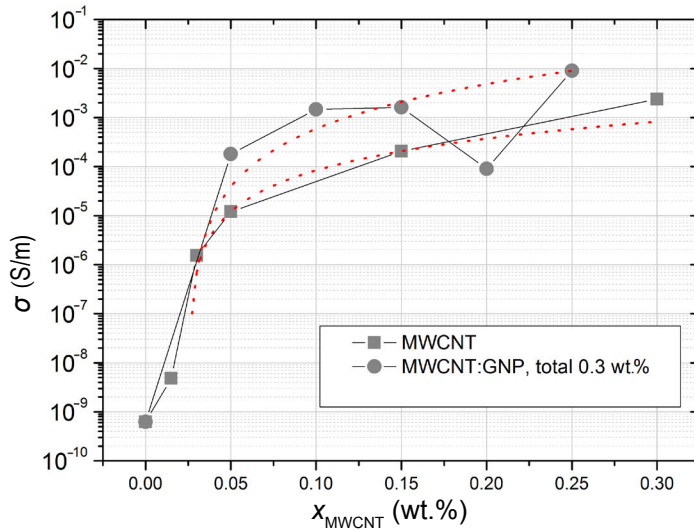
Fig. 5. Concentration dependences of the electrical conductivity at 1 kHz frequency for composites containing MWCNTs only and mixed MWCNT:GNP fillers. Dotted lines are the fits of the power law.

GNPs, therefore the conductivity of mixed composites clearly overcomes the values predicted by the ROM theory in all frequency range, including microwaves (Eq. 6), while in other works a similar effect was observed only at low frequences below 1 MHz [28]. An increase could be attributed to the formation of a more effective conductive network due to combining 2D MWCNT and 1D GNP conductive particles.

The electrical transport in mixed MWCNT/GNP composites can occur via 1) hopping and tunnelling of electrons in the MWCNT subsystem, 2) hopping and tunnelling of electrons in the GNP subsystem, and 3) tunnelling of electrons between the GNP and the MWCNT subsystems [29]. Increase of the conductivity with the increase of the MWCNT concentration for hybrid composites with the total 0.3 wt.% concentration of nanofillers indicates that the second conductivity mechanism is negligible in comparison with the first and third ones. Therefore, the electrical conductivity in mixed composites increases because of the better distribution of MWCNTs and the tunnelling of electrons between the GNPs and the MWCNTs.

Temperature dependences of the DC conductivity are presented in Fig. 6. Above the percolation threshold the DC conductivity below room temperature fits the electrical tunnelling model [30]

$$\sigma_{DC} = \sigma_0 \exp\left[\frac{T_1}{k(T+T_0)}\right], \tag{7}$$

where T_1 is the energy for an electron to cross the insulator gap between the conductive particles,

T_0 is the temperature above which thermally activated conductivity over the barrier occurs. The obtained tunnelling model fit parameters are listed in Table 1. The tunnelling model parameters T_1 and T_0 are related with the microscopic parameters [30]

$$T_1 = wA\beta_0/8\pi k \tag{8}$$

and

$$T_0 = 2T_1/\pi\chi w, \tag{9}$$

where $\chi = (2mV_0)^{0.5}/h$ and $\beta_0 = V_0/ew$, m and e are the electron mass and charge, respectively, V_0 is the potential barrier amplitude, w is the interparticle distance (gap width), and A is the area of capacitance formed by the junction. From Eqs. (8) and (9) it follows that T_1/T_0 is proportional to the gap width w and the potential barrier V_0 amplitude. The ratio T_1/T_0 decreases with the MWCNT concentration in single and hybrid composites (Table 1). Thus the interparticle distance and the potential barrier amplitude can decrease with the decrease of the MWCNT concentration for both single and hybrid composites. The gap width is approximately proportional to $p^{-1/3}$ in single composites [31]. The dependence T_1/T_0 is very similar in hybrid and single composites. However, the ratio T_1/T_0 is higher in single composites. According to SEM investigations, the smallest distance between nanoparticles is in mixed composites (Fig. 2). Therefore the ratio T_1/T_0 is lower in hybrid composites due to the better distribution of nanoparticles.
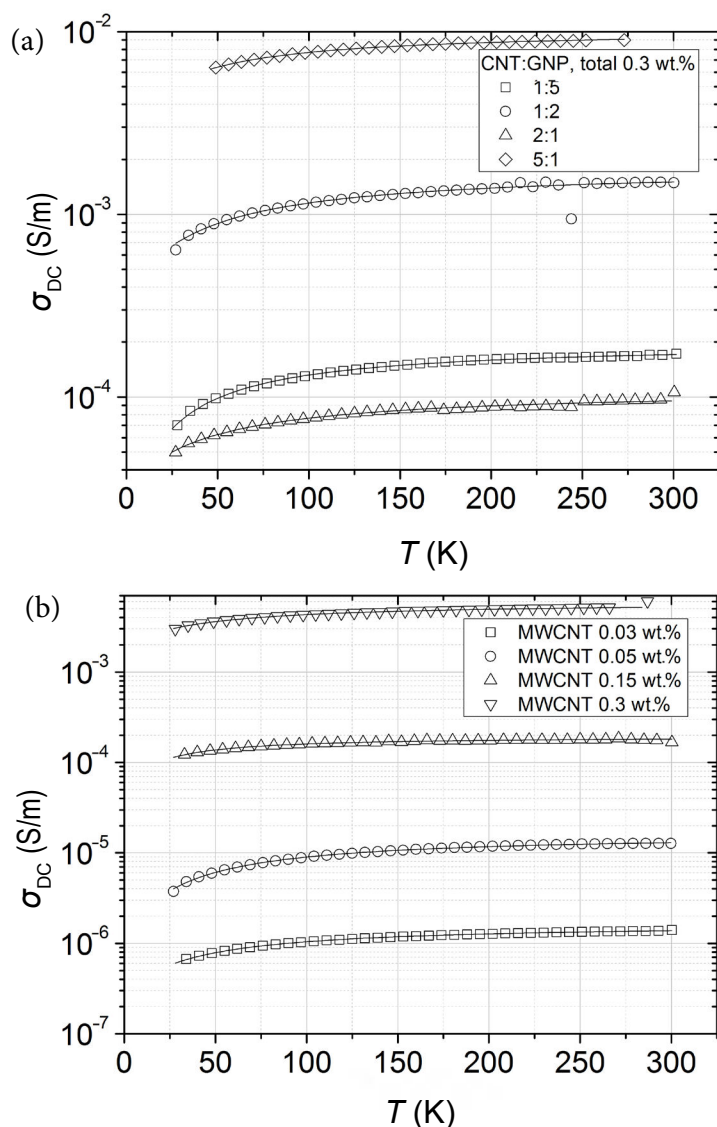
Fig. 6. Temperature dependence of DC conductivity for composites filled with (a) MWCNTs, (b) MWCNTs/GNPs; total concentration is 0.3 wt.%. Solid lines are fits of the tunnelling model.

Table 1. Tunnelling model fit parameters.

MWCNTs (wt.%)	σ_0 (S/m)	T_1 (K)	T_0 (K)
0.03	$1.6 \cdot 10^{-6}$	63	34
0.05	$1.5 \cdot 10^{-5}$	77	27
0.15	$2.1 \cdot 10^{-4}$	22	15
0.3	$6.1 \cdot 10^{-3}$	46	41
CNTs:GNPs (total 0.3 wt.%)			
1:5	$2.1 \cdot 10^{-4}$	50	20
1:2	$1.8 \cdot 10^{-3}$	61	37
2:1	$1.1 \cdot 10^{-5}$	52	41
5:1	$1.1 \cdot 10^{-2}$	36	27

4. Conclusions

MWCNT/epoxy and GNP/epoxy nanocomposites with different filler contents (0.015–0.3 wt.%) and hybrid epoxy nanocomposites filled with CNTs/GNPs in a total reinforcement of 0.3 wt.% were fabricated, and the effects of varying individual CNT/GNP contents and combination on electrical properties were evaluated.

The lowest electrical percolation threshold is observed in MWCNT composites (0.03 wt.% concentration). Although the percolation threshold in mixed MWCNTs/GNPs can be described by the excluded volume theory, the electrical conductivity of mixed composites is substantially higher in comparison with that of single composites. The electrical conductivity of hybrid nanocomposites containing 0.3 wt.% MWCNTs and GNPs in ratio 5:1 exhibits the highest value of 0.009 S/m, which is more than 4 times higher than that of composites containing only 0.3 wt.% MWCNTs (0.002 S/m). The concurrent 1D and 2D

particles did not affect the percolative behaviour of MWCNTs but led to an outstanding increment in the final electrical conductivity. That could be considered as a synergistic effect between GNPs and MWCNTs due to the better distribution of MWCNTs and the tunnelling of electrons between GNPs and MWCNTs.

Acknowledgements

References

[1] T. Kuilla, S. Bhadra, D. Yao, N.H. Kim, S. Bose, and J.H. Lee, Recent advances in graphene based polymer composites, Prog. Polym. Sci. **35**(11), 1350–1375 (2010).

[2] R.J. Young, I.A. Kinloch, L. Gong, and K.S. Novoselov, The mechanics of graphene nanocomposites: a review, Compos. Sci. Technol. **72**(12), 1459–1476 (2012).

[3] F. Qin and C. Brosseau, A review and analysis of microwave absorption in polymer composites filled with carbonaceous particles, J. Appl. Phys. **111**, 061301 (2012).

[4] G. Inzelt, *Conducting Polymers: A New Era in Electrochemistry* (Springer, Berlin, 2008).

[5] *Metal-filled Polymers*, ed. S.K. Battacharya (Dekker, New York, 1986).

[6] R. Strumpler and J. Glatz-Reichenbach, Conducting polymer composites, J. Electroceram. **3**(4), 329–346 (1999).

[7] J.N. Coleman, U. Khan, W.J. Blau, and Y.K. Gun'ko, Small but strong: A review of the mechanical properties of carbon nanotube–polymer composites, Carbon **44**(9), 1624–1652 (2006).

[8] J.K.W. Sandler, J.E. Kirk, I.A. Kinloch, M.S.P. Shaffer, and A.H. Windle, Ultra-low electrical percolation threshold in carbon-nanotube-epoxy composites, Polymer **44**(19), 5893–5899 (2003).

[9] C.A. Martin, J.K.W. Sandler, M.S.P. Shaffer, M.K. Schwarz, W. Bauhofer, K. Schulte, and A.H. Windle, Formation of percolating networks in multi-wall carbon-nanotube-epoxy composites, Compos. Sci. Tech. **64**(15), 2309–2316 (2004).

[10] S.Y. Fu, X.Q. Feng, B. Lauke, and Y.W. Mai, Effects of particle size, article/matrix interface adhesion and particle loading on mechanical properties of particulate–polymer composites, Compos. B Eng. **39**(6), 933–961 (2008).

[11] J.B. Bai and A. Allaoui, Effect of the length and the aggregate size of MWNTs on the improvement efficiency of the mechanical and electrical properties of nanocomposites – experimental investigation, Composites A **34**(8), 689–694 (2003).

[12] X.M. Chen, J.W. Shen, and W.Y. Huang, Novel electrically conductive polypropylene/graphite nanocomposites, J. Mater. Sci. Lett. **21**(3), 213–214 (2002).

[13] W.G. Weng, G.H. Chen, D.J. Wu, and W.L. Yan, HDPE/expanded graphite electrically conducting composite, Compos. Interface **11**(2), 131–143 (2004).

[14] I. Neitzel, V. Mochalin, and Y. Gogotsi, *Ultrananocrystalline Diamond* (Elsevier, 2012).

[15] T. Glaskova, M. Zarrelli, A. Borisova, K. Timchenko, A. Aniskevich, and M. Giordano, Method of quantitative analysis of filler dispersion degree in composite systems with spherical inclusions, Compos. Sci. Technol. **71**(13), 1543–1549 (2011).

[16] A.S. Patole, S.P. Patole, S.Y. Jung, J.B. Yoo, J.H. An, and T.H. Kim, Self assembled graphene/carbon nanotube/polystyrene hybrid nanocomposite by *in situ* microemulsion polymerization, Eur. Polym. J. **48**(2), 252–259 (2012).

[17] U. Khan, I. O'Connor, Y.K. Gun'ko, and J.N. Coleman, The preparation of hybrid films of carbon nanotubes and nano-graphite/graphene with excellent mechanical and electrical properties, Carbon **48**(10), 2825–2830 (2010).

[18] S. Chatterjee, F. Nafezarefi, N.H. Tai, L. Schlagenhauf, F.A. Nuesch, and B.T.T. Chu, Size and synergy effects of nanofiller hybrids including graphene nanoplatelets and carbon nanotubes in mechanical properties of epoxy composites, Carbon **50**(15), 5380–5386 (2012).

[19] M. Safdari, and M.S. Al-Haik, Synergistic electrical and thermal transport properties of hybrid

polymeric nanocomposites based on carbon nanotubes and graphite nanoplatelets, Carbon **64**, 111–121 (2013).

[20] J. Macutkevic, P. Kuzhir, A. Paddubskaya, S. Maksimenko, J. Banys, A. Celzard, V. Fierro, S. Bistarelli, A. Cataldo, F. Micciulla, and S. Bellucci, Electrical transport in carbon black-epoxy resin composites at different temperatures, J. Appl. Phys. **114**(3), 033707 (2013).

[21] I. Balberg, C.H. Anderson, S. Alexander, and N. Wagner, Excluded volume and its relation to the onset of percolation, Phys. Rev. B **30**(7), 3933–3943 (1984).

[22] A. Celzard, E. McRae, C. Deleuze, M. Dufort, G. Furdin, and J.F. Mareche, Critical concentration in percolating systems containing a high-aspect-ratio filler, Phys. Rev. B **53**, 6209 (1996).

[23] A. Li, C. Zhang, and Y.F. Zhang, Graphene nanosheets-filled epoxy composites prepared by a fast dispersion method, J. Appl. Polym. Sci. **134**(36), 45152 (2017).

[24] A. Plyushch, J. Macutkevic, P. Kuzhir, J. Banys, Dz. Bychanok, Ph. Lambin, S. Bistarelli, A. Cataldo, F. Micciulla, and S. Bellucci, Electromagnetic properties of graphene nanoplatelets/epoxy composites, Compos. Sci. Technol. **128**, 75–83 (2016).

[25] A.K. Jonsher, The universal dielectric response and its physical significance, IEEE Trans. Electr. Insul. **27**(3), 407–423 (1992).

[26] D. Stauffer and A. Aharony, *Introduction to Percolation Theory* (Taylor & Francis, London, 1994).

[27] U. Szeluga, B. Kumanek, and B. Trzebicka, Synergy in hybrid polymer/nanocarbon composites. A review, Composites A **73**, 204–231 (2015).

[28] Z.A. Ghaleb, M. Mariatti, and Z.M. Ariff, Synergy effects of graphene and multiwalled carbon nanotubes hybrid system on properties of epoxy nanocomposites, J. Reinf. Plast. Compos. **36**(9), 685–695 (2017).

[29] I. Balberg, Tunnelling and percolation in lattices and the continuum, J. Phys. D **42**(6), 064003 (2009).

[30] P. Sheng, E.K. Sichel, and J.I. Gettleman, Fluctuation-induced tunneling conduction in carbon-polyvinylchloride composites, Phys. Rev. Lett. **40**, 1197–1200 (1978).

[31] T.A. Ezquerra, M. Kulesza, and F.J. Balta Galleja, Electrical transport in polyethylene–graphite composite materials, Synth. Met. **41**, 915–920 (1991).

EPOKSIDINĖS DERVOS KOMPOZITŲ SU DAUGIASIENIAIS ANGLIES NANOVAMZDELIAIS ELEKTRINIO LAIDUMO GERINIMAS GRAFENO DALELĖMIS

I. Kranauskaitė [a], J. Macutkevič [a], A. Borisova [b], A. Martone [c], M. Zarrelli [c], A. Selskis [d],
A. Aniskevich [b], J. Banys [a]

[a] *Vilniaus universiteto Fizikos fakultetas, Vilnius, Lietuva*
[b] *Latvijos universiteto Medžiagų mechanikos institutas, Ryga, Latvija*
[c] *Nacionalinės mokslinių tyrimų tarybos Polimerų, kompozitų ir biomedžiagų institutas, Portiči, Italija*
[d] *Fizinių ir technologijos mokslų centras, Vilnius, Lietuva*

Santrauka

Tobulėjant technologijoms ir didėjant našesnių bei mažesnių matmenų prietaisų poreikiui reikalingos naujos medžiagos, atitinkančios kylančius reikalavimus. Vienos iš tokių medžiagų yra polimeriniai kompozitai su anglies nanodalelėmis, kurie pasižymi geromis mechaninėmis, terminėmis ir elektrinėmis savybėmis.

Straipsnyje aptariami mišraus užpildo kompozitų su anglies nanovamzdeliais ir grafeno dalelėmis elektrinio laidumo tyrimai. Anglies nanovamzdeliai ir grafenas sumaišyti įvairiomis proporcijomis, kai bendra dalelių procentinė masės dalis kompozite – 0,3 %. Palyginimui pagaminti kompozitai su anglies nanovamzdeliais, kurių procentinė masės dalis buvo nuo 0,025 iki 0,3 %.

Užpildo dalelių pasiskirstymas polimero matricoje įvertintas optinės mikroskopijos ir skenuojančios elektroninės mikroskopijos metodais. Elektrinių savybių tyrimai atlikti plačiame dažnių (20 Hz – 3 GHz) bei temperatūrų intervale (30–300 K).

Nustatyta, kad įterpiant nedidelį kiekį grafeno dalelių (0,05 % masės dalies) į kompozitus su anglies nanovamzdeliais, kai bendra užpildo dalelių koncentracija 0,3 %, elektrinis laidumas padidėja keturis kartus, palyginti su kompozitais, užpildytais tik anglies nanovamzdeliais esant tokiai pačiai dalelių koncentracijai. Tai gali būti siejama su geresniu vienmačių ir dvimačių dalelių tarpusavio pasiskirstymu mišraus užpildo kompozito polimerinėje matricoje.

VII

Size-dependent electrical and thermal properties of onion-like carbons/polyurethane composites

I.Kranauskaite, J. Macutkevic, J. Banys, V. Kuznetsov, M. Letellier, V. Fierro, A. Celzard, O. Shenderova

Size-Dependent Electrical and Thermal Properties of Onion-Like Carbons/Polyurethane Composites

Ieva Kranauskaite [ID],[1] Jan Macutkevic [ID],[1] Juras Banys,[1] Vladimir Kuznetsov,[2] Maxime Letellier,[3] Vanessa Fierro,[3] Alain Celzard,[3] Olga Shenderova[4]

[1]*Vilnius University, Vilnius, Lithuania*

[2]*Boreskov Institute of Catalysis SB RAS, Novosibirsk, Russia*

[3]*Université de Lorraine, CNRS, IJL, F-88000 Epinal, France*

[4]*International Technology Center, Raleigh, North Carolina 27715*

Results of dielectric/electrical studies of onion-like carbon (OLC)/polyurethane composite films in very broad frequency (20 Hz–3 THz) and temperature (26–300 K) ranges are presented. We show that the percolation threshold in these composites strictly depends on OLC aggregate size and is lower for composites having smaller OLC aggregates. The electrical conductivity in the composites is mainly due to electron tunneling between OLC clusters and quasi-one-dimensional hopping inside the clusters. The thermal diffusivity increases with OLC concentration and, as for electrical conductivity, is the highest for composites having the smallest OLC aggregates. POLYM. COMPOS., 00:000–000, 2018. © 2018 Society of Plastics Engineers

INTRODUCTION

Polymer-based composites presenting electrical percolation have attracted much attention because of their potential applications such as electroactive or sensitive materials, or as electromagnetic coatings [1]. Thermally conductive composites also find a lot of applications, since they can be used for example as heat sink in various electric and electronic systems [2]. In binary mixtures made of electrically conducting and non-conducting phases, an electrical percolation occurs at some critical filler concentration, called

percolation threshold [3]. It is an important task to reach as-low-as possible percolation threshold in order to maintain the mechanical properties of polymers and to save the cost of (generally expensive) fillers. The lowest percolation thresholds were generally observed in composites based on carbon nanotubes, due to their high aspect ratio [4]. Nevertheless, the percolation threshold in other composites, filled for instance by carbon blacks forming long chain-like aggregates, can be also very low [5]. But the percolation threshold of composites based on the same polymer matrix and on the same carbon nanotubes may take very different values [2]. This suggests that the percolation threshold is strongly influenced by the composite preparation technology. Additionally, a drawback of carbon nanotubes is their higher cost in comparison to other carbon allotropes, such as carbon blacks or graphites. Another serious disadvantage is the possible toxicity of CNTs, which has been debated for long [6], and which is still controversial today.

Herein, composites based on onion-like carbons (OLCs) are presented, which might be used for applications requesting high electrical conductivity, for example as antistatic materials, for electrostatic discharge, dissipation, electromagnetic interference shielding, temperature, pressure and gas sensors. OLCs are indeed stable, multi-shelled imperfect fullerenes, exhibiting electrical conductivity as high as about several hundred S/m at room temperature [7]. In comparison to other carbonaceous fillers, OLCs also combine many advantages such as easy preparation technology and low cost, tunable electrical conductivity (by annealing of OLC powder), hierarchical structure and defects which strongly absorb electromagnetic waves (required for electromagnetic shielding), and lower toxicity in comparison to carbon nanotubes [8, 9]. Many dielectric investigations of OLC-based composites were performed below the

---

percolation threshold, where the complex dielectric permittivity of composites increases slowly with OLC concentration according to the Maxwell-Garnett theory [10, 11]. It was also demonstrated that the electronic polarizability is almost independent of the OLC morphology, but is proportional to their volume fraction [12, 13]. Considering the electrical percolation, the threshold in OLC-polyurethane (PU) composites is 10 vol% for OLC with mean aggregate size of 130 nm [14]. Thus, the percolation threshold in OLC composites is significantly lower than the one predicted by Monte-Carlo calculations in three dimensions: 31.2 vol% [15, 16]. The aggregate structure of conductive particles thus has a strong impact on the threshold and on the related composite dielectric/electrical properties [17], as already observed for some carbon black composites [17]. OLCs, similarly to carbon blacks, may indeed have a complex aggregate structure [7] and it was found that, in OLC-polydimethylsiloxane composites, the percolation threshold is the lowest with the smallest OLC aggregates [19].

In this work, the way of further reducing the percolation threshold in OLC/polymer composites was investigated. Therefore, the aim of this article is to investigate the impact of OLC aggregate size on broadband electromagnetic and thermal properties of PU films filled with OLC. We found that the lowest percolation threshold and the highest thermal diffusivity were obtained in OLC/PU composites having the smallest OLC aggregates (40 nm).

EXPERIMENTAL

The OLC samples used to prepare OLC/PU composite films were synthesized as follows. Detonation nanodiamonds (DNDs) were first obtained by detonation of a mixture of trinitrotoluene and 1,3,5-trinitroperhydro–1,3,5-triazine in CO_2 atmosphere. It is known that DNDs exist in the form of strong aggregates (up to a few hundred nanometers) with coherent and incoherent interfaces between primary DND particles of size 4–7 nm [7]. The polydisperse DND material was thus separated by centrifugation into fractions with average aggregate sizes of 40 and 100 nm. Those sizes were measured by a dynamic light-scattering technique in water suspensions. The sp^2 carbon of the DND fractions was then oxidized in a mixture of concentrated sulfuric acid and chromic anhydride at 383 K, and the resultant material was washed with water and dried. The powder was heated in vacuum (10^{-4} Torr) at 1,923 K for 3 h. The sizes of OLC were measured by a dynamic light-scattering technique using N-Methyl-2-pyrrolidone (NMP) suspensions, in which OLC are well-dispersed. The distribution of sizes (average sizes 40 and 100 nm, respectively) was similar to that of the starting NDs in water suspensions.

Samples of OLC were subsequently mixed at different mass ratios with a Minwax "clear satin" commercial formulation of oil-based PU containing 60% of volatile compounds. After mixing with the OLC powder, the polymer suspension was stirred at 400 rpm overnight at 313 K. Then, the suspension was casted on a Teflon substrate and dried overnight at 318 K and room pressure. The samples were thus recovered in the form of films whose typical thicknesses ranged from 0.1 to 0.8 mm, depending on the OLC concentration that modified the viscosity of the corresponding suspensions.

Scanning electron microscopy (SEM) and transmission electron microscopy (TEM) images were obtained with JSM 6460 LV and JEM 2010 electron microscopes, respectively.

The complex effective permittivity was measured as a function of frequency and temperature using a HP4284A precision LCR meter in the frequency range 20 Hz–1 MHz. For the low-temperature measurements, a helium closed-cycle cryostat was used, while for the high-temperature measurements a home-made furnace was used. Each measurement was started at room temperature. In the frequency range 1 MHz–3 GHz, dielectric measurements were performed using an Agilent 8714ET vector network analyzer. In the microwave frequency range from 8 to 53 GHz, a home-made waveguide spectrometer was used; applying the thin rod method, the typical value of road diameter was about several hundred micrometers [20]. In the frequency range from 1 MHz to 53 GHz, the measurement accuracy was ~10%. Silver paste was used for making the contacts. In the terahertz frequency range (from 100 GHz to 3 THz), an Ekspla Ltd terahertz time-domain spectrometer based on a femtosecond laser was used. The spectrometer is based on femtosecond laser fiber (wavelength 1 µm, pulse duration <150 fs) and GaBiAs photoconductive terahertz emitter and detector [21]. The signal to noise ratio was as high as 60 dB at the frequency 0.5 THz. The complex effective permittivity was calculated according to the Fresnel *Equation* [22]. The measurements accuracy was better than 1% at 0.5 THz (where the signal to noise ratio is the highest) [23]. The real part σ' of the complex electrical conductivity was calculated as $\sigma' = \omega \, \varepsilon_0 \, \varepsilon''$, where ω is the angular frequency, ε_0 is the permittivity of vacuum, and ε'' is the imaginary part of the complex effective permittivity.

The thermal diffusivity was measured at room temperature with a Netzsch LFA 457 MicroFlash apparatus. The system comprised a Nd:glass laser of adjustable power (wavelength 1.054 nm, pulse width 0.3 ms) for flashing one side of the sample, and a liquid N_2-cooled MCT infrared detector for recording the increase of temperature on the opposite side. This method was used since it allows evaluating the thermal properties of small and thin samples, unlike usual methods of thermal conductivity measurement. Samples were cut into squares of dimensions 10 × 10 mm, and their thickness was cautiously measured with an electronic caliper. All samples presenting non-flat surfaces and/or inhomogeneous thickness were discarded. The films were then installed in a SiC sample holder, and submitted to laser pulses (three pulses separated by 5 min) of power around 5 mJ. The corresponding temperature increase was recorded, and the curve was fitted by the *Proteus* software, using the
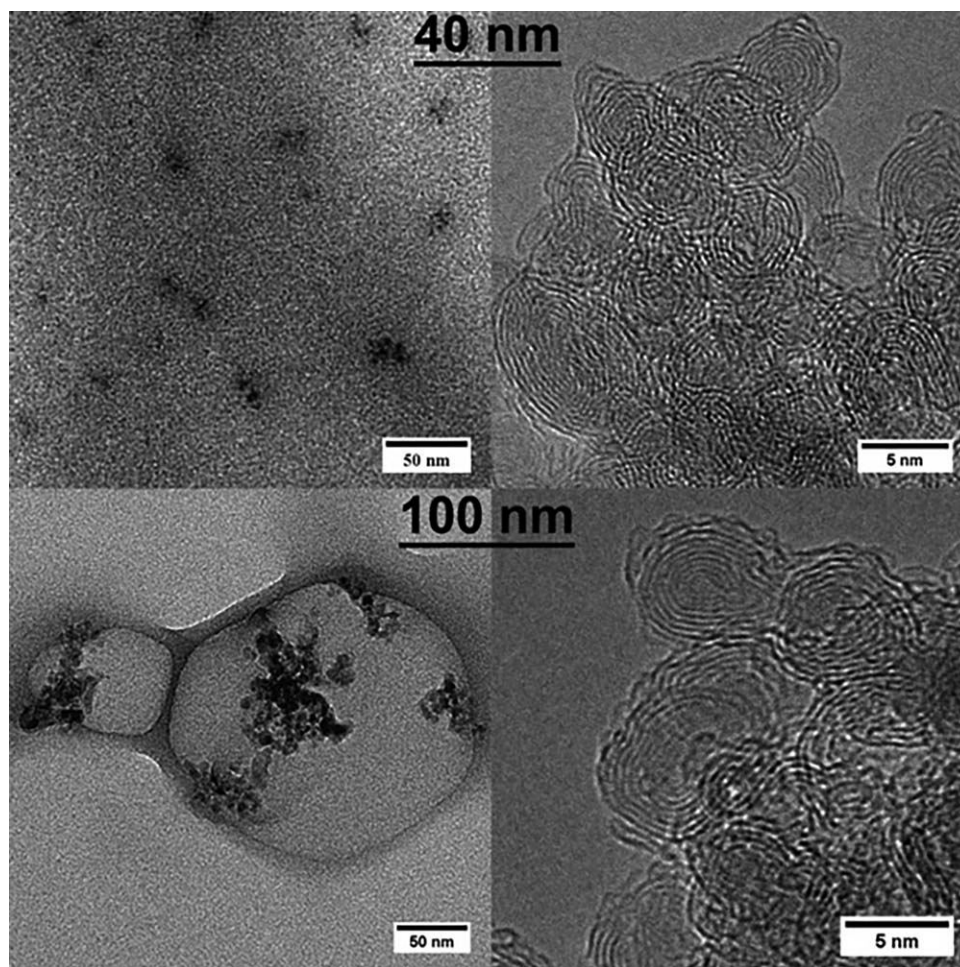
FIG. 1. TEM images of OLC with 40 and 100 nm average aggregate size. Left part—low magnification images of aggregates deposited on the amorphous carbon layer of TEM grid. Right part presents of HR TEM images of OLC aggregates.

radiation-corrected model. Because the method requires perfect thickness homogeneity, which is very hard to achieve with OLC/PU composite films, only a few selected samples could be accurately investigated.

RESULTS AND DISCUSSION

Room Temperature Dielectric Properties and Composite Structure

TEM images of OLC particles used in the present study and having average aggregate sizes of 40 and 100 nm are presented in Fig. 1. The left part of Fig. 1 illustrates low-magnification TEM images of the aggregates while the right part presents their high-resolution images. One can see that the primary OLC particles consist of defective fullerene-like shells, combined into aggregates with joint graphene layers rather similar to what is known for some carbon blacks. Therefore, it is likely that OLC form chainlike clusters. Whereas the latter don't have any particular shape, they can probably deform easily when submitted to shear stress during the

preparation of the composite: chains of carbon onions arranged in a pearl necklace structure are thus expected to be produced in the polymer matrix.

SEM images of OLC/PU composites with different aggregate sizes are presented in Fig. 2. It can be concluded that OLC particles are well dispersed in all cases, since all areas strictly looked equal, without obvious segregation or depletion at any place.

The frequency dependencies of dielectric permittivity and electrical conductivity for large aggregate size OLC/PU are presented in Fig. 3. The dielectric permittivity of composites with 3.5 vol% of OLC inclusions and pure PU is very low (<10) and almost constant in a wide frequency range, while the electrical conductivity of these materials strongly increases with frequency and no DC conductivity can be observed. Dielectric losses (which are strongly related with electrical conductivity) of these materials are also very low and caused by PU molecules dynamics [14]. Above an OLC concentration of 7 vol%, the dielectric permittivity starts decreasing with frequency, whereas a constant conductivity can be observed at low frequency (DC conductivity), as well as two
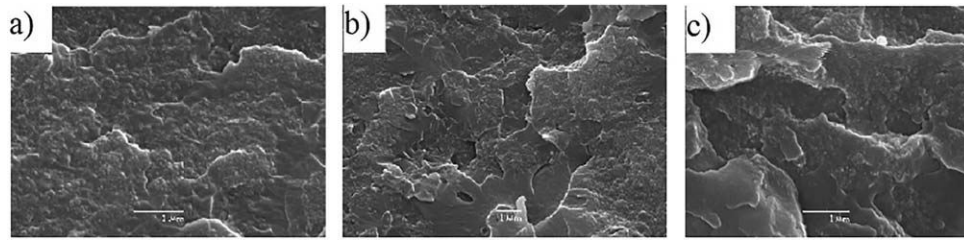
FIG. 2. SEM images of composite films based on PU matrix filled with: (a) 14 vol% of OLC of aggregate size 100 nm, (b) 11 vol% of OLC of aggregate size 40 nm; (c) 3.5 vol% of OLC of aggregate size 100 nm.

different dielectric dispersions obviously related to Maxwell-Wagner relaxation [24]. Therefore, the percolation threshold in composites with large OLC aggregates is close to 7.1 vol% concentration, while similar considerations of composites with small OLC aggregates allowed determining the percolation threshold value close to 5.4 vol%. Assuming that chains of carbon onions arranged in a pearl necklace structure are formed in the composite, as explained in the introduction, it is expected that aggregates based on small-sized OLC are more easily deformable, leading to more elongated aggregates in the polymer and hence to a lower percolation threshold. The present results agree with such assumption. The percolation

threshold value close to 5.4 vol. % for small-sized OLC is slightly lower than the percolation threshold observed in OLC/polydimethylsiloxane composites for the same aggregate size [19]. The huge values of dielectric permittivity and electrical conductivity in the microwave range (e.g. at 30 GHz) of composites above the percolation threshold indicate that those composites are suitable for electromagnetic shielding.

The concentration dependence of both dielectric permittivity and electrical conductivity for different OLC aggregate sizes is presented in Fig. 4. The electrical conductivity values were selected at 129-Hz frequency, since above the percolation threshold those values correspond
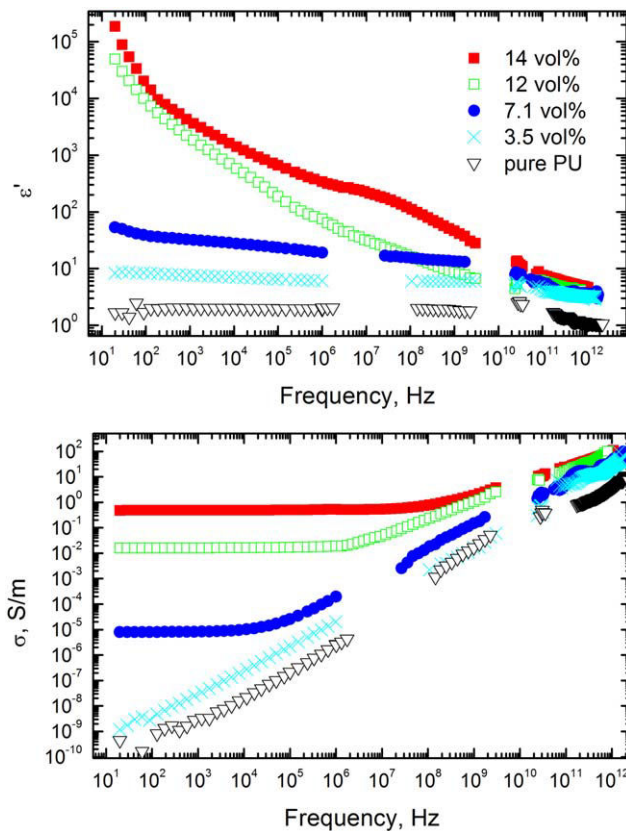

FIG. 3. Frequency spectra of real parts of complex dielectric permittivity and electrical conductivity of OLC/PU composites (with large OLC inclusions) at room temperature. [Color figure can be viewed at wileyonlinelibrary.com]
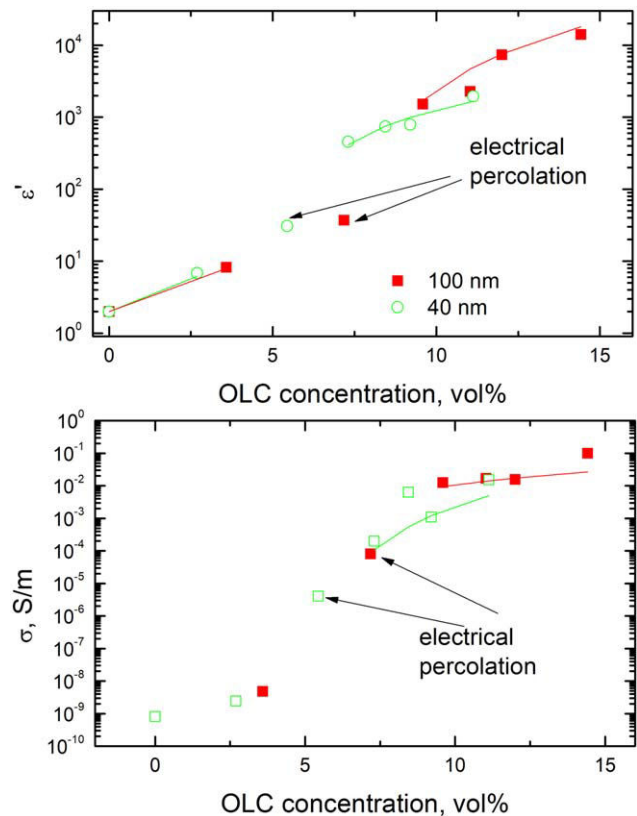
FIG. 4. Real parts of complex dielectric permittivity and complex electrical conductivity of OLC/PU composites versus OLC concentration and aggregate size at frequency 129 Hz and room temperature. [Color figure can be viewed at wileyonlinelibrary.com]
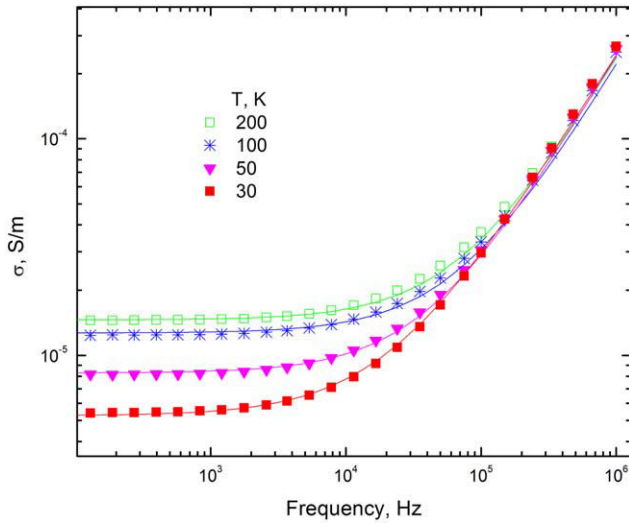
FIG. 5. Frequency dependence of the real part of complex electrical conductivity of OLC/PU (with 100-nm OLC inclusions at 7.5 vol%) at different temperatures (low-temperature region). [Color figure can be viewed at wileyonlinelibrary.com]

FIG. 6. Temperature dependence of OLC/PU with 40-nm OLC inclusions composites DC conductivity fitted by tunneling law (*Eq.* 4) in the low-temperature region. [Color figure can be viewed at wileyonlinelibrary.com]

to the DC conductivity. According to the classical percolation theory, the filler concentration dependence of both dielectric permittivity ε' and electrical conductivity σ' above the percolation threshold follows power laws with different critical exponents g and t [25]:

$$\varepsilon' = \varepsilon_p (f - f_c)^g \tag{1}$$

$$\sigma' = \sigma_p (f - f_c)^t \tag{2}$$

where f and f_c are the volume fraction and the critical volume fraction (percolation threshold) of filler, respectively, and ε_p and σ_p are the permittivity and the conductivity of the filler, respectively. Obtained parameters are $\varepsilon_p = 62.3 \times 10^3$, $g = 1.26$, $\sigma_p = 320$ S/m, $t = 3.5$, $f_c = 0.054$ for 40-nm OLC aggregate size, and $\varepsilon_p = 228.7 \times 10^3$, $g = 1.25$, $\sigma_p = 2.4$, $t = 1.5$ for 100-nm OLC aggregate size.

Frequency dependencies of the electrical conductivity of composites with 7.1 vol% of OLC at different temperatures are presented in Fig. 5. At low frequency, and as expected just above the percolation threshold, a frequency-independent plateau (DC conductivity) is observed but at higher frequency the conductivity increases as a power law of frequency. On cooling, the DC conductivity decreases and the changes of conductivity behavior can be fitted by Almond-West power law:

$$\sigma(\omega) = \sigma_{DC} + K\omega^s \tag{3}$$

where σ_{DC} and $K\omega^s$ are DC and AC conductivity, respectively. From this fit, the critical frequency at which the conductivity starts to increase from its DC values (here an increase by 10% was chosen) can be calculated. The resultant parameters are presented in Fig. 6.
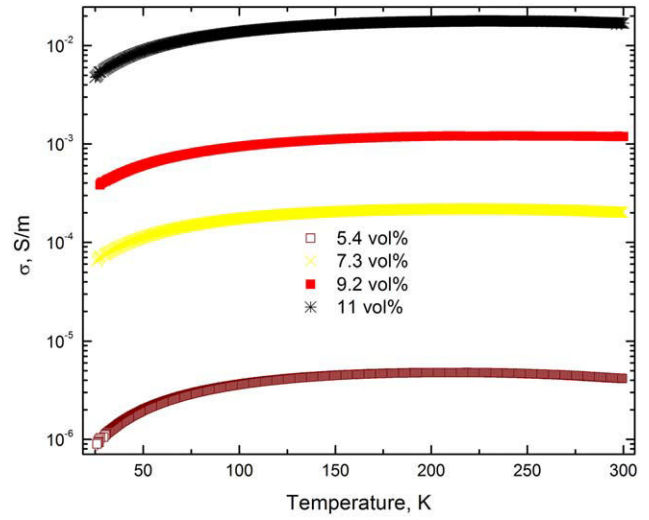
Below room temperature, the DC conductivity can be described by fluctuation-induced tunneling model, as presented in Fig. 6:

$$\sigma_{DC} = \sigma_{DC0} \, \exp\left(-\frac{T_1}{T + T_0}\right) \tag{4}$$

where σ_{DC0} is the conductivity at very high temperatures ($T \gg T_1$ and T_0), T is the absolute temperature, T_1 represents the energy required for an electron to cross the insulator gap between the conductive particles aggregates, and T_0 is the temperature above which thermally activated conduction over barriers starts to occur. The corresponding parameters are gathered in Table 1. According to the tunneling model:

$$T_1 = \frac{w \, A \, \beta_0}{8 \, \pi \, k} \tag{5}$$

$$T_0 = \frac{2 \, T_1}{\pi \, \chi \, w} \tag{6}$$

TABLE 1. Tunneling fit parameters for DC conductivity at low temperatures.

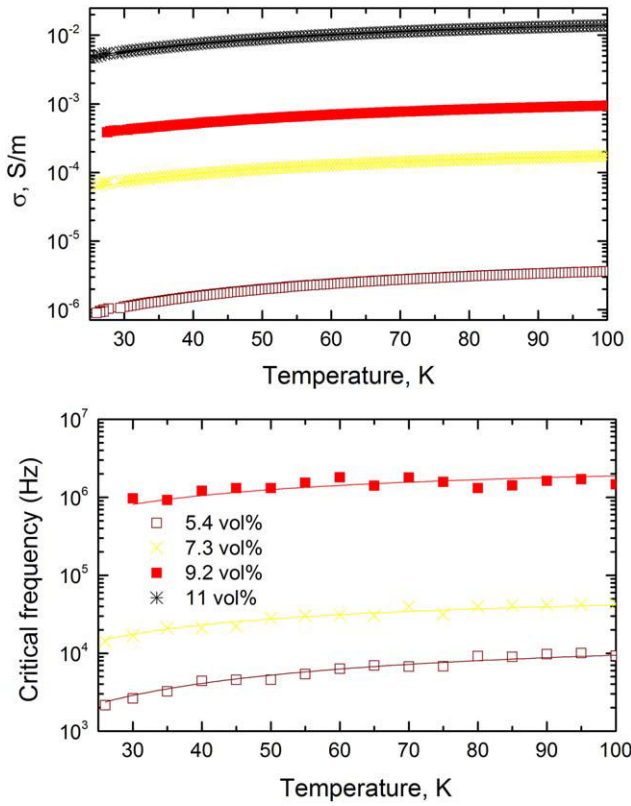| OLC aggregate size	Concentration, vol.%	σ_{DC0}, mS/m	T_1, K	T_0, K
Large	7.2	0.93	53	11
	9.5	16.9	36	7
	11	27	39	8
	12	10.5	31	7
	14	250	36	8
Small	5.4	0.006	63	3
	7.3	0.285	54	9
	8.4	8.18	58	6
	9.2	1.6	62	15
	11	22.7	53	7

FIG. 7. (a) Temperature dependence of OLC/PU with 40-nm OLC inclusions composites DC conductivity fitted by Mott's law (Eq. 7) in the low-temperature region; and (b) corresponding critical frequency. [Color figure can be viewed at wileyonlinelibrary.com]

where $\chi = (2~mV_0)^{0.5}/h$ and $\beta_0 = 4~V_0/ew$, m and e being the electron mass and charge, respectively, h is the Planck constant, V_0 is the potential barrier height, w is the interparticle distance (gap width), and A is the area of the capacitor formed by the junction.

However, at even lower temperatures, typically below 100 K, Mott's law describes also quite well the temperature dependence of the electrical conductivity (Fig. 7). It reads:

$$\sigma_{DC} = \sigma_{DC0}~\exp\left[-\left(\frac{T_m}{T}\right)^{1/n}\right] \qquad (7)$$

where T_m is a constant depending on the density of states and localisation length of the system, and $n = 1 + d$, d being the dimensionality of the system. The resultant parameters are given in Table 2, where it can be seen that the values of σ_{DC0} derived from the fits of either Eqs. 4 or 7 to the experimental data are quite consistent with each other. The dimensionality for all composites is close to 0.5, which is typical for pure OLC obtained by annealing nano-diamonds at 1,600 K [7]. Below 100 K, the critical frequency decreases on cooling according to the law:

$$f_{cr} = f_\infty~\exp\left[-\left(\frac{T_m}{T}\right)^{1/n}\right], \qquad (8)$$

TABLE 2. Mott's law fit parameters for DC conductivity at low temperatures.

OLC aggregate size	Concentration, vol.%	σ_{DC0}, mS/m	T_m, K	n	ω_0, kHz
Large	7.2	1.12	55	1.51	14.472
	9.5	17	31	1.24	268.874
	11	35.7	45	1.73	2213.310
	12	99	29	1.41	481.663
	14	254	29	1.09	-
Small	5.4	25.73	78	1.35	21.162
	7.3	0.33	56	1.46	81.226
	8.4	9.28	54	1.12	830.680
	9.2	2	64	1.62	402.834
	11	25.73	54	1.37	-

where f_∞ is the frequency at very high temperature. For 1D hopping conductivity, the dc hopping length reads:

$$R_{dc} = \sqrt{\frac{\Delta r}{2~\alpha~T}} \qquad (9)$$

while the ac hopping length is:

$$R_{ac} = \frac{1}{2}\alpha~\ln\frac{f_{fon}}{f_{cr}} \qquad (10)$$

where Δ determines an uniform distribution of carriers energies, r is the distance between two nearest OLC particles, α^{-1} is the localisation length, and f_{fon} is the attempt frequency. Assuming that both localisation length and attempt frequency don't depend on temperature and concentration, it can be concluded that the increase of critical frequency f_{cr} with OLC concentration seen in Fig. 7(b) is related to the decrease of ac hopping length, while the increase of critical frequency with temperature is related to the decrease of ac hopping length. Thus, the
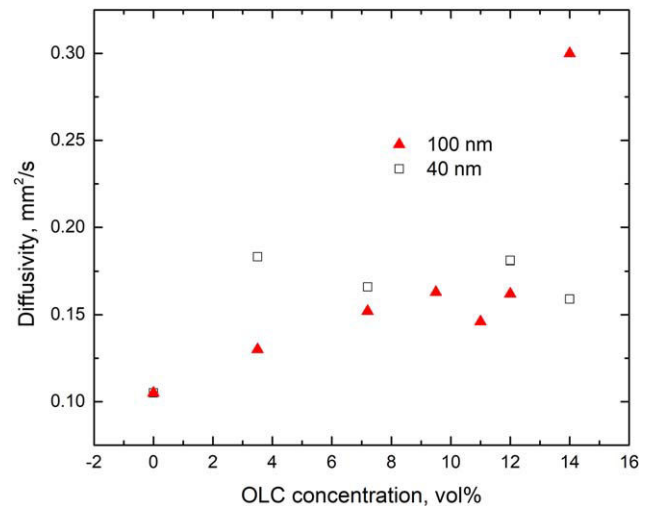

FIG. 8. Thermal diffusivity of OLC/PU composites as a function of OLC concentration and aggregate size. [Color figure can be viewed at wileyonlinelibrary.com]

electrical transport in PU matrices filled with OLC of different aggregate sizes proceeds by electron hopping inside OLC clusters and by tunneling between clusters.

The results of thermal diffusivity measurements are presented in Fig. 8. The thermal diffusivity, being the quantity describing the ability of the materials to rapidly transmit the heat, increases with OLC concentration. Since thermal conductivity is the product of diffusivity $\times$ heat capacity $\times$ bulk density of the material, and since heat capacity and density can be easily calculated by rules of mixtures, it is expected that the thermal conductivity presents the same qualitative behavior as the diffusivity. As for the effect of OLC aggregate size, the thermal diffusivity is higher for composites with smaller filler, in agreement with their higher electrical conductivity although the effect is far lower here, since no percolation occurs.

CONCLUSIONS

Composite films based on PU matrix filled with various volume fractions of OLC having two aggregate sizes, 40 and 100 nm, were investigated by dielectric/electrical and thermal diffusivity studies. The lowest percolation threshold in such materials was determined as 5.4 vol% in the case of 40-nm OLC aggregate size. The huge values of dielectric permittivity and electrical conductivity in the microwave range (e.g. at 30 GHz) of composites above the percolation threshold indicate that those composites are suitable for electromagnetic shielding. The electrical transport in OLC/PU composite films is controlled by quasi-1D electron hopping inside OLC clusters on the one hand, and by tunneling between OLC clusters on the other hand. The thermal diffusivity increases with OLC concentration, as expected, and is higher for composites with smaller OLC aggregates, in agreement with the lower percolation threshold evidenced by electrical conductivity measurements.

REFERENCES

1. F. Qin, and C. Brosseau, *J. Appl. Phys.*, **111**, 061301 (2012).

2. Z. Han, and A. Fina, *Prog. Polym. Sci.*, **36**, 914 (2011).

3. S. Kirkpatrick, *Rev. Modern Phys.*, **45**, 574 (1973).

4. W. Bauhofer, and Z. Kovacs, *Compos. Sci. Technol.*, **69**, 1486 (2009).

5. L.J. Adriaanse, J.A. Reedijk, P.A.A. Teunissen, H.B. Brom, M.A.J. Michels, and J.C.M. Brokken-Zijp, *Phys. Rev. Lett.*, **78**, 1755 (1997).

6. K. Kostarelos, *Nat. Biotechnol.*, **26**, 774 (2008).

7. V.L. Kuznetsov, Y.V. Butenko, A.L. Chuvilin, A.I. Romanenko, and A.V. Okotrub, *Chem. Phys. Lett.*, **336**, 397 (2001).

8. S. Kang, J.E. Kim, D. Kim, C.G. Woo, P.V. Pikhitsa, M.H. Cho, and M. Choi, *J. Nanoparticle Res.*, **17**, 378 (2015).

9. J. Bartelmess, and S. Giordani, *Belstein J. Nanotechnol.*, **5**, 1980 (2014).

10. S.A. Maksimenko, V.N. Rodionova, G.Y. Slepyan, V.A. Karpovich, O. Shenderova, J. Walsh, V.L. Kuznetsov, I.N. Mazov, S.I. Moseenkov, A.V. Okotrub, and P. Lambin, *Diamond Relat. Mater.*, **16**, 1231 (2007).

11. J. Macutkevic, P. Kuzhir, D. Seliuta, G. Valusis, J. Banys, A. Paddubskaya, D. Bychanok, G. Slepyan, S. Maksimenko, V. Kuznetsov, S. Moseenkov, O. Shenderova, A. Mayer, and P. Lambin, *Diamond Relat. Mater.*, **19**, 91 (2010).

12. R. Langlet, P. Lambin, A. Mayer, P.P. Kuzhir, and S.A. Maksimenko, *Nanotechnology*, **19**, 115706 (2008).

13. J. Macutkevic, R. Adomavicius, A. Krotkus, D. Seliuta, G. Valusis, S. Maksimenko, P. Kuzhir, K. Batrakov, V. Kuznetsov, S. Moseenkov, O. Shenderova, A.V. Okotrub, R. Langlet, and P. Lambin, *Diamond Relat Mater.*, **17**, 1608 (2008).

14. J. Macutkevic, D. Seliuta, G. Valusis, J. Banys, V. Kuznetsov, S. Moseenkov, and O. Shenderova, *Appl. Phys. Lett.*, **95**, 112901 (2009).

15. S. Kirkpatrick, *Phys. Rev. Lett.*, **36**, 69 (1976).

16. Y. Deng, H.W.J. Blöte, and M.P. Nightingale, *Phys. Rev. E*, **72**, 013126 (2005).

17. P.P. Kuzhir, A.G. Paddubskaya, S.A. Maksimenko, V.L. Kuznetsov, S. Moseenkov, A.I. Romanenko, O.A. Shenderova, J. Macutkevic, G. Valusis, and P. Lambin, *IEEE Trans. Electromagn. Compat.*, **54**, 6 (2012).

18. J. Liang, and Q. Yang, *J. Appl. Phys.*, **102**, 083508 (2007).

19. J. Macutkevic, I. Kranauskaite, J. Banys, S. Moseenkov, V. Kuznetsov, and O. Shenderova, *J. Appl. Phys.*, **115**, 213702 (2014).

20. J. Grigas, *Microwave Dielectric Spectroscopy of Ferroelectrics and Related Materials*, Gordon and Breach Science Publ., OPA Amsterdam (1996).

21. K. Bertulis, A. Krotkus, G. Aleksejenko, V. Pacebutas, R. Adomavicius, G. Molis, and S. Marcinkevicius, *Appl. Phys. Lett*, **88**, 201112 (2006).

22. I. Pupeza, R. Wilk, and M. Koch, *Opt. Exp.*, **15**, 4335 (2007).

23. S.R. Tripathi, M. Aoki, M. Takeda, T. Asahi, I. Hosako, and N. Hiromoto, *Jap. J. Appl. Phys.*, **52**, 042401 (2013).

24. J. Liu, C.G. Duan, W.G. Yin, W.N. Mei, R.W. Smith, and J.R. Hardy, *Phys. Rev. B*, **70**, 144106 (2004).

25. D.J. Bergman, *Phys. Rev. Lett.*, **44**, 1285 (1980).